INVESTIGATING THE ROLE OF HEPATOCYTE-DERIVED EXOSOMES IN DRUG-INDUCED LIVER INJURY

Natalie S. Holman

A dissertation submitted to the faculty of the University of North Carolina at Chapel Hill in partial fulfillment of the requirements for the degree of Doctor of Philosophy in the Curriculum in Toxicology in the School of Medicine.

Chapel Hill
2016

Approved by:

Edward L. LeCluyse

Paul B. Watkins

Ilona Jaspers

Mehmet Kesimer

Nigel Key

ABSTRACT

Natalie S. Holman: Investigating the role of hepatocyte-derived exosomes in drug-induced liver injury
(Under the direction of Edward LeCluyse and Paul Watkins)

Drug-induced liver injury (DILI) is the primary cause of acute liver failure in the United States and is responsible for a substantial number of drug failures both pre- and post-market. Over 1,000 drugs have been associated with DILI and as a result, understanding the mechanisms of toxicity has proved extremely difficult. A common theme across mechanisms is the involvement of the immune system in the etiology, exacerbation, or resolution of DILI. It has become apparent that events at the hepatocyte level prior to cell death may influence immune responses and mediate the outcome of DILI. Hepatocyte-derived exosomes (HDE) may constitute one such immunomodulatory signal. HDE are constitutively released lipid-bound particles that have the unique ability to pass through fenestrations in the sinusoidal endothelium and enter the systemic circulation, potentially delivering stress signals to local and distal immune cells. The current research sought to establish HDE as mediators of early immune responses in the absence of overt DILI. We present a comprehensive analysis of the kinetics, content, and immunologic activity of HDE from primary hepatocytes stressed by sub-toxic drug exposures. To our knowledge, this is the first report of content profiling and functional analysis using primary human HDE in the context of DILI. Studies in rats, rat hepatocytes, and human hepatocytes exposed to the prototypical hepatotoxicant acetaminophen (APAP) verified changes in the RNA content of HDE prior to overt injury. Next, HDE from control- and APAP-treated primary human

hepatocytes were collected for content profiling and functional analysis. The global profiles of mRNA and miRNA in HDE shifted as a result of drug exposure. Lastly, the immunologic activity of HDE was examined by exposing monocytes to HDE from control- and APAP-treated primary human hepatocytes. Differential gene expression in pathways related to immune cell function and cholesterol metabolism were observed. Functionally, APAP HDE exposure resulted in sensitization of monocytes to LPS stimulation. miRNA profiles in APAP HDE suggested that monocyte gene expression may have been mediated directly by exosomal miRNA. These results demonstrate that HDE influence immune cells before overt hepatotoxicity and highlight the mechanistic relevance of HDE in mediating DILI outcomes.

ACKNOWLEDGEMENTS

I would like to thank the Curriculum in Toxicology at the University of North Carolina. This education would not have been possible without my mentors Drs. Edward LeCluyse and Paul Watkins. I cannot thank you enough for believing in me and giving me the opportunity to learn from you. Ed, thank you for taking a risk and letting a graduate student come to The Hamner. I would not be where I am today had it not been for you. Thank you for sharing your hepatocyte wisdom with me, for always being patient and understanding, and for putting things back in perspective for me when I need it. Paul, I am forever grateful for your guidance and unwavering support. You'll never know how much I have learned from you and how much I appreciate the help you have given me. I also extend my sincerest gratitude to Dr. Merrie Mosedale, who has been instrumental in my development as a scientist and the success of this research. I thank my committee members, Drs. Ilona Jaspers, Mehmet Kesimer, and Nigel Key for their contributions to my research and education. Special thanks to Ilona for your strategic assistance, for taking my phone calls, and for trying to save me from RNA seq.

I have to thank Manda Edwards Miller, Kelly Rose, and Kirsten Wille for teaching me the basics, including how to culture primary hepatocytes. I think of you often and have missed you in the lab. Thank you to Dr. Katie Paul Friedman for your support and assistance over the years. You have always been willing to help and I am so very grateful for that generosity. Dr. Kristina Kathryn Wolf—thank you. I cannot express how much your friendship and advice have helped me through this process. You are an exceptional scientist

and human being. Your commitment, work ethic, and kindness are an inspiration to me. I am grateful for our Moe's trips and hope that they will continue long into the future! To my BFF Allison Stoklosa, thank you for being an amazing and thoughtful individual. Your friendship and support during this journey have meant so much to me. Thanks for always having my back. Above all I have to thank my mother for well, everything. Mom, this degree is as much yours as it is mine. I love you.

TABLE OF CONTENTS

LIST OF TABLES

LIST OF FIGURES

LIST OF ABBREVIATIONS

ALB	Albumin
ALF	Acute liver failure
ALT	Alanine aminotransferase
ANOVA	Analysis of variance
APAP	Acetaminophen
APR	Acute phase response
ATP	Adenosine triphosphate
BMDMϕ	Bone marrow derived macrophages
BMI	Body mass index
CAR	Constitutive androstane receptor
CC14	Carbon tetrachloride
cDNA	Complementary DNA
C_{max}	maximum plasma concentration
CO_2	Carbon dioxide
Ct	Cycle threshold
CYP	Cytochrome P450
D3T	3H-1,2-dithiole-3-thione
DAMP	Damage-associated molecular pattern
DE	Differentially expressed
DGAL	D-(+)-galactosamine
DPBS	Dulbecco's phosphate buffered saline
DILI	Drug-induced liver injury

DMEM	Dulbecco’s modified Eagle’s medium
DMSO	Dimethyl sulfoxide
EM	Electron microscopy
EQ	ExoQuick
EtBr	Ethidium bromide
EtOH	Ethanol
EV	Extracellular vesicle
FBS	Fetal bovine serum
FC	Fold change
FDR	False discovery rate
FXR	Farnesoid X receptor
GSH	Glutathione
H & E	Hematoxylin and eosin
HBV	Hepatitis B virus
HCV	Hepatitis C virus
HDE	Hepatocyte-derived exosome
HDL	High-density lipoprotein
HLA	Human leukocyte antigen
HMGB1	High mobility group box 1
I-DILI	Idiosyncratic drug-induced liver injury
IFN	Interferon
IL-1β	Interleukin-1 beta
IL-6	Interleukin-6

IL-6R	IL-6 receptor
IL-8	Interleukin 8
IPA	Ingenuity pathway analysis
KC	Kupffer cells
LB	Luria Bertani broth
LDH	Lactate dehydrogenase
LDL	Low-density lipoproteins
LPS	Lipopolysaccharide
LXR	Liver X receptor
MTI	miRNA-target interaction
NAC	N-acetylcysteine
NAFLD	Non-alcoholic fatty liver disease
NAPQI	N-acetyl-p-benzoquinone imine
NASH	Non-alcoholic steatohepatitis
NGS	Next-generation sequencing
NK	Natural killer cells
NPC	Non-parenchymal cells
PBS	Phosphate buffered saline
pDC	Plasmacytoid dendritic cells
pDNA	Plasmid DNA
PPP	Platelet-poor plasma
RIN	RNA integrity number
RXR	Retinoid X receptor

SNP	Single nucleotide polymorphism
TLR	Toll-like receptor
TNF-α	Tumor necrosis factor alpha
TNFR	TNF receptor
UC	Ultracentrifugation
WEM	William’s E Medium

CHAPTER 1.

INTRODUCTION

1.1 Overview

Drug-induced liver injury (DILI) is the primary cause of acute liver failure in the United States and Europe (Bernal *et al.*, 2010; Ostapowicz *et al.*, 2002; Wilke *et al.*, 2007). It remains a major problem in drug safety, impacting patients, physicians and the pharmaceutical industry. Many of the most serious clinical DILI reactions are idiosyncratic and poorly understood. To prevent DILI and reduce patient harm, a greater understanding of the pharmacological mechanisms that underlie DILI is needed. Growing evidence suggests that while an initial response begins at the hepatocyte level, communication with the immune system is essential for propagating both dose-dependent (intrinsic) and idiosyncratic DILI (I-DILI) reactions. We hypothesize that extracellular vesicles (EVs) called exosomes carry signals from stressed hepatocytes that modulate these early immune reactions. Exosomes are small (<150 nm) lipid bilayer-bound particles formed and secreted via the endolysosomal pathway as a means of cell-cell communication. Hepatocyte-derived exosomes (HDE) are capable of signaling locally and systemically, as they are small enough to diffuse into the circulation through fenestrations unique to the sinusoidal endothelium. HDE are constitutively released and thus present in biofluids such as plasma under basal conditions, but their abundance and

content are altered in overt DILI (Wetmore *et al.*, 2010). HDE contents include proteins and lipids, but the most well-studied alterations are those of HDE RNAs. The possible mechanisms of exosomal communication are vast, and include antigen presentation, receptor-mediated signaling, and the transfer of functional genetic material such as mRNA and miRNA (McKelvey *et al.*, 2015).

Studies have recently shown that HDE directly regulate innate and adaptive immune cell responses during liver disease. HDE influence adaptive immunity in the content of hepatitis C (HCV) infection (Dreux *et al.*, 2012; Harwood *et al.*, 2016), while models of non-alcoholic steatohepatitis (NASH) and alcoholic liver injury have identified a role for HDE in promoting innate immune cell responses (Hirsova *et al.*, 2016; Kakazu *et al.*, 2015; Momen-Heravi *et al.*, 2015a; Verma *et al.*, 2016). Based on the immunomodulatory activity of HDE in other contexts and the plasticity of their content, **we hypothesize that HDE carry signals of drug-induced hepatocellular stress to the immune system prior to overt hepatotoxicity, and that this communication may ultimately influence the outcome of DILI.**

The field of exosome research is relatively new, and as a result, little has been done to investigate the role of HDE in DILI. The majority of studies have focused on HDE as biomarkers of liver injury. The present research addressed a novel subject and required considerable optimization of methods for HDE analysis. Therefore, it was necessary to select a model hepatotoxic drug with well-defined and reproducible toxicity profiles in rats, rat hepatocytes, and human hepatocytes. To induce hepatocellular stress for the purposes of studying HDE release, the prototypical intrinsic hepatotoxicant acetaminophen (APAP) was selected.

To substantiate the role of HDE in early DILI events, three Specific Aims were pursued. In Aim 1, we sought to establish whether HDE could signal to the immune system prior to overt cytotoxicity by defining alterations in HDE following APAP-induced hepatocellular stress. The effects of APAP on specific RNA content and quantity of HDE were determined *in vivo* and *in vitro* using rats, primary rat hepatocytes, and primary human hepatocytes. Aim 2 incorporated next-generation sequencing techniques for global mRNA and miRNA profiling on primary human HDE to define differential RNA enrichment in APAP HDE across multiple donors. In Aim 3, the immunomodulatory effects of HDE from control- and APAP-treated primary human hepatocytes on THP-1 monocytes were examined by cytokine release and gene expression analysis. Differential gene expression in monocytes was correlated to increases in specific HDE miRNAs in an effort to identify miRNAs that could potentially be responsible for the biological effects of HDE.

These data provide the first report of immunomodulation by primary human HDE and define for the first time their mRNA and miRNA content under control and APAP-stressed conditions. By informing the human relevance of HDE in intrinsic DILI, this work will facilitate evaluation of HDE as a means to predict and explain mechanisms of I-DILI.

1.2 Drug-induced liver injury

DILI is the primary cause of liver failure in the United States and Europe (Bernal *et al.*, 2010; Ostapowicz *et al.*, 2002; Wilke *et al.*, 2007). It is a common adverse effect caused by drugs, due largely to the first-pass metabolism of orally administered compounds and the high metabolic activity of the liver. DILI is categorized as direct or intrinsic when the toxicity is dose-dependent and readily reproduced pre-clinically (Bass and Ockner, 1996). These reactions are often identified early in development and frequently result in abandonment of the drug candidate. However, the most problematic clinically relevant adverse liver reactions are idiosyncratic in nature, occurring on the order of 1 in 10,000 patients taking a drug within the therapeutic range (Fontana, 2014). Symptoms may not manifest for months and may still occur following cessation of treatment (Fontana, 2014). I-DILI reactions are often severe, and may result in liver or multi-organ failure, cerebral edema, and even death (Ostapowicz *et al.*, 2002; Ulrich, 2007). Such rare cases can lead to the withdrawal of approved drugs, making beneficial treatments unavailable to patients. As a result, DILI is responsible for a significant number of pre-and post-market drug failures.

Identification of underlying mechanisms has proved especially difficult as DILI has been associated with hundreds of drugs that elicit a broad spectrum of injuries (Bass and Ockner, 1996; Hussaini and Farrington, 2014). Differential diagnosis is hampered by the fact that DILI patients often remain asymptomatic until injury is extensive, and pathologic presentation of DILI is often indistinguishable from other liver diseases (Bass and Ockner, 1996; FDA CDER, 2009). In order to prevent DILI, a greater understanding of the cellular mechanisms that underlie intrinsic and idiosyncratic DILI is imperative.

1.3 Exosomes and extracellular vesicles

EVs are defined as sub-micron sized membrane-bound particles released from cells both actively and passively under various conditions. EVs were first discovered in 1946 in a study of clotting disorders (Chargaff and West, 1946) and were, for decades to follow, dismissed as cellular debris or "platelet dust" (Siekevitz, 1972; Wolf, 1967). It is not surprising that EVs were discovered in coagulation and platelet studies, because platelets are the most abundant source of circulating EVs in plasma (Aryani and Denecke, 2016). Although once classified as debris, EVs are now recognized as critical participants in intercellular communication. EVs play a role in paracrine and juxtacrine signaling by transporting cell-specific contents including protein, microRNA, and mRNA to recipient cells locally and systemically. EVs are separated into three classes: exosomes, microvesicles, and apoptotic bodies, based upon cellular biogenesis, size, and molecular content (Table 1.1) (Andaloussi *et al.*, 2013; Gyorgy *et al.*, 2011; Raposo and Stoorvogel, 2013). The relatively new field of EV research is plagued with inconsistencies in EV definition and nomenclature. For the purposes of this dissertation, exosomes are defined as small EVs (< 150 nm in diameter) secreted through the endolysosomal pathway that are enriched for proteins involved in formation of multivesicular bodies and exocytosis (Table 1.1). Exosomes are considered the most homogeneous class of EVs based on their size and enrichment profile. Microvesicles are a relatively heterogeneous class of EV that range from approximately 100 to 1,000 nm and are produced by outward blebbing of the plasma membrane (Table 1.1). Lastly, apoptotic bodies are those cellular fractions produced during apoptosis ranging from 1-5 μm and containing organelles as well as DNA (Table 1.1).

Table 1.1 Classes of extracellular vesicles. Approximate size, origin, and enriched molecule data were obtained from multiple publications to present a field consensus (Andaloussi *et al.*, 2013; Gyorgy *et al.*, 2011; Raposo and Stoorvogel, 2013).

EV Class	Approximate Size (nm)	Subcellular Origin	Enriched Markers	Typical Contents
Exosomes	40-150 (relatively homogeneous)	Endolysosomal pathway/multivesicular bodies	Tetraspanins ESCRT components Flotillin	mRNA, microRNA, non-coding RNA, ctyoplasmic and membrane proteins, MHC molecules
Microvesicles	100-1,000 (heterogeneous)	Membrane budding	Integrins External phosphatidylserine	mRNA, microRNA, non-coding RNA, proteins, surface receptors
Apoptotic Bodies	1,000-5,000	Apoptotic cell membrane blebbing	DNA	DNA, subcellular fractions, organelles

In vivo and *in vitro* research demonstrates that EVs are released from most mammalian cell types, including those of the human airway (Kesimer *et al.*, 2009), immune system (Wahlgren *et al.*, 2012), central nervous system (Faure *et al.*, 2006), stem cells (Ratajczak *et al.*, 2006), and tumor cells (Harris *et al.*, 2015). As such, EVs have been detected in virtually all biofluids including blood (Caby *et al.*, 2005), semen (Vojtech *et al.*, 2014), urine (Pisitkun *et al.*, 2004), breast milk (Admyre *et al.*, 2007), saliva (Ogawa *et al.*, 2011), ascites (Andre *et al.*, 2002), amniotic fluid (Asea *et al.*, 2008), bile (Masyuk *et al.*, 2010), bronchoalveolar lavage fluid (Torregrosa Paredes *et al.*, 2012), and cerebrospinal fluid (Vella *et al.*, 2007).

While exosomes and microvesicles are released constitutively, their content is highly regulated by the status of the parent cell. It follows that research has uncovered their ability to mediate myriad physiological and pathological processes, including tissue repair (Gatti *et al.*, 2011), cell fate and phenotype (Aliotta *et al.*, 2007), coagulopathy (Hisada *et al.*, 2016), metastasis (Bigagli *et al.*, 2016), viral transmission (Bukong *et al.*, 2014), and immune function (Dreux *et al.*, 2012). Their biological activity is attributed to receptor-mediated signaling (Taylor *et al.*, 2003), antigen presentation (Raposo *et al.*, 1996), and the ability to horizontally transfer cargo including mRNA and microRNA (Valadi *et al.*, 2007), protein (Ratajczak *et al.*, 2006), viral particles (Izquierdo-Useros *et al.*, 2009), and receptors (Al-Nedawi *et al.*, 2008) to recipient cells via fusion or endocytic mechanisms (McKelvey *et al.*, 2015; Mulcahy *et al.*, 2014) (Figure 1.1). The current research tests the hypothesis that HDE carry signals of drug-induced stress to immune cells, promoting immune response prior to overt cytotoxicity, and that the transfer of exosomal miRNA is in part responsible for these biological effects.

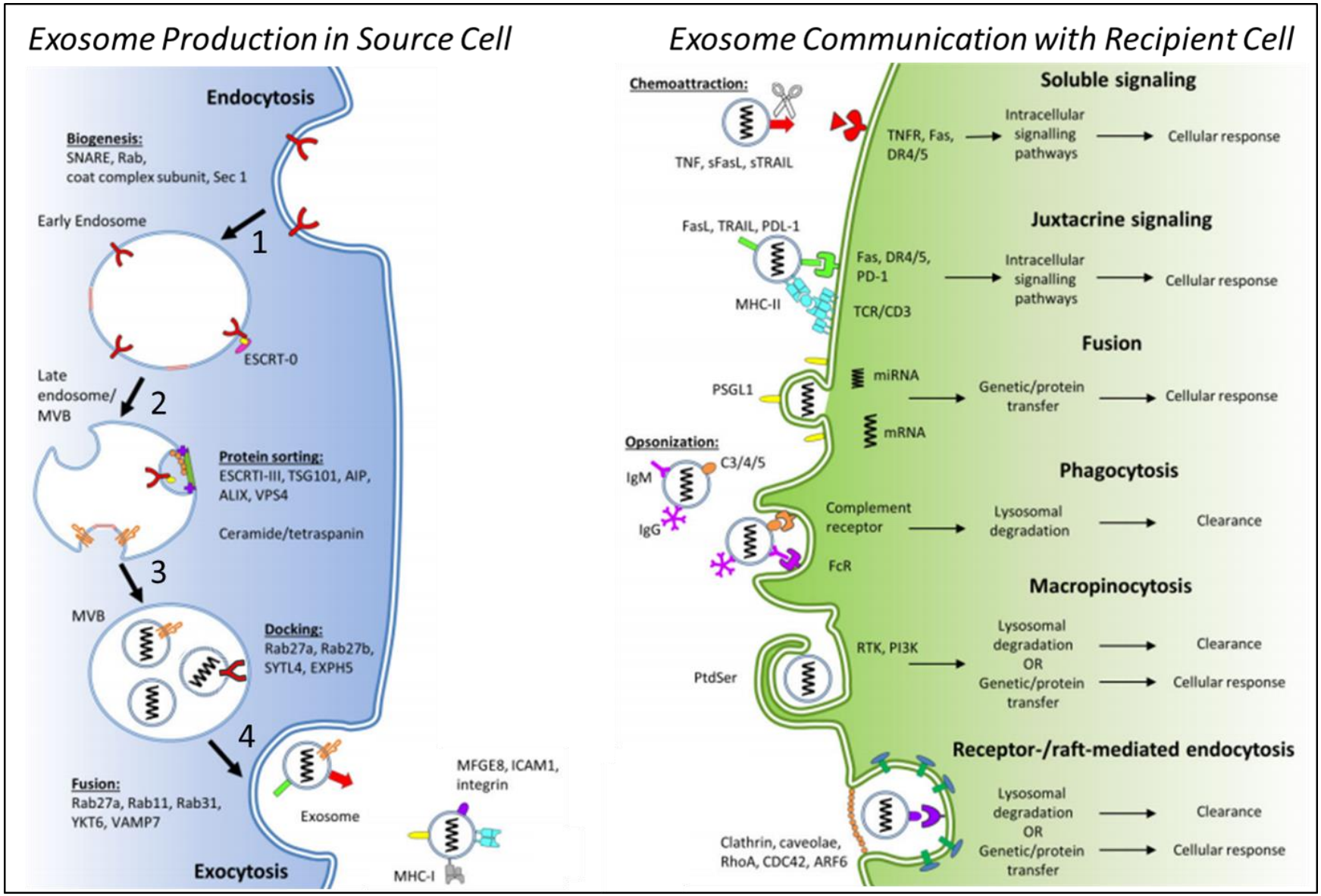
Exosome Production in Source Cell
Endocytosis
Biogenesis:
SNARE, Rab,
coat complex subunit, Sec 1
Early Endosome
1
ESCRT-0
Late
endosome/
MVB
2
Protein sorting:
ESCRTI-III, TSG101, AIP,
ALIX, VPS4
Ceramide/tetraspanin
3
MVB
Docking:
Rab27a, Rab27b,
SYTL4, EXPH5
4
Fusion:
Rab27a, Rab11, Rab31,
YKT6, VAMP7
Exosome
MFGE8, ICAM1,
integrin
MHC-I
Exocytosis
Exosome Communication with Recipient Cell
Chemoattraction:
TNF, sFasL, sTRAIL
Soluble signaling
TNFR, Fas,
DR4/5
Intracellular
signalling
pathways
Cellular response
FasL, TRAIL, PDL-1
MHC-II
TCR/CD3
Juxtacrine signaling
Fas, DR4/5,
PD-1
Intracellular
signalling
pathways
Cellular response
Fusion
PSGL1
miRNA
mRNA
Genetic/protein
transfer
Cellular response
Opsonization:
IgM
C3/4/5
IgG
FcR
Phagocytosis
Complement
receptor
Lysosomal
degradation
Clearance
Macropinocytosis
PtdSer
RTK, PI3K
Lysosomal
degradation
OR
Genetic/protein
transfer
Clearance
Cellular response
Receptor-/raft-mediated endocytosis
Clathrin, caveolae,
RhoA, CDC42, ARF6
Lysosomal
degradation
OR
Genetic/protein
transfer
Clearance
Cellular response

Figure 1.1. Mechanisms of exosome formation and uptake. Exosome biogenesis in source cell (blue) via multivesicular bodies and the endolysosomal pathway. This process can produce exosomes carrying receptors with the same outward orientation as in the plasma membrane. Exosomes can exert biological effects on recipient cells (green) through numerous molecular mechanisms, including endocytosis, fusion, and receptor-mediated signaling. Figure modified from (McKelvey *et al.*, 2015).

1.3.1 Exosomes mediate heterotypic hepatocellular communication

The liver is a structurally complex and physiologically diverse organ comprised of many cell types that fall into 2 categories: parenchymal (hepatocytes) and non-parenchymal cells (NPCs). Hepatic NPCs include sinusoidal endothelial cells (SECs; specialized high-permeability capillary lining), Kupffer cells (KCs; resident macrophages), cholangiocytes (biliary epithelial cells), stellate cells (pericytes), and various stem cell compartments. While much exosome research to date has focused on the biomarker potential of EVs and exosomes in various liver diseases, EVs and exosomes are now recognized as key mediators of interactions between hepatic and extra-hepatic cells. For example, in hepatitis C (HCV) and B (HBV) viral infection, SECs secrete exosomes that impart protective anti-viral activity to hepatocytes (Giugliano *et al.*, 2015; Li *et al.*, 2013). These SEC exosomes also help to control viral replication following interferon (IFN) stimulation. SECs themselves may be activated by stellate cell- and cholangiocyte-derived EVs after bile duct ligation, suggesting a potential role for EVs in the mechanisms of vasculopathy (Witek *et al.*, 2009). In turn, stellate cells are activated by HDE (Royo *et al.*, 2013) and cholangiocyte proliferation is promoted by the heterogeneous population of exosomes in bile (Masyuk *et al.*, 2010). Human adult liver stem cells produce EVs that enhance hepatic regeneration in rats following partial hepatectomy (Herrera *et al.*, 2010) and conversely inhibit growth of the hepatoma cell line HepG2 and ectopic murine tumors (Fonsato *et al.*, 2012).

1.3.2 HDE mediate communication between the liver and immune cells

HDE regulation of immune signaling in non-infectious liver disease has been best studied in models of non-alcoholic steatohepatitis (NASH) and non-alcoholic fatty liver disease (NAFLD). Broadly, these diseases are characterized by lipid-induced hepatocyte

toxicity, chronic inflammation, and compensatory wound healing leading to fibrosis. Evidence suggests that hepatocellular lipotoxicity is mediated by inflammatory signaling which has led to investigation of the link between hepatocyte lipoapoptosis and inflammatory response (Hirsova and Gores, 2015). In a recent study by Hirsova *et al*, murine bone marrow derived macrophages (BMDMϕ) were exposed to EV from mice with or without a high-fat diet as well as EV from mouse hepatocytes with or without toxic lipid treatment. EVs from mice on a high-fat diet and from lipoapoptotic hepatocytes induced expression of the interleukins IL-6 and IL-1β in BMDMϕ relative to control EVs (Hirsova *et al.*, 2016). A similar study found that palmitate exposure caused a mouse hepatocyte cell line to increase the production of ceramide-enriched EVs. These ceramide-loaded EVs chemotactically recruited more BMDMϕ than EVs from control-treated hepatocytes (Kakazu *et al.*, 2015).

Far less research has focused on the role of HDE in xenobiotic-induced liver injury. The most encouraging evidence has been observed in models of alcoholic liver disease. A comparison of the immunomodulatory effects of control- versus ethanol (EtOH)-treated Huh7.5 cells revealed that EtOH EVs synergize with lipopolysaccharide (LPS) to promote increased production of pro-inflammatory mediators tumor necrosis factor alpha (TNF-α), IL-1β, and monocyte chemoattractant protein 1 (MCP-1) in THP-1 monocytes (Momen-Heravi *et al.*, 2015a). To our knowledge, a direct relationship between drug-stressed primary human HDE and monocytes has not been established.

1.4 Immune-mediated DILI mechanisms

Immune responses in DILI are generally believed to initiate the injury (as in adaptive immune attack) or exacerbate existing injury (as with inflammation). A brief description of select canonical immune-mediated DILI reactions is provided below, with a summary in

Figure 1.2. These mechanisms do an excellent job of explaining how serious hepatotoxicity develops. We do not have a sufficient understanding of how the immune system participates in the events that precede fulminant hepatotoxicity, but it is likely that the first interaction between an injured cell and the immune system occurs prior to overt cytotoxicity. In a 2010 review, Adams and colleagues aptly summarized the issue: "…the direct effects of drugs on liver cells may be the initiating event for an immune response, which determines the extent of liver damage" (Adams *et al.*, 2010). **The present research addresses the hypothesis that HDE facilitate that initiating event, forming a connection between drug-stressed hepatocytes and the immune system that ultimately mediates the outcome of DILI.**

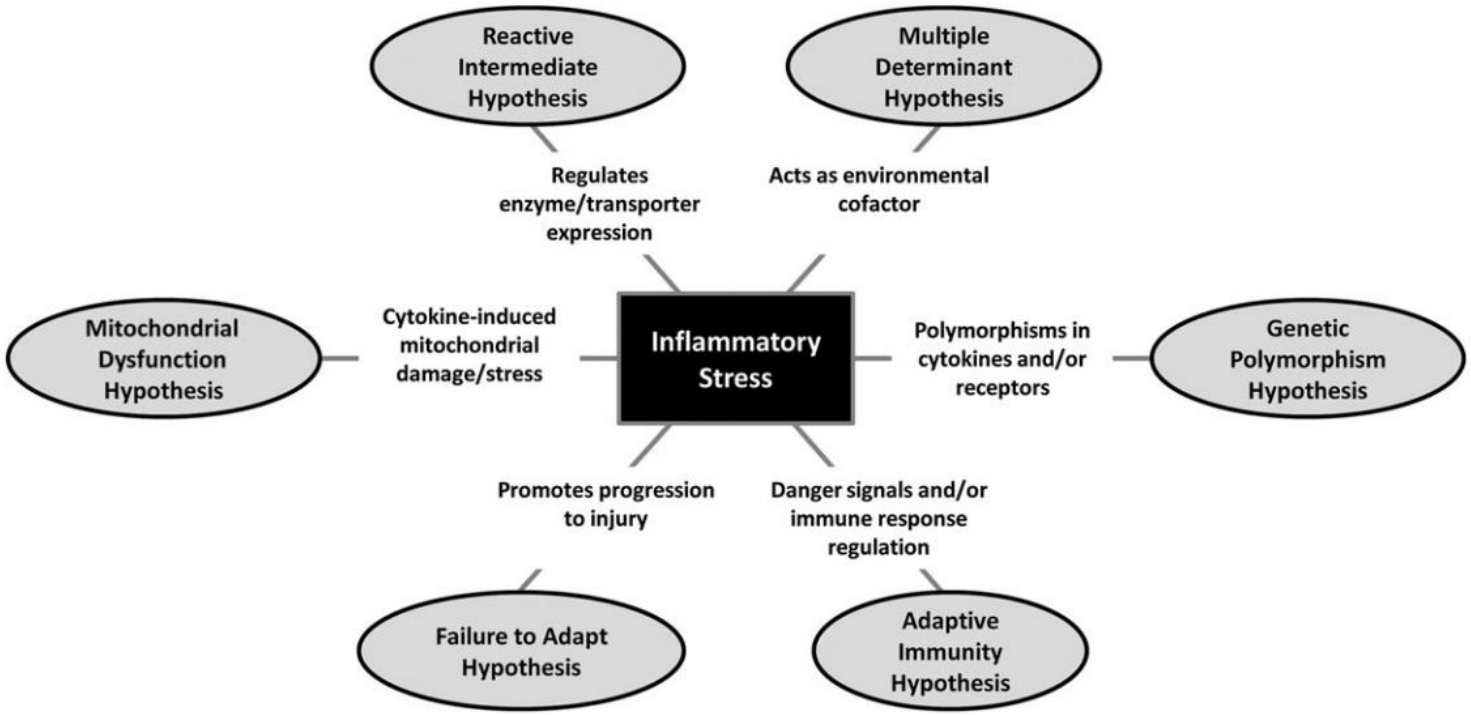

Figure 1.2. The links between inflammatory stress and modern DILI mechanisms. This figure is intended to orient the reader to current opinions regarding the role of inflammation in DILI, but also to highlight the potential downstream consequences of immune mediation by HDE. Reproduced from (Shaw *et al.*, 2010).

Adaptive immune attack

Increasing evidence suggests that intrinsic and idiosyncratic drug-induced hepatocellular death may often be mediated by adaptive immune responses (Adams *et al.*, 2010; Ju and Reilly, 2012; Russmann *et al.*, 2009). For example, human leukocyte antigen (HLA) genotype is a strong risk factor for DILI associated with a wide range of drugs, suggesting a role for the adaptive immune system in drug-mediated hepatotoxicity (Urban *et al.*, 2014). I-DILI may manifest as an adaptive immune attack on the liver as part of an allergic hypersensitivity response. However, it is rare that I-DILI cases present with symptoms indicative of allergic reactions such as rash, fever, and eosinophilia (Andrade *et al.*, 2005). As such, evidence of an adaptive immune I-DILI reaction may not be obtained until the patient recovers following treatment cessation and a "rechallenge" can be performed. In a rechallenge, the patient is re-exposed to the implicated I-DILI drug and monitored closely for signs of hepatotoxicity and a secondary immune reaction, known as a positive rechallenge (Tujios and Fontana, 2011). Typically, liver injury reappears quickly, which is consistent with adaptive immune memory. However, not all I-DILI events show recurrent injury upon rechallenge. It is difficult to determine whether negative rechallenge results are due to the lack of an adaptive immune mechanism, or whether these results indicate that some form of immune adaptation has occurred between the first drug regimen and rechallenge (Hunt, 2010; Tahaoglu *et al.*, 2001; Tujios and Fontana, 2011). For these reasons, earlier indicators of immune system involvement in DILI are needed.

Reactive metabolite formation and the hapten hypothesis

The liver's capacity to process xenobiotics and many endogenous substances is based largely on high levels of phase I oxidative metabolic enzymes which are designed to yield reactive metabolites for phase II conjugation and subsequent elimination. Many hepatotoxic drugs are bioactivated by phase I enzymes such as cytochrome P450s (CYPs) to produce highly reactive drug metabolites (Kaplowitz, 2005; Uetrecht, 2008). In fact, 62% of I-DILI drugs have been associated with reactive metabolites (Walgren *et al.*, 2005). These metabolites are electrophiles or free radicals that may bind to cellular targets before phase II enzymes can stabilize them. Consequences include glutathione depletion, covalent protein or DNA adduct formation, and redox-cycling to generate excess reactive oxygen species (Han *et al.*, 2006; Hanawa *et al.*, 2008; Jollow *et al.*, 1973; Kaplowitz, 2005). When reactive metabolites bind to mitochondrial proteins, the result can be electron transport chain interference or membrane permeability transition, resulting in adenosine triphosphate (ATP) depletion. It is believed that drug or metabolite protein binding may promote immune activation. While the molecular mechanisms that underlie this relationship are unclear, a popular hypothesis is that binding of a drug or its metabolite to hepatic proteins leads to formation of new antigens called haptens. These "neoantigens" or haptens may be presented on cell surface HLA molecules and recognized as foreign by adaptive immune cells. However, this process alone is often insufficient to cause an attack on the liver; it is believed that immune cell activation is also required to produce co-stimulatory signals and chemokines which recruit adaptive immune cells to the liver.

Inflammation and innate immunity

DILI is often accompanied by elevations in biomarkers that trigger an innate immune response such as high mobility group box 1 (HMGB1), and those that are suggestive of immune cell activation including miR-155 and acetylated HMGB1 (Antoine *et al.*, 2014; Bala *et al.*, 2012; Fontana, 2014). Intrinsic DILI often involves an immune cascade that follows overt cytotoxicity, as is the case with APAP. In APAP DILI, it is believed that infiltrating monocytes and resident liver macrophages (KCs) are stimulated by hepatocellular necrosis to produce pro-inflammatory cytokines. These cytokines may themselves be sufficient to exacerbate hepatocyte injury (Maiuri *et al.*, 2015; Shaw *et al.*, 2010), and such mechanisms are best modeled in a dynamic co-culture environment (Rose *et al.*, 2016) (Appendix). Cytokines and chemokines in turn recruit additional immune cells (*i.e.* neutrophils, lymphocytes, NK cells, monocytes), thus forming a link to the adaptive immune system. Whether immune cell recruitment promotes enhanced inflammation or encourages regeneration is dependent upon many factors including the tissue microenvironment. For example, infiltrating monocytes may differentiate into pro-inflammatory dendritic cells or reparative monocyte-derived macrophages (Shi and Pamer, 2011; Zigmond *et al.*, 2014).

1.5 Acetaminophen

To stimulate and characterize sub-toxic HDE release, this research utilized the prototypical intrinsic hepatotoxicant N-acetyl-*p*-aminophenol (APAP). While the ultimate application of this research is to understand the role of HDE in mediating immune responses in I-DILI, it was necessary to first substantiate our hypothesis using a drug with well-defined mechanisms and established toxicity profiles across multiple experimental platforms.

APAP is an analgesic and antipyretic that has been in use since the 1800's (Hinson *et al.*, 2010). It is the active ingredient in Tylenol® and has become a ubiquitous additive in hundreds of over-the-counter and prescription medications for allergies, pain, cold, flu, cough, and fatigue (FDA, 2016). As a result, many consumers receive APAP in multiple products at once, but if taken appropriately, as 95% of consumers do, APAP is considered an extremely safe drug (Kaufman *et al.*, 2012).

APAP-induced liver injury was first reported in 1966 (Davidson and Eastham, 1966) and is now a widespread concern as a growing number of patients intentionally or accidentally exceed the maximum daily dose of 4 g APAP (CHPA, 2014). While there are known susceptibility factors including alcohol use (Larson *et al.*, 2005) and genetic polymorphisms (Harrill *et al.*, 2009b), APAP is a prototypical dose-dependent toxicant and can cause DILI in anyone who ingests a high enough dose. In fact, APAP overdose is responsible for 80,000 emergency room visits and hospitalizations annually (Serper *et al.*, 2016). It follows that APAP is the leading cause of acute liver failure in the United States (Larson *et al.*, 2005).

APAP, ingested orally, is quickly absorbed in the gut and reaches maximum plasma concentration (C_{max}) within 1.5 h (Hodgman and Garrard, 2012). The drug is subject to hepatic first-pass metabolism and is mostly glucuronidated or sulfated by phase II detoxifying enzymes in humans (Mazaleuskaya *et al.*, 2015). A fraction of APAP is metabolized by CYP enzymes including CYP3A4, CYP2E1, CYP1A2, and CYP2D6 (Laine *et al.*, 2009). The principal CYP enzymes involved vary depending on APAP dose, but CYP34 and CYP2E1 are generally considered the primary metabolizers of APAP in humans. The CYPs oxidize APAP in a process that bioactivates it to a toxic intermediate known as N-

acetyl-p-benzoquinone imine (NAPQI) (Hinson *et al.*, 2010). NAPQI is highly reactive and is neutralized by binding to glutathione (GSH) under normal conditions (Jollow *et al.*, 1974). At intermediate and high APAP doses, the sulfation and glucuronidation pathways, respectively, become saturated (Mazaleuskaya *et al.*, 2015). When these processes are overwhelmed, greater proportions of APAP are available for CYP bioactivation, leading to increased production of the toxic metabolite, NAPQI. Eventually GSH stores are exhausted and NAPQI is free to bind cellular macromolecules, including those critical for energy production, leading to oxidative stress and impaired homeostasis that result in cytotoxicity (Bessems and Vermeulen, 2001; James *et al.*, 2003; Prescott, 1981). APAP exhibits a centrilobular zonal toxicity, which can be explained by the higher CYP2E1 expression and smaller stores of GSH in centrilobular hepatocytes (Jaeschke, 2008). The most effective treatment for APAP overdose, N-acetylcysteine (NAC), works by restoring GSH levels and is highly efficient if administered 8-10 h following overdose (Prescott, 1981). APAP also causes kidney injury via similar bioactivation mechanisms.

The severity of APAP DILI is linked to innate immune activation in rodent models and humans, but there is significant conflict regarding whether immune activity is deleterious or advantageous. Evidence for the benefit of innate immune cells in APAP DILI includes mechanistic findings that these cells support resolution or, at best, do not actively promote toxicity. For instance, mice treated with the KC depleting compound clodronate showed lower IL-6 and IL-10 gene expression, which was associated with enhanced APAP susceptibility (Ju *et al.*, 2002). Similarly, humans with APAP-induced liver failure have high concentrations of proliferating KCs at sites of hepatic regeneration (Antoniades *et al.*, 2012; Widmann and Fahimi, 1975). Despite increased KC activity, anti-inflammatory cytokines

predominated, suggesting that KC activation was not patently detrimental following APAP overdose. Another mouse model of APAP injury showed that monocytes infiltrating the liver negatively regulated neutrophil activation while supporting tissue regeneration and angiogenesis (Zigmond *et al.*, 2014). Recruited monocytes have also been shown to differentiate into hepatic macrophages that assist in clearing dead cells and promoting the pro-restorative activity of neutrophils (Holt *et al.*, 2008). With regard to neutrophils, mouse and human APAP overdose cases show sustained neutrophil activation in the aftermath of acute injury, suggesting that these cells were not actively promoting the toxicity (Williams *et al.*, 2014). In contrast, other reports indicate that immune cell infiltration is associated with increased APAP hepatotoxicity. In liver-specific HMGB1 knockout mice, neutrophil accumulation was positively correlated with enhanced liver injury (Huebener *et al.*, 2015). In an MCP-1 receptor (CCL2R) knockout mouse model, monocyte recruitment to the liver corresponded to increased APAP DILI (Mossanen *et al.*, 2016). It is important to note, however, that these results were observed in models of APAP overdose, leaving the role of innate immunity in early stages of injury largely unknown.

The current research does not address the beneficial or detrimental nature of immune activation in APAP DILI. Here, APAP is used to stress hepatocytes for the purpose of studying sub-toxic HDE responses; the mechanisms of APAP overdose are not the focus of these investigations. Recent evidence suggests that immune responses after sub-toxic APAP exposure manifest prior to overt hepatocellular injury in healthy volunteers (Fannin *et al.*, 2015), a process that we believe likely involves the release of hepatocellular stress signals contained in HDE.

1.6 Summary and dissertation content

The purpose of the current research was to characterize the role of HDE in directly mediating early immune events in DILI (Figure 1.3). When we began this work, a single method to generate HDE from rat hepatocytes had been published and the number of hepatocytes required was prohibitively high (Conde-Vancells *et al.*, 2008; Royo *et al.*, 2013). There were no reports on the isolation, content, or function of HDE from primary human hepatocytes. Therefore, it was necessary to develop fit-for-purpose methods for the harvest and analysis of HDE from primary rat and human hepatocytes. In Chapter 2, HDE enrichment and RNA content analysis techniques were extensively validated and optimized. Using these methods, we evaluated the kinetics of APAP-induced HDE release to assess the likelihood that HDE were altered before overt hepatocellular death. In Chapter 3, translationally relevant sub-toxic HDE alterations were observed following APAP exposure in rats, primary rat hepatocytes, and primary human hepatocytes (Aim 1). These results confirmed that HDE content is affected by drug-induced stress in both species, and may serve as a signaling mechanism to immune cells prior to the onset of hepatocyte death. We provide novel evidence of HDE alterations in the absence of overt APAP-induced toxicity. Also presented is the first characterization of baseline mRNA levels in primary human HDE, which may be related to body mass index (BMI). We then applied next-generation sequencing techniques to comprehensively profile the mRNA and miRNA content of HDE from control- and APAP-treated primary human hepatocytes (n=5) (Aim 2). HDE from the same hepatocytes were incubated with THP-1 human monocytes to address the hypothesis that exosomes from drug-stressed hepatocytes are capable of immunomodulation in the absence of toxicity (Aim 3). Gene expression profiling of THP-1 monocytes revealed that

exposure to APAP HDE altered genes related to cholesterol metabolism and lipid homeostasis. Cytokine release from monocytes exposed to HDE and then stimulated with LPS revealed differences in the effects of control HDE and APAP HDE. HDE from control-treated human hepatocytes suppressed LPS-induced cytokine secretion. However, APAP HDE did not demonstrate cytokine suppression, perhaps suggesting monocyte predisposition to LPS activation. Many of the significant differentially expressed genes in APAP HDE-treated monocytes have been associated with increased pro-inflammatory mediator production in the literature, and may explain this effect. In addition, genes involved in immune cell trafficking and lymphoid development were also differentially expressed as a result of APAP HDE. The findings of Aims 2 and 3 are presented in Chapter 4, including the correlation of exosomal miRNA content with the biological effects of HDE. We observed biologically plausible associations between the miRNAs differentially enriched in APAP HDE and down-regulation of their target genes in monocytes treated with APAP HDE. These observations support the hypothesis that HDE may transfer miRNAs that are potentially responsible for pro-inflammatory priming effects of APAP HDE on immune cells. Conclusions, limitations, and future directions of this work are discussed in Chapter 5.

In summary, this research highlights HDE as a critical means of communication between hepatocytes and immune cells following drug-induced hepatocellular stress. These findings validate application of the approaches developed here to understanding the role of HDE in I-DILI. We have shown:

1. *The liver-specific RNA contents of HDE in rat and human model systems are altered prior to overt hepatotoxicity*

2. *Global mRNA and miRNA profiles within primary human HDE are altered in response to drug-induced stress and may reflect changes in hepatocyte gene expression*

3. *Primary human HDE from control- and APAP-treated hepatocytes directly influence monocyte gene expression and subsequent cytokine response to LPS, which may ultimately result in modulation of DILI*

4. *Delivery of specific miRNA via HDE may be responsible for the immunomodulatory activity of HDE, including sensitization of monocytes to inflammatory stimuli*

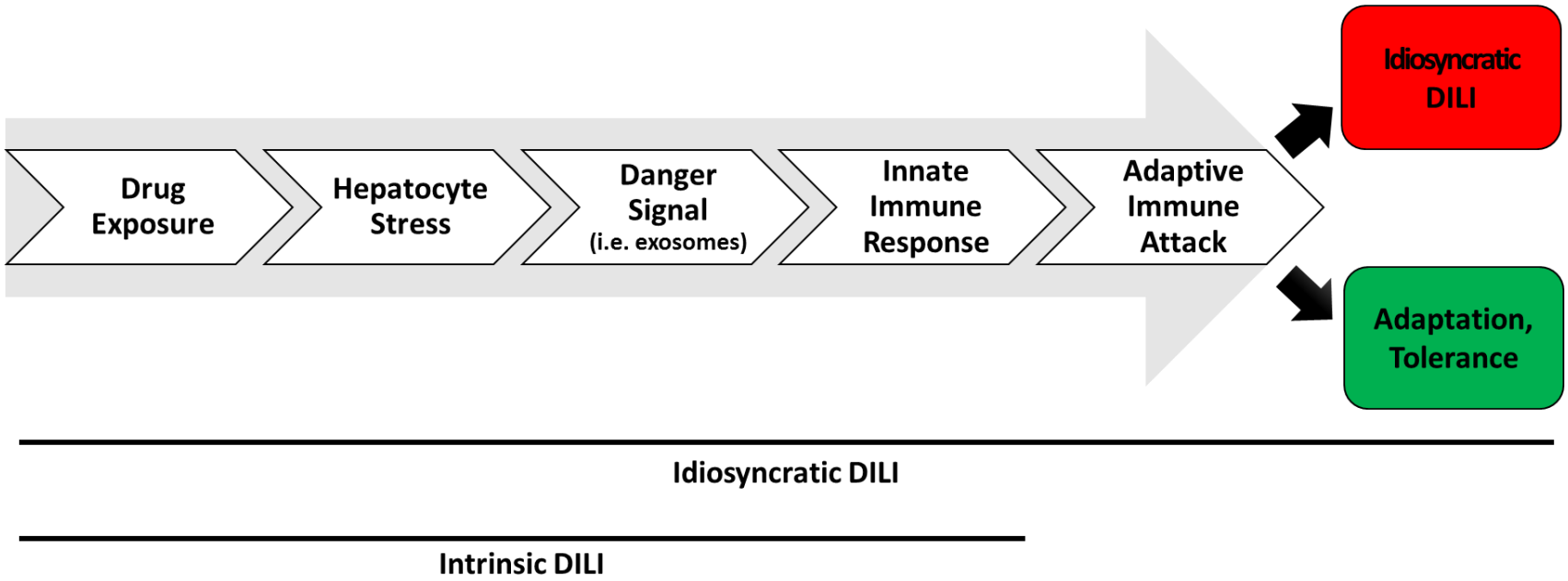

Figure 1.3. Schematic representation of the current hypothesis. Hepatocyte stress may be communicated to the immune system in the absence of cytotoxicity via danger signals such as HDE. The immune response to HDE may ultimately impact the outcome or extent of DILI. We believe that the process of early HDE-mediated interactions with the immune system is conserved across DILI mechanisms and types.

CHAPTER 2.

OPTIMIZATION OF METHODS FOR THE STUDY OF PRIMARY HEPATOCYTE-DERIVED EXOSOMES

2.1 Introduction

In the last decade, extracellular vesicles (EVs) have received enormous attention in the research community for their value as mechanistic mediators, biomarkers, drug delivery vehicles, and drug targets. It follows that methods of EV analysis continue to evolve at a rapid pace, and due to the infancy of this field, no standardized methods exist. In such a new and emerging field, the means by which EVs like exosomes are isolated and studied is widely regarded, even among professional EV-focused societies, as specific to the goal of the research (Witwer *et al.*, 2013). This chapter describes the optimization and validation of project-specific methods for the study of exosomes released by primary rat and human hepatocytes.

To date, the two most widely used methods for exosome isolation are ultracentrifugation (UC) and polymer precipitation. Alternative methods include size-exclusion column chromatography and immuno-affinity isolation including modified flow cytometry protocols and immunoprecipitation (Taylor and Shah, 2015). Most protocols introduce some form of size-exclusion either by filtration or other means. Many methods are a hybrid of two or more approaches.

It is important to note that while the term "isolation" is commonly employed, no currently available technique offers complete separation and purification of different vesicle types. All methods use either size or molecular markers to separate exosomes from other vesicles, but size, buoyant density, content, and exterior molecular tags may overlap across classes (Witwer *et al.*, 2013). To be technically correct, current approaches may "enrich" for exosomes, but cannot fully isolate them.

The selection of an enrichment method also influences the outcome of downstream analyses including microRNA, mRNA, and protein profiles (Alvarez *et al.*, 2012; Taylor and Shah, 2015; Taylor *et al.*, 2011; Van Deun *et al.*, 2014). Therefore, method(s) must be validated for each new research inquiry, cell type, sample source, and endpoint.

Ultracentrifugation (UC)

UC utilizes differential sedimentation and high speed (100,000-120,000 x *g*) centrifugation to enrich for the smallest class of EVs. While sequential spins may improve separation, UC is subject to several limitations. For instance, sedimentation is influenced by particle density, which is not consistent across exosomes. UC will also pellet contaminants such as protein aggregates and lipoproteins (Witwer *et al.*, 2013; Yuana *et al.*, 2014). In addition, aggregation-prone EVs may form larger complexes that could be removed erroneously in the supernatant (Witwer *et al.*, 2013).

Gradient-based UC or "buoyant velocity separation" is the most time consuming and technically challenging protocol; however, it is considered very stringent and is often employed as a means of "cleaning up" preparations produced by other methods (Witwer *et al.*, 2013). Unfortunately, this approach is low-throughput and results in vastly decreased

exosomal protein and RNA yields relative to polymer precipitation or UC without a density gradient (Van Deun *et al.*, 2014). While the addition of a density gradient does separate a number of contaminants, particles with the same density as EVs, such as high-density lipoproteins (HDL), which also carry RNA, will segregate with EVs (Vickers *et al.*, 2011; Witwer *et al.*, 2013). The EV product of gradient-based UC is heavily influenced by such details as tube length, rotor type, speed, and centrifugation time, making it the least replicable approach (Cvjetkovic *et al.*, 2014; Witwer *et al.*, 2013).

Polymer precipitation

Commercially available polymer precipitation reagents such as ExoQuick™ (SBI) or the Total Exosome Isolation Kit (Thermo Fisher) can be used on culture medium, urine, plasma, serum, and other biofluids. Once samples are cleared of cellular debris, the reagent is added for an incubation period ranging from 30 min to 24 h, depending on sample type and precipitation kit. The reagent's polymers form a mesh-like network that traps exosome-sized vesicles while leaving larger particles in solution. This exosome "trapping" facilitates precipitation of an exosome pellet with relatively low centrifugal forces (System Biosciences, 2013). While polymer precipitation does not require laborious sample handling, it may co-precipitate non-exosomal material as with most other methods. Exosomes isolated by ExoQuick-TC™ (EQ), the version of ExoQuick™ (SBI) designed for tissue culture supernatants, demonstrate biological activity (Kaur *et al.*, 2014; Koeck *et al.*, 2014) and functional RNA transfer (Giugliano *et al.*, 2015; Momen-Heravi *et al.*, 2015a). Therefore, this method represents a reliable, fast, and non-destructive technique for exosome enrichment and downstream functional studies.

2.2 Exosome enrichment method validation

2.2.1 Initial proof of concept for studying primary human hepatocyte-derived exosomes (HDE)

At the time this work was initiated, no group had published research on primary human HDE. A handful of studies had been conducted using primary rat hepatocytes (Conde-Vancells *et al.*, 2008; Royo *et al.*, 2013), but the majority of hepatic exosome research employed hepatocyte-like cell lines. The paucity of manuscripts addressing primary HDE was likely due to the difficulty of culturing primary hepatocytes and the availability of primary human hepatocytes. As an initial proof of concept, we sought to empirically determine whether HDE could be detected in the media supernatant of primary human hepatocytes cultured on a small scale relative to primary rat hepatocyte studies (Royo *et al.*, 2013).

Freshly isolated primary human hepatocytes were obtained from Triangle Research Labs (Research Triangle Park, NC). Hepatocytes were cultured on a rigid collagen I substratum in 6-well plates (Corning) at 1.5e6 or 2.25e6 cells per well. Given that primary human hepatocytes had not yet been utilized for exosomal RNA experiments, the cell and medium requirements to achieve sufficient exosome material by UC were not known. To induce stress and promote exosome accumulation, cultures were starved for 120 h following a 24 h acclimation period. Media samples were collected from single wells of 1.5e6 hepatocytes, single wells of 2.25e6 hepatocytes, and two wells of 1.5e6 hepatocytes pooled (3e6 cells total). Exosomes were isolated from cell culture medium using UC. Cell debris was removed by clarification at 1,300 x *g* for 10 min at 4 ºC. The resulting supernatant was transferred to a new tube and clarified at 16,000 x *g* for 10 min at 4 ºC to remove large

microparticles. Supernatants were transferred to autoclaved polycarbonate ultracentrifuge tubes (Beckman) and balanced with sterile phosphate-buffered saline (PBS) (Gibco). Exosomes were enriched by centrifugation at 100,000 x *g* for 60 min at 4 ºC. The pellet was washed with PBS and centrifuged again under the same conditions as described previously (Taylor *et al.*, 2011).

Immediately following UC, RNA was isolated from exosomes using the miRCURY Cell & Plant RNA Isolation Kit (Exiqon), which was selected for its superior performance in isolating high quality microRNA and mRNA from exosomes (Eldh *et al.*, 2012). The manufacturer's protocol for mammalian cells was followed. Total RNA concentration was analyzed using a NanoDrop 1000 spectrophotometer (Thermo). Exosomal RNA yield was compared across hepatocyte densities (Figure 2.1). Results confirmed that UC-based enrichment of primary human HDE produces detectable quantities of RNA, and that there is a linear relationship between exosomal RNA quantity and the number of hepatocytes producing exosomes *in vitro*.

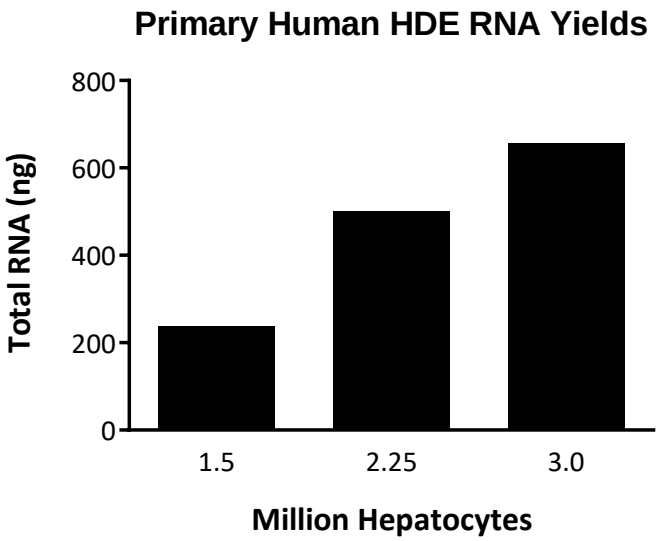

Figure 2.1. Human hepatocyte-derived exosomes isolated by ultracentrifugation on a small scale contain detectable quantities of RNA that are proportionate to the number of cultured hepatocytes. Data were collected from exosomes produced by primary human hepatocytes cultured without media change for 120 h to stimulate cell stress and exosome accumulation.

With the knowledge that EQ-based polymer precipitation usually produces higher quantities of exosomal RNA than UC (Pisitkun *et al.*, 2004; Taylor *et al.*, 2011), we were confident using EQ for the study of primary human HDE going forward. Using EQ, we were able to detect highly abundant exosomal RNAs such as albumin mRNA and miR-122, in HDE from as little as 1 ml of primary human hepatocyte culture supernatant (data not shown). When performing experiments for publication (Chapter 3), the optimal media volume for HDE enrichment was determined to be 2 ml.

2.2.2 Enrichment method comparison using primary rat HDE

Freshly isolated primary male Sprague-Dawley rat hepatocytes were obtained from The Hamner Institutes for Health Sciences (Research Triangle Park, NC). Hepatocytes were cultured on a rigid collagen I substratum in 6-well plates (Corning) at 1.5e6 cells per well. Following a 24 h acclimation period and second media change, media was not replaced for 120 h to promote stress-related exosome release and accumulation. Cell starvation was intentional in order to maximize the release of exosomes, as this experimental design represented a 10-20-fold reduction in rat hepatocytes relative to previously published exosome studies (Royo *et al.*, 2013). Media samples were collected from single wells of 1.5e6 hepatocytes and two pooled wells of 1.5e6 hepatocytes per well. Exosomes were isolated from equal volumes of cell culture medium (2 ml from 1.5e6 cells and 4 ml from 3e6 cells) using UC or EQ polymer precipitation. UC was performed as previously described, using UC tubes treated with RNase inhibitor to reduce RNA degradation. Polymer precipitation samples were prepared using EQ reagent according to the manufacturer's instructions for cell culture supernatant, with an overnight incubation.

Immediately following enrichment, exosome pellets were processed for RNA or protein yield. Exosomal RNA from both methods was isolated and quantified according to hepatocellular input as previously described. Aliquots of RNA were converted to complementary DNA (cDNA) for quantitative real-time polymerase chain reaction (qRT-PCR) analysis using a High Capacity cDNA Reverse Transcription Kit (Applied Biosytems) according to the manufacturer's instructions, using equal volumes of exosomal RNA across samples (Eldh *et al.*, 2012). RT-PCR was performed on a 7900HT Fast RT-PCR System (Applied Biosystems) using the rat albumin TaqMan Gene Expression Assay (Rn00592480_m1) and Fast Advanced Master Mix. Absolute quantities of mRNAs were calculated using a rat albumin cDNA standard curve generated from bacterial plasmids.

Exosomal protein was extracted from exosomes by lysis with RIPA Lysis and Extraction buffer with protease inhibitors (Thermo). Samples were mixed thoroughly and incubated at 4 ºC for 30 min with agitation. Following lysis, protein was separated from nucleic acids by centrifugation at 10,000 x *g* for 2 min at 4 ºC. Supernatants were stored at -80 ºC until protein quantification with a BCA Protein Assay Kit (Thermo) according to the manufacturer's instructions.

Across all endpoints, EQ enrichment produced higher yields of exosomal protein, RNA, and albumin (Figure 2.2). These metrics of exosomal material increased with hepatocyte density in the EQ preparations while total RNA, protein, and albumin copy number in HDE enriched by UC did not increase with cell number. From this work, we determined that EQ is a reliable means of exosome enrichment from primary rat hepatocytes cultured on a small scale.

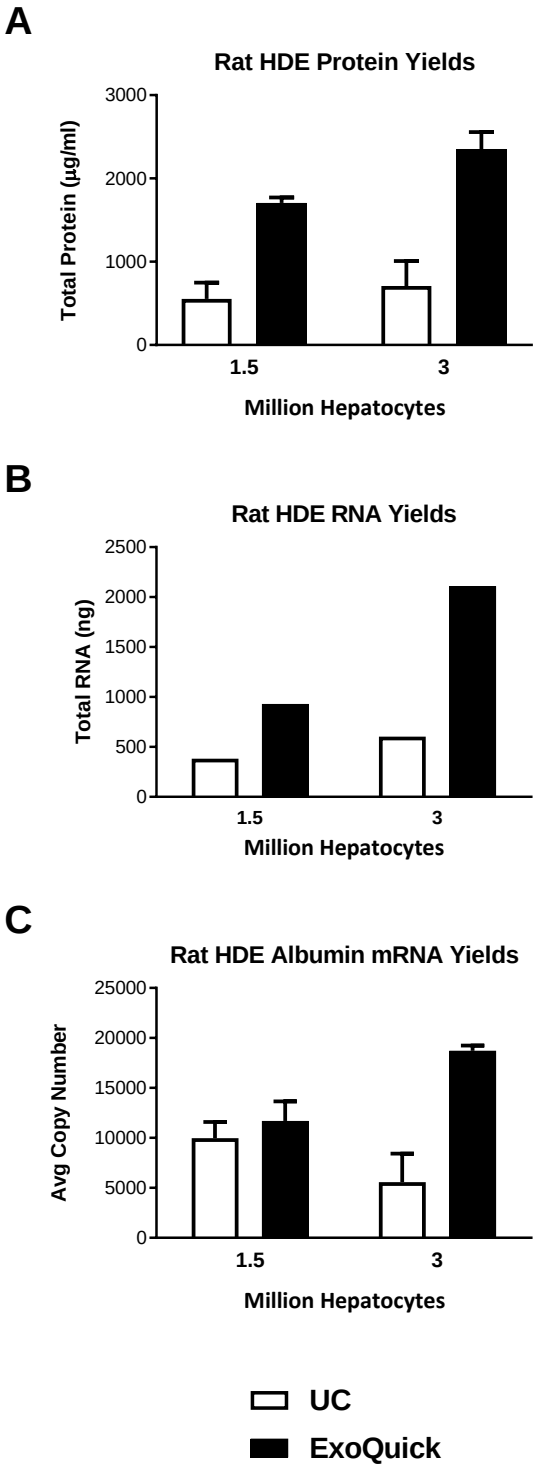

Figure 2.2. ExoQuick-TC precipitation produces superior exosome yields relative to ultracentrifugation. Comparison of total exosomal protein (A), RNA (B), and albumin copy number (C) between exosomes isolated from equal volumes of rat hepatocyte conditioned medium.

2.2.3 Enrichment method comparison using rat plasma

The purpose of this work was to select an appropriate exosome enrichment method for future processing of *in vivo* samples. When isolating exosomes from biofluids such as blood, there are arguably more variables to be aware of that can influence exosome status and therefore data quality. For instance, thought must be given to the type of anticoagulant and the gauge of needle used for blood collection. EDTA is largely preferred as an anticoagulant over heparin because it interferes less with downstream PCR reactions, including qRT-PCR on both mRNA and microRNA (Beutler *et al.*, 1990; Johnson *et al.*, 2003; Kim *et al.*, 2012). Interference with RNA content analysis is a critical consideration when handling small quantities of RNA such as those within EVs. Similarly, care must be taken to avoid shear forces when collecting blood by using a large-bore needle. This consideration is driven by platelets and their sensitivity to activation, as platelet activation induced by handling may result in massive EV release and skewing of the true EV population within a sample (Witwer *et al.*, 2013).

Whole blood was collected from adult male, Sprague-Dawley rats following euthanasia by CO_2 inhalation and subsequent exsanguination. Blood was collected by cardiac puncture with an 18-gauge needle and transferred to K_2EDTA Vacutainer tubes (Beckton Dickinson). The anticoagulant and needle gauge were selected to minimize platelet activation according to previously published methods used to study liver-derived EVs (Brodsky *et al.*, 2008). Tubes were immediately inverted and incubated for 5 min on ice prior to plasma isolation by centrifugation at 1,300 x *g* for 10 min at 4 ºC. To generate platelet-poor plasma (PPP), the resulting supernatant was centrifuged at 16,000 x *g* for 10 min at 4 ºC, conditions which represent a harmonization of previously published methods

(Cattaneo *et al.*, 2007; Yuana *et al.*, 2011). Supernatants were removed and separated into 250 µl aliquots for exosome enrichment by UC or EQ precipitation. UC was conducted as described previously. Polymer precipitation was carried out using EQ reagent according to the manufacturer's protocol for serum. Albumin mRNA copy number analysis and protein isolation were performed on exosomes as described prevoiusly.

From the same volume of plasma, exosomes prepared via EQ have a higher protein concentration compared to exosomes from UC (Figure 2.3). However, the copies of albumin mRNA detected by qRT-PCR were similar across methods (Figure 2.3). Albumin mRNA quantity is often used to approximate HDE number, and if this assumption is made, these qPCR data may indicate that UC and EQ enrichment produce a similar exosome yield. If true, this finding would indicate that the higher protein concentration observed with EQ was due to extra-exosomal protein precipitation. However, following incubation with EQ, the plasma exosome pellet could not be fully resuspended due to dense, insoluble material in the tube. Further investigation revealed that the insoluble material was likely fibrin protein aggregates, and that plasma should be pre-treated with thrombin to defibrinate, producing a more "serum-like" form that is compatible with EQ (System Biosciences, 2013). Given that exosomal protein concentration and albumin copy number showed similar trends *in vitro* (Figure 2.2), we hypothesize that the addition of thrombin to the EQ plasma samples would likely have increased the albumin mRNA yields, and that this method is suitable for future *in vivo* studies (Chapter 3).

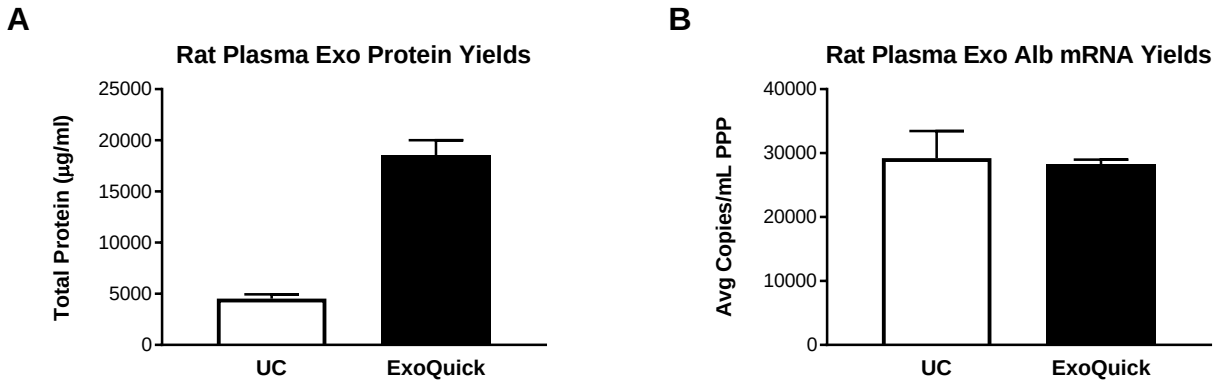

Figure 2.3. Plasma-derived exosome enrichment by ultracentrifugation and ExoQuick. By exosomal protein (A), EQ produces more material but, by qRT-PCR for the HDE marker albumin (B), no difference was observed.

2.3 Methods for exosomal RNA isolation and analysis

2.3.1 RNA elution volume

Given that our experiments utilize a significantly reduced culture medium input to generate HDE, a primary concern was the yield and quality of exosomal RNA that could be isolated for analysis. Based on a rigorous comparison of exosomal RNA isolation kits, the miRCURY™ Cell & Plant kit (Exiqon) was selected as it produces the highest exosomal RNA yield, wide size distribution (allowing for enrichment of miRNA), and sufficient quality for qPCR analysis (Eldh *et al.*, 2012). In their work, Eldh and colleagues isolated exosomes from a large volume of cell culture supernatant (85 ml) and obtained an average of 11 µg exosomal RNA from all methods. Using 1-2 ml of primary hepatocyte culture supernatant, we obtain 0.2-1 µg exosomal RNA eluting in the same volume (50 µl). To increase the concentration of exosomal RNA for downstream analysis, we examined the effect of decreasing the elution volume using the miRCURY kit.

We validated this method modification by preparing 9 samples of 2e6 fresh primary human hepatocytes from the same donor. The isolation process was the same for all samples and was conducted according to the manufacturer's instructions. At the elution step, samples were separated into 3 groups: single 50 µl elution, single 25 µl elution, and a group in which 12.5 µl of elution buffer was added to the column and eluted (n=3/group). For the 12.5 µl group, a second aliquot of 12.5 µl was added to the column and eluted into the same tube, resulting in a final volume of 25 µl. This condition was included to examine whether washing of the column increased or decreased total yield. The concentration of RNA in each sample was measured in triplicate on a NanoDrop 1000 spectrophotometer.

The concentration of RNA eluted in 50 µl was roughly half that of the samples eluted in 25 µl, with a yield of 36.9 and 35.5 µg, respectively. The lack of significant difference ($p = 0.76$ by Student's t-test) between the yield in these samples indicates that eluting in 25 µl was a viable option to concentrate RNA without loss of yield. However, samples generated by two consecutive 12.5 µl elutions had highly variable RNA yields (17.5 ± 7.7 µg) that were lower than a single 25 µl elution, likely because such a small volume cannot adequately or reliably saturate the surface area of the column. Exosomal RNA was eluted in a single aliquot of 25 µl for all remaining miRCURY kit isolations.

2.3.2 Exosome-specific optimization of qRT-PCR

A common challenge for exosome researchers is the absence of housekeeping molecules that are reliably detected at consistent levels across samples. Exosome constituents, including lipid, protein and RNA, are largely specific to the parent cell type and are very sensitive to changes in the cellular environment. Therefore, it has been very difficult to identify exosome components that are suitable for normalization (i.e., that are not altered by treatment or experimental conditions) (Witwer *et al.*, 2013; Yang *et al.*, 2014). As the quantification of HDE RNA is a primary metric proposed here, we have chosen absolute qRT-PCR to circumvent the need for a housekeeping gene. The data product of absolute quantification is the definitive copy number of a given target based upon a dilution series of known target cDNA copy number.

Generation of cDNA standard curves via bacterial cloning

Initially, standard curves for each mRNA analyte were generated by bacterial cloning as previously described (Wetmore *et al.*, 2010). Bacteria transformed to express the DNAs of interest were obtained as glycerol stocks, either from Dr. Barbara Wetmore or purchased from Dharmacon (Table 2.1). For both human and rat constructs, DNAs were cloned by culturing the transformed bacteria in sterile Miller's Luria Bertani broth (LB; Fisher Scientific) prepared with the appropriate concentration of selective antibiotic (Table 2.1). Starter cultures were generated by inoculating 5 ml of the antibiotic-containing LB with a pipette tip that had been pressed into a tube of frozen bacterial stock and were incubated with shaking (300 rpm) for approximately 8 h at 37 ºC. When the starter cultures became turbid, suggesting log-phase growth, the cultures were expanded for bulk cDNA production. Based on the turbidity of starter culture, 250-500 µl was transferred into a sterile vented flask containing 250 ml of fresh LB broth. Flasks were incubated with shaking (300 rpm) overnight (approximately 16 h) at 37 ºC. The remaining starter culture was used to create frozen glycerol stocks for future use. Briefly, bacteria were pelleted by centrifugation at 3,500 x *g* for 5 min and resuspended in 950 µl of antibiotic-containing LB. This solution was combined with an equal volume of 60% glycerol (Fisher Scientific) to give a final concentration of 30% glycerol. Stocks were stored at -80 ºC. Following the overnight incubation, bacteria were spun out of the bulk cultures at 3,500 x *g* for 5 min at 4 ºC. Pellets were frozen at -20 ºC until processing or were used directly for DNA isolation. Plasmid DNA (pDNA) was isolated from each batch of bacteria (clone) using a HiSpeed Plasmid Purification Kit (Qiagen) according to the manufacturer's protocol.

Upon elution, the pDNA concentration was obtained using a NanoDrop 1000 spectrophotometer (Thermo). Based on the size and weight of each individual vector (Table 2.1) and the concentration of plasmid DNA produced by that clone, the number of cDNA copies per preparation was calculated. With this information, each pDNA was diluted to 1e12 and 1e9 copies per microliter and stored as concentrated stocks. A standard curve consisting of 10-fold serial dilutions with final copy numbers ranging from 1e6 to 10 was prepared fresh in nuclease-free water immediately prior to each qRT-PCR reaction.

Absolute qRT-PCR copy number calculation

The cycle threshold (Ct) values for each standard dilution were plotted against the log of the copy number to produce a linear regression formula $y = mx + b$ where *y* is the Ct value, *m* is the slope, and *b* is the y-intercept. Solving this equation for *x* facilitates quantification of copy number for each unknown exosomal cDNA sample. Linearity of the curve was also utilized to characterize individual assay reaction or amplification efficiency such that $E = [10^{(-1\text{-slope})} - 1]$, where *E* is efficiency. Efficiency is considered optimal between 0.90 and 1.05.

Table 2.1. Plasmid DNA vector information for preparation of qRT-PCR standard curves by bacterial cloning. Rat (A) and human (B) constructs are described. Amp: ampicillin; Chlor: chloramphenicol. * indicates custom TaqMan Gene Expression Assay primers were designed to avoid known SNPs.

A

cDNA Amplicon	Entrez Gene ID	IMAGE Consortium Clone ID	Plasmid Vector	Coding Sequence Length (bp)	Total Vector Size (bp)	Antibiotic Resistance	TaqMan Gene Expression Assay
Albumin	24186	7303856	pExpress-1	2020	6137	Amp (100 μg/ml)	Rn00592480_m1 (a) Rn01413927_g1 (b)
Fibrinogen β-chain polypeptide	24366	7371665	pExpress-1	1604	5721	Amp (100 μg/ml)	Rn01459028_m1
Haptoglobin	24464	7321960	pExpress-1	1239	5356	Amp (100 μg/ml)	Rn00561393_m1
α-1-microglobulin/bikunin precursor	25377	7368246	pExpress-1	1180	5297	Amp (100 μg/ml)	Rn01458278_m1
Apolipoprotein H	287774	7364928	pExpress-1	1175	5292	Amp (100 μg/ml)	Rn01467588_m1
Group-specific component	24384	7130137	pExpress-1	1684	5801	Amp (100 μg/ml)	Rn01414180_m1
Retinol binding protein 4	25703	7369314	pExpress-1	939	5056	Amp (100 μg/ml)	Rn01451315_g1
Transferrin	24825	7132382	pExpress-1	2323	6440	Amp (100 μg/ml)	Rn01445479_m1
Serpin peptidase inhibitor A1	24648	7131535	pExpress-1	1603	5720	Amp (100 μg/ml)	Rn00574670_m1

B

cDNA Amplicon	Entrez Gene ID	IMAGE Consortium Clone ID	Plasmid Vector	Coding Sequence Length (bp)	Total Vector Size (bp)	Antibiotic Resistance	TaqMan Gene Expression Assay
Albumin*	213	4734617	pDNR-LIB	2068	6229	Chlor (25 μg/ml)	Forward: TACTCTGTCGTGCTGCTGCT Reverse: CAGGGCATTCTTTTTGCTTC
Fibrinogen β-chain polypeptide	2244	4734415	pDNR-LIB	1948	6109	Chlor (25 μg/ml)	Hs00905942_m1
Haptoglobin	3240	4716454	pDNR-LIB	1139	5300	Chlor (25 μg/ml)	Hs00605928_g1
α-1-microglobulin/bikunin precursor	259	5433460	pOTB7	1413	3228	Chlor (25 μg/ml)	Hs01089670_m1
Apolipoprotein H	350	4734357	pDNR-LIB	1201	5362	Chlor (25 μg/ml)	Hs00979400_m1
Group-specific component	2638	4767205	pDNR-LIB	1720	5881	Chlor (25 μg/ml)	Hs00167096_m1
Retinol binding protein 4	5950	4767481	pDNR-LIB	950	5111	Chlor (25 μg/ml)	Hs00928627_g1
Transferrin	7018	5264299	pBluescriptR	2330	5320	Amp (100 μg/ml)	Hs01067774_m1
Serpin peptidase inhibitor A1	5265	3859644	pCMV-SPORT6	1584	5980	Amp (100 μg/ml)	Hs01097800_m1

Performance of plasmid-based standard curves

Validating the rat albumin mRNA qPCR assay (Rn00592480_m1) for HDE content analysis was the focus of early efforts. The assay performed well in preliminary experiments (Figure 2.4), but efficiency declined over time. A fresh rat albumin pDNA standard curve was generated, and 5 and 20 µl qRT-PCR reaction volumes were tested on two different qPCR instruments (7900 HT Fast RT-PCR System and 7900 HT Sequence Detection System; ABI) in an attempt to improve amplification efficiency. Regardless of reaction volume, the efficiencies were closer to acceptable limits and the standard deviations were lower with the 7900 Fast RT-PCR System (data not shown). Despite improved instrument performance, standard curve results remained inconsistent across multiple qPCR plates.

The predominant form of albumin pDNA was presumably circular given that the construct had not been gel-purified. We hypothesized that the standard curve could be affected negatively by contaminants, including alternate forms of pDNA. It has also been shown that the conformation of DNA cloned via cellular methods can significantly bias quantification and alter efficiency due to differential primer binding, with circular pDNA resulting in drastic copy number over-estimations in both SYBR Green and TaqMan platforms (Hou *et al.*, 2010; Lin *et al.*, 2011). While efficiency differences depend on the target being quantified, linearized pDNA curves generate more accurate copy number extrapolations and therefore, were the conformation of choice for future standard curves (Hou *et al.*, 2010).

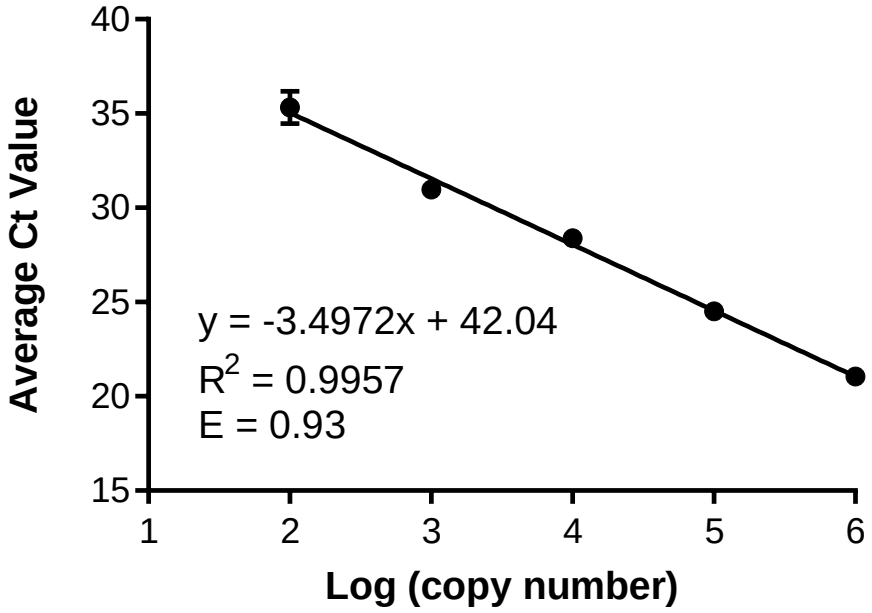

Figure 2.4. Representative rat albumin standard curve generated from uncut pDNA. Data represent an average of triplicate qPCR wells fitted with a linear regression model. Initial amplification efficiency (E) is within the ideal range (0.90-1.05).

Linearization of pDNA standard curves

Focusing on the rat albumin construct, pDNA was linearized via restriction digest using an enzyme with a single cut site, *XhoI* (Figure 2.5). Digests were prepared in a 50 µl reaction volume with 2 µg circular DNA, 20 units *XhoI* (New England Biolabs; NEB), Buffer 2 (NEB), and nuclease-free water. Following a 16 h incubation at 37 ºC, digests were combined with Track-It Cyan/Orange gel loading buffer (Invitrogen), and electrophoresed in parallel with 2 µg uncut plasmid and Track-It 100 bp DNA ladder (Thermo) in a horizontal mini 1% agarose gel (Sigma) containing 1.5 µg/ml ethidium bromide (EtBr) with 1x tris/borate/EDTA (TBE) buffer (Sigma) at 100 V constant for 90 min. Migration was visualized with an ultraviolet (UV) transilluminator (Figure 2.5) and the linearized band was excised from the gel with a scalpel. The linear albumin DNA fragment was purified from the agarose using a QIAquick Gel Extraction Kit (Qiagen) pursuant to the manufacturer's "Quick Start" protocol. Upon elution of the purified linear albumin, the eluate concentration was determined using a NanoDrop 1000 spectrophotometer and the copy number was determined as outlined in an earlier section. Concentrated stocks were stored in aliquots at -80 ºC. The same procedure was followed to generate linearized human standards from constructs described in Table 2.1.

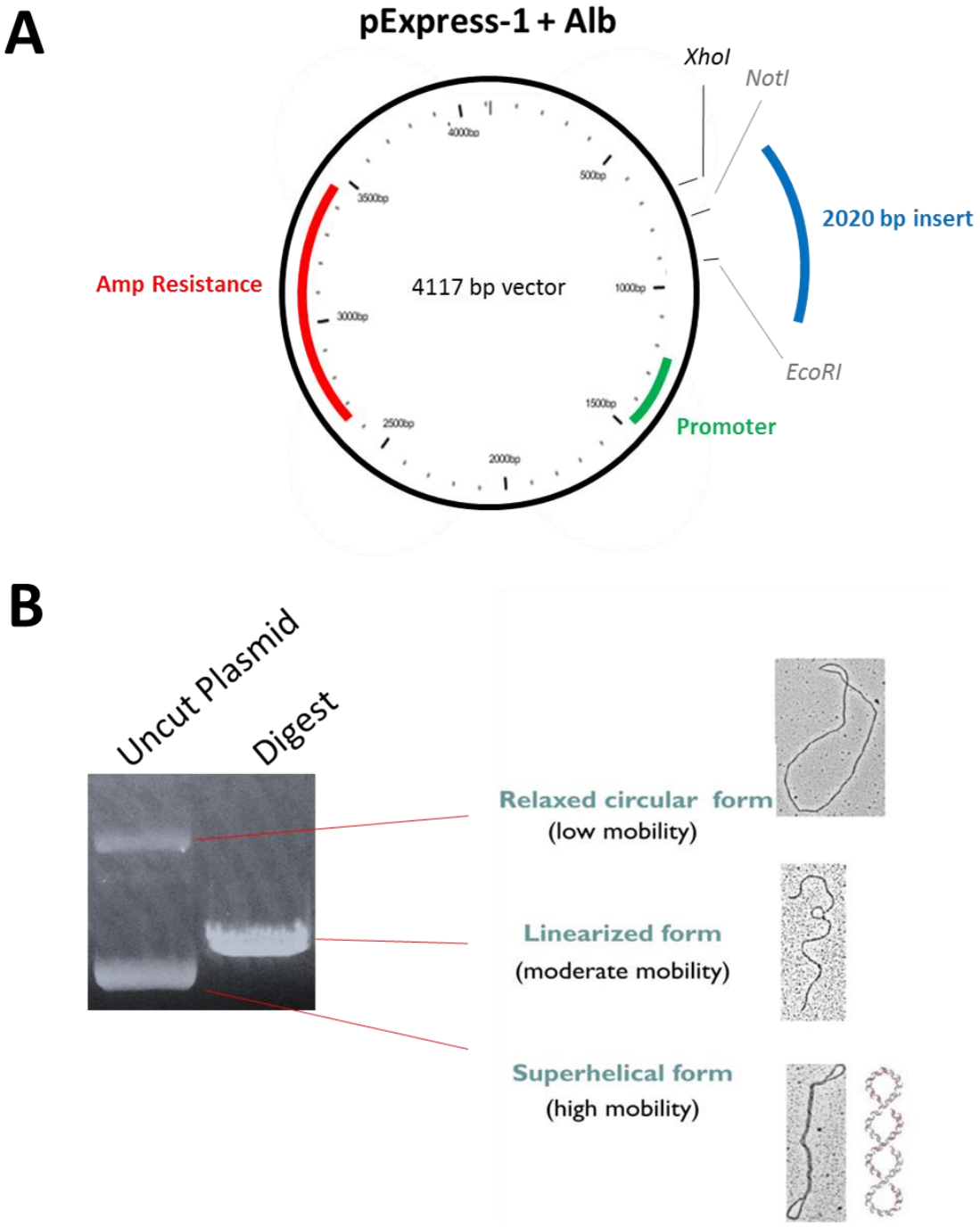

Figure 2.5. Linearization of pDNA carrying insert for qPCR standard curve. Illustration of rat albumin DNA vector and restriction site targeted to linearize plasmid (A). Representative gel of uncut and linearized pDNA for rat *Ambp* standard curve (B). Image demonstrates differential gel migration of various pDNA conformations. For all pDNA standards, the linearized band represented in the "Digest" lane was excised for purification. Image of pDNA forms (right portion of panel B was adapted from (Hegyi *et al.*, 2013)).

Comparison of circular vs. linear pDNA curves

Rat Albumin

Freshly diluted circular and linearized standard curves were prepared with copy numbers ranging from 1e6 to e10 in 10-fold serial dilutions. These curves were assayed in parallel using the rat albumin TaqMan Gene Expression Assay (Rn00592480_m1) with 5 and 20 µl total reaction volumes. For both reaction sizes, the linearized pDNA curve demonstrated much lower Ct values relative to the circular pDNA curve with the same copy numbers (Table 2.2). These findings agree with existing evidence that circularized plasmid-based qPCR standard curves generate inflated copy number estimations (Hou *et al.*, 2010).

Table 2.2. Linearized pDNA standard curve for rat albumin shows universally lower average Ct values than circular pDNA.

	5 µl Reaction		*20 µl Reaction*	
Copies	**Linear Ct**	**Circular Ct**	**Linear Ct**	**Circular Ct**
1.00E+06	16.8	24.2	19.0	24.7
1.00E+05	21.3	27.4	23.3	28.2
1.00E+04	25.3	31.8	27.2	33.0
1.00E+03	29.3	36.6	31.4	36.6
1.00E+02	33.3	35.0	34.9	36.5
1.00E+01	34.8	36.0	36.0	35.6

Human Constructs

Freshly diluted circular and linearized pDNA standard curves for all human TaqMan assays (Table 2.1) were prepared with copy numbers ranging from 1e6 to 10 in 10-fold serial dilutions, as described above. These curves were assayed in parallel using 5 µl total reaction volumes. For 6 out of 8 constructs, the linearized plasmid DNA curve demonstrated much lower Ct values relative to the same copy number using the circular plasmid curve (Figure 2.6). While 2 linearized curves (Gc and ApoH) were not detected at lower Cts than the corresponding circular standards, these linearized standards had superior linearity and reaction efficiency. For human ApoH, the uncut standard curve yielded $R^2 = 0.9808$ and E = 1.23 while the linearized curve showed $R^2 = 0.9979$ and E = 0.985. The human Gc curve had $R^2 = 0.9711$ in the circular form versus 0.9984 in the linear form and E = 1.13 versus 0.903. The linearized standard curves were used for qPCR analyses of human HDE content described in Chapter 3.

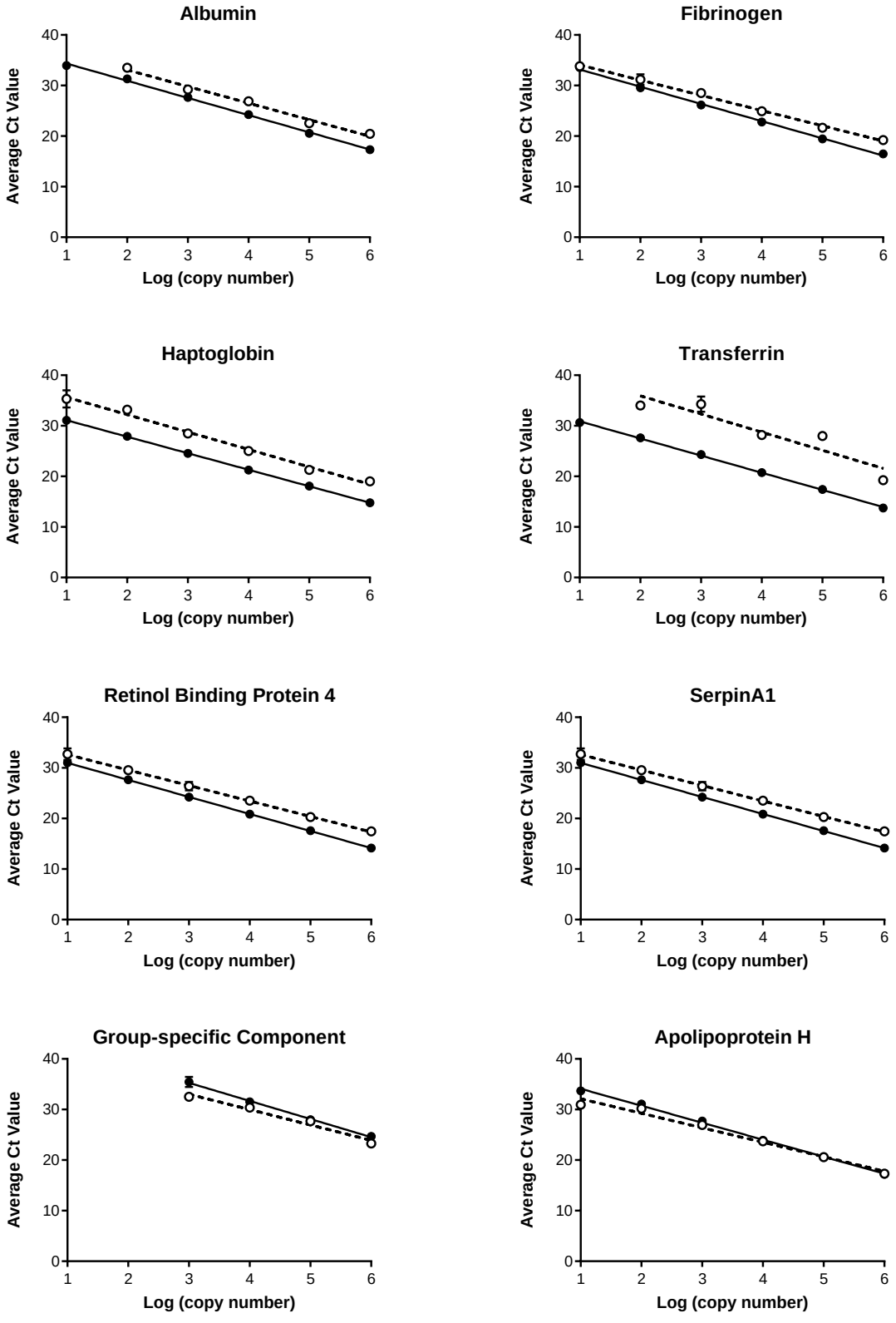
Albumin
Fibrinogen
Haptoglobin
Transferrin
Retinol Binding Protein 4
SerpinA1
Group-specific Component
Apolipoprotein H
Average Ct Value
Log (copy number)
0
10
20
30
40
1
2
3
4
5
6
Circular
Linearized

Figure 2.6. Linear versus circular pDNA standard curves for human exosome qRT-PCR assays. All 8 human constructs are represented with open circles indicating curves generated from uncut pDNA and the closed circles representing curves from linearized pDNA. In all cases, the linearized standard curves were detected at lower Ct values and/or showed better linearity and amplification efficiency than the corresponding circular pDNA curves.

Optimization of rat exosomal albumin qRT-PCR

While the linearized conformation of pDNA was superior to the circular form, within a month of generation, Ct values for the standard curve in 5 µl albumin qPCR reactions had increased from 16.8 (Table 2.2) to 19.2, despite storage in aliquots to prevent multiple freeze/thaw cycles (data not shown). We next investigated an alternative TaqMan Gene Expression Assay in addition to molecular cloning for stable standard curve generation.

Validation of an alternative qPCR assay for detection of albumin in rat HDE

To detect exosomal albumin in rat HDE, we initially used the TaqMan Gene Expression Assay Rn00592480_m1 (Table 2.1) because it had been used in earlier EV studies (Wetmore *et al.*, 2010) and was found to identify the most rat albumin transcripts by the manufacturer. However, underperformance of the assay was a concern, as this primer/probe set targets the 5' end of rat albumin cDNA. Therefore, we selected an alternative assay, Rn01413927_g1 (Table 2.1), which targets the 3' region and had also been validated in EV samples (Wetmore *et al.*, 2010). Using the same linearized pDNA standard curve and qPCR plate, these two assays were compared in 5 µl qPCR reactions. The new assay (Rn01413927_g1) had superior linearity and lower Ct values for the same standard curve, allowing all six standards to be detected relative to only five standards with the original assay (Figure 2.7). All further analyses of albumin mRNA quantity in rat HDE were conducted using this new qPCR assay.

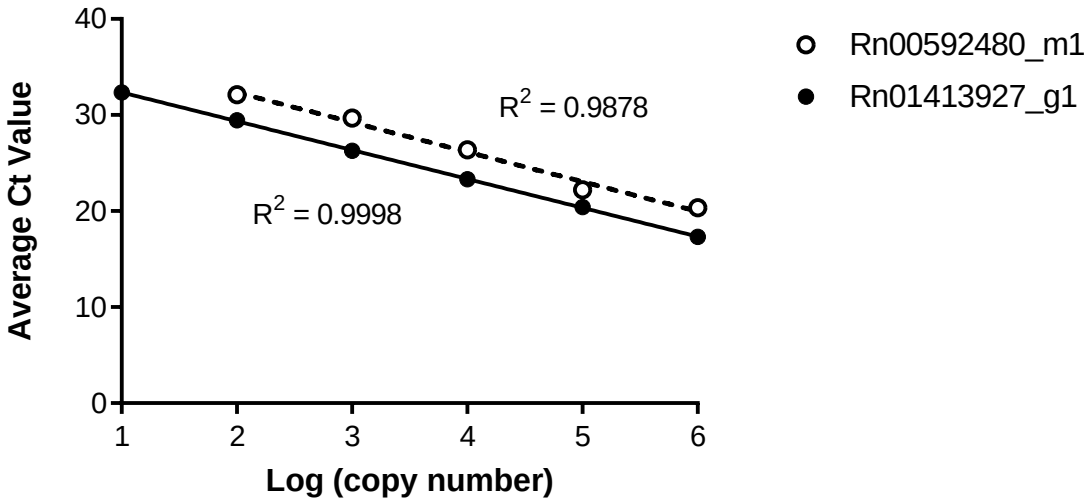

Figure 2.7. Side-by-side performance of two qRT-PCR assays for rat albumin. Lines represent linear regression analyses with respective R^2 values next to each curve. The alternative assay (Rn01413927_g1) shows lower Ct values for the same standards and detects as few as to 10 copies, while the original assay (Rn00592480_m1) detection limit is 100 copies.

Primer design

Prior to designing PCR primers, the mRNA/cDNA sequence for the target of interest must be known. Given that the PCR amplicon will be measured in a qPCR assay, the region within the PCR amplicon targeted by the qPCR assay must be preserved. While TaqMan Gene Expression Assay primer sequences are proprietary, the start position and size of the rat albumin TaqMan amplicon were known. Using this information, flanking forward and reverse PCR primers were selected to generate a PCR amplicon of approximately 500 bp, which is generally considered the optimal amplicon size for traditional PCR (New England Biolabs; Premier Biosoft) (Figure 2.8). Primers were designed to be roughly 18-22 bp in length with a GC percentage between 40 and 60% and melting temperature (T_m) between 42 and 65 ºC (New England Biolabs; Premier Biosoft). Custom primers were synthesized by Invitrogen and provided as lyophilized stocks.

CTAGCCTCTGGCACAATGAAGTGGGTAACCTTTCTCCTCCTCCTCTTCATCTCCGGTTCTGCCTTTTCCAGGGGTGTGTTTCGCC
GAGAAGCACACAAGAGTGAGATCGCCCATCGGTTTAAGGACTTGGGAGAACAGCATTTCAAAGGCCTAGTCCTGATTGCCTTT
TCCCAGTATCTCCAGAAATGCCCATATGAAGAGCATATCAAATTGGTGCAGGAAGTAACAGACTTTGCAAAAACATGTGTCGC
TGATGAGAATGCCGAAAACTGTGACAAGTCCATTCACACTCTCTTCGGAGACAAGTTATGCGCCATTCCAAAGCTTCGCGACAA
CTACGGTGAACTGGCTGACTGCTGTGCAAAACAAGAGCCCGAAAGAAACGAGTGTTTCCTGCAGCACAAGGATGACAACCCC
AACCTGCCACCCTTCCAGAGGCCGGAGGCTGAGGCCATGTGCACCTCCTTCCAGGAGAACCCTACCAGCTTTCTGGGACACTA
TTTGCATGAAGTTGCCAGGAGACATCCTTATTTCTATGCCCCAGAACTCCTTTACTATGCTGAGAAATACAATGAGGTTCTGACC
CAGTGCTGCACAGAGTCTGACAAAGCAGCCTGCCTGACACCGAAGCTTGATGCCGTGAAAGAGAAAGCACTGGTCGCAGCTG
TCCGTCAGAGGATGAAGTGCTCCAGTATGCAGAGATTTGGAGAGAGAGCCTTCAAAGCCTGGGCAGTAGCTCGTATGAGCCA
GCGATTCCCCAATGCTGAGTTCGCAGAAATCACCAAATTGGCAACAGACCTCACCAAAATCAACAAGGAGTGCTGTCACGGCG
ACCTGTTGGAATGCGCGGATGACAGGGCGGAACTTGCCAAGTACATGTGTGAGAACCAGGCCACTATCTCCAGCAAACTGCA
GGCTTGCTGTGATAAGCCAGTGCTGCAGAAATCCCAGTGTCTCGCTGAGATAGAACATGACAACATTCCTGCCGATCTGCCCTC
AATAGCTGCTGACTTTGTTGAGGATAAGGAAGTGTGTAAGAACTATGCTGAGGCCAAGGATGTCTTCCTGGGCACGTTTTTGT
ATGAATATTCAAGAAGGCACCCCGATTACTCCGTGTCCCTGCTGCTGAGACTTGCTAAGAAATATGAAGCCACACTGGAGAAG
TGCTGTGCTGAAGGCGATCCTCCTGCCTGCTACGGCACAGTGCTTGCAGAATTTCAGCCTCTTGTAGAAGAACCTAAGAACTTG
GTCAAAACTAACTGTGAGCTTTACGAGAAGCTTGGAGAGTATGGATTCCAAAACGCCATTCTGGTTCGATACACCCAGAAAGC
ACCTCAGGTGTCGACCCCAACTCTCGTGGAGGCAGCAAGAAACCTGGGAAGAGTGGGCACCAAGTGTTGTACCCTTCCTGAA
GCTCAGAGACTGCCCTGTGTGGAAGACTATCTGTCTGCCATCCTGAACCGTCTGTGTGTGCTGCATGAGAAGACCCCAGTGAG
CGAGAAGGTCACCAAGTGCTGTAGTGGGTCCCTGGTGGAAAGACGGCCATGTTTCTCTGCTCTGACAGTTGACGAGACATATG
TCCCCAAAGAGTTTAAAGCTGAGACCTTCACCTTCCACTCTGATATCTGCACACTCCCAGACAAGGAGAAGCAGATAAAGAAG
CAAACGGCTCTCGCTGAGCTGGTGAAACACAAGCCCAAGGCCACAGAAGATCAGCTGAAGACGGTGATGGGTGACTTCGCAC
AATTCGTGGACAAGTGTTGCAAGGCTGCCGACAAGGATAACTGCTTCGCCACTGAGGGGCCAAACCTTGTTGCTAGAAGCAA
AGAAGCCTTAGCCTAAACACATCACAACCATCTCAGGCTACCCTGAGAAAAAAAGACATGAAGACTCAGGACTCATCTCTTCTG
TTGGTGTAAAACCAACACCCTAAGGAACACAAATTTCTTTGAACATTTGACTTCTTTTCTCTGTGCCGCAATTAATAAAAAATAG
AAAGAAAAAAAAAAAAAAAAAAAAA

Custom Primer Sequence	%GC Content	Base Range	Size (bp)	T_m (ºC)
GAAGGTCACCAAGTGCTGTAGTG	52	1500-1522	23	61
TGCGGCACAGAGAAAAGAA	47	1962-1980	19	61

Figure 2.8. Rat albumin mRNA sequence (NCBI Reference Sequence NM_134326.2) used for custom PCR primer design. TaqMan assay (Rn01413927_g1) amplicon of 76 bp in size (1734-1874 bp) is highlighted in yellow and the binding sites of the flanking forward and reverse primers are indicated by a red underline. The embedded table shows the sequences of the forward primer (top) and the reverse primer (bottom).

Polymerase chain reactions

Rat liver cDNA (1 µg) was used as the template in 25 µl PCR reactions. Reaction components included GC Enhancer and AmpliTaq Gold polymerase from an AmpliTaq Gold 360 Master Mix kit (Thermo), as well as forward and reverse primers at a final concentration of 0.2 µM. The volume was adjusted to 25 µl with nuclease-free water. No template control reactions were also prepared with water in place of the cDNA template. Using a thermal cycler, PCR reactions were run under the following conditions: 95 ºC for 10 min (*Taq* polymerase activation); 35 cycles of 95 ºC for 30 sec (denaturation), 60 ºC for 30 sec (annealing) and 72 ºC for 30 sec (extension); 72 ºC for 7 min (final extension); and held at 4 ºC.

The PCR product was subjected to gel electrophoresis to confirm appropriate amplicon size (~500 bp) and purity (Figure 2.9). Electrophoresis was performed as previously described with the exception of voltage (200 V constant) and time (70 min). Gel purification of the PCR product was conducted as described and the eluate concentration was measured by NanoDrop for copy number calculations.

Assessing performance of PCR-based standard curve by qPCR

The gel-purified PCR product was diluted in a series of six 10-fold dilutions to generate the qRT-PCR standard curve for rat albumin. Using the newly validated TaqMan Gene Expression Assay, linearity and amplification efficiency of the PCR-based standard curve were determined. All standards down to 10 copies were detected ($E = 0.940$; $R^2 = 0.9999$). Concentrated stocks of this curve were stored at -80 ºC. The Ct signals for each standard remained stable for the duration of our qRT-PCR experiments.

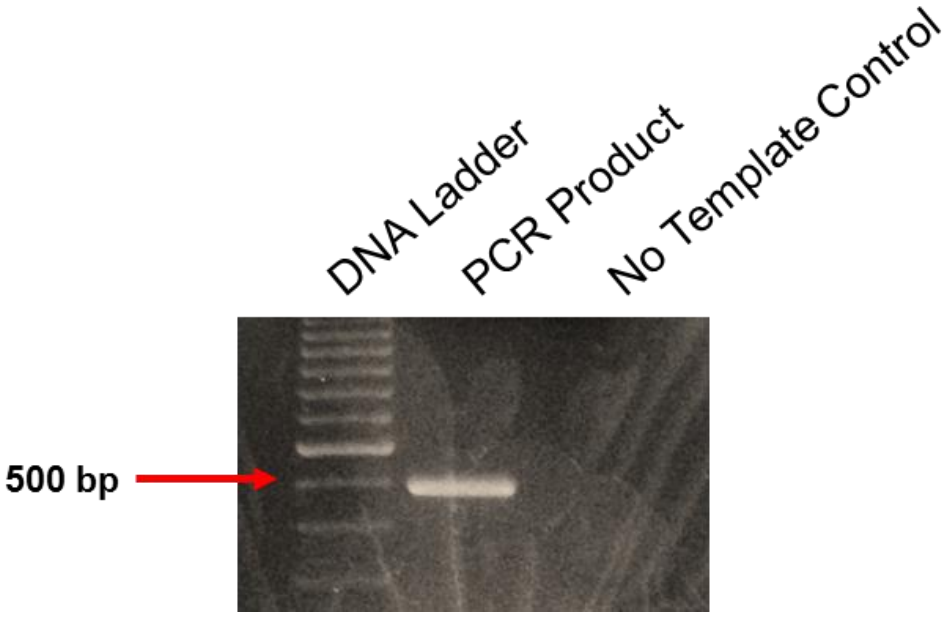

Figure 2.9. Gel electrophoresis of rat albumin PCR product confirming amplicon size. No template control indicates a PCR reaction that was carried out with water instead of template DNA. The lack of a band in this lane demonstrates an absence of non-specific PCR amplification.

Assessing performance of PCR-based standard curve by qRT-PCR

The gel-purified PCR product was diluted in a series of six 10-fold dilutions to generate the qRT-PCR standard curve for rat albumin. Using the newly validated TaqMan Gene Expression Assay, linearity and amplification efficiency of the PCR-based standard curve were determined. All standards down to 10 copies were detected ($E = 0.940$; $R^2 = 0.9999$). Concentrated stocks of this curve were stored at -80 ºC. The Ct signals for each standard remained stable for the duration of our qRT-PCR experiments.

Generation of a standard qRT-PCR curve for miR-122

As with albumin mRNA, we sought to quantify the copy number of hepatocyte-specific microRNA miR-122 within rat and human HDE using TaqMan qRT-PCR. Fortunately, miRNA sequences are highly conserved across species, and the TaqMan assay for miR-122 (hsa-miR-122-5p; Applied Biosystems) detects both rat and human miR-122, among other species. We generated a universal miR-122 standard curve of known copy number for qRT-PCR of human and rat exosomal miR-122 using a miScript miRNA Mimic (Qiagen). A lyophilized stock of synthetic miR-122 was reconstituted with nuclease-free water to a concentration of 1.2e13 copies/µl. Given the high quantities of miR-122 within hepatocytes and HDE, an 8-point standard curve was preferred. From the stock, an intermediate dilution of 2e10 copies/µl was prepared to facilitate generation of the highest standard at 2.5e8 copies/µl. Six serial 10-fold dilutions of the highest standard were generated with the final standard being a zero copy blank (also serving as a no template control for the RT reactions).

The standard curve of synthetic miR-122 was reverse-transcribed using a TaqMan miRNA Reverse Transcription Kit (Applied Biosystems) with miR-122-specific primers in a 5 µl total reaction volume scaled according to the manufacturer's instructions. The resultant cDNA was diluted to produce a set of standards whose final concentrations in a qPCR reaction would be 1e7 copies to 10 copies (Table 2.3). This standard curve remained stable through the completion of exosomal miR-122 quantification experiments.

Table 2.3. Preparation of the miR-122 qRT-PCR standard curve. Schematic shows how copy numbers were tracked and adjusted during standard preparation from stock dilution to qRT-PCR input.

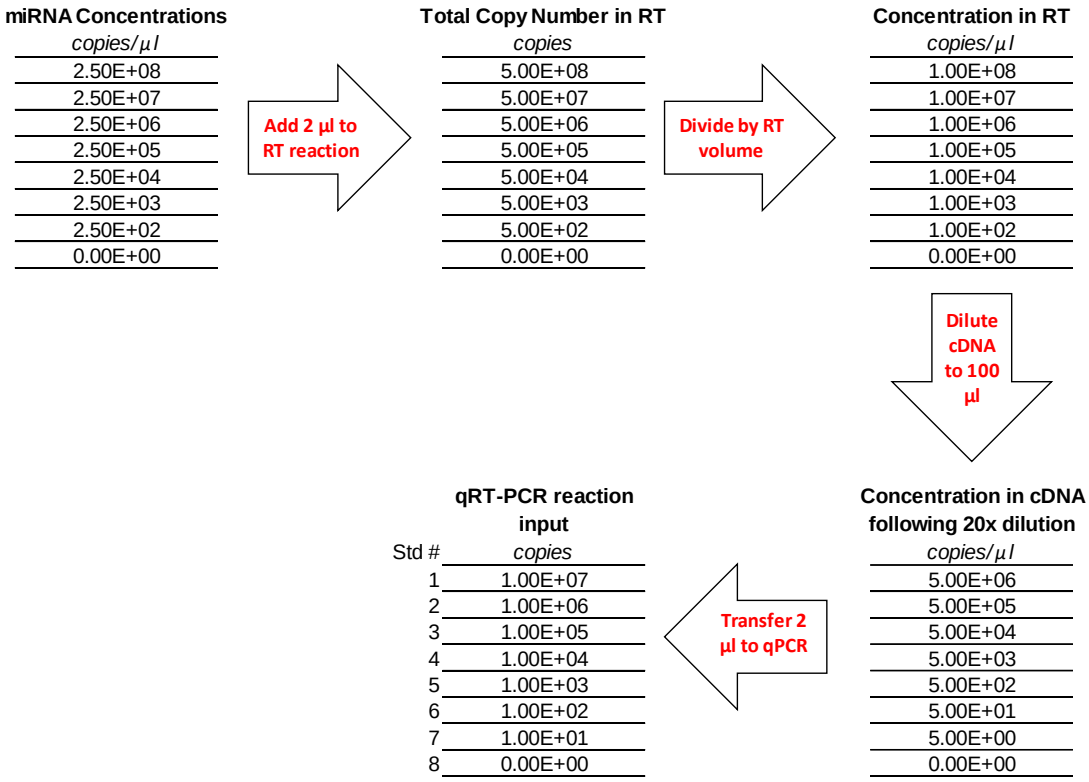

2.3.3 Exogenous mRNA spike-in control

In addition to standardizing qRT-PCR results across plates with the use of absolute quantification, we wanted to normalize for slight differences in RNA isolation efficiency across exosome samples and batches. Since no endogenous reference or housekeeping genes have yet been identified in exosomes, we selected an exogenous non-mammalian spike-in to serve as a pseudo-housekeeping marker. An exogenous reference mRNA control was spiked in to all samples at an equal quantity prior to RNA extraction. The recovery of this mRNA was assessed in parallel with target mRNAs of interest during qRT-PCR and used to adjust Ct values for the gene of interest.

Preparation and addition of mRNA spike-in

The addition of exogenous mRNA reference controls for qRT-PCR is a well-established practice (Johnston *et al.*, 2012; Revilla-Fernandez *et al.*, 2005; Smith *et al.*, 2003) deemed useful for cellular applications since traditional internal housekeeping genes such as glyceraldehyde 3-phosphate dehydrogenase (GAPDH) or hypoxanthine phosphoribosyl-transferase 1 (HPRT) are often subject to endogenous transcription changes. Exogenous RNA introduced at a known concentration for the purposes of normalizing qRT-PCR data from exosomal samples is highly desirable because exosomes do not currently have housekeeping genes that remain constant across experimental conditions. We selected synthetic luciferase mRNA Luciferase Control RNA (Promega) as a validated exogenous reference gene (Johnston *et al.*, 2012).

The copy number of stock Luciferase Control RNA was calculated based on construct size as described in an earlier section. To test the spike-in using actual exosomes, various

concentrations of luciferase were spiked in to human HDE (2 µl per sample) prior to RNA isolation, immediately following addition of miRCURY Lysis Buffer. Linear acrylamide carrier was added to each sample and RNA isolation was performed according to our established protocol with elution in 25 µl. A High Capacity cDNA Reverse Transcription Kit (Applied Biosytems) was used to generate cDNA from all samples. This kit uses random primers, allowing for reverse transcription of exosomal mRNA and exogenous luciferase mRNA to occur in the same reaction.

Based on the multiplexed qPCR data shown below, we selected a working spike-in concentration of 1.6e8 copies/µl to be added to all subsequent exosome samples (2 µl per sample).

Validation of exosomal albumin and exogenous luciferase multiplexed qRT-PCR

The most value would be gained from a reference gene (endogenous or exogenous) that is measured in the same qPCR reaction as the target, eliminating a number of confounding variables. We wished to combine qPCR assays for albumin and luciferase. With multiplexing in mind, we selected a TaqMan gene expression assay for luciferase that was "primer-limited" because of the over-abundance of luciferase relative to albumin in our samples (Applied Biosystems, 2010; Henegariu *et al.*, 1997). Choosing a primer-limited assay for the more abundant target helps ensure that luciferase does not out-compete albumin for reagents and does not confound albumin Ct values. The TaqMan qPCR master mix we used was optimized for multiplexing (Applied Biosystems, 2010), and the combined assays had distinct reporter dyes (albumin = FAM, luciferase = VIC).

To validate this duplex approach, the performance of individual assays was compared to their performance when multiplexed in an effort to identify possible interference. Human HDE prepared with increasing concentrations of luciferase spike-in were analyzed by qPCR using the luciferase assay alone and in combination with albumin (Figure 2.10). The Ct values of luciferase were not affected by the addition of the albumin assay. We also compared the Ct values from human and rat albumin standard curves using the albumin assay alone and multiplexed with luciferase (Figure 2.10). No changes in the Ct values of either albumin standard curve were detected using the albumin assay alone versus in conjunction with luciferase. This work confirmed that the exogenous normalization gene luciferase can be measured in the same qPCR reaction as human or rat albumin.

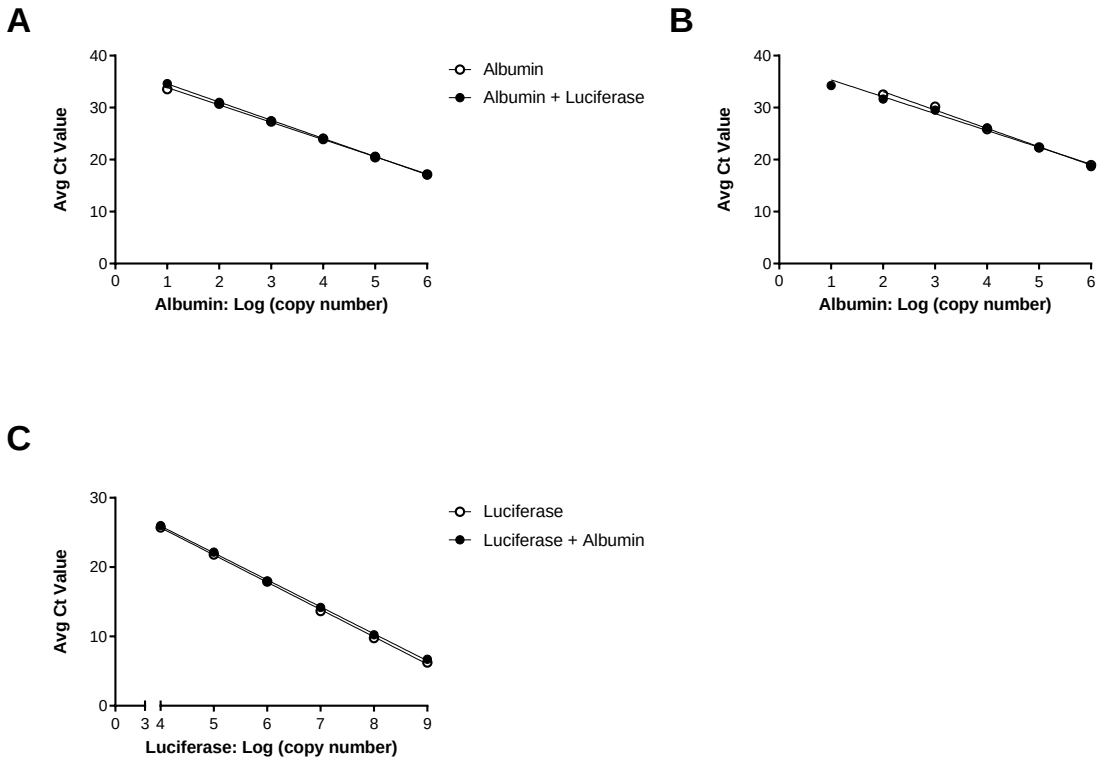

Figure 2.10. Validation of qRT-PCR multiplexed assays for albumin and exogenous luciferase reference mRNA. Addition of the luciferase TaqMan assay does not interfere with detection of the human (A) or rat (B) albumin standard curves (both A and B share the same graph legend). Detection of luciferase across a range of concentrations is not affected by the albumin assay (C). Data points represent the mean Ct value for triplicate qPCR reaction wells and are fit with linear regression models.

Normalization of qRT-PCR data using exogenous mRNA

Multiplexed qPCR for albumin and luciferase produced Ct values for both genes. Normalization to luciferase as a reference gene was performed by the following process. First, luciferase Ct values were averaged across triplicate wells of each sample. The median of these averages was calculated. On a per-sample basis, the average luciferase Ct was subtracted from the median of all luciferase averages. The result is a normalization factor for each sample. This sample-specific normalization factor was added to the corresponding albumin Ct values for a given sample. The sum represents a normalized albumin Ct that can be used to calculate copy number in the unknown samples as previously described in the copy number calculation section. The luciferase normalization factor was also applied to other mRNAs in those samples that were run on the same qPCR plate.

2.4 Initial acetaminophen exposures and concentration selection for *in vitro* HDE studies

2.4.1 Rat hepatocytes

Freshly isolated primary Sprague-Dawley (SD) rat hepatocytes were obtained from the Hamner Institutes for Health Sciences (Research Triangle Park, NC). Hepatocytes were seeded in culture plates coated with collagen type I (Corning) at a density of 1.5×10^6 cells per well in plating medium (high-glucose Dulbecco's modified Eagle's medium [DMEM], penicillin-streptomycin, sodium pyruvate, fetal bovine serum [Thermo Fisher Scientific], insulin, and dexamethasone [Sigma-Aldrich]). Culture plates were incubated at 37ºC with 5% CO_2. After attachment, non-adherent cells were removed and fresh plating medium was added. Cultures were transitioned to serum-free hepatocyte maintenance medium (Modified Chee's Medium, custom formulation) 4 h after plating. Following a 24 h acclimation period,

hepatocyte cultures were exposed to acetaminophen (APAP; 0, 0.37, 1.1, 3.3, 10, or 30 mM) in medium for 72 h. Treatment-induced effects on cell health were determined by measuring alanine aminotransferase (ALT) in the medium with an Infinity ALT/GPT Reagent kit (Thermo) modified for platereader format. Reagent was warmed to 37 ºC and 200 µl were added to each well containing 20 µl of sample, media blank, or high and low controls. The assay plate was incubated for 30 sec at 37 ºC before data collection. The change in absorbance at 340 nm was measured every 60 sec for 8 min total on a SpectraMax M3 microplate reader (Molecular Devices) in kinetic mode.

After 72 h APAP exposure, the levels of ALT in culture medium as a function of APAP concentration demonstrated a pattern indicative of cell health at low concentrations, slight toxicity at intermediate concentrations, and overt necrosis at high concentrations (Figure 2.11). However, the assay had a narrow dynamic range and was deemed inappropriate for *in vitro* hepatocellular toxicity approximation. Morphologically, toxicity was apparent at 10 and 30 mM APAP.

HDE and exosomal RNA were isolated as previously described. Increases in exosomal albumin mRNA relative to untreated controls were observed at sub-toxic concentrations as low as 1.1 mM (Figure 2.11) and became statistically significant at 3.3 mM ($p < 0.05$, one-way ANOVA with Bonferonni's multiple comparison test). We selected this concentration range for acute 24 h exposures *in vitro* to study the early, sub-toxic responses of HDE to APAP.

To examine the toxicity of a range of APAP concentrations in rat hepatocytes over 24 h, we exposed primary rat hepatocytes to 0, 5, 10, or 20 mM APAP and measured lactate dehydrogenase (LDH) in the medium as described elsewhere (Holman *et al.*, 2016). We

empirically determined that overt APAP cytotoxicity after 24 h does not occur below 20 mM in rat hepatocytes (Figure 2.12) and that these concentrations were suitable to induce low to high levels of sub-toxic hepatocyte stress.

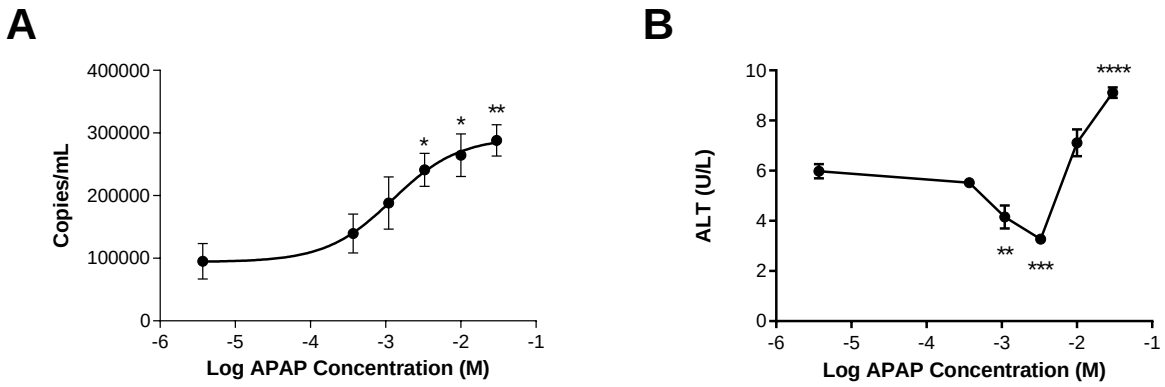

Figure 2.11. Primary rat hepatocyte responses following a range of APAP exposures for 72 h. Exosomal albumin mRNA (A) increased consistently with APAP exposure, while ALT was significantly decreased prior to elevations (B). * $p < 0.05$, ** $p < 0.01$, *** $p < 0.001$, **** $p < 0.0001$; one-way ANOVA with Bonferroni's multiple test correction.

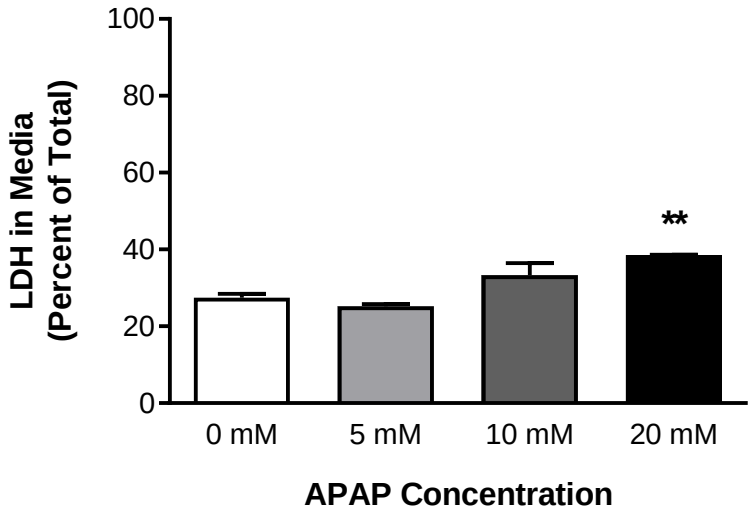

Figure 2.12. Overt cytotoxicity in primary rat hepatocytes is statistically significant following 24 h exposure to 20 mM APAP. Data are presented as the mean + SEM across 3 biological replicates assayed in triplicate. ** $p < 0.01$; one-way ANOVA with Dunnett's post-test relative to vehicle.

2.4.2 Human hepatocytes

We next sought to establish the appropriate concentration of APAP to stress primary human hepatocytes *in vitro* within 24 h. Freshly isolated primary hepatocytes were cultured as previously described and exposed to 5 mM APAP for 24 h. Cytotoxicity was determined by LDH leakage into medium and cellular ATP content using methods described in Holman *et al* 2016 (Figure 2.13).

The average fold change in LDH measured in culture medium following APAP exposure was 1.4 (representing an increase from 9 to 13% of total LDH in the system) and the average fold change in cellular ATP was 0.95 relative to controls. These alterations were minor and deemed to be biologically insignificant because in overt APAP hepatotoxicity, ATP, which is indicative of mitochondrial stress and energy imbalance, would be greatly decreased prior to the necrotic cell death indicated by increased LDH leakage. The lack of significant APAP cytotoxicity was supported by the fact that no changes in exosomal albumin mRNA were detected. We concluded that to induce biologically relevant hepatocellular stress in human hepatocytes within 24 h for the study of exosomal alterations, a concentration of 10 mM APAP would be required. Our results agree with published data from primary human hepatocytes which revealed that within 24 h, APAP does not cause significant LDH elevations until 30 mM (Kia *et al.*, 2015). Therefore, 10 mM APAP was used for subsequent primary human hepatocyte exposures.

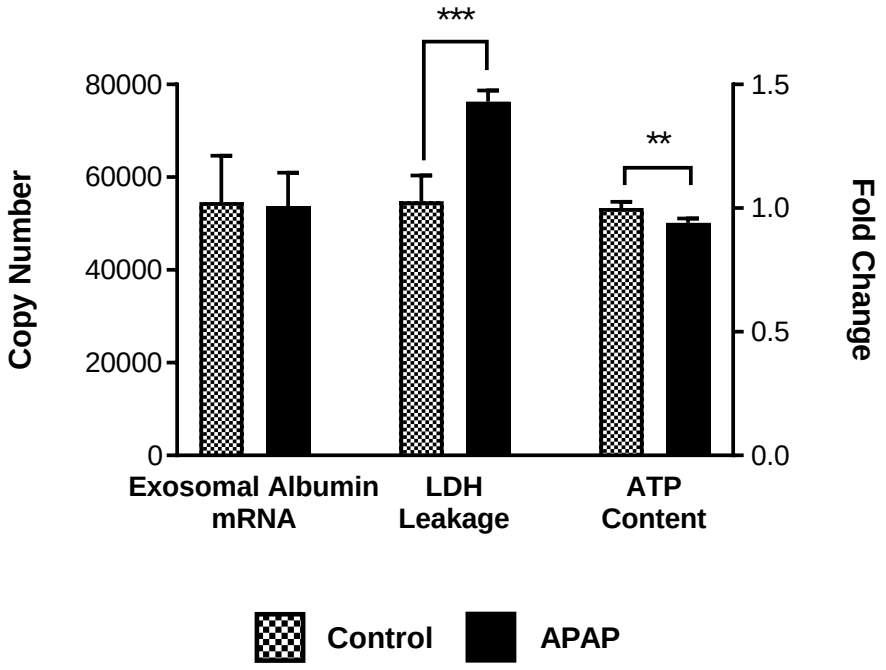

Figure 2.13. Overt cytotoxicity is not observed in primary human hepatocytes following 24 h exposure to 5 mM APAP. Data are presented as the mean + SEM across 3 biological replicates assayed in triplicate. ** $p < 0.01$, *** $p < 0.001$; one-way ANOVA with Dunnett's post-test relative to vehicle.

CHAPTER 3.

SUBTOXIC ALTERATIONS IN THE RNA CONTENT OF HEPATOCYTE-DERIVED EXOSOMES FROM HUMAN AND RAT MODELS OF DRUG-INDUCED LIVER INJURY[1]

3.1 Introduction

Drug-induced liver injury (DILI) is responsible for significant pre- and post-market drug failures and is the primary cause of acute liver failure in the United States and Europe (Bernal *et al.*, 2010; Ostapowicz *et al.*, 2002; Wilke *et al.*, 2007). DILI, therefore, represents a major economic and clinical challenge for patients, healthcare providers, and pharmaceutical companies. Identification of underlying mechanisms has proved especially difficult as DILI has been associated with hundreds of drugs that elicit a broad spectrum of injuries (Hornby *et al.*, 2014; Hussaini and Farrington, 2014). However, increasing evidence suggests that drug-induced hepatocellular death may often be mediated by immune responses (Adams *et al.*, 2010; Ju and Reilly, 2012; Russmann *et al.*, 2009). For example, human leukocyte antigen (HLA) genotype is a strong risk factor for DILI associated with a wide range of drugs, suggesting a role for the adaptive immune system in drug-mediated hepatotoxicity (Urban *et al.*, 2014). In addition, elevations in biomarkers that trigger an

[1] This chapter has been published as an original research article in Toxicological Sciences and is presented according to journal convention. The original citation is as follows: Holman *et al*. 2016. Sub-toxic alterations in hepatocyte-derived exosomes: an early step in drug-induced liver injury?, Toxicological Sciences, 151(2):365-375; Epub 2016 Mar 8.

innate immune response such as high mobility group box 1 (HMGB1), and those that are suggestive of immune cell activation including miR-155 and acetylated HMGB1, have been associated with DILI (Antoine *et al.*, 2014; Bala *et al.*, 2012; Fontana, 2014). Furthermore, immune reactions are triggered by hepatocellular danger signals, which can be released in the absence of hepatocyte death and communicate to other cell types as part of a stress response (Uetrecht and Naisbitt, 2013).

Extracellular vesicles released by hepatocytes, principally hepatocyte-derived exosomes (HDE), may constitute one such danger signal (Conde-Vancells *et al.*, 2008; De Maio, 2011; Royo and Falcon-Perez, 2012; Royo *et al.*, 2013). By virtue of their small size (<150 nm), HDE can readily cross through fenestrations in the sinusoidal endothelium and enter the bloodstream (Conde-Vancells *et al.*, 2008), carrying liver-specific contents that are modified during DILI (Wetmore *et al.*, 2010). Clinically relevant alterations in HDE content and quantity have been detected in multiple models of liver injury including viral hepatitis (Zhang *et al.*, 2014), alcoholic hepatitis (Momen-Heravi *et al.*, 2015b), non-alcoholic steatohepatitis (Hirsova *et al.*, 2016), cirrhosis, and hepatocellular carcinoma (Bernal *et al.*, 2010). Moreover, exosomes are immunomodulatory and can carry damage-associated molecular patterns (DAMPs), antigens, and cytokines to recipient cells (Beninson and Fleshner, 2014; De Maio, 2011; Liu *et al.*, 2006; Robbins and Morelli, 2014). In the liver, HDE released by hepatitis C-infected hepatocytes activate dendritic cells and those released during lipotoxicity influence macrophage phenotype (Dreux *et al.*, 2012; Hirsova *et al.*, 2016). Recent experiments have demonstrated that one means by which HDE evoke immune responses is the delivery of functional genetic material such as microRNA (miRNA) and messenger RNA (mRNA). For example, HDE-based RNA species miR-122 and albumin

mRNA (*ALB*) have been shown to activate recipient monocytes and fibroblasts, respectively (Momen-Heravi *et al.*, 2015a; Royo *et al.*, 2013).

HDE may play a critical role in the initiation of and response to DILI by transmitting signals of hepatocellular stress that directly or indirectly stimulate an immune response. For HDE to mediate early DILI events, we hypothesized that significant alterations in HDE content and/or number must occur prior to, or in the absence of, overt hepatocellular injury. To better understand the potential of HDE to modulate early immune-driven DILI events, we sought to establish that sub-toxic drug-induced HDE alterations were consistent *in vivo* and *in vitro*, and relevant in human DILI. Acetaminophen (APAP) was selected as the model hepatotoxicant due to its well-defined *in vivo* and *in vitro* toxicity profiles. We utilized this prototypical intrinsic hepatotoxicant for verification that the exosomes released by hepatocytes following drug exposure were altered in the absence of overt injury. Although the role of immune reactions in APAP-induced liver injury is controversial, there is recent evidence of induction of immune tolerance in healthy adults that do not develop ALT elevations after recurrent therapeutic doses of APAP (Fannin *et al.*, 2015), further supporting selection of APAP as our model toxicant. This finding also suggests that some stress-induced HDE alterations may promote an adaptive response to toxicity rather than an exacerbation of injury.

We therefore evaluated the dose- and time-dependent effects of APAP on HDE-associated RNAs in rats, primary rat hepatocytes, and primary human hepatocytes. Because exosomes in the blood are derived from multiple cell types, exosome-associated liver-enriched *ALB* mRNA and liver-specific miR-122 were assayed as a means to confirm the

presence of, and track alterations in, HDE across platforms (Bandiera *et al.*, 2015; Miyamoto *et al.*, 2008).

3.2 Materials and Methods

3.2.1 Animal exposures

Male Sprague-Dawley rats (Crl:SD), 7-9 weeks of age, were purchased from Charles River Laboratories and allowed to acclimate in-house for 7-10 days prior to study initiation. Water and food (pelleted PicoLab Rodent Diet 20 [Lab Diet]) were available *ad libitum* during this time. Food was removed during an 18 h fasting period immediately prior to compound administration. APAP (Sigma-Aldrich) was administered in 0.5% (w/v) methylcellulose (Sigma-Aldrich) at 0, 500, or 1400 mg/kg by oral gavage. After dosing, food was provided *ad libitum* until necropsy. Studies were conducted in accordance with the Guide for the Care and Use of Laboratory Animals, and were approved by the Mispro Institutional Animal Care and Use Committee (Mispro Biotech Services Inc.).

3.2.2 Necropsy and histology

Rats were euthanized by CO_2 inhalation and subsequent exsanguination at 0, 1, 2, 4, 8, 12, and 24 h post-dose (n=6 per group). Blood was collected in K_2EDTA Vacutainer® tubes (Becton Dickinson). Portions of the liver (median lobe) were minced and placed in RNAlater® Stabilization Solution (Applied Biosystems) for gene expression analysis. Sections from the left and median lobes were fixed in 10% neutral buffered formalin followed by 70% ethanol. Paraffin-embedded blocks were sectioned (5 µm) and stained with hematoxylin and eosin (H&E). Histopathological examination was performed by a board-

certified veterinary pathologist. Severity scores were assigned for centrilobular degeneration and necrosis (+1, minimal; +2, mild; +3, moderate; +4, marked). Degeneration was defined as pre-necrotic hepatocellular change in centrilobular areas, including cytoplasmic hypereosinophilia, nuclear condensation and cellular dissociation. Degeneration is assumed to precede fulminant necrosis such that, if given more time, degenerating cells likely would have progressed to necrosis. Necrosis was marked by areas of complete hepatocellular destruction and neutrophil infiltration.

3.2.3 Plasma isolation and plasma-derived exosome enrichment

Within 15 min of collection, blood was centrifuged to obtain cell-free plasma. Alanine aminotransferase (ALT) activity in fresh plasma was determined using a CLC 720 clinical chemistry analyzer (Carolina Liquid Chemistries). Additional aliquots of plasma were frozen at -80ºC until exosome isolation. Thawed plasma was treated with Purified Thrombin Plasma Reagent and exosomes were isolated with ExoQuick™ Exosome Precipitation Solution (System Biosciences) according to the manufacturer's instructions. The post-ExoQuick supernatant was reserved for RNA isolation to analyze liver-specific RNAs in the extra-exosomal, protein-rich plasma fraction.

3.2.4 Primary hepatocyte culture and medium-derived exosome enrichment

Freshly isolated primary hepatocytes from human donors (n=7; Table 3.1) and male Sprague-Dawley rats (n=3) were obtained from commercial sources (QPS Hepatic Biosciences and Triangle Research Labs). Individual batches of fresh hepatocytes were seeded into 12-well plates coated with collagen type I (Corning) at a density of 0.9×10^6 cells per well in hepatocyte plating medium (William's E medium, penicillin-streptomycin,

GlutaMax™, HEPES, sodium pyruvate, fetal bovine serum [Thermo Fisher Scientific], insulin, and dexamethasone [Sigma-Aldrich]). Culture plates were incubated at 37ºC with 5% CO_2. After attachment, non-adherent cells were removed and fresh plating medium was added. Cultures were transitioned to hepatocyte maintenance medium without fetal bovine serum after 3-4 h. Following a 24 h acclimation period, hepatocyte cultures were exposed to APAP or a medium control (vehicle) for 24 h. All conditions were tested in triplicate culture wells for each rat or human donor.

Hepatocyte-conditioned medium (1-2 ml) was collected after 24 h and clarified by centrifugation at 3000*g* for 15 min. Exosomes were precipitated from medium with ExoQuick-TC™ (System Biosciences) following the protocol for this sample type. LDH activity was assayed with a Cytotoxicity Detection Kit (Roche) as described previously (Kia *et al.*, 2015). Cellular ATP content was measured with CellTiter-Glo® Luminescent Cell Viability Assay (Promega) according to the manufacturer's instructions. Data were collected using a SpectraMax® M3 microplate reader (Molecular Devices).

Table 3.1 Characteristics of primary human hepatocyte donors.

Age (yr)	BMI	Sex	Race
<1	15	M	African-American
3	17	M	Caucasian
14	24	F	Caucasian
26	32	M	Caucasian
30	33	F	African-American
48	24	F	Caucasian
74	23	F	Caucasian

3.2.5 Extracellular vesicle characterization and validation of exosome enrichment

Nanoparticle tracking analysis

Nanoparticle tracking analysis was performed on exosomes produced *in vitro* using a NanoSight NS500 (Malvern Instruments). The instrument was calibrated using polystyrene bead standards (100 nm) before each use (Malvern Instruments). Diluted samples were advanced through the detection chamber to obtain 5 readings per sample, each with a capture period of 60 sec. Particle concentration and size were determined using NTA software version 3.0 (Malvern Instruments).

Electron microscopy

Exosomes were precipitated from filtered (0.2 μm PES) hepatocyte-conditioned culture medium using ExoQuick-TC. Exosome preparations were diluted 1:1000 in Dulbecco's phosphate buffered saline (DPBS) to start the assembly reaction. At 10 min, samples were applied to glow-discharged 200 mesh Quantifoil R 2/1 grids (Electron Microscopy Sciences), blotted briefly, and plunged into liquid ethane as described previously (Dokland, 2006). The frozen grids were transferred to a Gatan 622 cryo-holder and imaged using an FEI Tecnai™ F20 transmission electron microscope, operated at 200 kV with magnifications from 5,000x to 29,000x and defocus settings of -6.0 to -10.0 μm. Images were collected on a Gatan Ultrascan™ 4000 CCD camera.

Immunoblot analysis

Protein extracts were prepared from hepatocyte monolayers or exosomes using RIPA Lysis and Extraction Buffer (Thermo) with Halt Protease Inhibitor Single-Use Cocktail (Thermo) and Triton X-100 (hepatocytes only). Protein concentration was determined using the BCA Protein Assay Kit (Thermo). Equal protein quantities of each sample were

separated on 4-12% NuPAGE Bis-Tris gels (Life Technologies) and transferred to Immobilon®-FL PVDF membranes (Millipore). Membranes were blocked with either 5% (w/v) non-fat dry milk in PBS or Odyssey PBS Blocking Buffer (Licor Biosciences). The following primary antibodies were used for immunoblotting: Flotillin-1 (BD Transduction Laboratories), CD63 (Abcam), CD81 (AbD Serotech), Prohibitin-1 (Santa Cruz Biotechnology Inc.), and Grp78 (BD Transduction Laboratories). Proteins were detected using IRDye secondary antibodies (Licor Biosciences) or Alexa Fluor® 680-conjugated AffiniPure IgG (Jackson Immunoresearch Laboratories). Blots were imaged using an Odyssey® Classic Imaging System (Licor Biosciences).

3.2.6 Total RNA isolation and analysis by absolute qRT-PCR

Total RNA was isolated from plasma- and culture medium-derived exosomes using the miRCURY Cell & Plant Isolation Kit (Exiqon) according to the manufacturer's instructions for RNA isolation from blood. To analyze extracellular RNA in the protein-rich compartment of culture medium and plasma, total RNA was isolated from culture medium samples or post-ExoQuick plasma supernatants, respectively, using the miRNeasy Serum/Plasma Kit (Qiagen) and manufacturer's protocol. Total RNA from rat liver, rat hepatocytes, and human hepatocytes was isolated with the miRNeasy Mini Kit (Qiagen) according to the manufacturer's instructions. For all RNA isolations, a spike-in cocktail consisting of linear acrylamide carrier (Applied Biosystems) and exogenous RNA controls, Luciferase mRNA mimic (Promega) and *C. elegans* miR-39 (Qiagen), was added.

Synthesis of cDNA for mRNA analysis was performed with equal volumes of RNA using a High-Capacity cDNA Reverse Transcription Kit (Applied Biosystems). Quantitative

real-time PCR (qRT-PCR) was performed on a 7900HT Fast Real-Time PCR System (Applied Biosystems) using TaqMan® Gene Expression Assays and Fast Advanced Master Mix. Absolute quantities of mRNAs were calculated using a species-matched standard curve generated from bacterial plasmids or PCR amplification of liver cDNA. Synthesis of cDNA for analysis of miR-122 copy number was performed using a TaqMan® miRNA Reverse Transcription Kit (Applied Biosystems). Absolute qRT-PCR was performed on a 7900HT Fast Real-Time PCR System (Applied Biosystems) using TaqMan® MicroRNA Assays (hsa-mir-122-5p) and Universal Master Mix II (no UNG). Absolute quantities of miR-122 in cells, exosomes, and the protein-rich fraction were computed from a standard curve of synthetic miR-122 cDNA.

3.2.7 Statistical analysis

Analyses were conducted using GraphPad Prism 6 (GraphPad Software, Inc.) unless otherwise noted. For all tests, $p<0.05$ was considered statistically significant. Mean values from plasma-based endpoints (i.e. exosomal RNA and ALT activity) were analyzed using a two-way analysis of variance (ANOVA). Results from APAP-treated animals were compared to time-matched control groups with Fisher's Least Significant Difference (Fisher's LSD) test. *In vitro* data from rat hepatocytes were averaged across triplicate wells and a fold change relative to control was calculated for each rat. Fold changes across rats (n=3) were averaged and compared by one-way ANOVA. Results from each APAP concentration were compared to controls using Dunnett's test for multiple comparisons. *In vitro* data from each human hepatocyte batch were averaged across triplicate wells and a fold change relative to donor-matched controls was calculated. From individual fold changes, a

mean across all donors was obtained. Mean fold changes of control and APAP-treated groups were compared by Student's two-tailed t-test.

3.3 Results

3.3.1 Exosomal albumin transcript quantities are significantly elevated prior to APAP-induced hepatic necrosis in rats

Adult male Sprague-Dawley rats were administered a low (500 mg/kg) or high (1400 mg/kg) dose of APAP or a vehicle control and were sacrificed at 0, 1, 2, 4, 8, 12, or 24 h post-dose. Liver injury was determined by histology and plasma ALT activity. Liver-specific RNAs isolated from circulating exosomes were quantified to determine the relationship between hepatocyte-derived exosome (HDE) alterations and liver injury. Histological findings of necrosis (Figure 3.1; Table 3.2) and elevated plasma ALT activity (Figures 3.2, 3.3) were observed only in rats treated with the high dose of APAP at 24 h post-exposure. Exosomal albumin transcript (*ALB*) quantity, however, was significantly elevated in APAP-treated animals (relative to time-matched, vehicle-treated controls) prior to histological observations of necrosis or increases in plasma ALT (Figures 3.2, 3.3). Drug-induced elevations in mean exosomal *ALB* quantity were detected as early as 4 h post-dose; these elevations became dose-dependent at 8 h post-dose. By 12 h, mean exosomal *ALB* mRNA had increased 30- and 50-fold in the low- and high-dose groups, respectively (Figure 3.2). Increases in exosomal *ALB* reached statistical significance in the high dose group at 12 h and in the low dose group at 24 h, without signs of liver injury (Figures 3.2, 3.3). Together, these data suggest that changes in HDE release occur as a result of sub-toxic APAP exposure *in vivo*.

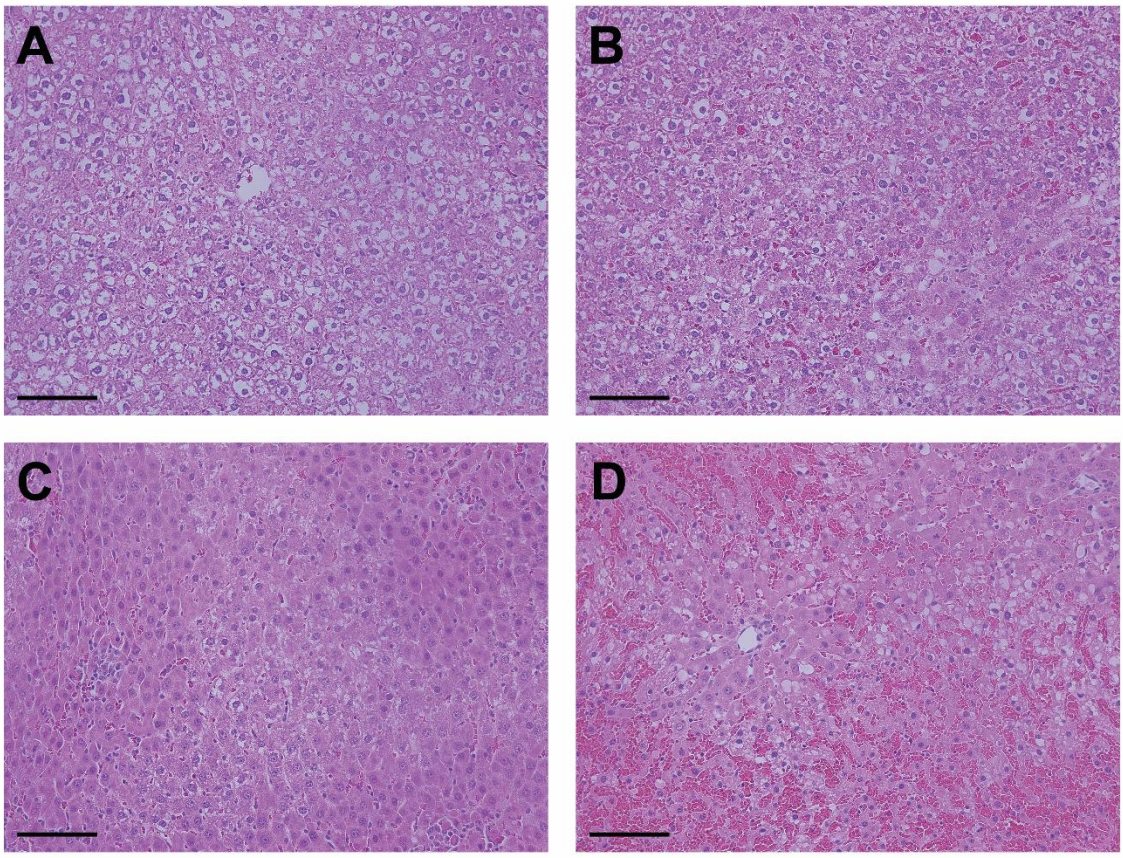

Figure 3.1. Histopathology of rat liver sections 24 h after APAP treatment. Representative photomicrographs of H&E stained liver sections from rats 24 h after administration of (A) 0.5% methylcellulose vehicle, (B) 500 mg/kg APAP, or 1400 mg/kg APAP with (C) moderate or (D) marked centrilobular necrosis. Bars indicate 200 µm.

Table 3.2. Histopathological scoring of APAP-treated rat livers stained with H&E. Scoring: +1, minimal; +2, mild; +3, moderate; +4, marked. *, indicates outlier removed from data set.

Treatment (mg/kg)	Time (h)	Score:	Number of animals								
			No findings	Centrilobular degeneration				Centrilobular necrosis			
			0	+1	+2	+3	+4	+1	+2	+3	+4
0	4		6	0	0	0	0	0	0	0	0
500	4		6	0	0	0	0	0	0	0	0
1400	4		0	6	0	0	0	0	0	0	0
0	8		6	0	0	0	0	0	0	0	0
500	8		5	0	0	0	0	0	0	0	1*
1400	8		1	4	1	0	0	0	0	0	0
0	12		6	0	0	0	0	0	0	0	0
500	12		6	0	0	0	0	0	0	0	0
1400	12		1	2	3	0	0	0	0	0	0
0	24		6	0	0	0	0	0	0	0	0
500	24		2	2	0	1	0	0	0	1	0
1400	24		0	1	0	0	0	1	1	2	1

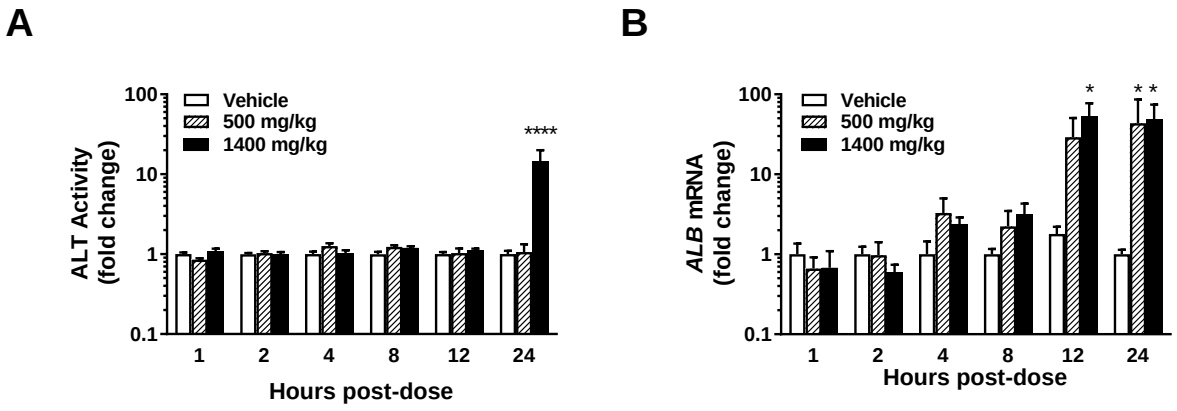

Figure 3.2. *In vivo* elevations in ALT activity and exosomal *ALB* as a function of APAP dose and exposure time. APAP-induced elevations in (A) plasma ALT activity and (B) exosomal *ALB* mRNA. Data are presented as mean + SEM of fold change over time-matched controls (n=5-6 rats/group). * $p < 0.05$, **** $p < 0.0001$; two-way ANOVA with Fisher's LSD.

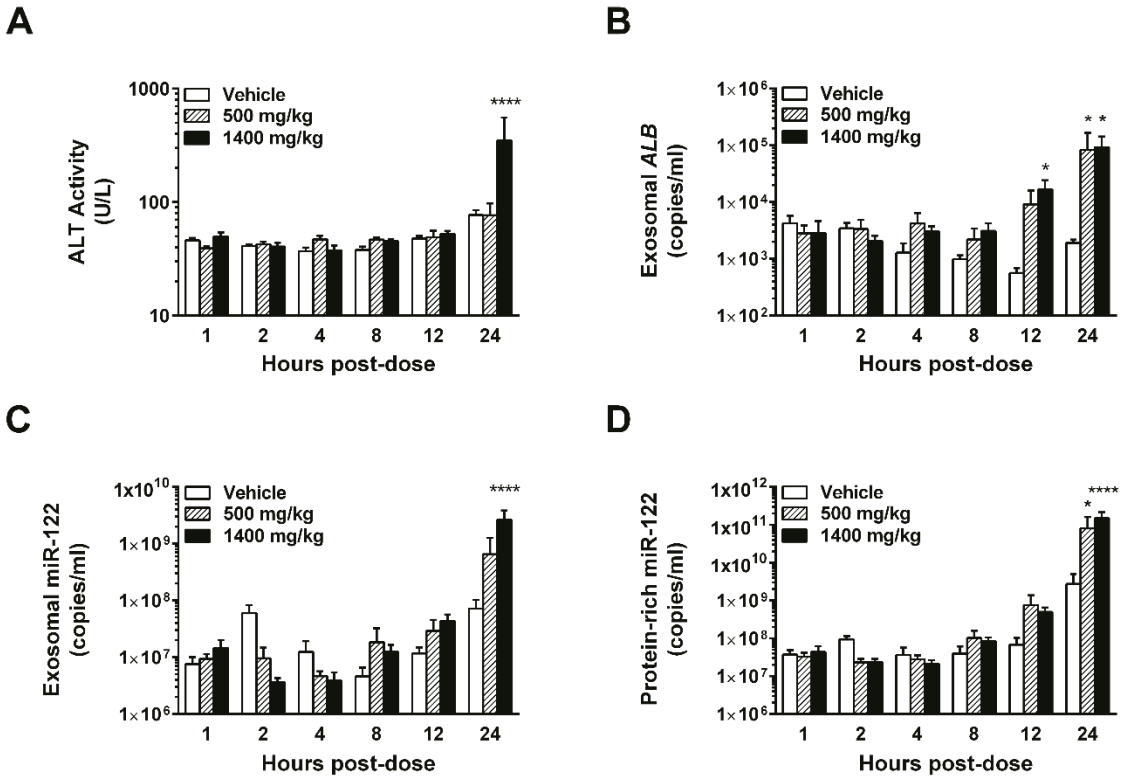

Figure 3.3. Absolute values of ALT activity and circulating liver-specific RNAs as a function of APAP dose and exposure time *in vivo*. APAP-induced elevations in (A) plasma ALT activity, (B) exosomal *ALB* mRNA copy number, (C) exosomal miR-122 copy number, and (D) protein-rich miR-122 copy number. Data are presented as mean + SEM (*n*=5-6 rats/group). * $p < 0.05$, **** $p < 0.0001$; two-way ANOVA with Fisher's LSD.

3.3.2 Quantity and distribution of extracellular miR-122 are altered by sub-toxic APAP exposure *in vivo*

Unlike *ALB* mRNA which was not detected outside of the exosomal plasma fraction (data not shown), circulating miR-122 is stable in exosomes and in a "protein-rich" Argonaute-bound form (Arroyo *et al.*, 2011; Hornby *et al.*, 2014). In order to determine if miR-122 followed a similar trend as exosomal *ALB* upon *in vivo* APAP exposure, we measured exosomal and protein-rich fractions of circulating miR-122. A trend toward increased exosomal miR-122 was observed in APAP-treated animals at 8 h post-dose (Figures 3.3, 3.4). This trend continued, with mean levels reaching 3- and 4-fold over controls in the low- and high-dose groups at 12 h, respectively. At 24 h post-dose, mean exosomal miR-122 quantities in the low-dose group reached 9-fold that of vehicle-treated controls, despite a lack of hepatocellular toxicity. miR-122 in the protein-rich fraction showed trends similar to exosomal miR-122 but was significantly elevated in the low-dose group after 24 h (Figures 3.3, 3.4). Whereas the content of miR-122 in both exosomal and protein-rich compartments was increased by APAP exposure in our study, the distribution of miR-122 between these plasma compartments shifted over time. In the high-dose group, the percentage of circulating miR-122 within HDE decreased over time and reached statistical significance at 12 h, prior to overt liver injury (Figure 3.4).

Unexpectedly, we observed previously undocumented dose-dependent decreases in exosomal and protein-rich miR-122 fractions after 2 h of APAP exposure, which were not accompanied by decreases in exosomal *ALB* (Figure 3.4). To determine whether the decreases in exosomal miR-122 reflected selective packaging of RNA into HDE or decreased hepatocyte miR-122 content, we quantified miR-122 in liver tissue obtained from the 2 h

post-exposure animals. There was a trend toward increased hepatic miR-122 copy number coincident with statistically significant dose-dependent decreases in exosomal miR-122 (Figure 3.4). Exosomal *ALB*, however, was not significantly affected in circulating exosomes or liver tissue.

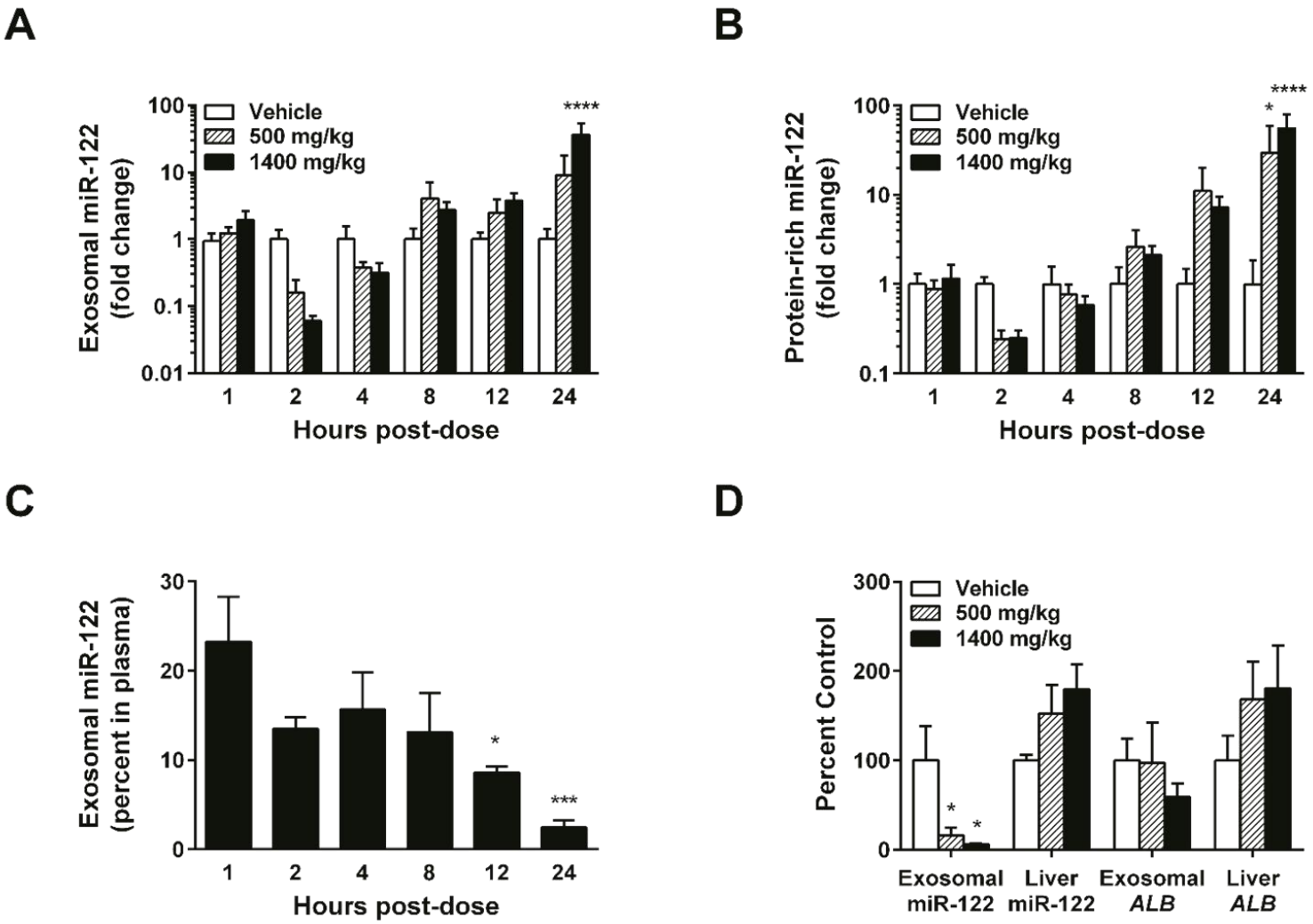
A
Exosomal miR-122
(fold change)
Vehicle
500 mg/kg
1400 mg/kg
100
10
1
0.1
0.01
****
1
2
4
8
12
24
Hours post-dose
B
Protein-rich miR-122
(fold change)
Vehicle
500 mg/kg
1400 mg/kg
100
10
1
0.1
*
****
1
2
4
8
12
24
Hours post-dose
C
Exosomal miR-122
(percent in plasma)
30
20
10
0
*
***
1
2
4
8
12
24
Hours post-dose
D
Percent Control
Vehicle
500 mg/kg
1400 mg/kg
300
200
100
0
*
*
Exosomal miR-122
Liver miR-122
Exosomal ALB
Liver ALB

Figure 3.4. Alterations in exosomal and protein-rich fractions of miR-122 following *in vivo* APAP exposure. Fold change in (A) exosomal and (B) protein-rich miR-122 plasma compartments relative to time-matched vehicle controls (*n*=5-6 rats/group). * $p < 0.05$, **** $p < 0.0001$; two-way ANOVA with Fisher's LSD. (C) Percentage of circulating miR-122 in HDE from 1400 mg/kg APAP-treated rats. * $p < 0.05$, *** $p < 0.001$; one-way ANOVA with Dunnett's post-test relative to t=1 h. (D) Relationship between liver-specific RNAs measured in exosomes and liver tissue at 2 h post-dose. * $p < 0.05$; one-way ANOVA with Dunnett's post-test relative to vehicle. Data are presented as mean + SEM.

3.3.3 EV preparations from primary rat and human hepatocyte cultures are highly enriched for exosomes

We selected a well-characterized exosome enrichment method for our *in vivo* studies, and evidence suggests that most extracellular vesicles (EV) released by hepatocytes are exosomal in size (Giugliano *et al.*, 2015; Koeck *et al.*, 2014; Momen-Heravi *et al.*, 2015a; Royo *et al.*, 2013). However, multiple cell types and tissues contribute to the population of circulating vesicles, and therefore we could not study the nature of hepatocyte-specific vesicles isolated from the *in vivo* samples. To confirm the presence of exosomes in EVs isolated by ExoQuick, we analyzed the size, morphology, and protein enrichment of EVs produced *in vitro* by primary rat and human hepatocytes.

EVs were isolated from conditioned medium of untreated primary rat or human hepatocytes by ExoQuick-TC polymer precipitation. Nanoparticle tracking analysis of rat and human EV preparations revealed a majority of small exosome-sized particles less than 200 nm in diameter, with the greatest concentration of particles being less than 100 nm in size (Figure 3.5). These results were confirmed using a ZetaView® instrument (ParticleMetrix) (data not shown). Cryo-electron microscopy verified exosome enrichment in precipitated rat and human EV preparations, which contained circular membrane-bound vesicles smaller than 100 nm (Figure 3.5).

Western immunoblot analyses of rat EVs confirmed the presence of exosomal protein markers CD81 and CD63 (Figure 3.5). Prohibitin-1, a mitochondrial membrane protein, was detected in rat hepatocytes but was not present in rat HDE, suggesting a lack of cellular contamination in exosomal samples (Figure 3.5). Human EV preparations were positive for exosomal markers CD63 and Flotillin-1 and did not contain detectable cellular

contamination, as measured by Prohibitin-1 and Grp78, a protein found in the endoplasmic reticulum (Figure 3.5). These results confirm that our ExoQuick preparations contain mostly HDE.

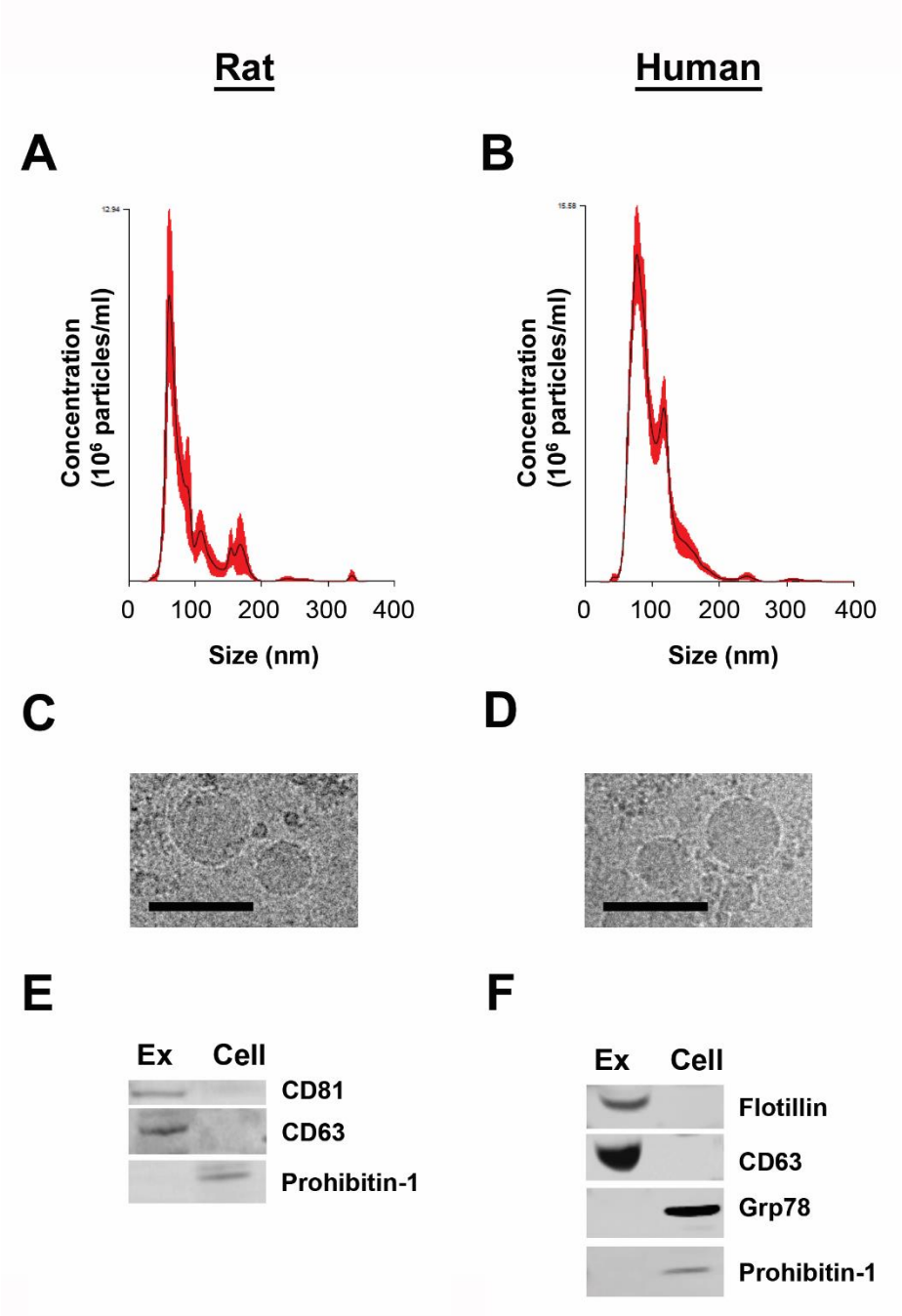

Figure 3.5. Characterization of exosome enrichment in extracellular vesicles secreted by primary rat and human hepatocytes. Representative nanoparticle tracking analyses illustrating the average size distribution of EVs isolated from untreated (A) rat and (B) human hepatocyte-conditioned culture medium; red indicates SEM. Representative cryo-electron micrographs of (C) rat and (D) human hepatocyte-derived EV preparations. Bars indicate 100 nm. Western blot analysis of exosomal and cellular markers in (E) rat and (F) human HDE ("Ex") relative to hepatocytes ("Cell").

3.3.4 Sub-toxic APAP exposure elicits exosomal RNA elevations in primary rat hepatocytes

To further characterize HDE release from drug-treated hepatocytes, we explored whether APAP-dependent changes in exosomal RNA content observed *in vivo* could be reproduced in monocultures of primary rat hepatocytes. Primary rat hepatocytes were exposed to a concentration range of APAP (0-30 mM) for 24 h. Across 3 rat hepatocyte batches, statistically significant elevations in LDH leakage and decreases in cellular ATP were not observed at concentrations less than 30 mM APAP (Figure 3.6). However, statistically significant increases in exosomal *ALB* mRNA were evident at concentrations as low as 1.1 mM APAP (Figure 3.6). Hepatocellular *ALB* levels were not altered significantly at any APAP concentration, suggesting that increased exosomal *ALB* was not a result of increased expression at the cellular level. In contrast to our *in vivo* findings, miR-122 was not elevated significantly in the exosome- or protein-rich fractions prior to the onset of overt cytotoxicity (Figure 3.6).

We then tested the hypothesis that liver-specific exosomal RNA levels are indicative of HDE number, which cannot currently be assessed *in vivo*. We performed nanoparticle tracking analysis on HDE from primary rat hepatocyte cultures exposed to 0, 10, or 30 mM APAP for 24 h (n=2 rats). No statistically significant changes in HDE quantity were observed at any concentration (Figure 3.6).

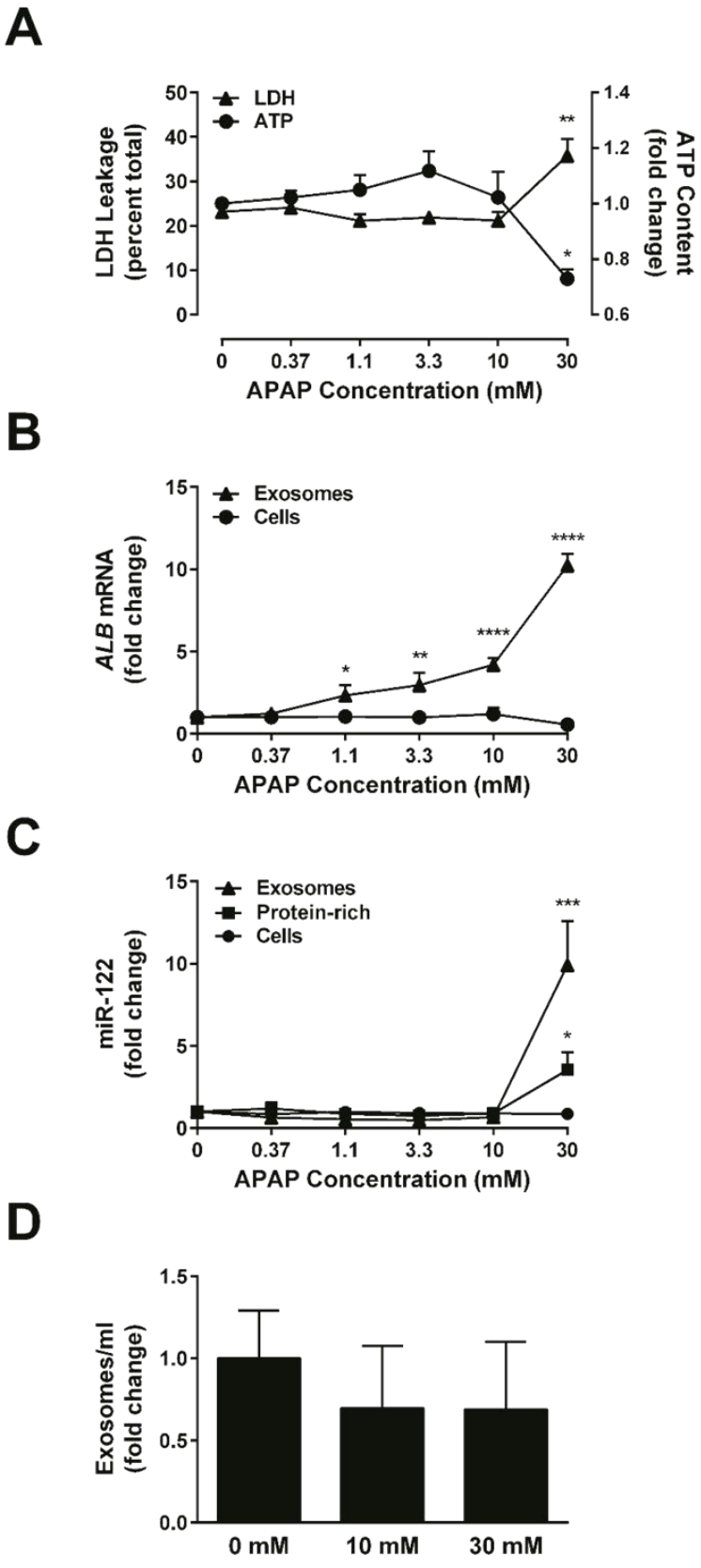

Figure 3.6. APAP-induced alterations in exosomes released by primary rat hepatocytes. Data are presented as mean + SEM (*n*=3 rats) after 24 h APAP exposure. (A) Cytotoxicity, as indicated by cellular ATP and LDH activity in medium. (B) Exosomal and cellular levels of *ALB* in response to APAP. (C) miR-122 in exosomal, protein-rich, and cellular fractions in response to APAP. * $p < 0.05$, ** $p < 0.01$, *** $p < 0.001$, **** $p < 0.0001$; one-way ANOVA with Dunnett's post-test relative to vehicle. (D) Nanoparticle tracking analysis on HDE preparations from primary rat hepatocytes (*n*=2 rats) following 24 h incubation with APAP. Data are presented as the mean + SEM of fold change in exosomes/ml relative to control. No statistically significant differences in exosome quantity between treated and untreated groups were observed; one-way ANOVA with Dunnett's post-test relative to vehicle.

3.3.5 Increased secretion of exosomal RNA in the absence of overt APAP toxicity translates to primary human hepatocyte cultures

To determine whether primary human hepatocytes would respond to APAP exposure by increasing production of exosomal RNAs, we separately exposed individual batches of freshly isolated primary hepatocytes (n=7 donors) to a sub-toxic APAP concentration (10 mM) for 24 h (Figure 3.7). APAP treatment caused increases in mean exosomal *ALB* (not statistically significant) and miR-122 (p<0.001) levels in the absence of overt injury (Figure 3.7). Quantities of *ALB* and miR-122 in cells and protein-rich medium fractions were not affected by APAP exposure (Figure 3.7).

To define the relationship between drug-induced changes in liver-specific exosomal RNA and HDE number in a human system, nanoparticle tracking analysis was performed on exosomes isolated from control and treated (0 vs. 10 mM APAP) primary human hepatocyte cultures (n=4 donors). As observed in the rat experiments, APAP exposure did not cause statistically significant changes in exosome quantity (Figure 3.7).

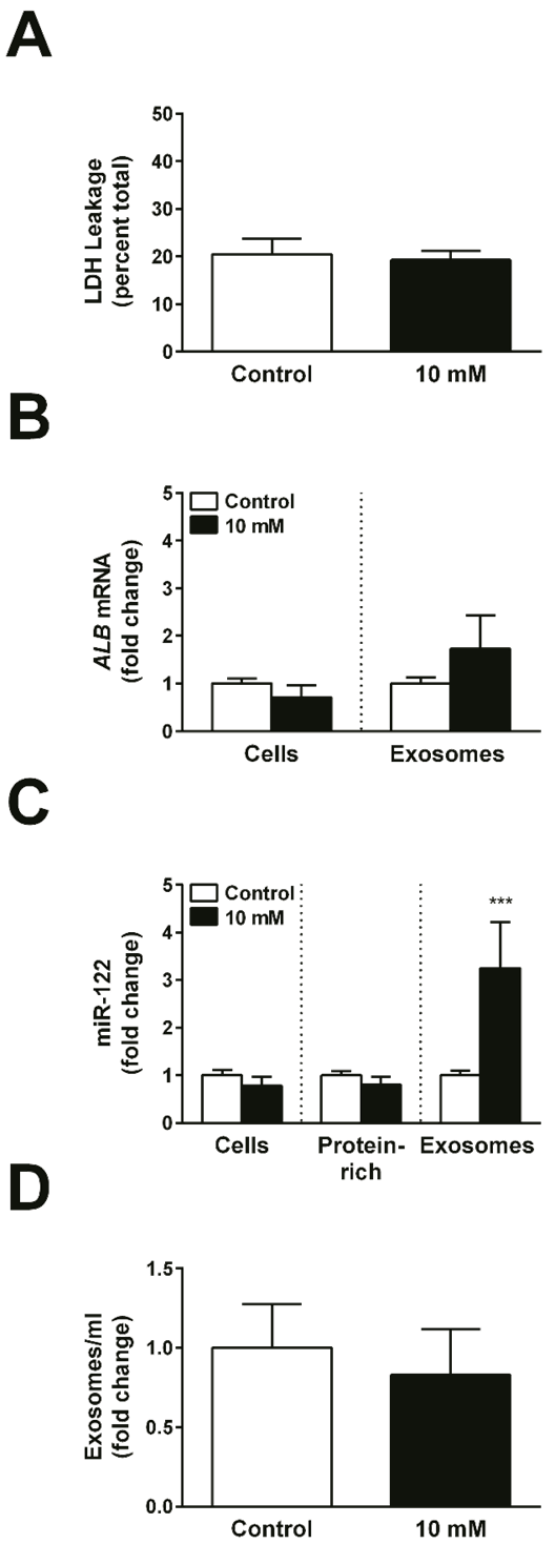

Figure 3.7. Alterations in exosomes released by primary human hepatocytes with and without APAP exposure. (A) LDH leakage, (B) *ALB* mRNA, and (C) miR-122 after 24 h of exposure to APAP (10 mM). Data are presented as the mean + SEM across 7 donors. *** $p < 0.001$; Student's t-test comparing treatment and control. (D) Nanoparticle tracking analysis on HDE preparations from primary human hepatocytes (n=4 donors) after 24 h incubation with APAP. Data are presented as the mean + SEM of fold change in exosomes/ml relative to control. No statistically significant differences in exosome quantity between treated and untreated groups were observed; Student's t-test.

3.3.6 Establishing baseline quantities of liver-specific RNAs in exosomes from primary human hepatocytes

Individual lots of primary human hepatocytes (*n*=7) were cultured for 24 h with or without 10 mM APAP. Substantial donor-to-donor variability in the exosomal quantities of *ALB* and miR-122 was apparent. To identify donor characteristics that potentially influenced exosomal content, we related characteristics such as sex, age, BMI, and race to the quantity of liver-specific exosomal RNAs from medium control- and APAP-treated hepatocytes (Figure 3.8). No association reached statistical significance, but we observed a relationship between exosomal *ALB* and BMI (p=0.074, regression analysis) in untreated hepatocytes (Figure 3.8).

In an effort to establish healthy ranges of exosomal *ALB* and miR-122, we examined absolute copy numbers of these exosomal RNAs across hepatocyte donors (*n*=7) under control conditions. We found that quantities of exosomal miR-122 generally corresponded with levels of protein-rich miR-122, although this relationship did not hold true for every donor (Figure 3.9). We did not observe a consistent relationship between exosomal and cellular *ALB*. Absolute copy numbers of exosomal miR-122 ranged from approximately 10^7-10^9, while exosomal *ALB* ranged from approximately 10^3-10^6 (Figure 3.9).

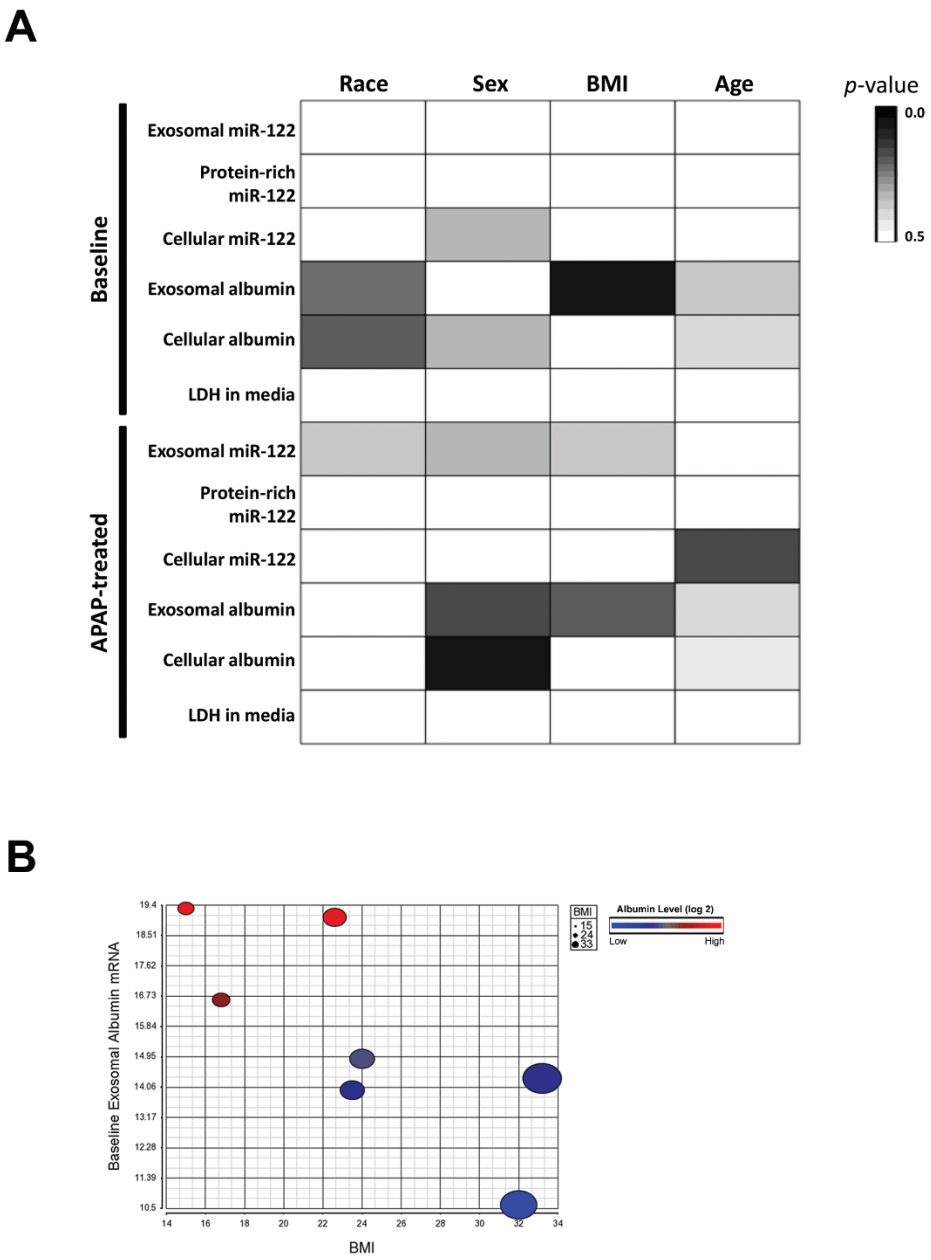

Figure 3.8. Relationships between human donor characteristics and HDE endpoints before and after *in vitro* APAP exposure. (A) Data are presented as *p*-values obtained by Student's t-test (categorical variables) or regression (continuous variables); darker cells indicate lower *p*-values. The most significant relationship was observed between BMI and baseline exosomal *ALB* quantity (p=0.074). (B) High BMI (indicated by circle size) corresponded to lower exosomal *ALB* (indicated by circle color).

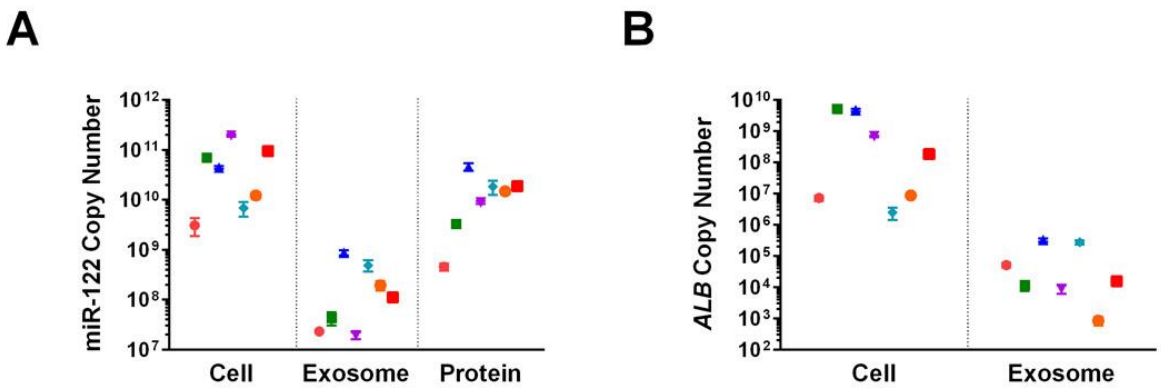

Donor	Age (yr)	BMI	Sex	Race
●	3	17	M	Caucasian
■	30	33	F	African-American
▲	< 1	15	M	African-American
▼	48	24	F	Caucasian
◆	74	23	F	Caucasian
●	26	32	M	Caucasian
■	14	24	F	Caucasian

Figure 3.9. Quantification of miR-122 and *ALB* mRNA in HDE from untreated primary human hepatocytes. Absolute copy numbers of (A) miR-122 and (B) *ALB* mRNA in cellular, exosomal, and protein-rich ("protein") fractions from 7 primary human hepatocyte donors. Data represent the mean + SEM of triplicate culture wells for each donor. Corresponding age, BMI, sex, and race are also presented.

3.3.7 Additional liver-enriched transcripts are present in human hepatocyte-derived exosomes

Finally we sought to confirm that additional liver-enriched mRNAs previously identified in rat EVs, and enriched in both rat and human liver, were packaged within human HDE (Miyamoto *et al.*, 2008; Okubo *et al.*, 2013; Royo *et al.*, 2013; Yu *et al.*, 2010). Exosomes were precipitated from the culture medium of untreated primary human hepatocytes (n=3 lots), and exosomal transcripts were quantified by absolute qRT-PCR. All 7 liver-enriched transcripts were detected in human HDE under control conditions, and although the absolute amounts varied, the relative proportions of each mRNA across donors were consistent (Figure 3.10).

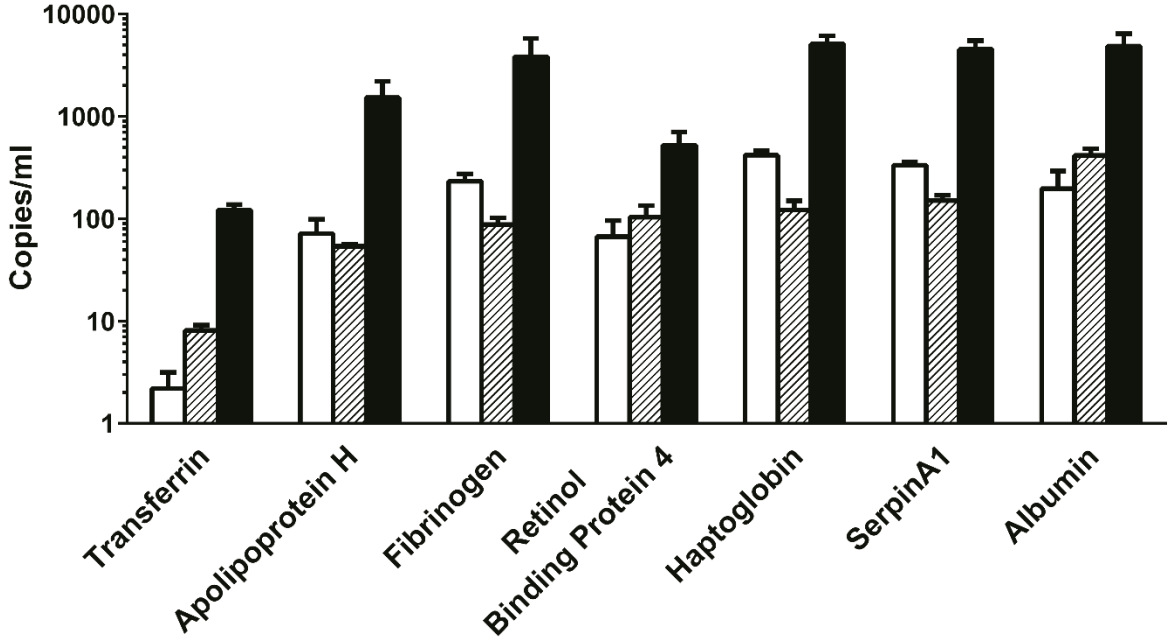

Figure 3.10. Analysis of additional liver-enriched transcripts within exosomes released by untreated primary human hepatocytes. Bar color denotes different donors (*n*=3). Data represent the mean + SEM of exosomal mRNAs across triplicate culture wells for each donor. Transcript quantities are expressed as exosomal copy number per ml of culture medium used to isolate HDE.

3.4 Discussion

To determine whether HDE could mediate the immune reactions that occur without overt hepatotoxicity following drug exposure, we tested the hypothesis that HDE content and/or number would be altered by drug-induced hepatocellular stress in the absence of cell death. We found that the RNA content of HDE was affected prior to, and in the absence of, overt hepatocellular injury in rats receiving both toxic and sub-toxic doses of APAP. These results translated across experimental models and species as similar phenomena were observed in primary hepatocyte cultures from both rats and humans.

APAP was selected for this work largely for its defined toxicity profile *in vivo* and in cultured hepatocytes from both rats and humans. Although we are ultimately interested in the role of exosomes in immune signaling, the current study does not address the consequences of the immune component of APAP-induced hepatotoxicity, a topic that remains controversial. Whether advantageous (Antoniades *et al.*, 2012; Jaeschke *et al.*, 2012; Ju *et al.*, 2002; Williams *et al.*, 2014) or damaging (Fannin *et al.*, 2015; Ferreira *et al.*, 2016; Huebener *et al.*, 2015; Tujios and Fontana, 2011), there is no question that inflammatory and immune responses are associated with APAP-induced hepatotoxicity in humans. In a study of recurrent therapeutic APAP dosing, activation of immune tolerance was evident in the peripheral blood transcriptome of healthy adults without APAP-induced ALT elevations (Fannin *et al.*, 2015). This suggests that immune responses after APAP exposure manifest prior to overt hepatocellular injury, a process that likely involves sub-toxic hepatocellular release of stress signals such as HDE.

Although mouse models are generally considered to be more appropriate for the study of APAP-induced hepatotoxicity mechanisms (Jaeschke *et al.*, 2014; McGill *et al.*, 2012), the

goal of the current work was to evaluate early changes in HDE that occur during APAP-induced stress, prior to hepatocellular injury. Therefore, the rat was intentionally selected as a relatively resistant preclinical species to extend the duration of APAP-induced stress *in vivo* so that HDE alterations could be observed prior to overt DILI. Evidence suggests that this latency may be more similar to humans than the latency to fulminant hepatotoxicity observed in mice (Jaeschke *et al.*, 2014). Because mouse hepatocytes are difficult to culture, selection of a rat model also facilitated comparisons of data collected from primary hepatocytes relative to *in vivo* data from the same species.

In the current study, we selected liver-specific exosomal contents *ALB* mRNA and miR-122 as translational markers of HDE alteration that also elicit immunologically relevant responses when transferred to other cell types (Momen-Heravi *et al.*, 2015a; Royo *et al.*, 2013). Circulating *ALB* mRNA and miR-122 have been identified previously as more sensitive and specific biomarkers of liver injury in both preclinical species and humans (Antoine *et al.*, 2013; Okubo *et al.*, 2013; Starckx *et al.*, 2013; Wang *et al.*, 2009; Zhang *et al.*, 2014). In particular, the value of miR-122 in peripheral blood as a biomarker of APAP overdose is well established (Antoine *et al.*, 2013). Therefore, the biomarker potential of miR-122 and HDE was not a focus of the current work.

In our *in vivo* rat model of APAP-induced liver injury, the proportion of plasma miR-122 contained within exosomes decreased over time in the high dose group, presumably as a function of increased hepatocellular damage. These data are in agreement with what is known about the active nature of exosome release and the passive, necrotic release of protein-rich miR-122 (Bobrie *et al.*, 2011; Dear and Antoine, 2014; Kia *et al.*, 2015; Turchinovich *et al.*, 2013; Turchinovich *et al.*, 2011; Villarroya-Beltri *et al.*, 2014). Similar

shifts in miRNA localization between protein-rich and exosomal fractions have been observed in DILI, and the nature of these shifts may reflect different mechanisms of liver injury (Bala *et al.*, 2015; Bala *et al.*, 2012). We propose that shifts in miRNA localization, such as those shown here, may serve a biological signaling purpose. For example, miR-122 in HDE released by alcohol-treated hepatocytes can prime monocytes for activation, while biological activity has yet to be attributed to miRNA in the protein-rich form (Momen-Heravi *et al.*, 2015a; Turchinovich *et al.*, 2013). Similarly, the effects of inflammatory mediators such as Hsp70 are amplified when they are delivered to recipient cells via exosomes (De Maio, 2011). While it is unlikely that exosomal miR-122 is a driving factor or major inflammatory mediator in overt APAP hepatotoxicity, during which necrosis releases massive amounts of DAMPs, the present miR-122 results support the assertion that HDE alterations may be actively mediated and functionally relevant in the early stages of hepatocyte stress.

In vivo, parallel increases in HDE-associated *ALB* mRNA and miR-122 were generally observed. However, exosomal *ALB* mRNA did not decrease *in vivo* at early time points alongside exosomal miR-122, providing evidence for the selective packaging of RNA into HDE. Selective mRNA packaging into exosomes has been observed in circulating vesicles from rats treated with APAP or D-(+)-galactosamine (DGAL), which contained distinct transcript profiles suggestive of compound-specific exosomal content (Wetmore *et al.*, 2010). We confirmed these results with HDE, as different trends in exosomal *ALB* mRNA and miR-122 were observed following APAP and DGAL exposures in primary rat hepatocytes (Figure 3.11). While sub-toxic concentrations of DGAL elicited increases in both exosomal RNAs, neither reached statistical significance prior to overt cytotoxicity. Our

nanoparticle tracking results also recapitulate the selective packaging hypothesis by indicating that the quantity of exosomal RNA does not correspond to HDE number. As such, the APAP-induced exosomal *ALB* mRNA elevations observed *in vivo* and *in vitro* are likely the result of increased *ALB* packaging within a similar number of HDE rather than an increase in overall HDE production with constant *ALB* mRNA content. While these findings are novel, it is important to note that exosome quantification could be affected by the stability of HDE in culture, which is currently unknown. Future experiments to establish the half-life and clearance rate of HDE will be imperative for understanding the biological implications of HDE in DILI.

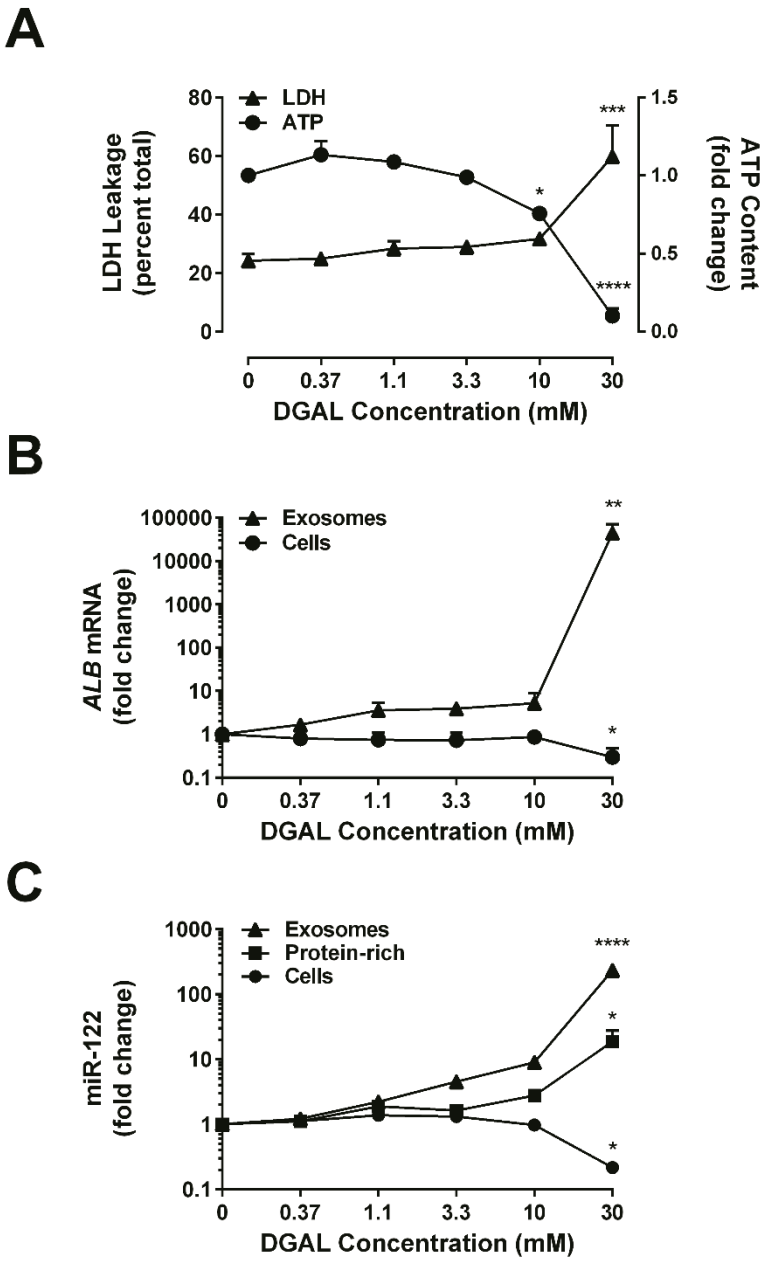

Figure 3.11. D-(+)-galactosamine-induced alterations in exosomes released by primary rat hepatocytes. Data are presented as mean + SEM (*n*=3 rats) following 24 h DGAL exposure. (A) Cytotoxicity, as indicated by cellular ATP and LDH activity in medium. (B) Fold change in exosomal and cellular *ALB* in response to DGAL. (C) Fold change in miR-122 within exosomal, protein-rich, and cellular fractions in response to DGAL. * $p < 0.05$, ** $p < 0.01$, *** $p < 0.001$, **** $p < 0.0001$; one-way ANOVA with Dunnett's post-test relative to vehicle.

Although the intent of this work was not to study biomarkers, by defining the kinetics and dose-dependence of HDE release prior to overt DILI, the current study could help to validate HDE as sensitive, translational, and clinically relevant biomarkers of DILI. We assayed 7 liver-enriched transcripts within primary human HDE from 3 separate donors. To our knowledge, this is the first characterization of the mRNA content of HDE from primary human hepatocytes. All 7 liver-enriched transcripts were measurable, and there was some consistency in the relative abundance of each transcript across the 3 donors, suggesting that these mRNAs, originally detected in rat HDE (Miyamoto *et al.*, 2008; Okubo *et al.*, 2013; Royo *et al.*, 2013), may also be used to identify human HDE. In addition, we have begun to define normal levels of exosomal *ALB* mRNA and miR-122 across donors. Despite the small donor pool, potential relationships were identified between donor characteristics and exosomal content. Continuing to study donor characteristics that influence HDE RNA content and to define a healthy range of HDE-based RNA levels will be important for interpreting biomarker data in the future. These data will need to be considered in the context of disease, which is known to affect basal HDE quantity and content. For instance, recent evidence suggests that high hepatocellular lipid content and non-alcoholic fatty liver disease correspond to increased extracellular vesicle production by hepatocytes (Hirsova *et al.*, 2016; Kakazu *et al.*, 2015).

In summary, we detected significant alterations in the liver-specific RNA content of HDE at sub-toxic doses of the prototypical hepatotoxicant APAP in rats and in primary rat and human hepatocytes. These alterations appear to reflect differential packaging of select RNAs in HDE rather than HDE number. The changes in HDE content observed prior to and in the absence of overt hepatocellular injury, together with growing data on the role of

exosomes in stimulating immune responses, support the hypothesis that HDE released from drug-stressed hepatocytes may transmit signals that mediate critical early immune responses across multiple forms of DILI. While this hypothesis was substantiated using an intrinsic hepatotoxicant, future work will address the release kinetics and signaling potential of HDE released by hepatocytes exposed to idiosyncratic DILI compounds.

CHAPTER 4.

MECHANISTIC INTEGRATION OF HUMAN HEPATOCYTE-DERIVED EXOSOME CONTENT AND IMMUNOLOGIC ACTIVITY

4.1 Introduction

It is widely accepted that intrinsic and idiosyncratic drug-induced hepatocellular death are often mediated by immune responses (Adams *et al.*, 2010; Ju and Reilly, 2012; Russmann *et al.*, 2009). For example, human leukocyte antigen (HLA) genotype is a strong risk factor for idiosyncratic DILI (I-DILI) associated with a wide range of drugs, suggesting a role for the adaptive immune system in drug-mediated hepatotoxicity (Urban *et al.*, 2014). In addition, elevations in biomarkers that are suggestive of immune cell activation, including miR-155 and acetylated high mobility group box 1 (HMGB1), have been associated with intrinsic DILI (Antoine *et al.*, 2014; Bala *et al.*, 2012; Fontana, 2014). Such immune reactions may be triggered in part by hepatocellular danger signals or damage-associated molecular patterns (DAMPs), which communicate to immune cells as part of a stress response (Uetrecht and Naisbitt, 2013). Recent evidence indicates that hepatocytes can release these signals prior to overt cell death, suggesting that the first interaction between an injured hepatocyte and cells of the immune system may occur much earlier than previously thought.

Exosomes released by drug-stressed hepatocytes may constitute an early link between hepatocellular distress and the immune system. The immunomodulatory activity of

hepatocyte-derived exosomes (HDE) has been validated in various models of liver disease. In the context of viral hepatitis, hepatitis C (HCV)-infected Huh7.5 cells release exosomes that transfer viral RNA to plasmacytoid dendritic cells (pDCs) and promote the release of interferon (IFN-α) as part of the body's defense against HCV (Dreux *et al.*, 2012). HCV-infected Huh7.5 cells alter monocyte secretion of the adaptive immune response mediator galectin-9, a process which is thought to be mediated by HDE (Harwood *et al.*, 2016). In hepatitis B viral infection (HBV), exosomes can actively transfer the virus to other hepatocytes and have a deleterious effect on natural killer (NK) cell proliferation (Yang *et al.*, 2016).

Exosome regulation of immune signaling in non-infectious liver disease has been best studied in models of non-alcoholic steatohepatitis (NASH) and non-alcoholic fatty liver disease (NAFLD). Broadly, these diseases are characterized by lipid-induced hepatocyte toxicity, chronic inflammation, and compensatory wound healing leading to fibrosis. Evidence suggests that hepatocellular lipotoxicity is mediated by inflammatory signaling which has led to investigation of the link between hepatocyte lipoapoptosis and inflammatory response (Hirsova and Gores, 2015). In a recent study by Hirsova *et al*, murine bone marrow-derived macrophages (BMDMϕ) were exposed to EV from mice fed a control or high-fat diet as well as EV from mouse hepatocytes exposed to control or toxic lipid treatment. EVs from mice on a high-fat diet and from lipoapoptotic hepatocytes induced expression of the interleukins IL-6 and IL-1β in BMDMϕ relative to control EVs (Hirsova *et al.*, 2016). A similar study found that a mouse hepatocyte cell line exposed to palmitate produced greater quantities of ceramide-enriched EVs that chemotactically recruited more BMDMϕ than EVs from control-treated hepatocytes (Kakazu *et al.*, 2015).

Few studies have focused on the role of HDE in xenobiotic-induced liver injury, although there is encouraging evidence from models of alcoholic liver disease. A comparison of the immunomodulatory effects of control- versus ethanol (EtOH)-treated Huh7.5 cells revealed that EtOH EVs synergize with lipopolysaccharide (LPS) to promote increased production of the pro-inflammatory mediators tumor necrosis factor alpha (TNF-α), IL-1β, and monocyte chemoattractant protein 1 (MCP-1) in THP-1 monocytes (Momen-Heravi *et al.*, 2015a). Similarly, THP-1 cells, primary murine macrophages, and primary human monocyte-derived macrophages showed significant increases in pro-inflammatory cytokines following treatment with EVs from EtOH-treated, CYP2E1-overexpressing HepG2 human hepatocyte-like cells (Verma *et al.*, 2016). Other xenobiotic studies have utilized the overt hepatotoxicant carbon tetrachloride (CCl4) to study the functional activity of EVs from injured hepatocytes. For example, Simon *et al* co-cultured a subpopulation of bone marrow-derived monocytes (BMDM) with primary rat hepatocytes isolated from a CCl4-induced acute liver failure (ALF) model or healthy rats (2015). In the presence of ALF hepatocytes, BMDM internalized hepatocyte EVs and began to express hepatocyte progenitor markers (Simon *et al.*, 2015). However, whether hepatocyte EVs were involved in mediating the BMDM phenotypic changes in co-cultures was not examined.

The molecular basis of exosome-mediated activity in recipient cells is not well defined. One possible mechanism is the transfer of exosomal content (lipid, protein, and/or RNA cargo) into the recipient cell via fusion or endocytosis. The transfer of RNA species like miRNA and mRNA by exosomes is well-established, an example being the transfer of viral RNA described previously. An attractive argument for this mechanism is the fact that stress and toxicity influence the RNA content of exosomes from various cell types, including

hepatocytes (de Jong *et al.*, 2012; Eldh *et al.*, 2010; Holman *et al.*, 2016; Wetmore *et al.*, 2010). Evidence supports the transfer of functional mRNA and miRNA by hepatocyte EVs. For example, following exposure to human liver stem cell-derived EVs, rat hepatocytes *in vivo* translate EV-delivered human *AGO2* mRNA into protein (Herrera *et al.*, 2010). In the aforementioned study of EtOH HDE activating monocytes, a set of elegant and thorough experiments showed that hepatocyte-specific exosomal miRNA miR-122 was elevated in EtOH HDE over controls, and that this miRNA was responsible for the pro-inflammatory phenotype in recipient cells (Momen-Heravi *et al.*, 2015a).

Surprisingly, despite convincing evidence of immune mediation by HDE, to our knowledge, no studies have examined the role of HDE in DILI reactions, representing a clear knowledge gap in this field. Most exosome research related to DILI has focused on their biomarker potential, which is a promising area of study. As a result, HDE are often studied in the context of drug overdose or drug-induced ALF.

To better understand the biological activity of HDE in early immune-driven DILI events, we sought to establish that sub-toxic drug-induced HDE alterations could influence THP-1 human monocytes. Acetaminophen (APAP) was selected as our model hepatotoxicant due to its well-defined *in vivo* and *in vitro* toxicity profiles. We have already confirmed significant sub-toxic alterations in the albumin mRNA and miR-122 content of HDE released by rat and human hepatocytes following sub-toxic APAP exposures (Chapter 3) (Holman *et al.*, 2016), and both of these RNAs are implicated in the functional effects of HDE (Momen-Heravi *et al.*, 2015a; Royo *et al.*, 2013). In addition, there is no doubt that immune responses play a role in APAP-induced liver injury. For example, recent evidence from a healthy volunteer study revealed pro-inflammatory transcriptomic signatures in

subjects who developed ALT elevations following therapeutic doses of APAP (Fannin *et al.*, 2015). While a consensus regarding the positive or negative impact of immune reactions is lacking, the human relevance is not.

Based on this evidence, we sought to: (1) establish a role for HDE in the regulation of early DILI immune responses, (2) comprehensively profile the mRNA and miRNA content of exosomes released by control- and APAP-treated primary human hepatocytes, and (3) link HDE miRNA profiles to their biologic activity. In addressing these goals, we provide the first next-generation sequencing (NGS) analysis of the RNA in primary human HDE. This research is the first to report immunologic activity of primary human HDE in a model of DILI.

4.2 Materials and Methods

4.2.1 EV pathway activation experiments with the potent Nrf2 activator 3H-1,2-dithiole-3-thione (D3T)

In vivo rat exposures

Male Sprague-Dawley rats (Crl:SD), 10-12 weeks of age, were purchased from Charles River Laboratories and allowed to acclimate in-house for 10-15 days prior to study initiation. Water and food (pelleted NIH-07 diet [Ziegler Brothers]) were available *ad libitum* during this time. D3T (LKT labs) was administered once daily for 4 days in sterile saturated sucrose vehicle at 0, 0.1 mmol/kg, or 0.3 mmol/kg by oral gavage (n=14/group). The rats were not fasted at any point during this study. Studies were conducted by Drs. Rusty Thomas, Barbara Wetmore, and Reetu Singh in accordance with the Guide for the Care and Use of Laboratory Animals, and were approved by The Hamner Institutes for Health Sciences Institutional Animal Care and Use Committee.

At necropsy, blood was collected for circulating EV RNA analysis and liver tissue was collected for histology as well as gene expression analysis. Total RNA was isolated from plasma with a QIAmp Viral RNA Kit (Qiagen) according to the manufacturer's instructions. Liver and plasma cDNA was generated with a High Capacity cDNA RT Kit (Applied Biosystems) and qRT-PCR was performed as described in previous chapters.

In vitro exposures and analysis of hepatocyte-specific exosome content

Freshly isolated primary hepatocytes from male Sprague-Dawley rats were plated as previously described (Holman *et al.*, 2016). Cultures were treated with 0, 10, 50, or 100 µM D3T (LKT Labs) in 0.2% (v/v) dimethyl sulfoxide (DMSO) vehicle (Sigma). These

concentrations are well below peak plasma concentrations observed in rats treated with high doses of D3T (0.4-4 mM) (Brown *et al.*, 2000) but were the highest that could be achieved with the compound's solubility limitations. A concentration of 10 µM was previously used to induce Nrf2 *in vitro* and was deemed to be suitable for Nrf2 activation and down-stream gene target up-regulation (Kwak *et al.*, 2002).

While D3T is widely considered non-toxic, we wished to confirm that the concentrations used to induce Nrf2 in rat hepatocytes over a 24 h period would not cause cell death. To assess cytotoxicity, LDH in culture medium was assayed as described in earlier sections. RNA was collected from hepatocytes and HDE precipitated by EQ to compare the content of Nrf2-regulated genes *Gsta3, Nqo1, Hmox1, Gclc,* and *Ugt1a6* in both sample types. TaqMan qRT-PCR was performed as stated earlier.

Given that the Nrf2 target genes being measured in HDE are not as abundant as the highly liver-enriched RNAs albumin or miR-122, we investigated the validity of isolating HDE from large volumes of conditioned rat hepatocyte culture medium via centrifugal concentration. We compared quantities of exosomal albumin obtained by EQ precipitation from equal volumes of un-concentrated medium, medium processed using an Amicon Ultra 3kDa molecular weight cutoff concentrator or a Centricon Plus 10 kDa concentrator. Upon validating that no exosomal material was lost with medium concentration, rat hepatocyte cultures were scaled to the maximum feasible level to determine whether a larger quantity of exosomes would yield detectable Nrf2 target mRNAs.

4.2.2 Generation of primary human HDE

Primary human hepatocyte cultures

Primary human hepatocytes from 5 donors were obtained from commercial sources (QPS Hepatic Biosciences and Triangle Research Labs) (Table 4.1). Freshly isolated hepatocytes were used (n=3 donors) when available. Cryopreserved hepatocytes were also utilized (n=2 donors). Individual batches of hepatocytes were seeded into 10 cm dishes coated with collagen type I (Corning) at a density of 10×10^6 cells per dish in hepatocyte plating medium (William's E medium, penicillin-streptomycin, GlutaMax™, HEPES, sodium pyruvate, fetal bovine serum [Thermo Fisher Scientific], insulin, and dexamethasone [Sigma-Aldrich]). Culture plates were incubated at 37ºC with 5% CO_2. After attachment, non-adherent cells were removed and fresh plating medium was added. Cultures were then transitioned to hepatocyte maintenance medium without fetal bovine serum within 6-12 h of plating. Following a 24 h acclimation period, hepatocyte cultures were exposed to APAP (10 mM) or a vehicle control (medium) for 24 h.

Treatment-induced effects on cell health and function were determined by measuring cellular ATP, urea production, and LDH leakage. Cellular ATP content was measured with CellTiter-Glo® Luminescent Cell Viability Assay (Promega) and urea production was assayed in cell culture supernatant with a Urea Nitrogen BUN kit (Stanbio) using modified methods. Briefly, a urea nitrogen standard curve of 2-fold serial dilutions from 100 to 1.56 µg/ml was prepared in culture medium. Clarified media supernatants and standards were added to a clear 96-well assay plate in 10 µl/well. Working BUN reagent was prepared according to manufacturer's instructions and added to the assay plate at 150 µl/well. The

plate was incubated in an oven at 60 ºC for 90 min prior to data collection. LDH activity was determined as described previously (Kia *et al.*, 2015). Data for all cytotoxicity endpoints were collected using a SpectraMax® M3 microplate reader (Molecular Devices).

Human HDE enrichment

Hepatocyte-conditioned medium from control- or APAP-treated cells was collected after the 24 h exposure and clarified by centrifugation at 3000 x *g* for 15 min to remove cellular debris. Medium supernatants were filtered at 0.45 µm and subsequently concentrated using Centricon-70 centrifugal filter units with a 10,000 Da cut-off (Millipore) per manufacturer's instructions. The resultant concentrates were subjected to a second filtration (0.22 µm) and processed under sterile conditions for the remainder of the preparation. Exosomes for quantification, content analysis, and non-parenchymal cell exposure were precipitated from these concentrates with ExoQuick-TC™ (System Biosciences) following the protocol for tissue culture supernatants. The use of ExoQuick-TC™ for primary human hepatocyte-derived exosome enrichment has been previously validated by our group (Holman *et al.*, 2016).

Table 4.1. Characteristics of primary human hepatocyte donors.

Donor ID	Age (yr)	BMI	Sex	Race	Cells Obtained
1	55	29	F	Caucasian	Cryopreserved
2	63	24	F	Caucasian	Freshly isolated
3	27	27	M	Hispanic	Freshly isolated
4	35	21	M	Caucasian	Freshly isolated
5	28	26	F	Caucasian	Cryopreserved

4.2.3 Exosomal mRNA sequencing (RNA-seq)

Preparation of RNA-seq samples

Total RNA was isolated from exosomes using the miRCURY Cell & Plant Isolation Kit (Exiqon) according to the manufacturer's instructions for RNA isolation from blood. Sample concentrations were obtained using an Experion RNA HighSens Analysis kit (BioRad). It is important to note that exosomal RNA cannot be quality controlled in the traditional manner using RIN numbers based on 18S and 28S peaks because exosomes do not carry significant levels of rRNA (Eldh *et al.*, 2012; Royo *et al.*, 2013). cDNA was prepared with a SMART-Seq® v4 Ultra Low Input RNA Kit for Sequencing (Clontech Laboratories, Inc.) and libraries were created using the Nextera XT (Ilumina) library preparation workflow as previously described (Welch *et al.*, 2016). Libraries were QC'd as described above and pooled for 50 bp paired-end sequencing on a single lane of an Ilumina HiSeq system.

RNA-seq data analysis

Two fastq files representing both paired-end reads were generated for each sample and Q scores were generated using FastQC (version 0.11.5). Files were trimmed for adapter k-mers with BBDuk software and aligned to UCSC human genome build Hg19 (BBMap version 36.32). Within R, the *subread* package and featureCounts command were used to generate count matrices, which were loaded into DESeq2 for differential expression analysis (Love *et al.*, 2014). Log2 fold change values were used to observe the most differentially expressed genes between HDE from APAP- versus control-treated human hepatocytes. Using raw counts, pathway enrichment analysis was performed to identify the best-represented pathways within HDE from untreated human hepatocytes using Ingenuity

Pathway Analysis (IPA) software (Qiagen, version 28820210). The 150 genes that exhibited the highest fold change in APAP HDE relative to control HDE were then cross-referenced with genes known to be differentially expressed in primary human hepatocytes following 10 mM APAP exposure for 24 h. These data were obtained from microarray analyses of primary human hepatocytes treated with 0 or 10 mM APAP (n=5 donors) from the NCBI GEO2R database (GSE13430). Within the GEO2R microarray data set, DE analysis was performed via the *limma* R package using standard GEO2R parameters.

4.2.4 Exosomal microRNA profiling

HTG EdgeSeq miRNA Whole Transcriptome assay

We selected the HTG EdgeSeq miRNA Whole Transcriptome Assay v2 Kit (HTG Molecular Diagnostics) for miRNA profiling. This kit was designed to measure all 2,083 miRNAs currently annotated in miRbase version 20. Samples (isolated total RNA or intact exosomes) were washed 1x with PBS and centrifuged at 10,000 x *g* for 60 min at the UNC High Throughput Sequencing Facility. The supernatants were removed and 30 µl of HTG Lysis Buffer was added to each exosome sample. Lysates (25 µl) were loaded onto an EdgeSeq plate and processed according to the manufacturer's instructions for cells. Briefly, libraries were prepared in two steps: nuclease protection on an HTG Edge processor followed by PCR labeling and amplification. Library concentration and quality were determined using a High Sensitivity DNA Assay Kit on an Agilent 2100 Bioanalyzer. Libraries were pooled and sequenced in a single lane on an Ilumina MiSeq system for 50 bp single-end reads. Data were parsed using HTG EdgeSeq software.

Optimization of exosomal input for HTG miRNA assay

Due to rapid advancement in the technologies available to analyze miRNAs many kits no longer require RNA extraction which can significantly bias results, allowing cells or exosomes to be used directly as input. Use of exosomes as starting material is possible with the HTG technology, and we wished to ensure that the miRNA profiles obtained with this assay would be the same using intact exosomes versus total exosomal RNA. We isolated exosomes from a single primary human hepatocyte donor with EQ and reserved an aliquot for direct miRNA profiling. RNA, including mRNA and miRNA, was isolated using the miRCURY Cell & Plant kit (Exiqon) as described previously. Duplicates of both sample types were analyzed to evaluate the technical variability inherent in this assay.

Profiling of differentially expressed miRNAs in HDE from primary human hepatocytes with and without APAP exposure

Median-normalized counts for all 2,083 miRNAs were used for data analysis (Anders and Huber, 2010). Results were filtered by liver expression, including only those miRNAs detected in 100% of 79 human liver samples in the analysis (Gamazon *et al.*, 2013). ANOVAs were performed in Partek Genomics Suite (version 6.6) on these data to examine differential miRNA enrichment in HDE from APAP- and control-treated hepatocytes across 4 human hepatocyte donors.

4.2.5 *In vitro* HDE exposures

Pilot studies to examine biological effects of human HDE across cell types

Exosome exposures were first conducted in human macrophage, monocyte, and sinusoidal endothelial cell (SEC) lines to evaluate HDE activity in representative non-parenchymal cell (NPC) populations.

Macrophages were generated from THP-1 human monocytes (TIB-202, ATCC) cultured in RPMI-1640 (ATCC) supplemented with 10% (v/v) Exosome-Depleted FBS (Gibco), penicillin-streptomycin (Gibco), and 0.05 mM β-mercaptoethanol (Sigma). THP-1 cells were differentiated in 24-well culture plates by incubation with 50 ng/ml phorbol 12-myristate 13-acetate (PMA; Sigma) for 48 h (Park *et al.*, 2007). Upon differentiation, adherent macrophages were exposed to 20 µg/ml human HDE from hepatocytes that had been cultured with either 10 or 30 mM APAP for 24 h. Exosomes were cultured with macrophages for 8 h followed by an 8 h wash-out period and a subsequent 6 h LPS-

activation, according to a previously validated experimental design (Momen-Heravi *et al.*, 2015a). Gene expression changes associated with stimulation were measured in control- and HDE-treated macrophages by relative RT-PCR.

Immortalized human SECs, TMNK-1 cells (Japanese Cell Research Bank), were also exposed to HDE in initial studies. TMNK-1 cells were maintained in MCDB-131 medium (Life Technologies) supplemented with 10% (v/v) Exosome-Depleted FBS (Gibco), penicillin-streptomycin (Gibco), and EGM-2 SingleQuot Kit (50% strength, Clonetics). Cells were subcultured with Accutase cell detachment solution and seeded in 96-well plates for 24 h HDE exposure experiments. Human HDE at 200 μg/ml were co-incubated with TMNK-1 cells for 24 h prior to a 6 h activation period with or without LPS (50 ng/ml, Sigma) to induce validated activation markers such as cell adhesion molecules (Matsumura *et al.*, 2004). Expression of these markers was measured by relative RT-PCR using GAPDH as an internal normalization gene.

THP-1 cells were cultured as above without PMA differentiation and were exposed to HDE (100 or 200 μg/ml) as monocytes in suspension culture to understand whether exosomes exert concentration-dependent effects on immune cells. For these experiments, monocytes were co-cultured with HDE or medium alone for 24 h followed by a 6 h LPS activation to stimulate cytokine release. Pro-inflammatory cytokines IL-8 and TNF-α were measured to determine whether HDE augmented monocyte cytokine secretion (see Cytokine and chemokine analysis section).

Mitigating potential biological effects of EQ polymer in HDE exposure studies

Removal of EQ polymer

Great care must be taken when assessing the biological functionality of exosomes prepared using EQ precipitation, because results may be confounded by effects of the polymer itself on recipient cells. For activity studies, SBI recommends polymer removal via G-25 Sephadex resin desalting columns (GE Healthcare Life Sciences). Prior to conducting HDE exposures, we attempted to remove EQ from HDE preparations according to the manufacturer's instructions. HDE with and without column-based polymer removal were visualized via cryo-electron microscopy according to published methods (Holman *et al.*, 2016).

Preparation of mock controls to account for EQ matrix effects

For each primary human hepatocyte exposure experiment used to generate HDE, portions of control and APAP dosing solutions were reserved. A volume of unconditioned dosing solution equal to that of conditioned medium from each treatment was processed in parallel for mock "exosome enrichment" as described above. Unconditioned dosing solution concentrates were brought to the same volume as true exosome samples with sterile PBS and EQ was added in equal amounts to both the unconditioned and conditioned samples. Unconditioned media samples did not contain HDE or any source of exogenous exosomes, and were used as an EQ vehicle or "mock" control in monocyte exposures. In addition to controlling for the amount of EQ in each exosome preparation, these controls allowed us to examine the effect of residual hepatocyte maintenance medium and APAP that may have carried over from the hepatocyte dosing solutions to the monocyte cultures. Following the

centrifugation step in our precipitation protocol, pellets of EQ polymer were seldom observed. Whether a pellet was visible or not, the majority of supernatant was removed and a volume equivalent to the volume of the corresponding true HDE pellet was saved as the mock control. This solution was diluted in monocyte culture medium exactly as the matching exosomes were diluted for monocyte treatment (see *Monocyte HDE exposures* section).

Monocyte HDE exposures

THP-1 human monocytes (TIB-202, ATCC) were cultured in suspension in RPMI-1640 (ATCC) supplemented with 10% (v/v) Exosome-Depleted FBS (Gibco), penicillin-streptomycin (Gibco), and 0.05 mM β-mercaptoethanol (Sigma). Exposures were conducted in 96 well round-bottom plates (Corning) at a density of 1 x 10^5 cells per well. THP-1 monocytes were exposed to 200 µg/ml exosomes derived from control and APAP-treated hepatocyte cultures or matched EQ mock controls (described above) in separate experiments for each hepatocyte donor (Table 4.2). In each well, monocytes were seeded at the desired density in 100 µl of medium and a 2x solution of exosomes in 100 µl medium was added for a total of 200 µl final volume. Donor-specific exosome concentration for exosomes harvested from control- and APAP-exposed hepatocytes was determined using total exosomal protein measured by a BCA Protein Assay Kit (Thermo). Normalizing exosome preparations for *in vitro* exposure based on total protein concentration is a common practice in mechanistic experiments (Chiba *et al.*, 2012; Giugliano *et al.*, 2015; Li *et al.*, 2013). The final concentration of 200 µg/ml exosomal protein was modeled after total exosomal protein concentrations in human plasma (Momen-Heravi *et al.*, 2015a; Muller *et al.*, 2014).

Following 24 h of exosome co-culture, THP-1 monocytes were lysed in QIAzol (Qiagen) for gene expression analysis. The effects of control- and APAP-treated hepatocyte-derived exosomes on human monocyte function were examined by quantifying pro-inflammatory cytokine release in co-cultures after incubating them for an additional 6 h following a spike-in of 5 ng/ml LPS (*E. coli* 0111:B4; Sigma) or medium vehicle.

Table 4.2. Definition of THP-1 culture conditions in HDE exposure studies.

Treatment Name	Condition
Control HDE	monocytes exposed to HDE from control-treated hepatocytes
APAP HDE	monocytes exposed to HDE from APAP-treated hepatocytes
Mock Control	mock HDE preparation containing ExoQuick for Control HDE matrix effects
Mock APAP	mock HDE preparation containing ExoQuick and APAP for APAP HDE matrix effects
Medium	monocytes exposed to medium alone

Cytokine and chemokine analysis

Pro-inflammatory cytokines TNF-α, IL-8, IL-6, and IL-1β were measured in clarified culture supernatant using a multiplex MSD V-plex assay (Meso Scale Discovery) according to the manufacturer's protocol for cell culture supernatant samples. Release of the chemokine MCP-1 was quantified using an MSD Single Spot assay according to the manufacturer's instructions. MSD plates were run on a Meso QuickPlex SQ 120 instrument and analyzed using Discovery Workbench 4.0 software (Meso Scale Discovery).

4.2.6 Exosome uptake imaging

Exosomes from control- and APAP-treated hepatocytes were stained using a PKH67 dye kit (Sigma). Exosomes were diluted to 200 µg/ml with Diluent C and were combined with an equal volume of 1:250 dye solution and incubated according to the manufacturer's protocol. Following incubation, 3 ml of complete exosome-free medium was added to terminate the labeling reaction. Labeled exosomes were harvested and washed once with 1x PBS by centrifugation (100,000xg for 1 h at 4 ºC). Exosomes were suspended in warm monocyte culture medium and were incubated with THP-1 cells for 8 h at 37 ºC. Monocytes were then harvested and labeled for visualization of exosome uptake. Monocytes were incubated with Alexa Fluor® 647 anti-human CD32 antibody (BioLegend) to define cell boundaries and permeabilized with Cytofix/Cytoperm Fixation and Permeabilization Kit (BD). DAPI nucleic acid stain (BD Pharmingen) was added to delineate nuclei post-fixation. Image acquisition was performed on an Amnis ImageStreamX Mark II Imaging Flow Cytometer with INSPIRE® software at 60x magnification. Focused, single, and DAPI positive cells were first gated and an internalization score (uptake of PKH67+ exosomes by

CD32+ cells) was generated with the IDEAS® software package (v6.2) as previously described (Ackerman et al., 2011).

4.2.7 Monocyte gene expression analysis

Gene expression microarrays

Global gene expression from HDE-exposed THP-1 monocytes was evaluated using a microarray platform. Total RNA from THP-1 monocytes incubated for 24 h with control HDE, APAP HDE, treatment-matched EQ mocks, or medium alone was isolated with the miRNeasy Mini Kit (Qiagen) according to the manufacturer's instructions. Lysates from replicate wells were pooled and linear acrylamide carrier (Applied Biosystems) was added prior to RNA isolation. Total RNA samples were submitted to the UNC Functional Genomics Core for microarray analysis. All RIN values, assessed using an Agilent 2200 TapeStation, were ≥ 9.7 using TapeStation Software (version A.01).

An Affymetrix GeneChip® WT PLUS Reagent Kit (Afftymetrix) was used according to the manufacturer's protocol to generate, fragment, and label sense-strand cDNA from total RNA. Fragmented and labeled cDNA was used to prepare a hybridization cocktail with the Affymetrix GeneTitan Hybridization Wash and Stain Kit for WT Arrays. Samples were hybridized onto a Clariom™ S HT Human peg plate (Affymetrix), washed, stained, and scanned using the Affymetrix GeneTitan MC Instrument. GeneChip Command Console Software (AGCC, version 4.3) was used for GeneTitan Instrument control. Affymetrix Expression Console Software (version 1.4) was used for basic data analysis and quality control.

Differential gene expression (DE) analysis

Normalized $\log_2$ probe intensities were analyzed in Partek Genomics Suite, version 6.6. Rather than adhere to a pre-determined intensity cutoff, data were filtered to include only probe sets whose maximum intensity across all samples was greater than the 25th percentile. Analyses were batch-corrected for the greatest source of variability by defining HDE donor (n=5) as a random factor. Treatment groups (Table 4.1) were compared by ANOVA. To account for the potential biological activity of EQ, exosome treatments (APAP and mock APAP EQ control) were compared directly to their mock EQ controls by linear contrasts with false discovery rate (FDR) $p < 0.05$ and fold change (FC) > |1.5|. Statistically significant DE genes were analyzed for enriched pathways using IPA software. Linear contrasts were also performed on microarray data from monocytes exposed to APAP HDE or mock control from individual donors. The top 100 genes most impacted by APAP HDE exposure from each donor were analyzed for pathway enrichment to identify the immunomodulatory influence of individual donor APAP HDE. Pathway enrichment revealed two subsets of donors whose APAP HDE induced similar gene expression changes in monocytes. Network analysis was performed on overlapping genes from these two subsets, respectively, to identify biological functions impacted by binding, activation, translocation, degradation, or biochemical reactions with these gene products. Networks were generated using a curated database of interactions cross-referenced with NCBI, Ensembl, UniProt, UCSC Genome Browser, HapMap, KEGG, ChEBI, PubMed and GO resources (http://www.reactome.org; v58).

4.2.8 Integration of exosomal miRNA and recipient THP-1 cell gene expression patterns

Reverse prediction of differentially expressed exosomal miRNAs

miRNAs targeting the significant DE genes in exosome-treated THP cells were retrieved from the miRTarBase database (version 6.0), which is manually curated to include the most current experimentally validated miRNA-target interactions. The miRNAs predicted from our list of DE THP genes was compared to the exosomal miRNAs enriched in APAP HDE versus vehicle HDE.

Prediction of differentially expressed genes in exosome-exposed THP-1 cells

The 50 most differentially enriched exosomal miRNAs in APAP HDE relative to control HDE were used to generate a list of target genes predicted to be affected in exosome-exposed THP cells. Likely mRNA targets were inferred via the IPA microRNA Target Filter (IPA software), which retrieves results from 3 interaction databases: miRecords, TarBase, TargetScan. IPA analysis was performed on these predicted gene targets to determine whether the over-represented pathways in exosome-exposed THP cell microarrays matched with the pathways inferred from exosomal miRNA profiling. This process was performed using the top 50 most increased miRNA from the global data set (n=4 donors) as well as the top 50 most increased miRNAs on an individual donor basis. Pathways predicted from individual donor analyses were compared to donor-specific pathway enrichment observed in monocytes.

4.3 Results

4.3.1 Exosomal mRNA content and hepatocellular pathway activation

In vivo, rats treated with D3T to activate the Nrf2 oxidative stress response pathway demonstrated robust hepatic induction of Nrf2 target genes. Expression of a representative target gene, *Gsta3*, is shown in Figure 4.1. *Gsta3* levels were also measured in plasma and were detectable due to their encapsulation within EVs. While hepatic expression was dose-dependently elevated by increasing D3T exposures, EV levels were dose-dependently decreased (Figure 4.1), suggesting an inverse relationship between liver and EV mRNA content. Albumin mRNA was also measured as a control to ensure that D3T did not produce off-target gene induction. Levels of albumin mRNA were not affected by D3T treatment in the liver or plasma samples (Figure 4.1). As albumin mRNA is used as a surrogate marker of HDE, it was hypothesized that overall HDE release was unchanged while *Gsta3* was selectively retained by stressed hepatocytes.

Although D3T significantly up-regulates hepatic Nrf2-mediated gene expression, neither its effects nor the genes it influences are specific to the liver. With the knowledge that many cell types contribute to the circulating population of exosomes *in vivo*, we used an *in vitro* model to directly investigate the relationship between hepatocellular Nrf2 activation and exosomal Nrf2 target gene content. Primary rat hepatocytes were exposed to D3T across a range of concentrations and exhibited robust induction of all target genes analyzed (Figure 4.2). However, these same mRNAs were not detected in HDE at any concentration of D3T (Figure 4.2). While D3T is considered non-toxic, we evaluated LDH leakage into medium at all concentrations in our culture system. LDH was not increased relative to vehicle at any

D3T concentration; we observed a small but statistically significant decrease in LDH leakage at 100 μM D3T ($p < 0.0001$, Student's t-test, data not shown).

Experiments were then scaled-up to determine whether the lack of detection of these mRNAs was due to insufficient exosomal material. First, HDE preparation from concentrated medium was validated for downstream RT-PCR. Between unconcentrated medium and medium concentrated with 2 different methods, there were no differences in exosomal albumin mRNA recovery (data not shown). We then employed these medium concentration techniques to 150 ml of rat hepatocyte-conditioned medium and measured Nrf2 target genes by RT-PCR. It is important to note that the hepatocyte cultures were un-stimulated with D3T. We hypothesized that if the *in vivo* results held true, control exosomes would actually contain the highest levels of Nrf2 targets. Therefore, if Nrf2 target genes could not be detected in control HDE, there was little chance they could be detected in D3T experiments. Despite increasing culture scale, Nrf2 target genes remained undetectable in rat HDE (data not shown). These data suggest that the decrease in circulating Nrf2 target genes observed *in vivo* following D3T exposure is unlikely due to hepatocyte EVs. It is possible that these experiments were limited because we only measured a handful of targets via RT-PCR, and supports a more global profiling approach to investigating lower abundance exosomal RNAs.

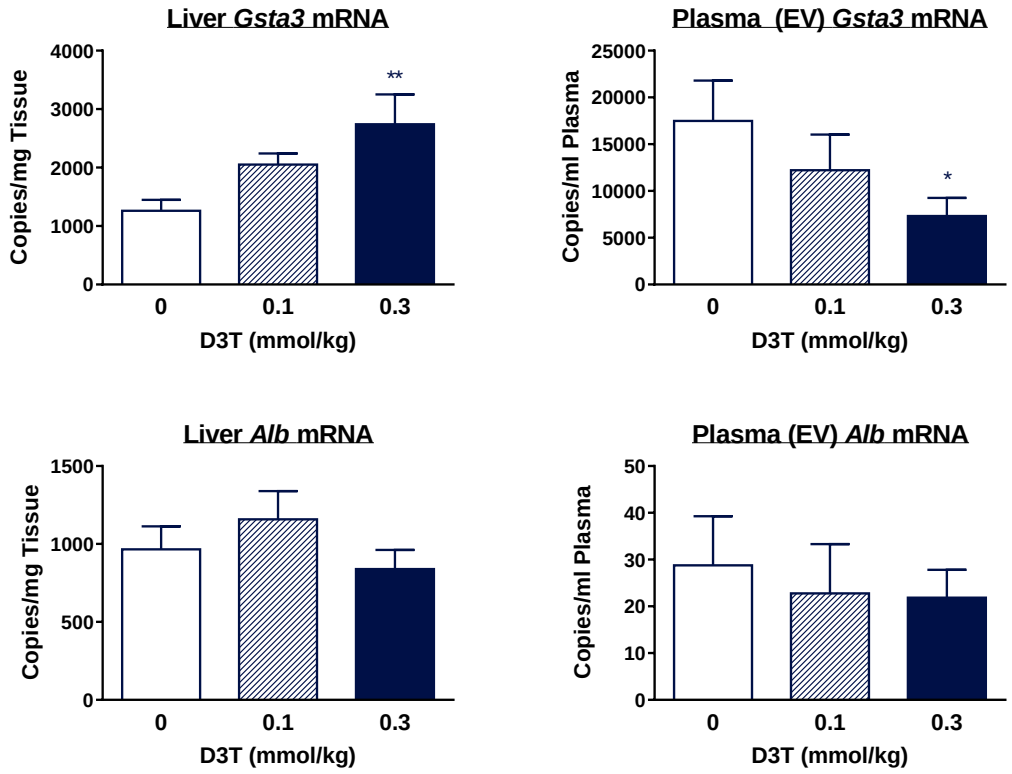

Figure 4.1. Relationship between Nrf2 target mRNA levels in liver and circulating exosomes. Male Sprague-Dawley rats were treated once daily for 4 days (*p.o.*) with non-toxic Nrf2 pathway activator D3T or saturated sucrose vehicle. Data represent mean + SEM (n=14-15 rats). Transcripts detected in plasma are packaged within extracellular vesicles (EV). * $p < 0.05$, ** $p < 0.001$; one-way ANOVA with Sidak's test.

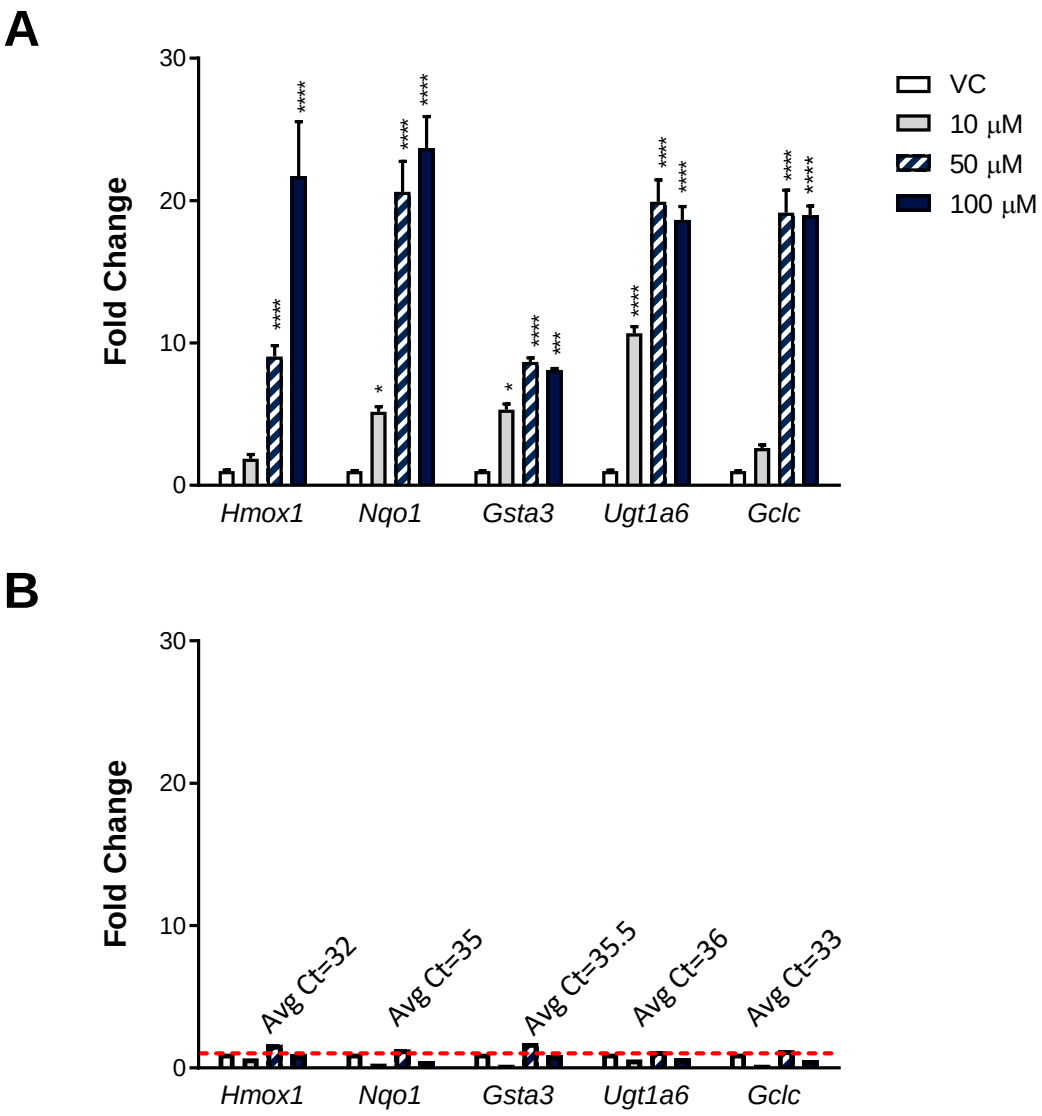

Figure 4.2. Induction of Nrf2 target genes by D3T is apparent in rat hepatocytes but not rat HDE. Male Sprague-Dawley rat hepatocytes were treated once for 24 h with non-toxic Nrf2 pathway activator D3T or 0.2% DMSO vehicle. Target genes were measured by RT-PCR in hepatocytes (A) and HDE (B). Data represent mean + SEM of triplicate reactions. * $p < 0.05$, ** $p < 0.01$, *** $p < 0.001$, **** $p < 0.0001$; one-way ANOVA with Dunnett's post-test relative to vehicle.

4.3.2 RNA sequencing of primary HDE transcripts

Earlier results from this research have confirmed that liver-enriched miRNAs and transcripts that are abundant in hepatocytes can be detected in primary rat and human HDE. The results of our earlier D3T studies suggest that certain mRNAs are not detectable in HDE with RT-PCR which is considered one of the most sensitive detection techniques. In the present work, we employed an RNA sequencing approach to globally profile the mRNA content of primary human HDE under control conditions and following APAP exposure. Next-generation sequencing (NGS) approaches such as RNA sequencing have distinct advantages over microarray analysis. RNA sequencing was pursued in the current research because it directly counts transcripts and provides a more quantitative dataset than microarrays, which is important for exosomes because they are not known to carry housekeeping genes. With the knowledge that most exosomal RNA is non-coding as opposed to full length transcripts, we selected sequencing library preparations to select for mRNA specifically. Exosomes are a challenging material for RNA profiling because they contain such small quantities of RNA, and little of the total RNA concentration is full-length mRNA (Hill *et al.*, 2013; Huang *et al.*, 2013; Nolte-'t Hoen *et al.*, 2012). Very few next-generation sequencing (NGS) studies have been conducted using exosomes, and most are focused on miRNAs. Only a single publication has examined the transcript content of HDE (Royo *et al.*, 2013), and this was done using primary rat hepatocytes and gene expression microarray. To our knowledge, our earlier measurements of mRNA within primary human HDE was the first study of its kind. We sought to expand upon those findings with global mRNA sequencing.

Because there are no standardized techniques or precedents for exosomal RNA sequencing, we first assessed the quality of sequencing read alignments. An early metric of quality is the Q score, which is a loose representation of base call accuracy. It gives the probability that a given base was incorrect, such that a Q score of 30 for a region indicates that there is a 1:1000 chance a base was wrongly assigned. Desirable Q scores are generally considered 25 or above, and our exosomal RNA sequencing Q scores did not fall below 27 with the exception of one read (Table 4.3). Another measure of data quality is the percentage of mated pairs, which is relevant for paired-end sequencing. This metric quantifies concordance between sequencing reads from either end of the cDNA and demonstrates proportion of read 1 (R1) and read 2 (R2) sequences that aligned to the same genomic region, giving confidence in the identified gene. Mated pairs above 80% are considered reliable, and all but 2 samples (control and treated samples from the same donor) met these standards (Table 4.3). Overall, the technical quality of exosomal RNA sequencing was ideal. Upon mapping the sequence alignments to the human genome, 2% of all sequences mapped to coding sequences. While this mapping rate is low for traditional samples, it is not unusual for exosomes (Huang *et al.*, 2013; Santangelo *et al.*, 2016). This result is not uncommon for HDE either: Bioanalyzer profiles on HDE from a mouse hepatocyte cell line have shown enrichment for small, likely non-coding RNAs (Momen-Heravi *et al.*, 2015a). It should be noted, however, that primary rat hepatocyte Bioanalyzer profiles and those from a different mouse hepatocyte cell line present much higher levels of large RNAs, suggesting that different hepatocyte lines may have unique RNA profiles (Royo *et al.*, 2013). Taking into consideration both the unique RNA profiles of exosomes and the high quality of our

sequencing data, we interpret the low mapping rate to be a true reflection of the abundance of coding sequences in human HDE.

Due to the low proportion of coding sequence maps in our data set, robust statistical comparisons between the mRNA content of HDE from control versus APAP-treated human hepatocytes could not be performed. However, we obtained sufficient data to perform pathway enrichment on control HDE and on APAP HDE relative to control HDE. First, we used raw counts to identify the most abundant mRNAs in untreated (control) primary human HDE (Table 4.4). Of these genes, many were also detected in rat HDE *in vitro* and *in vivo*, suggesting that these contents may be germane to hepatocyte EVs (Miyamoto *et al.*, 2008; Okubo *et al.*, 2013; Royo *et al.*, 2013); they are marked in Table 4.4 with an asterisk. These mRNAs are highly expressed in both rat and human liver (Yu *et al.*, 2010) and were detected by qRT-PCR in our earlier analyses of primary human HDE mRNA (n=3 donors) (Holman *et al.*, 2016). IPA was used to define over-represented pathways in these data (Figure 4.3), some of which were also identified in rat HDE by Royo *et al*. Shared pathways included acute phase response, clathrin-mediated endocytosis, LXR/RXR activation, and cholesterol metabolism.

Statistical RNA-seq package DESeq2 was used to generate $\log_2$ fold change values for transcripts elevated in APAP HDE versus vehicle (control) HDE. Given the small sample size and low mapping frequency, statistically significant differences were not observed. However, a shift in the exosomal mRNA enrichment was observed between HDE from APAP treated human hepatocytes (Figure 4.4). Interestingly, many of the differentially enriched mRNAs in APAP HDE have been associated with APAP-induced stress at the hepatocyte level. For instance, components of the electron transport chain (*COX7B, ATP5,*

UQCR, NDUFB) were differentially increased in APAP HDE and were significantly up-regulated in HepG2 cells following exposure to the same concentration of APAP we employed (10 mM) (Jiang *et al.*, 2015). The abundance of multiple ribosomal mRNAs associated with EIF signaling also increased in APAP HDE, many of which were differentially regulated in HepG2 spheroids following APAP exposure (Wojdyla *et al.*, 2016). These mitochondrial and ribosomal mRNAs are mechanistically relevant to APAP toxicity as they represent altered ATP production and protein production, respectively. Abundant transcripts in APAP HDE were then compared to genes that were significantly altered in primary human hepatocytes exposed to 10 mM APAP for 24 h relative to untreated controls. Of the top 150 most increased mRNAs in APAP HDE, 99 overlapped with significant DE genes in APAP hepatocytes (Table 4.5). Pathway enrichment analysis revealed that the overlapping genes from APAP HDE represent biological and toxicological processes that are mechanistically relevant in APAP DILI (Figure 4.5). These data suggest that the mRNA contents of HDE following drug-induced stress may indeed reflect gene expression changes within hepatocytes.

Table 4.3. Sequence quality metrics from human exosomal RNA-seq samples

Sample	R1 Minimum Q-score	R2 Minimum Q-score	Mated Pairs (%)
Donor 1 Control	31	31	87.1
Donor 1 APAP	32	31	85.2
Donor 2 Control	16	27	60.7
Donor 2 APAP	27	31	71.8
Donor 3 Control	32	31	85.2
Donor 3 APAP	31	31	85.4
Donor 4 Control	31	31	86.8
Donor 4 APAP	31	31	85.5
Donor 5 Control	31	31	83.5
Donor 5 APAP	32	31	84.4

Table 4.4. Top 50 most abundant mRNAs in control human HDE. * indicates mRNAs that overlap with the top 50 most abundant mRNAs in control rat HDE (Royo *et al.*, 2013).

Gene Symbol	Gene Name	Counts
*FTL**	ferritin light chain	13486
ALB	albumin	13393
*HP**	haptoglobin	8775
SAA1	serum amyloid A1	7950
ORM1	α-1-acid glycoprotein 1 (orosomuscoid 1)	5704
APOA1	apolipoprotein A1	3991
*SERPINA1**	serpin family A member 1	3923
*APOA2**	apolipoprotein A2	3431
ROCK1P1	Rho-associated coiled-coil containing protein kinase 1	3137
*FTH1**	ferritin heavy chain 1	2782
*AMBP**	α-1-microglobulin bikunin precursor	2178
SAA2	serum amyloid A2	2145
*APOC3**	apolipoprotein C3	1964
GAPDH	glyceraldehyde-3-phosphate dehydrogenase	1830
*RBP4**	retinol binding protein 4	1738
TAOK1	TAO kinase 1	1452
*TTR**	transthyretin	1443
*APOC1**	apolipoprotein C1	1267
*APOE**	apolipoprotein E	1256
TTN	titin	1080
KCNQ1OT1	KCNQ1 opposite strand/antisense transcript 1	1064
*ACTB**	actin beta	987
TFPI	tissue factor pathway inhibitor	966
CLU	clusterin	943
DUX2	DUX4L8 double homeobox 4 like 8	831
CDC27	cell division cycle 27	818
ORM2	orosomucoid 2	805
UBC	ubiquitin C	795
KNG1	kininogen 1	786
FGG	fibrinogen gamma chain	698
SOD2	superoxide dismutase 2, mitochondrial	676
CCDC168	coiled-coil domain containing 168	669
REXO1L1	REX1, RNA exonuclease 1 homolog-like 1 pseudogene	657
SERPINA3	serpin family A member 3	631
*APOH**	apolipoprotein H	626

Table 4.4. *continued*

Gene Symbol	Gene Name	Counts
*B2M**	β-2 microglobulin	617
SH3KBP1	SH3 domain containing kinase binding protein 1	612
IL32	interleukin 32	595
VTN	vitronectin	594
LOC100272216	uncharacterized LOC100272216	586
LOC388692	uncharacterized LOC388692	579
ANKRD20A9P	ankyrin repeat domain 20 family member A9 pseudogene	576
HYDIN2	axonemal central pair apparatus protein pseudogene	574
FGL1	fibrinogen like 1	571
UBB	ubiquitin B	569
LOC440297	chondroitin sulfate proteoglycan 4 pseudogene, discontinued	562
CLDN11	claudin 11	545
CFB	complement factor B	529
FGB	fibrinogen beta chain	514
AKR1C2	aldo-keto reductase family 1 member C2	512

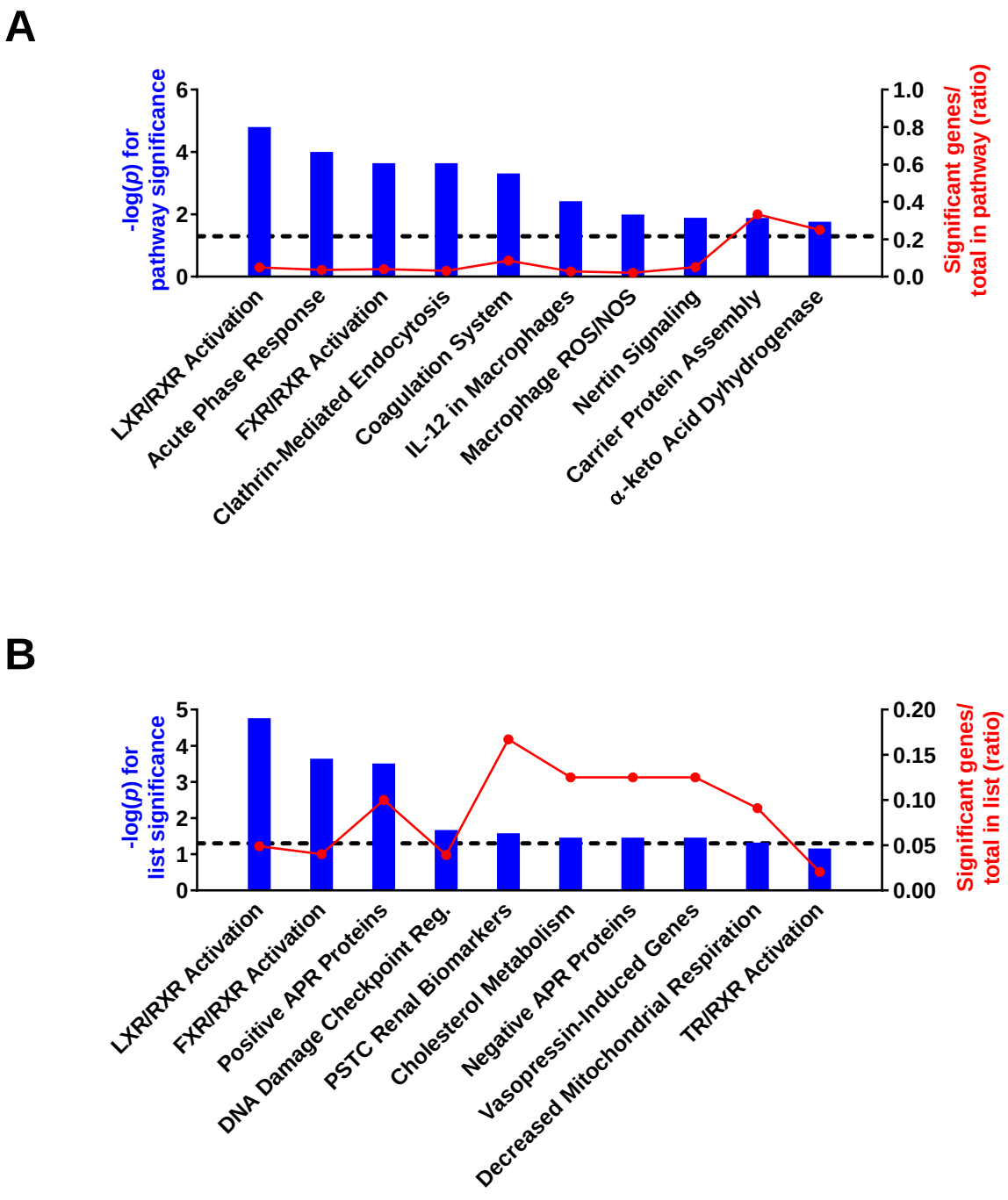

Figure 4.3. Top 10 pathways enriched in exosomal mRNA from untreated primary human hepatocytes. Pathway enrichment was performed on the 100 most abundant exosomal mRNAs based on maximum count across donors (n=5). Canonical pathways (A) and toxicity-related pathways (B) are represented. The dashed line indicates a –log(*p*) > 1.3 threshold for pathway significance.

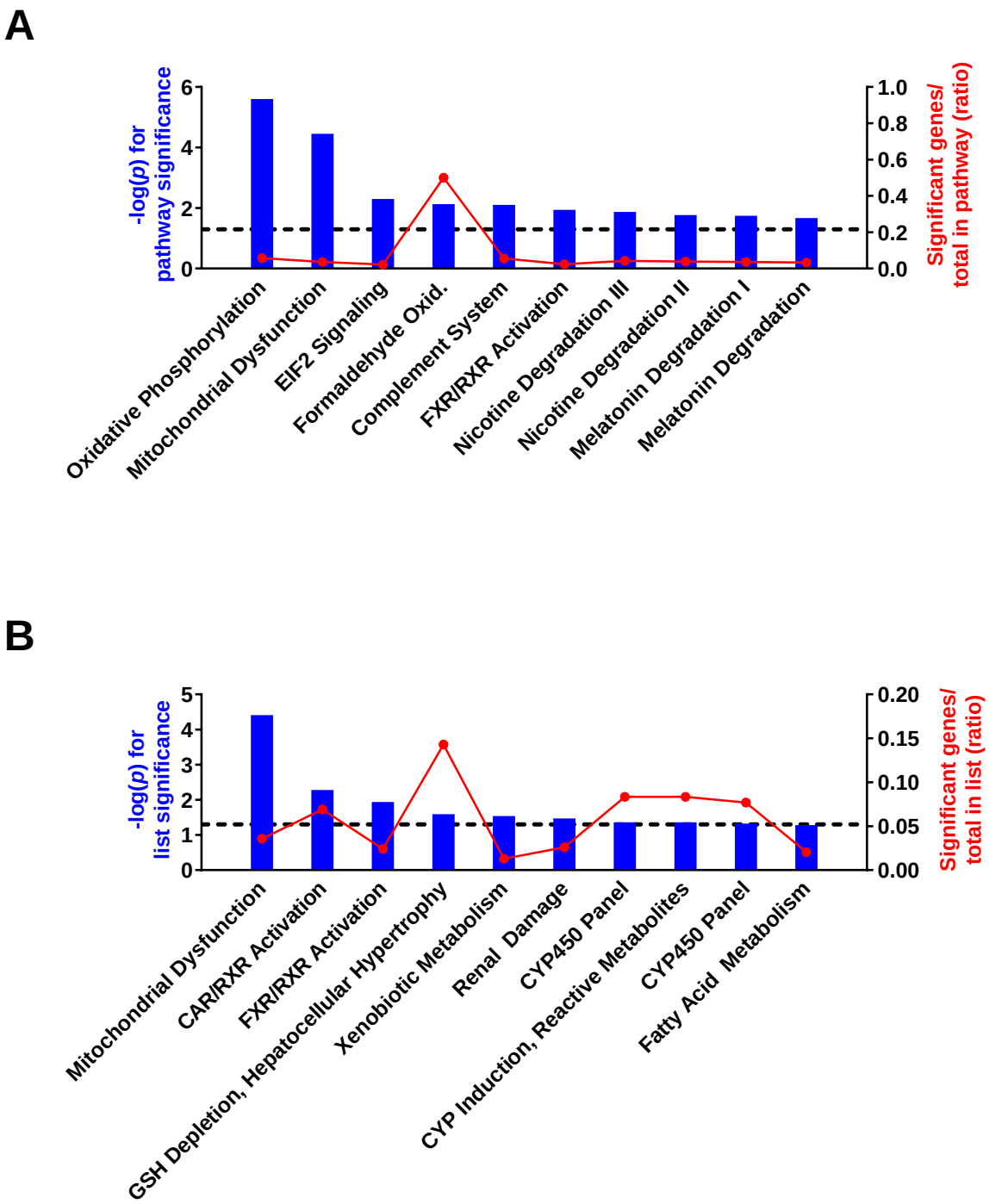

Figure 4.4. Top 10 pathways enriched in exosomal mRNA from APAP-treated primary human hepatocytes. Pathway enrichment was performed on the 100 most differentially expressed exosomal mRNAs across donors (n=5) relative to controls. Canonical pathways (A) and toxicity-related pathways (B) are represented. The dashed line indicates a –log(*p*) > 1.3 threshold for pathway significance.

Table 4.5. Transcripts increased within APAP HDE that overlap with differentially expressed genes in APAP-exposed primary human hepatocytes.

Gene Symbol	Name
ACBD6	acyl-CoA binding domain containing 6
ACP1	acid phosphatase 1, soluble
ADH1A	alcohol dehydrogenase class 1A, alpha polypeptide
ADH1C	alcohol dehydrogenase class 1C, gamma polypeptide
AHSG	alpha 2-HS glycoprotein
AIMP2	aminoacyl tRNA synthetase complex interacting multifunctional protein 2
ALDH1A1	aldehyde dehydrogenase 1 family member A1
APOH	apolipoprotein H
APRT	adenine phosphoribosyltransferase
ATP5A1	mitochondrial complex V: ATP synthase subunits
ATP5I	mitochondrial ATP synthase, H+ transporting, mitochondrial F0 complex subunit E
ATPIF1	APTase inhibitory factor 1
BARHL2	BarH like homeobox 2
C9orf16	chromosome 9 open reading frame 16
CALM1	calmodulin 1
CBR1	carbonyl reductase 1
CFB	complement factor B
CFH	complement factor H
CHCHD2	coiled-coil helix coiled-coil helix domain containing 2
CNN3	calponin 3
COX4I1	mitochondrial complex IV: cytochrome C oxidase subunit 4I1
COX5A	cytochrome c oxidase subunit 5A
COX5B	cytochrome c oxidase subunit 5B
COX6C	cytochrome c oxidase subunit 6C
COX7B	cytochrome c oxidase subunit 7B
CYP2C9	cytochrome P450 family 2 subfamily C member 9
CYSTM1	cysteine rich transmembrane module containing 1
DAD1	defender against cell death 1
DCAF12	DDB1 and CUL4 associated factor 12
DCD	dermicidin
DYNLL1	dynein light chain LC8 type 1
ECHS1	enoyl-CoA hydratase, short chain 1
EPHA4	EPH receptor A4

Table 4.5. *continued*

Gene Symbol	Name
ESD	esterase D
FSHR	follicle stimulating hormone receptor
FUCA2	fucosidase, alpha L2, plasma
GC	vitamin D binding protein
HMGN1	high mobility group nucleosome binding domain 1
IGBP1	immunoglobulin (CD79A) binding protein 1
ISCA1	iron-sulfur cluster assembly 1
ISG20	interferon stimulated exonuclease gene 20
KPNA3	karopherin subunit alpha 3
KRTCAP2	keratinocyte associated protein 2
LIPI	lipase I
MOSPD1	motile sperm domain containing 1
MRGPRX2	MAS related GPR family member X2
MRPL37	mitochondrial ribosomal protein L37
MRPL39	mitochondrial ribosomal protein L39
MRPL54	mitochondrial ribosomal protein L54
MRPS5	mitochondrial ribosomal protein S5
NDUFB1	NADH:ubiquinone oxidoreductase subunit B1
NDUFB9	NADH:ubiquinone oxidoreductase subunit B9
NFIL3	nuclear factor, interleukin 3 regulated
NUDCD2	NudC domain containing 2
OAZ1	ornithine decarboxylase antizyme 1
OR10A7	olfactory receptor family 10 subfamily A member 7
OR10AD1	olfactory receptor family 10 subfamily AD member 1
OR1A1	olfactory receptor family 1 subfamily A member 1
OR4K17	olfactory receptor family 4 subfamily K member 17
OR51I1	olfactory receptor family 51 subfamily I member 1
OR7E5P	olfactory receptor family 7 subfamily E member pseudogene
PABPC3	poly(A) binding protein cytoplasmic 3
PEBP1	phosphatidylethanolamine binding protein 1
PLSCR1	phospholipid scramblase 1
PQLC3	PQ loop repeat containing 3
PSMB6	proteasome subunit beta 6
PSMB7	proteasome subunit beta 7
PSMB9	proteasome subunit beta 9
PSMC1	proteasome subunit 26S, ATPase 1
PTGR1	prostaglandin reductase 1
RPL19	ribosomal protein L19

Table 4.5. *continued*

Gene Symbol	Name
RPL31	ribosomal protein L31
RPLP1	ribosomal protein lateral stalk subunit P1
RPS12	ribosomal protein S12
RPS16	ribosomal protein S16
RPS18	ribosomal protein S18
SBDS	SBDS ribosome assembly guanine nucleotide exchange factor
SEPP1	selenoprotein P1, plasma
SERF2	small EDRK-rich factor 2
SIGLEC1	sialic acid binding Ig like lectin 1
SLC35A1	solute carrier family 35 member A1
SNRPD2	small nuclear ribonucleoprotein polypeptide N
SNRPN	SNRPN upstream reading frame-like (pseudogene)
TAAR6	trace amine associated receptor 6
TCEA3	transcription elongation factor A3
TCEB2	transcription elongation factor B subunit 2
TDO2	tryptophan 2,3-dioxygenase
TMEM117	transmembrane protein 177
TMEM199	transmembrane protein 199
TMEM99	transmembrane protein 99
TNFAIP8	TNF alpha induced protein 8
TP53TG1	TP53 target 1 (non-protein coding)
TPT1	tumor protein, translationally-controlled 1
TXNL1	thioredoxin like 1
UGT2B4	UDP glucuronosyltransferase family 2 member B4
UQCRB	ubiquinol-cytochrome C reductase binding protein
UQCRQ	ubiquinol-cytochrome C reductase complex III subunit VII
YBX1	Y-box binding protein 1
ZNF155	zinc finger protein 155

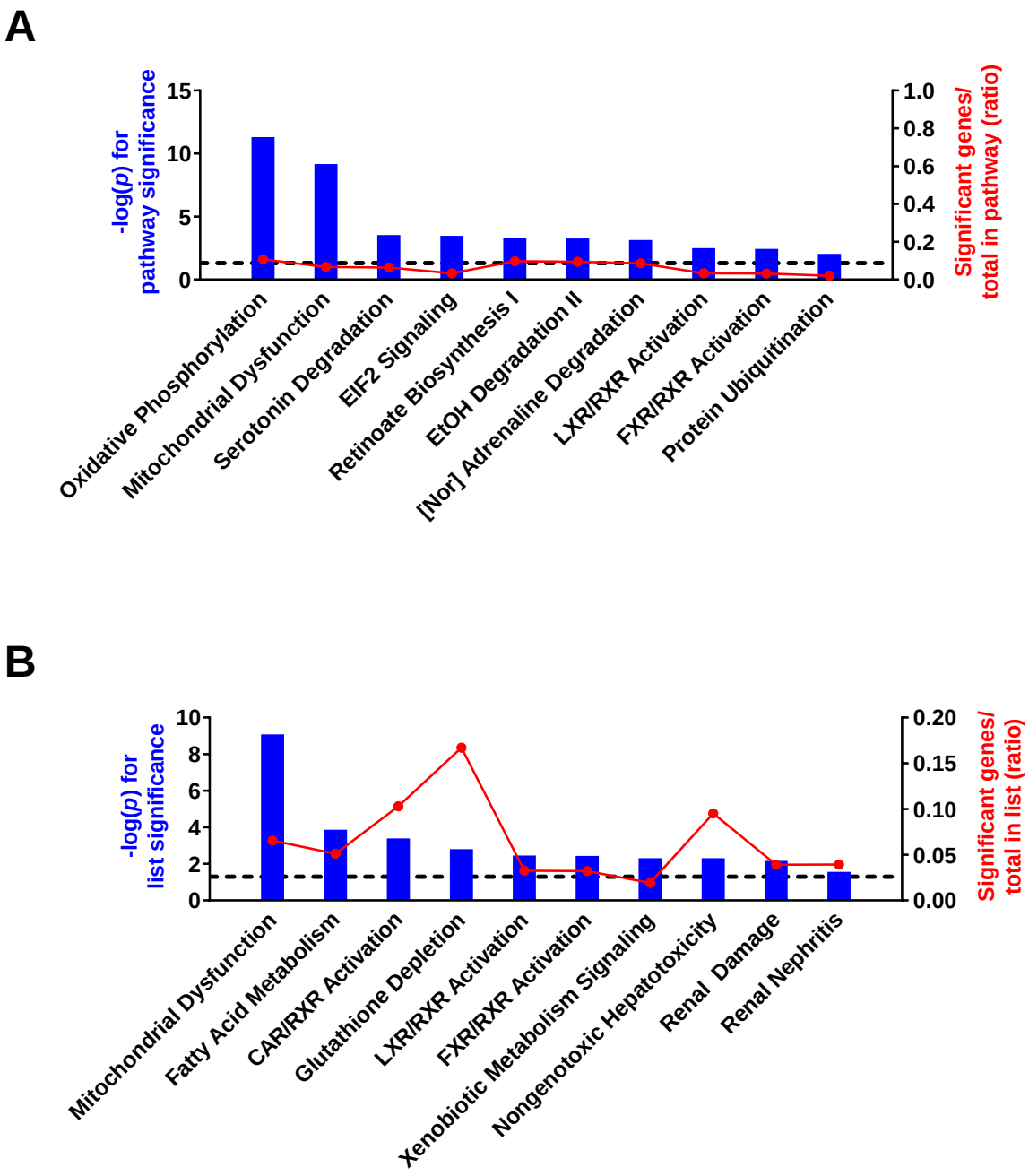

Figure 4.5. Top 10 pathways represented by genes common to APAP HDE and APAP-treated hepatocytes. Pathway enrichment was performed on the 99 differentially enriched genes in APAP HDE that were significantly increased in primary human hepatocytes (n=5 donors per data set). Canonical pathways (A) and toxicity-related pathways (B) are presented. The dashed line indicates a –log(*p*) > 1.3 threshold for pathway significance.

4.3.3 Cytotoxicity measurements in primary human hepatocytes following APAP exposure

At the end of each APAP exposure, medium was collected for exosome enrichment and cytotoxicity assays were conducted to measure urea production, cellular ATP, and LDH leakage. Results from these assays across 5 donors are shown in Figure 4.6. In 3 cases, LDH, a necrotic cell death marker, was significantly decreased following APAP treatment. When assessed in the context of mild urea and ATP decreases, these results suggest cellular stress rather than overt injury with 10 mM APAP for 24 h, which is consistent with prior findings (Holman *et al.*, 2016; Kia *et al.*, 2015). The exception is donor 3, which appears uniquely sensitive to APAP.

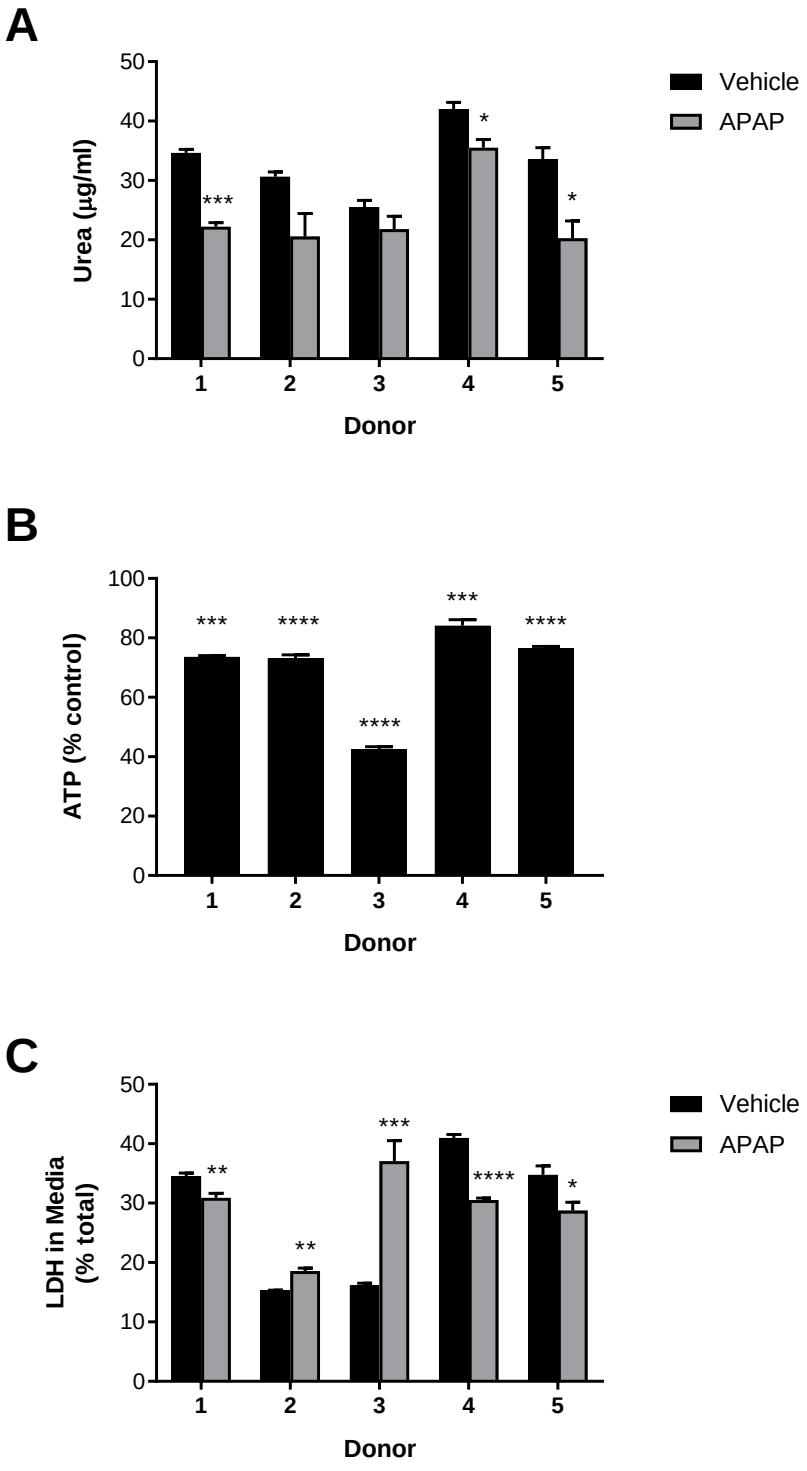

Figure 4.6. Cytotoxicity measured in primary human hepatocytes used for HDE generation. Data represent mean + SEM of biological replicates and duplicate assay wells from n=5 donors following 24 h of 10 mM APAP or vehicle exposure. * $p < 0.05$, ** $p < 0.01$, *** $p < 0.001$, **** $p < 0.0001$; Student's t-test comparing vehicle to APAP for each donor.

4.3.4 miRNA profiling results are consistent across replicates and sources of exosomal RNA

We compared HTG miRNA profiling results across replicates as well as across input types (whole exosomes and isolated exosomal RNA) and treatment groups (APAP and control). We observed good concordance between data collected from whole exosomes and total RNA isolated from the same exosome sample (Figure 4.7), which confirmed that whole HDE were a viable input material for our purposes. Elimination of RNA extraction is optimal because it eliminates excessive sample handling and any inherent bias introduced by the RNA isolation method. Upon verifying HDE as an appropriate sample type, we evaluated the reproducibility of data by profiling the miRNA content of 2 identical HDE aliquots prepared from either control- or APAP-treated primary human hepatocytes. Replicates of both groups were highly correlated (Figure 4.7) suggesting low technical variability, and validated the use of the HTG miRNA profiling platform for global HDE miRNA analysis.

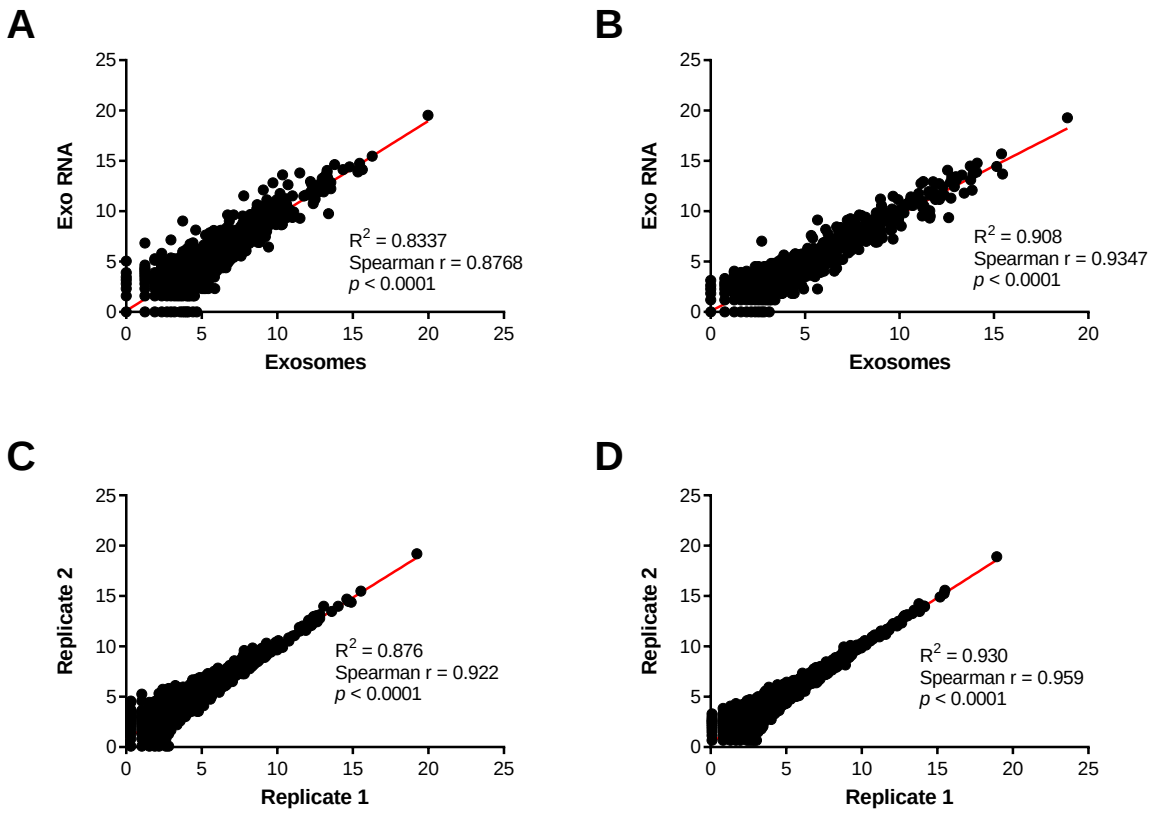

Figure 4.7. miRNA profiling validation across sample types and replicates. Exosomes or corresponding exosomal RNA from control-treated hepatocytes (A) and APAP-treated hepatocytes (B) were analyzed side-by-side to validate whole exosomes as a suitable input for HTG miRNA Whole Transcriptome profiling. Two identical replicates from control HDE (C) and APAP HDE (D) were profiled to ensure reproducibility. Black dots represent $\log_2$ normalized counts and red lines show the data fitted with linear regression models.

4.3.5 Global miRNA profiles in human HDE shift as a result of APAP exposure

Data from control and APAP HDE from Donor 4 did not pass quality control filters due to inefficient sample lysis and were discarded. Median-normalized exosomal miRNA results from the remaining donors (n=4) were filtered by a list of miRNAs with consistent expression in human liver samples, obtained via personal communications with Dr. Wanqing Liu, a contributing author to the Gamazon *et al* manuscript. Partek Genomics Suite (version 6.6) was used for statistical analysis of differential miRNA enrichment between HDE from control- and APAP-treated human hepatocytes by linear contrast. With a data set of this size and exposure to a sub-toxic APAP concentration, the power to detect statistically significant differences in miRNA profiles was limited. As a result, no statistically significant differences between APAP and control HDE across all donors were observed. This outcome may be due in part to the distinct differences in exosomal miRNA patterns observed between donors in response to APAP exposure (Figure 4.8). Donor was the most significant source of variability, and global exosomal miRNA profiles following APAP-induced hepatocellular stress were donor-specific. The cytotoxicity data collected from these same donors (Figure 4.6) was not highly variable across individuals, and would suggest that hepatocyte responses to APAP did not differ greatly across donors, while the exosomal miRNA content reveals extensive donor-to-donor variation. These results underscore the importance of integrating primary cells into exosome activity studies, as exosomes from immortalized cell lines fail to capture the extensive diversity of human donors.

Although none of the miRNA changes were statistically significant, there were marked shifts in miRNA abundance between APAP HDE and control HDE. Figure 4.9 presents miRNAs with the highest and lowest fold changes in APAP HDE relative to control

HDE. We compared the differentially expressed miRNAs in our exosomal data set to miRNAs that have been altered in plasma in at least 2 other studies of APAP DILI, either from published work (Krauskopf *et al.*, 2015; Starkey Lewis *et al.*, 2011; Vliegenthart *et al.*, 2015; Ward *et al.*, 2014) or an in-house rat study (data unpublished). The fold changes of miRNAs that were detected in our data set and also differentially expressed in at least 2 additional studies of APAP DILI are shown in Figure 4.10.

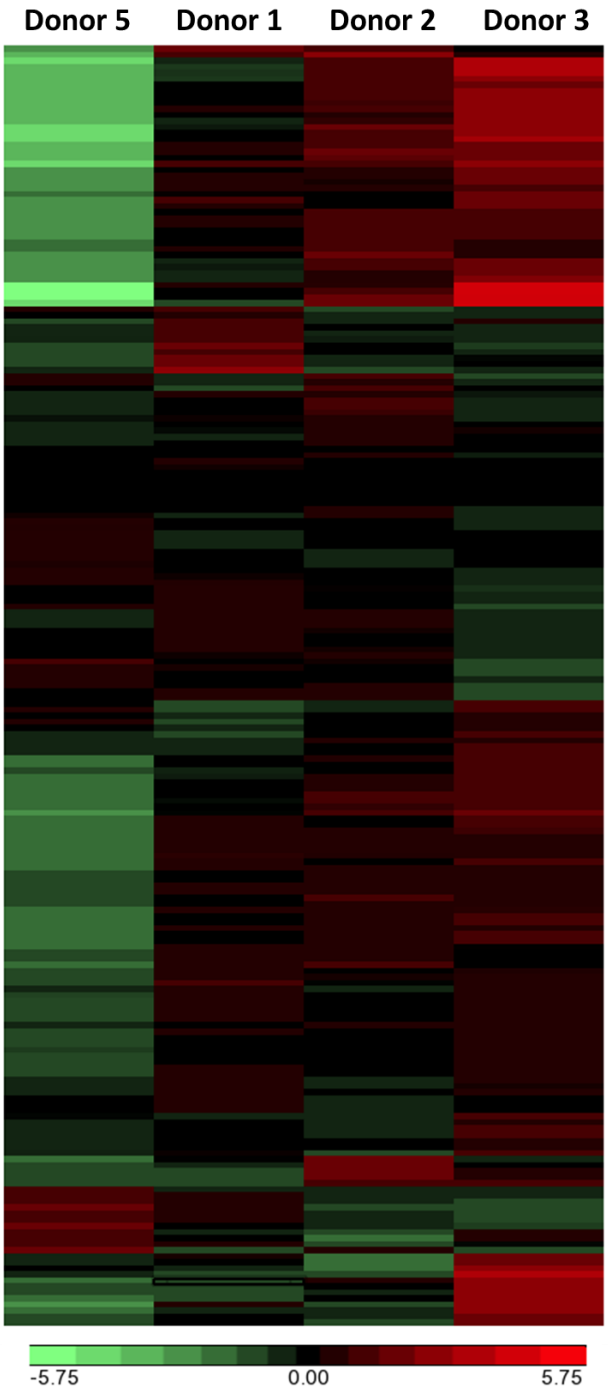

Figure 4.8. Distinct donor-specific responses to APAP are captured by exosomal miRNA profiling. Differential expression for each donor was determined by linear contrasts between the miRNA content of HDE from APAP-treated hepatocytes and control-treated hepatocytes. Coloration reflects directionality of $\log_2$ ratio of the contrast (green, down-regulated in APAP HDE; red, up-regulated in APAP HDE).

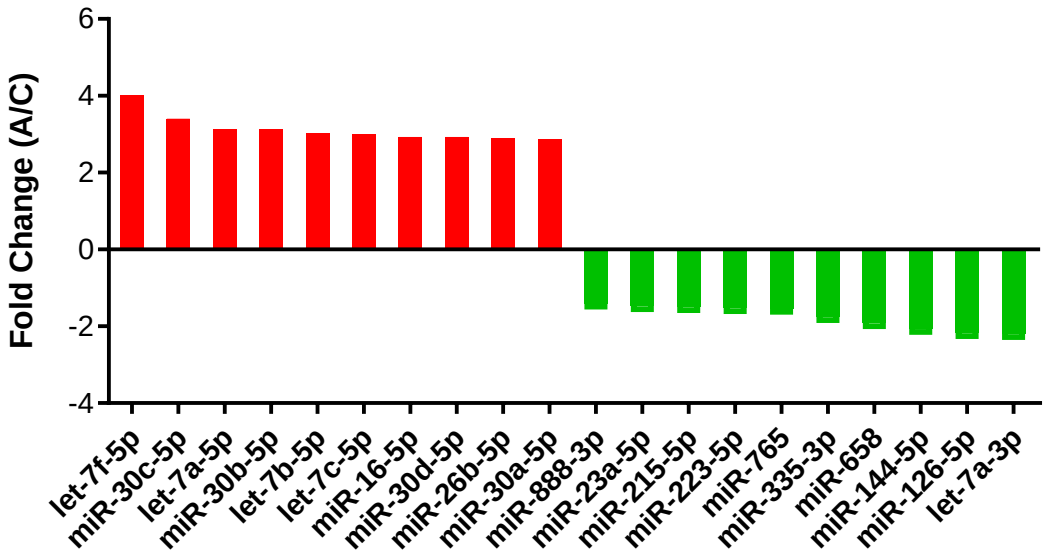

Figure 4.9. Top 10 up- and down-regulated miRNAs in human HDE as a result of APAP exposure. Data represent fold changes in HDE from APAP-treated hepatocytes relative to control-treated hepatocytes across all donors.

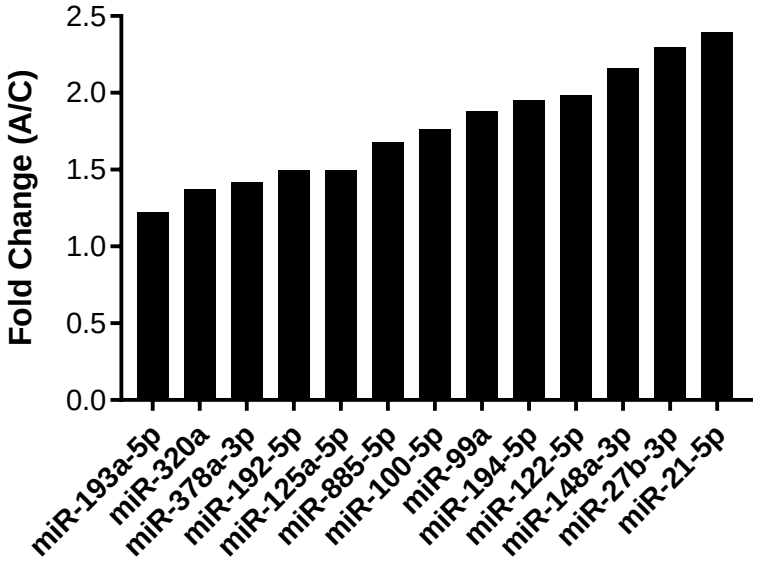

Figure 4.10. Fold changes of exosomal miRNAs associated with APAP-induced liver injury. Data represent fold changes in HDE from APAP-treated hepatocytes relative to control-treated hepatocytes across all donors. Candidate miRNAs were selected if they were differentially regulated in the circulation of treated subjects from 2 or more *in vivo* studies of APAP DILI.

4.3.6 Verification of HDE biological activity using models of non-parenchymal and immune cells

The effects of exosomes from control- and APAP-treated human hepatocytes were initially investigated on multiple representative human non-parenchymal cell types: THP-1 macrophages to mimic resident hepatic Kupffer cells, TMNK-1 immortalized SECs, and THP-1 monocytes to mimic infiltrating immune cells. This work was conducted to substantiate the hypothesis that HDE exert biological activity on hepatic cell types prior to deeper mechanistic inquiries.

Macrophages

First, adherent macrophages were derived from THP-1 monocytes via PMA differentiation. Macrophages were incubated with HDE from human hepatocytes exposed to vehicle, 10, or 30 mM APAP for 8 h to mimic baseline conditions, drug-induced stress, and overt cytotoxicity, respectively. Following HDE incubation and an 8 h washout period, macrophages were transitioned to medium +/- LPS for a total experimental duration of 24 h. The addition of LPS served as a positive control to invoke *NOX2* gene expression (Kim *et al.*, 2010).

Cells were then lysed for RNA isolation and the prototypical immune activation markers NADPH oxidase 2 (*NOX2*) and heme oxygenase 1 (*HO-1*) were measured in cells by RT-PCR. Interestingly, in the macrophages that were exposed to HDE but were not stimulated with LPS, *NOX2* expression was decreased (Figure 4.11). Cells that were treated with the same HDE and were subsequently stimulated with LPS showed a reversal of this trend such that *NOX2* levels were increased relative to medium alone. *HO-1* expression was

significantly affected by the addition of HDE but was not impacted by the addition of LPS (Figure 4.11). *HO-1* was induced most strongly by control HDE and this induction decreased in relation to the APAP concentration given to the hepatocytes.

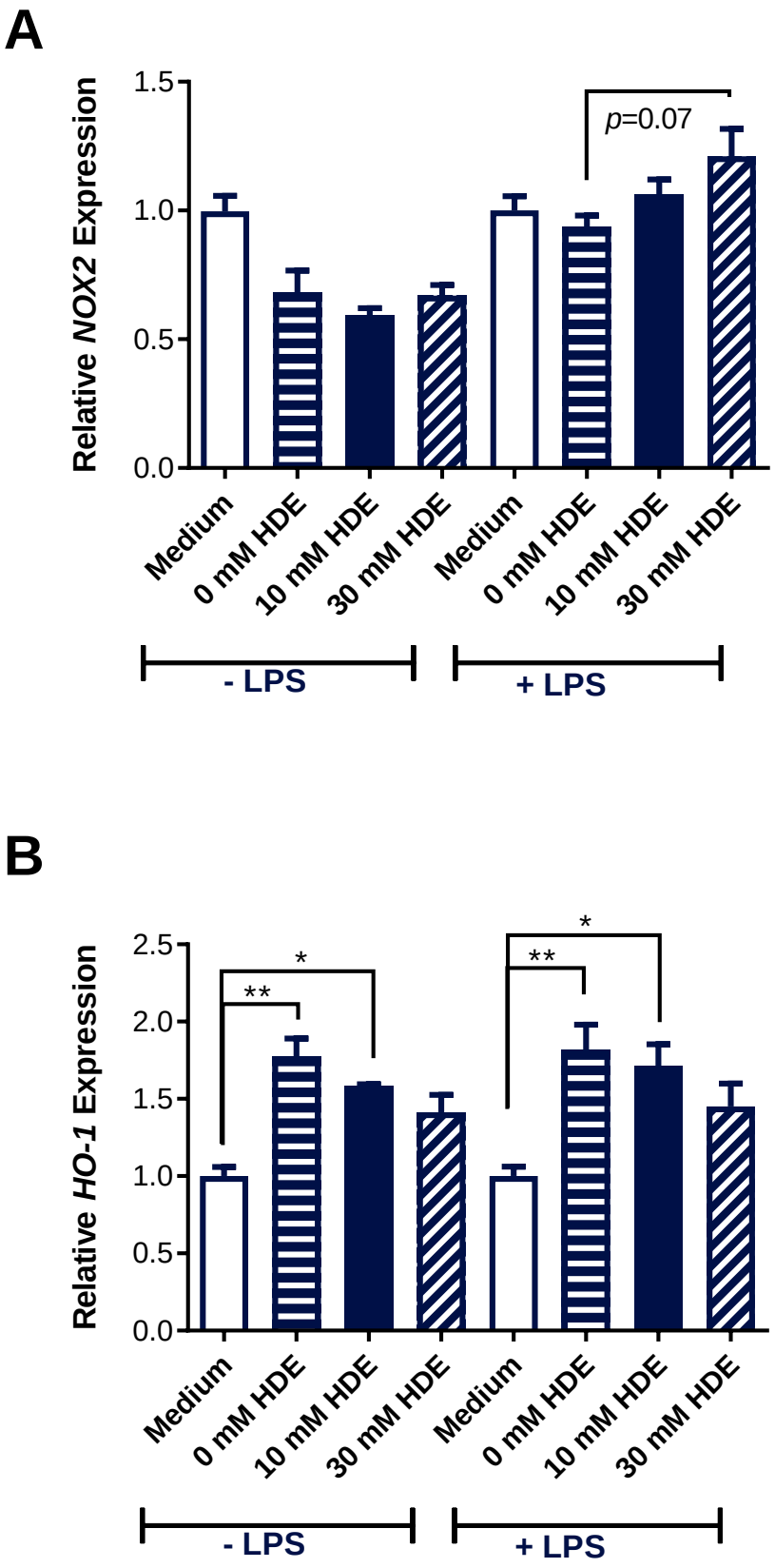
A
Relative NOX2 Expression
1.5
1.0
0.5
0.0
p=0.07
Medium
0 mM HDE
10 mM HDE
30 mM HDE
Medium
0 mM HDE
10 mM HDE
30 mM HDE
- LPS
+ LPS
B
Relative HO-1 Expression
2.5
2.0
1.5
1.0
0.5
0.0
*
**
**
*
Medium
0 mM HDE
10 mM HDE
30 mM HDE
Medium
0 mM HDE
10 mM HDE
30 mM HDE
- LPS
+ LPS

Figure 4.11. Impact of primary human HDE on prototypical immune response genes in macrophages. Data represent the mean + SEM of replicate culture wells and triplicate RT-PCR reactions for *NOX2* (A) and *HO-1* (B). Statistical comparisons were made within each stimulation group (i.e. all treatments without LPS were compared to one another but not to the LPS-activated group). * $p < 0.05$, ** $p < 0.01$; one-way ANOVA with Tukey's multiple comparisons test.

Sinusoidal endothelial cells

Cells from the immortalized human SEC line TMNK-1 were also exposed to HDE from control- and APAP-treated human hepatocytes. Following a 24 h incubation with HDE, SECs were stimulated with LPS to induce expression of cellular adhesion molecules, used as a physiologically relevant readout of SEC activation and possible HDE effects (Giugliano *et al.*, 2015; Matsumura *et al.*, 2004). Expression of intracellular adhesion molecule 1 (*ICAM1*), vascular endothelial cadherin (*CDH5*), and E-selectin (*SELE*) were measured by RT-PCR relative to *GAPDH* (Figure 4.12). All three genes were down-regulated by HDE regardless of hepatocyte treatment (control or APAP) relative to medium + LPS. Small but statistically significant decreases were observed for all genes, with the most pronounced down-regulation by HDE occurring for *SELE*. *SELE* expression was not significantly affected by control HDE, but was greatly suppressed in the presence of APAP HDE.

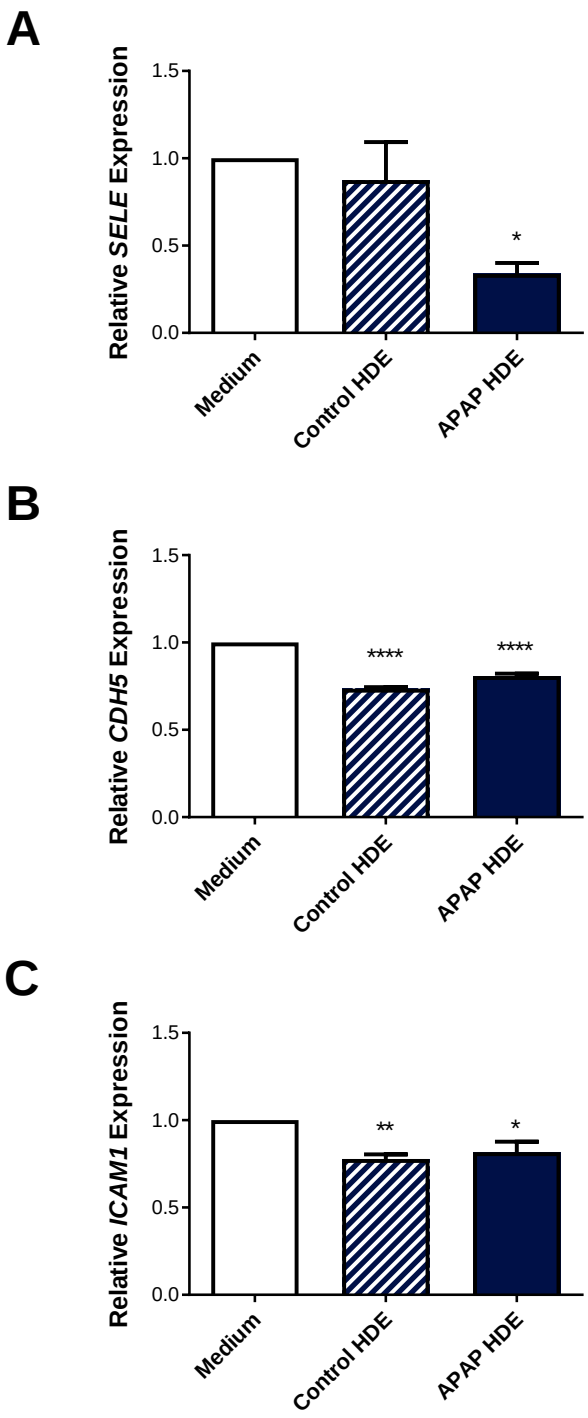

Figure 4.12. Impact of primary human HDE on expression of cellular adhesion molecules in LPS-stimulated sinusoidal endothelial cells. Data represent the mean + SEM of replicate culture wells and triplicate RT-PCR reactions for *SELE* (A), *CDH5* (B), and *ICAM1* (C). * $p < 0.05$, ** $p < 0.01$, **** $p < 0.0001$; one-way ANOVA with Dunnett's post-test relative to medium.

Monocytes

Monocytes are the principal cell type of interest for HDE exposures because they are some of the first cells to be recruited to sites of injury such as hepatocellular necrosis (Antoniades *et al.*, 2012). For these initial experiments, we used cytokine secretion as a functional endpoint to indicate if HDE had any overt immune effects. To accomplish this, we exposed THP-1 monocytes to medium, 100 µg/ml, or 200 µg/ml HDE from control- and APAP-treated human hepatocytes. Monocytes were incubated with HDE for 24 h followed by a 6 h LPS stimulation to induce cytokine response. The level of LPS (5 ng/ml) was selected from empirical concentration-response tests to produce sub-maximal cytokine release, allowing us to observe both increases and decreases in cytokine response induced by HDE exposure (Figure 4.13).

To select cytokines of interest, we first performed a 10-plex analysis on LPS-stimulated monocytes and found that IL-8 and TNF-α were most robustly affected compared to IL-1β which was poorly expressed and IL-6 which was almost undetectable (data not shown). It has been established that THP-1 cells do not express IL-6 and IL-1β at the same levels as primary monocytes (Schildberger *et al.*, 2013), but evidence is conflicting depending on the number of cells used and the stimulus (Bretz *et al.*, 2013; Skazik-Voogt *et al.*, 2016).

Secretion of pro-inflammatory cytokines TNF-α and IL-8 was decreased in monocytes treated with control HDE relative to no-exosome (LPS alone) control (Figure 4.14). The reduction of cytokine secretion by control HDE-treated monocytes appeared to be dependent upon exosome concentration: suppression was slightly greater in the 200 µg/ml cultures than in the 100 µg/ml cultures (Figure 4.14). Interestingly, THP-1 cells exposed to

APAP HDE produced higher levels of both cytokines than those exposed to control HDE, but quantities did not exceed LPS alone. APAP HDE produced a concentration-responsive increase in IL-8, but not in TNF-α.

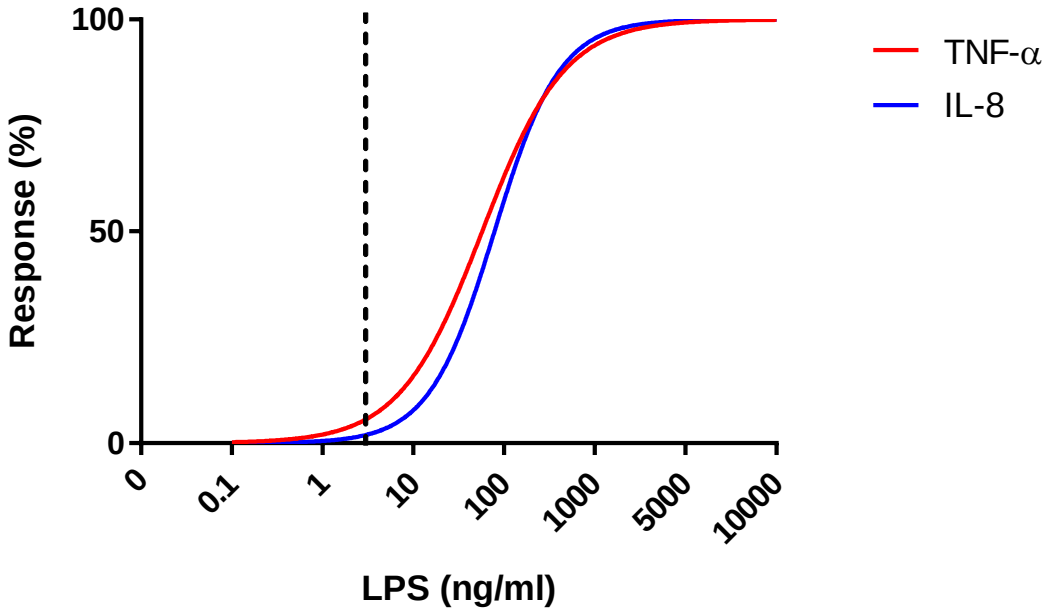

Figure 4.13. Selection of LPS concentration for monocyte stimulation using pro-inflammatory cytokine responses. Data represent the mean + SEM of triplicate culture wells and duplicate assay wells for TNF-α and IL-8. Non-linear regression was performed on normalized data to illustrate minimum and maximum concentration responses. The dashed line indicates 5 ng/ml, the selected concentration for future *in vitro* LPS exposures.

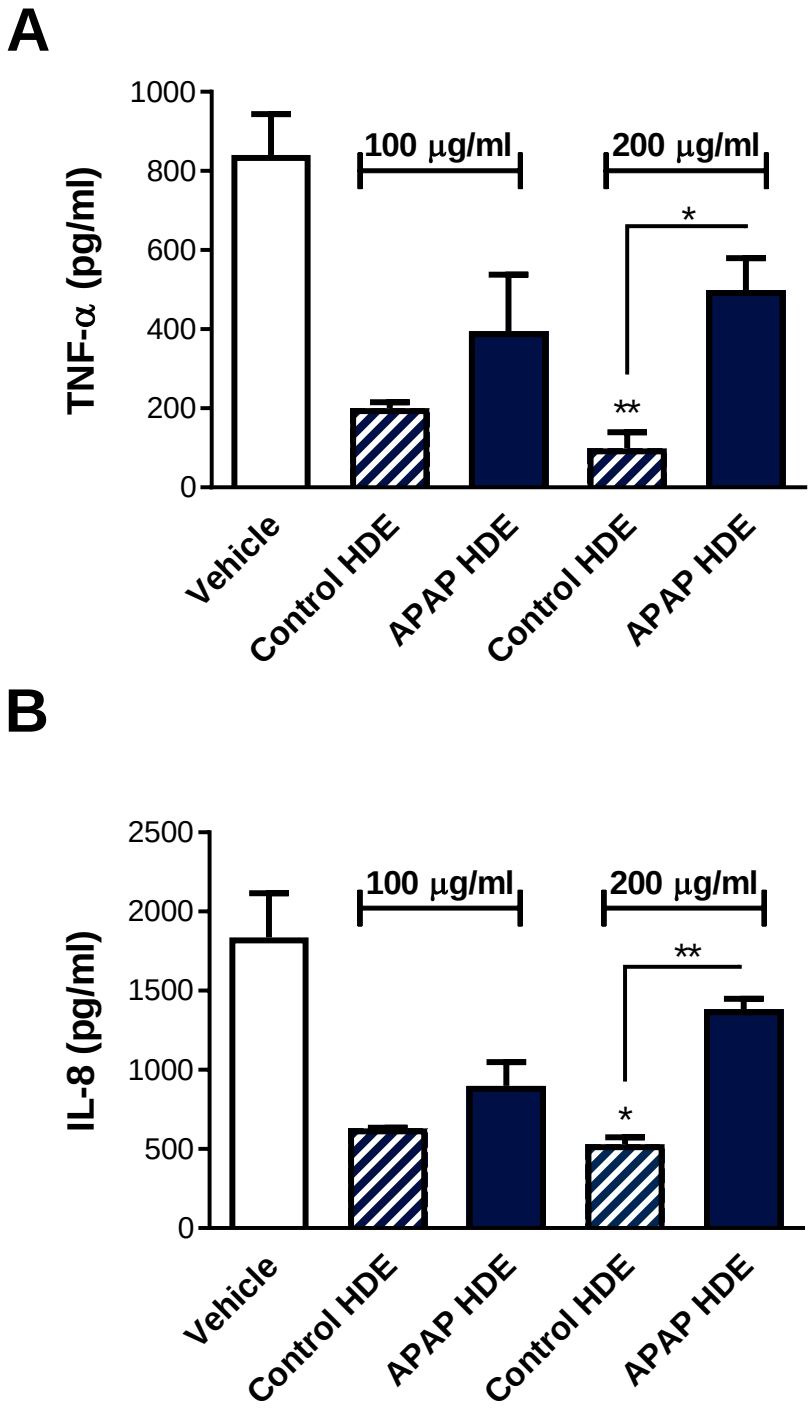

Figure 4.14. HDE from control- and APAP-treated hepatocytes mediate pro-inflammatory cytokine response in LPS-stimulated monocytes. Data represent the mean + SEM of triplicate culture wells and duplicate assay wells for TNF-α (A) and IL-8 (B). * $p < 0.05$, ** $p < 0.01$, Student's t-test.

4.3.7 Accounting for the matrix effects of EQ polymer in HDE activity assays

Recognizing that EQ is an undefined synthetic matrix, we wished to separate EQ-precipitated HDE from the reagent prior to examining the biological activity of exosomes. The manufacturer's protocol was followed to remove EQ polymer via desalting columns and preparations with and without polymer removal were visualized using cryo-electron microscopy (EM) as previously described (Holman *et al.*, 2016). The desalting columns effectively removed most of the EQ polymer, which appears as clouds of granular particles in Figure 4.15. However, in doing so, all of the HDE were also eliminated. From these results, we ascertained that HDE are incorporated into a network of EQ polymer such that one cannot be removed without also removing the other. It was clear that the potential confounding biological effects of EQ itself on recipient cells needed to be accounted for.

To ensure that HDE activity was not due to EQ, we prepared mock controls of control (medium vehicle) and APAP dosing solutions for every hepatocyte donor (n=5). These mock controls were concentrated, precipitated with EQ, and applied to monocytes alongside the corresponding HDE preparations. Adding these experimental conditions allowed us to control for potential activity of not only EQ, but also any residual APAP left in APAP HDE. EQ appeared to have inconsistent but potentially relevant effects on monocyte cytokine secretion induced by LPS (Figure 4.16). Microarray data (described below) suggest that EQ exerts small but statistically significant effects on monocytes relative to medium alone, and that the gene expression changes induced by EQ largely overlap between control and APAP mock preparations (data not shown). For analysis of significant HDE-induced gene expression changes, microarray results from monocytes exposed to exosomes were compared to monocytes exposed to the respective EQ mock (*i.e.* significance of APAP HDE effects

were determined via linear contrast to APAP mock control). These findings represent valuable contributions because, to our knowledge, the gene expression effects of EQ have not previously been described or taken into account in previous functional studies of EQ-precipitated exosomes.

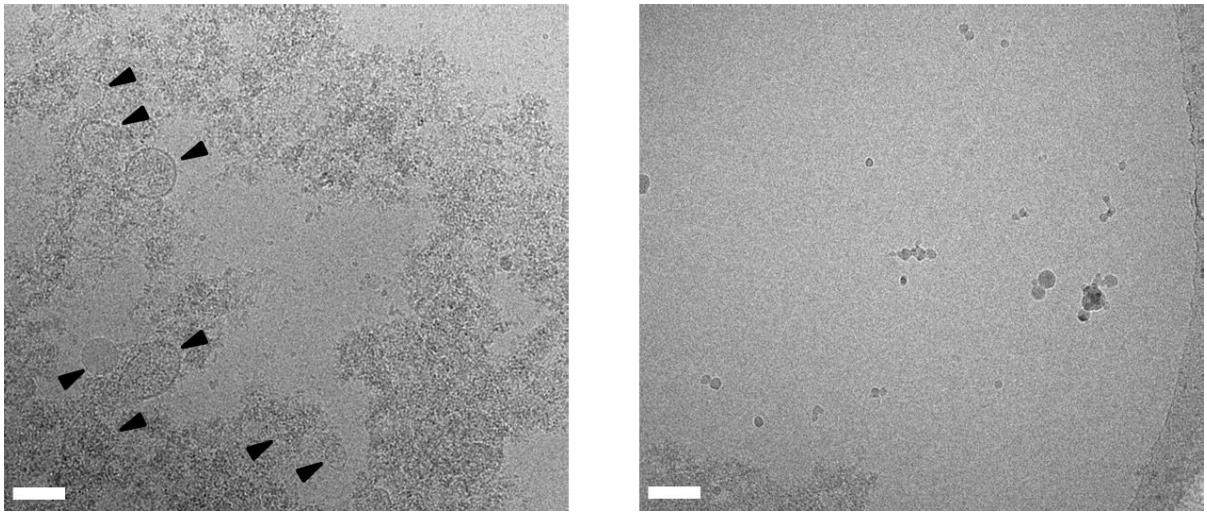

Figure 4.15. Cryo-EM of ExoQuick-TC HDE preparations with and without polymer removal. Representative electron photomicrographs of unprocessed HDE precipitated with EQ (left), arrows indicate HDE surrounded and obscured by clouds of granular EQ reagent. HDE preparations in which an attempt at EQ removal was made (right), showing some residual EQ (bottom left corner) and an absence of HDE. The small circular shapes in the right-hand image are imperfections in the ice. Scale bar, 100 nm.

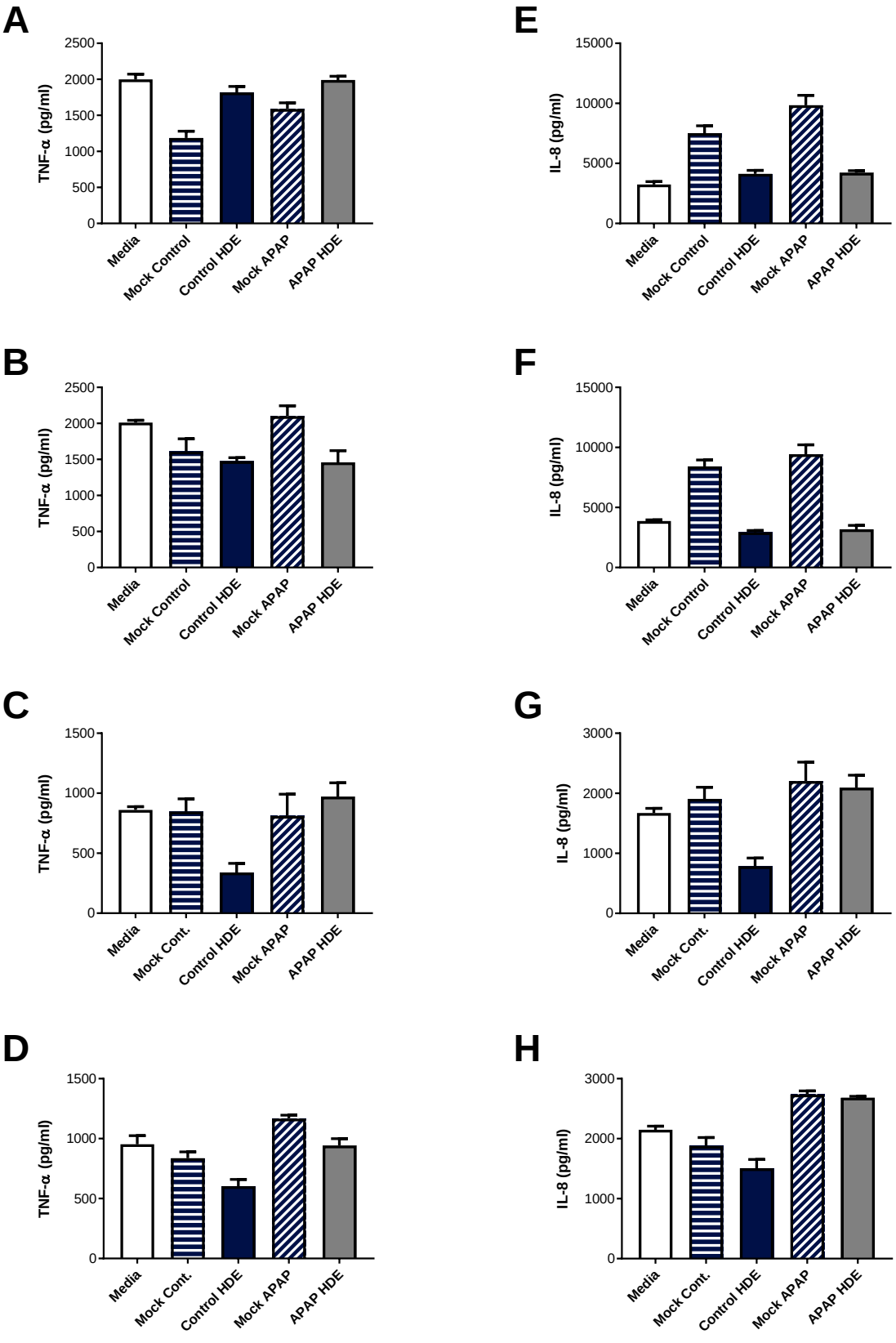
A
TNF-α (pg/ml)
2500
2000
1500
1000
500
0
Media
Mock Control
Control HDE
Mock APAP
APAP HDE
E
IL-8 (pg/ml)
15000
10000
5000
0
Media
Mock Control
Control HDE
Mock APAP
APAP HDE
B
TNF-α (pg/ml)
2500
2000
1500
1000
500
0
Media
Mock Control
Control HDE
Mock APAP
APAP HDE
F
IL-8 (pg/ml)
15000
10000
5000
0
Media
Mock Control
Control HDE
Mock APAP
APAP HDE
C
TNF-α (pg/ml)
1500
1000
500
0
Media
Mock Cont.
Control HDE
Mock APAP
APAP HDE
G
IL-8 (pg/ml)
3000
2000
1000
0
Media
Mock Cont.
Control HDE
Mock APAP
APAP HDE
D
TNF-α (pg/ml)
1500
1000
500
0
Media
Mock Cont.
Control HDE
Mock APAP
APAP HDE
H
IL-8 (pg/ml)
3000
2000
1000
0
Media
Mock Cont.
Control HDE
Mock APAP
APAP HDE

Figure 4.16. Cytokine release from monocytes may be affected by ExoQuick-TC. Data represent mean + SEM of triplicate culture wells assayed in duplicate for TNF-α (A-D) and IL-8 (E-H) from LPS-stimulated monocytes exposed to HDE or mock controls (n=4 donors).

4.3.8 HDE from control- and APAP-treated human hepatocytes are internalized by monocytes

To ensure that EQ-isolated HDE from both control- and APAP-treated human hepatocytes were taken up by recipient monocytes and to examine HDE subcellular localization, we performed uptake imaging and internalization analysis with an Amnis ImageStreamX Mark II Imaging Flow Cytometer. Control and APAP HDE were diluted to the same concentration used for functional analysis (200 µg/ml) and stained using PKH67 lipid dye. Labeled HDE were incubated with monocytes for 8 h at 37 ºC prior to antibody staining for surface marker AF647-CD32 (FcγR2), fixation/permeabilization, and DAPI staining. Imaging was performed on monocytes exposed to labeled control or APAP HDE, as well as separate preparations of labeled monocytes and HDE alone (Figure 4.17). Monocyte uptake of both HDE types was confirmed and internalization scores calculated from approximately 10,000 cells in each treatment group indicated no significant difference between control HDE and APAP HDE uptake (Figure 4.17). These results suggest that treatment-specific HDE effects on THP-1 cells are likely due to exosomal content alterations as opposed to differential uptake. They also confirm that in this model system, HDE are capable of transferring cargo to the interior of recipient cells. It is unlikely that areas of diffuse PKH67 (green) cytoplasmic staining in HDE-treated monocytes (Figure 4.17) are the result of non-specific PKH binding, given that its lipid intercalating properties would theoretically cause it to be localized to the outer membrane. More plausible is the idea that diffuse green signal is caused by distribution of exosomal material within the recipient cells.

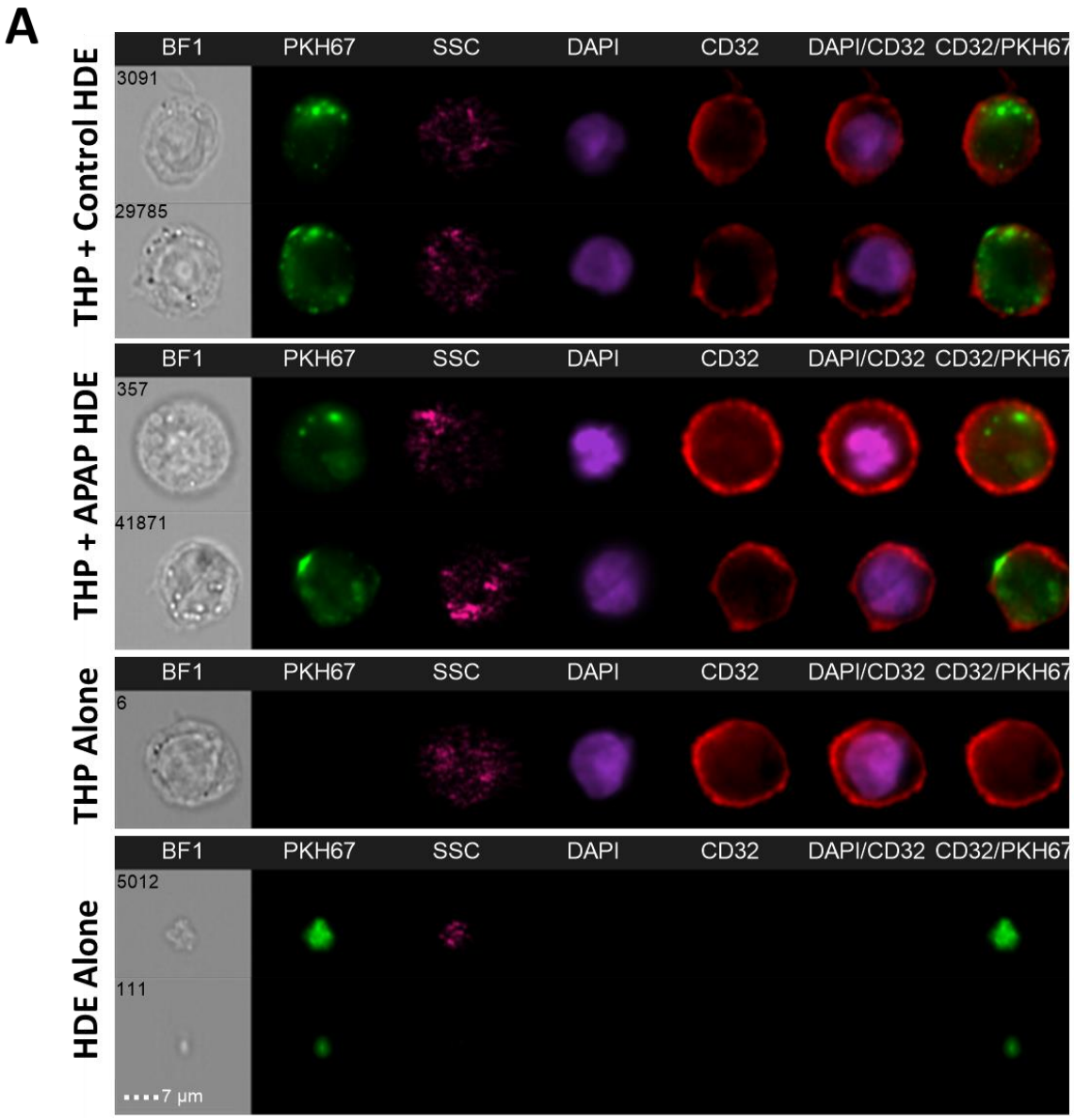

Figure 4.17. Monocytes internalize HDE from control- and APAP-treated human hepatocytes. Representative ImageStream-acquired brightfield (BF1), side-scatter (SSC), and fluorescent images of PKH67-stained HDE (green) within CD32+ THP-1 monocytes (red) counterstained with DAPI nuclear dye (violet) (A). Internalization scores generated from analysis of approximately 10,000 cells by IDEAS software for control HDE (B) and APAP HDE (C) in monocytes *(continued on next page).*

B

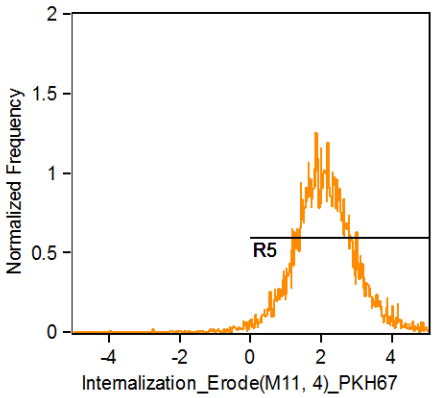

Internalization_Erode(M11, 4)_PKH67

Population	Count	%Gated	Mean
R4 & R3 & R2 & R1	9815	100	2.09
R5 & R4 & R3 & R2 & R1	9672	98.5	2.128

C

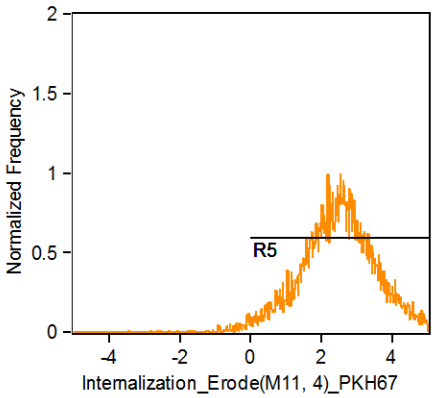

Internalization_Erode(M11, 4)_PKH67

Population	Count	%Gated	Mean
R4 & R3 & R2 & R1	9413	100	2.483
R5 & R4 & R3 & R2 & R1	9242	98.2	2.538

Figure 4.17. *continued*

4.3.9 HDE differentially regulate monocyte response to endotoxin

THP-1 monocytes were exposed to medium, mock controls, control HDE or APAP HDE (Table 4.2) from primary human hepatocytes for 24 h. HDE activity was analyzed on a per-donor basis such that HDE preparations from individual donors (n=5; Table 4.1) were tested in separate THP-1 experiments. To observe HDE-induced alterations in cytokine response, HDE-exposed monocytes were stimulated with LPS for 6 h prior to cytokine analysis. As noted in HDE concentration-response studies (Figure 4.14), control HDE from all donors decreased TNF-α secretion relative to medium alone while APAP HDE reversed this trend (Figure 4.18). The effects of HDE were similar for IL-8, although control HDE from Donor 5 uniquely increased IL-8 relative to LPS alone (no exosomes). APAP HDE from Donors 2, 3, and 5 produced levels of IL-8 that exceeded the LPS alone group (Figure 4.18). These results indicate that exposure to control HDE suppresses the pro-inflammatory response of monocytes, suggesting that HDE from healthy human hepatocytes may in fact be anti-inflammatory. Control HDE may confer some of the liver's inherent immune tolerance for bacterial endotoxins from the gut to immune cells. Conversely, HDE from APAP-treated hepatocytes do not have anti-inflammatory activity and appear to enhance LPS-induced IL-8 secretion.

Levels of MCP-1 were also assayed in HDE-exposed THP-1 monocytes. MCP-1, also known as CCL2, is a chemotactic cytokine that is produced by monocytes in response to inflammation by stimuli including LPS and pro-inflammatory cytokines like TNF-α and IL-1β (Bossink *et al.*, 1995; Chensue *et al.*, 1996; Zisman *et al.*, 1997). MCP-1 mediates recruitment and infiltration of additional immune cells including monocytes, neutrophils, lymphocytes (natural killer [NK] and T cells), and to a lesser extent basophils and mast cells

(Bossink *et al.*, 1995; Chensue *et al.*, 1996; Zigmond *et al.*, 2014). MCP-1-recruited cells adopt pro- or anti-inflammatory properties depending on the stage of injury and tissue microenvironment (Shi and Pamer, 2011). THP-1 monocytes increase MCP-1 production in response to exosomes from amniotic fluid, ascites, and EtOH-treated Huh7.5 hepatocyte-like cells (Bretz *et al.*, 2013; Momen-Heravi *et al.*, 2015a). Our results demonstrate that HDE from control-treated primary human hepatocytes significantly increase LPS-induced MCP-1 production in monocytes (Figure 4.19). HDE from APAP-treated primary human hepatocytes promote greater elevations in MCP-1 that are significantly different from LPS alone and control HDE (Figure 4.19). To support the assertion that the observed effects are exosome-related, we performed a concentration-response at 100 and 200 µg/ml HDE as described earlier. MCP-1 release from LPS-stimulated monocytes was responsive to APAP HDE concentration such that the effects were significantly increased at 200 µg/ml relative to 100 µg/ml (Figure 4.19). Control HDE did not appear to elicit concentration-dependent effects. HDE-induced MCP-1 elevations were also observed in un-stimulated monocyte cultures in the absence of LPS, albeit at much lower levels (Figure 4.19). MCP-1-mediated monocyte recruitment is a well-established and integral part of the "necroinflammatory" process in APAP DILI (Zigmond *et al.*, 2014). We present the first evidence that HDE released by APAP-treated hepatocytes mediate MCP-1 secretion in the absence of overt hepatocellular necrosis, and that the influence of HDE on monocyte-derived MCP-1 is enhanced by LPS.

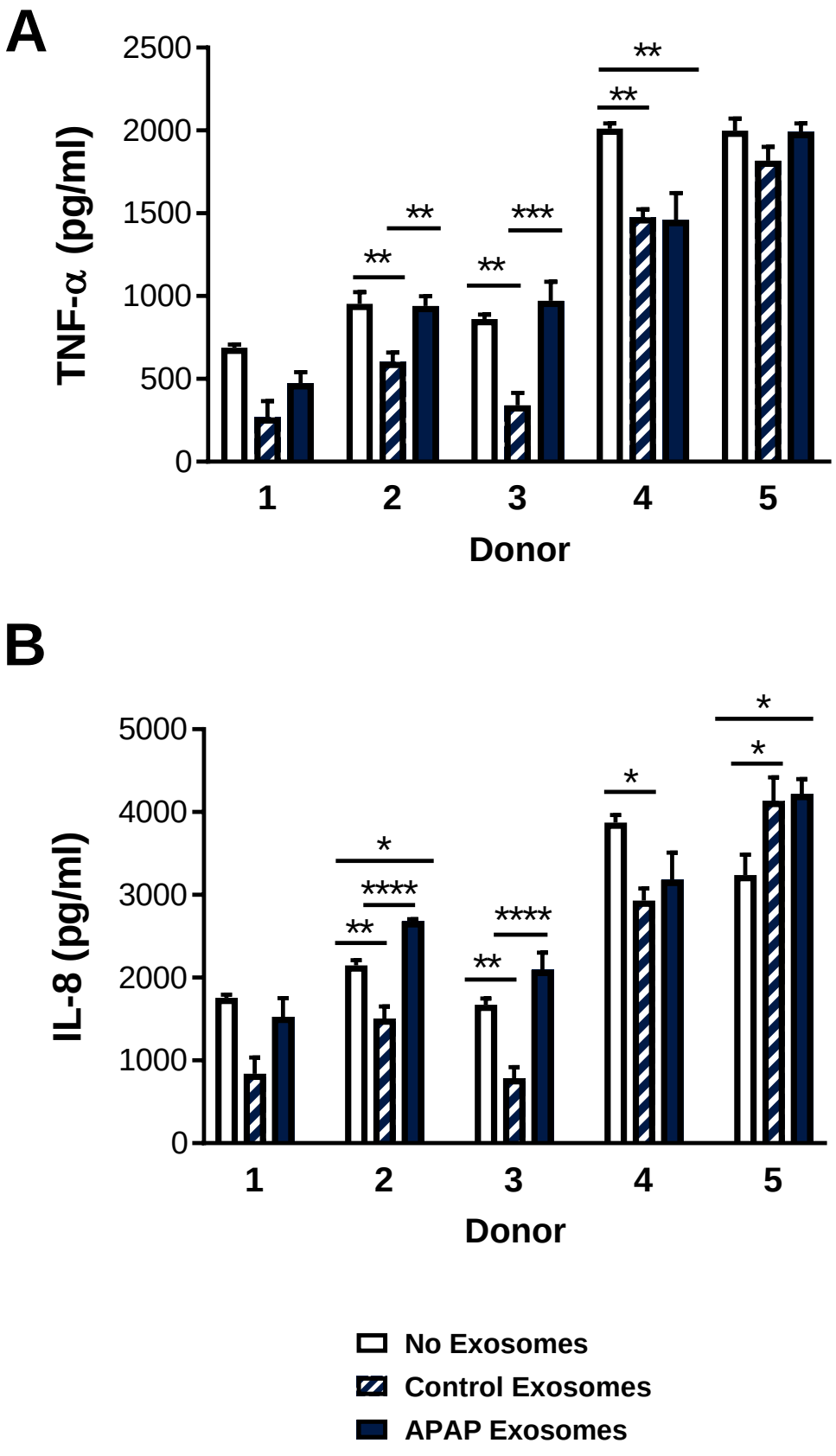
A
TNF-α (pg/ml)
2500
2000
1500
1000
500
0
**
**
**
***
**
**
1
2
3
4
5
Donor
B
IL-8 (pg/ml)
5000
4000
3000
2000
1000
0
*
****
**
**
****
*
*
*
1
2
3
4
5
Donor
No Exosomes
Control Exosomes
APAP Exosomes

Figure 4.18. HDE from control- and APAP-treated human hepatocytes alter monocyte response to endotoxin. Data represent the mean + SEM of triplicate culture wells and duplicate assay wells for TNF-α (A) and IL-8 (B) released by LPS-stimulated monocytes following 24 h of HDE exposure (n=5 hepatocyte donors). Donor IDs correspond to those listed in Table 4.1. * $p < 0.05$, ** $p < 0.01$, *** $p < 0.001$, **** $p < 0.0001$; one-way ANOVA with Tukey's multiple comparisons test.

A

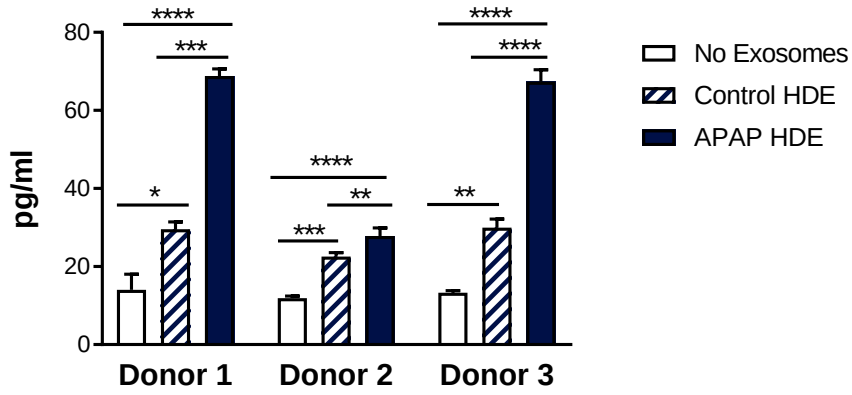
pg/ml
80
60
40
20
0
****
***
*
****
**
***
****
****
**
Donor 1
Donor 2
Donor 3
No Exosomes
Control HDE
APAP HDE

B

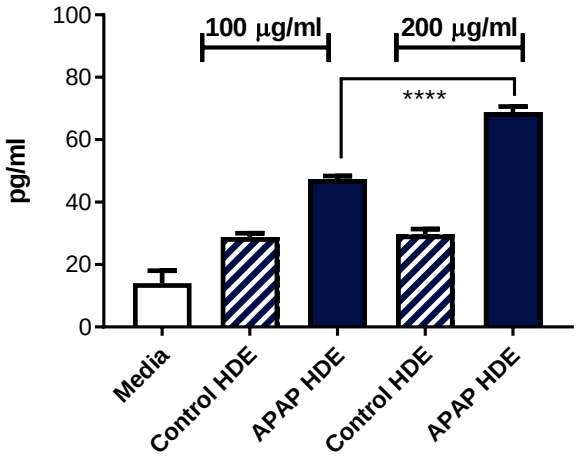
pg/ml
100
80
60
40
20
0
100 µg/ml
200 µg/ml
****
Media
Control HDE
APAP HDE
Control HDE
APAP HDE

C

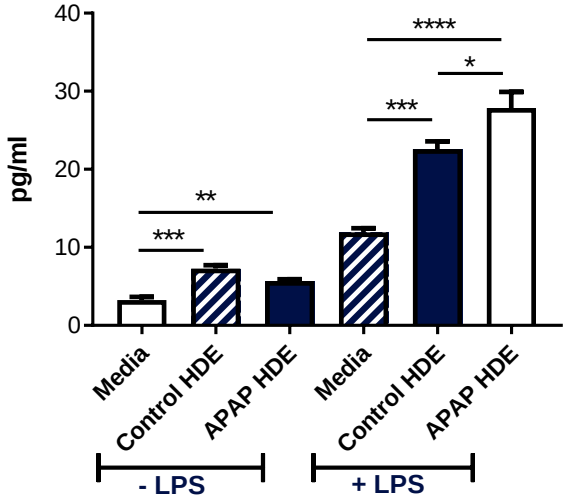
pg/ml
40
30
20
10
0
****
*
***
**
***
Media
Control HDE
APAP HDE
Media
Control HDE
APAP HDE
- LPS
+ LPS

Figure 4.19. HDE from control- and APAP-treated hepatocytes increase MCP-1 secretion by monocytes. MCP-1 in HDE-treated LPS-stimulated cultures (A, n=3 HDE donors); APAP HDE induce concentration-responsive MCP-1 elevations (B, n=1 HDE donor); MCP-1 is increased by HDE in the presence and absence of LPS stimulus (C, n=1 HDE donor). Data represent the mean + SEM of triplicate culture wells and duplicate assay wells. Donor IDs correspond to those listed in Table 4.1. * $p < 0.05$, ** $p < 0.01$, *** $p < 0.001$, **** $p < 0.0001$; one-way ANOVA with Tukey's multiple comparisons test.

4.3.10 HDE from drug-stressed hepatocytes significantly alter the monocyte transcriptome

Gene expression microarrays were performed on THP-1 monocytes following 24 h exposure to medium alone, control HDE, control mock, APAP HDE, or APAP mock to assess the transcriptome-level effects of HDE on immune cells. As previously described, the effects of EQ polymer in HDE preparations were taken into account by comparing HDE to their respective mock controls by linear contrast with FDR $p < 0.05$ and fold change > |1.5|. Performing the analysis in this manner allowed us to factor out the influences of residual APAP and EQ on monocyte gene expression. Hierarchical clustering of significant probe sets revealed that control HDE influence monocyte gene expression in a different manner than APAP and that the expression profiles of EQ matrix controls are more closely related to each other than to HDE (Figure 4.20).

There were 138 significantly DE genes from APAP HDE exposure relative to mock APAP control. Control HDE relative to the mock EQ control produced 13 significantly DE genes, and 12 were common to APAP HDE as well (Table 4.6). To analyze the genes uniquely affected by APAP HDE, we removed the 12 DE probe sets overlapping with control HDE to generate a list of 126 genes. Of those, 7 were up-regulated (Table 4.7) and 119 were significantly down-regulated (top 50, Table 4.8). IPA pathway enrichment analysis was run on significant genes to identify over-represented biological and pathological functions in monocytes that were influenced by APAP HDE. The most prominent pathways uniquely affected by APAP HDE are those centered around cholesterol homeostasis and lipid metabolism, with connections to fatty liver disease (Figure 4.21). These pathways were also enriched when we directly compared DE genes in APAP HDE versus control HDE (data not

shown), suggesting that the method we adopted to correct for EQ effects did not detrimentally affect or skew the results.

Select up- and down-regulated genes that were significantly influenced by APAP HDE have been linked to enhanced pro-inflammatory response in the literature, thus providing a plausible explanation for the cytokine secretion patterns we observed in APAP HDE-treated monocytes following LPS stimulation (Figure 4.22). APAP HDE also influenced a number of relevant innate and adaptive immune pathways falling into 2 broad categories: lymphoid tissue development (29 genes) and immune cell trafficking (25 genes) (Table 4.9). While most of the DE genes were down-regulated, it is important to note that the pathways these genes participate in may be activated or repressed.

While global analysis of gene expression changes induced by all APAP HDE treatments (n=5 donors) demonstrated an enrichment for cholesterol pathways, the effects of APAP HDE from individual donors revealed unique pathway trends. For each donor, probe set fold changes between APAP HDE and APAP mock control were generated. As the majority of monocyte genes were decreased due to APAP HDE exposure, the 100 most down-regulated genes were selected for pathway analysis. Results demonstrated two groups within the donor pool: APAP HDE from two donors affected cholesterol-related pathways while APAP HDE from three donors influenced immune pathways (Figure 4.23). These immune pathways were under-represented in the global data set and reveal that the immunomodulatory effects of APAP HDE on a gene expression level are more pronounced than initially thought. Donors whose exosomes initiated cholesterol-related responses shared a number of significant pathways; the same was true of donors whose exosomes promoted immune-relevant gene expression changes (Table 4.10). "Reactome" analysis was performed

on genes shared across donors within each subset to identify networks impacted by these gene products (Figures 4.24 and 4.25). Reactome data were not available for 8 genes from the immune subset and 2 genes from the cholesterol subset. The available donor characteristics (Table 4.1) do not reveal any obvious similarities between the donors in each group. Regardless, these findings may be indicative of the donor-specific systemic immune responses to APAP that been observed in humans (Fannin *et al.*, 2016).

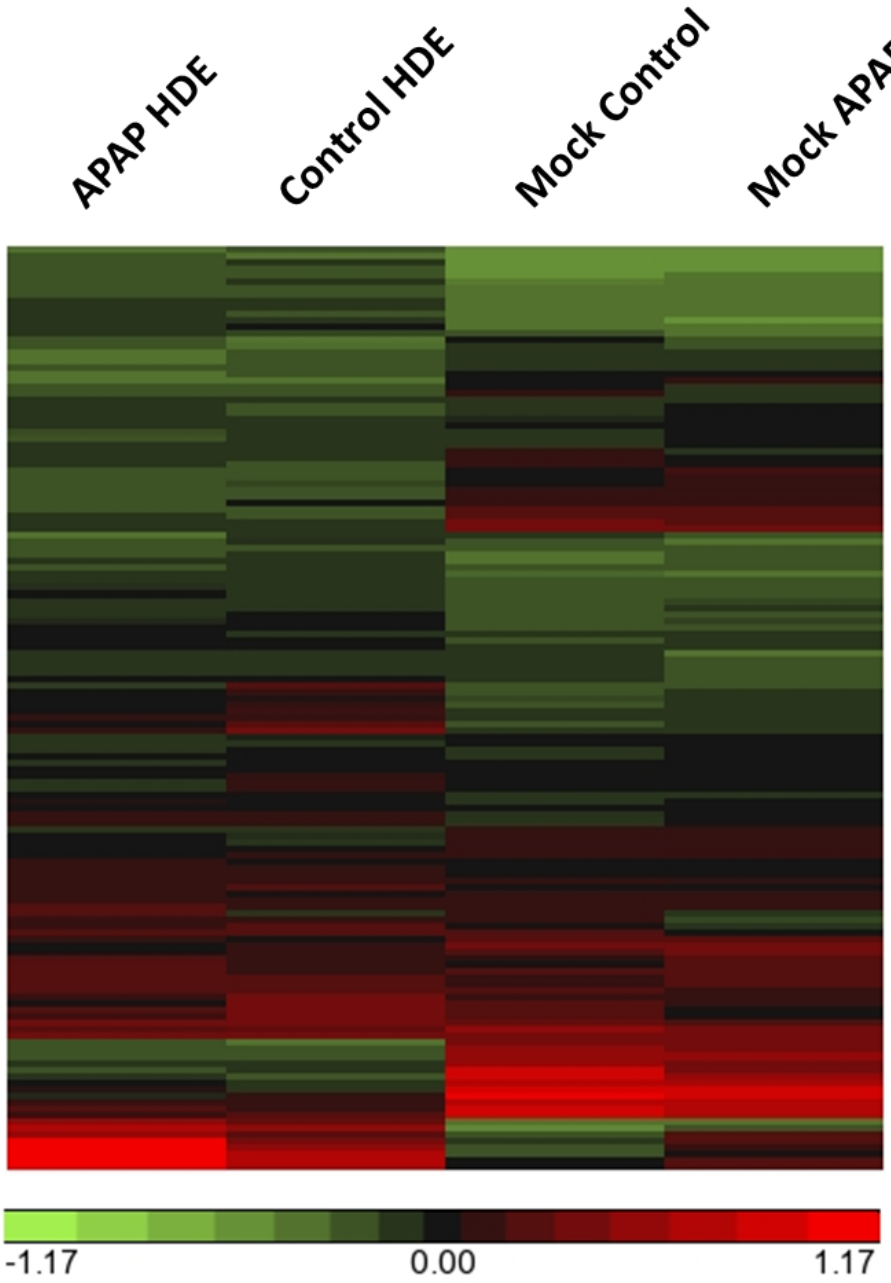

Figure 4.20. Hierarchical clustering across treatments of the significant probe sets differentially regulated by APAP HDE. Signals indicate $\log_2$ ratios determined by linear contrasts between each treatment and medium alone. Coloration reflects directionality of the $\log_2$ ratio of the contrast (green, down-regulated; red, up-regulated). The probes clustered represent those that showed significant DE in APAP HDE versus mock APAP (FDR $p < 0.05$ and FC > |1.5|).

Table 4.6. Differentially regulated genes in monocytes exposed to control HDE relative to control mock. * indicates significant genes that were unique to control HDE.

Gene Symbol	Gene Name	Gene FC	*p* -value	Relevant Gene Product Functions
ACSS2	acetyl-CoA synthetase short-chain family member 2	-3.62	0.0000012	acetate activation for lipid synthesis and energy production; "hub gene" for nutrient-sensing transcript cluster in monocytes, within QTL associated with blood glucose and body weight (Martinez-Micaelo, et al. 2016)
SLCO4C1	solute carrier organic anion transporter family member 4C1	-2.68	0.0000379	sodium-independent organic ion transport, associated with cell differentiation; over-expression decreases inflammation in models of chronic kidney disease (Toyohara, et al. 2009)
HSD17B7	hydroxysteroid (17-β) dehydrogenase 7	-2.66	0.0000021	participates in cholesterol and estrogen biosynthesis; down-regulated relative to healthy controls in models of cystic fibrosis and polycystic ovarian syndrome (Ogilvie, et al. 2011 & Salilew-Wondim, et al. 2015)
PNPLA3	patatin-like phospholipase domain containing 3	-2.18	0.0000152	glycerolipid metabolism; SNP associated with hepatic lipid accumulation and increased odds ratios for alcoholic and non-alcoholic liver disease in multiple patient cohorts (Awai, et al. 2016)
IDI1	isopentenyl-diphosphate delta isomerase 1	-2.14	0.0000252	isoprenoid and cholesterol biosynthesis; down-regulation associated with impaired regulatory T cell proliferation (Zeng, et al. 2013); expression altered by glucocorticoid receptor and NFκB activation (Rao, et al. 2011)
CLCN6	chloride channel, voltage-sensitive 6	-2.08	0.0000114	voltage-gated chloride channel that functions in late endosomes as a chloride/proton antiporter; SNP associated with hypertension and renal damage in humans (Flister, et al. 2013)
HMGCR	3-hydroxy-3-methylglutaryl-CoA reductase	-2.02	0.0000564	transmembrane glycoprotein that serves as a rate-limiting factor in cholesterol biosynthesis; auto-antibodies are directly related to peripheral immune myopathy (Alshehri, et al. 2015)

Table 4.6. *continued* * indicates significant genes that were unique to control HDE.

Gene Symbol	Gene Name	Gene FC	*p* -value	Relevant Gene Product Functions
STARD4	steroidogenic acute regulatory (STAR) related lipid transfer domain containing 4	-1.87	0.0000210	intracellular sterol/lipid transport that is highly expressed in THP-1 cells, Kupffer cells, and hepatocytes (positive regulation of bile acid synthesis); localization and expression directly linked to sterol levels (Rodriguez-Agudo, et al. 2011)
SC5D	sterol-C5-desaturase	-1.78	0.0000279	cholesterol biosynthesis and lipid metabolism; knock-out models have altered protein synthesis and oxidative stress responses (Jiang, et al. 2010)
FDPS	farnesyl diphosphate synthase	-1.67	0.0000241	enzyme involved in isoprenoid biosynthesis and post-translational protein modifications; down-regulation associated with disruption of plasma membrane lipid rafts; mediates NK cell signaling and activation of γδ T cells (Ciaglia, et al. 2013)
C14orf1	chromosome 14 open reading frame 1	-1.62	0.0000555	probable ergosterol biosynthetic protein; assembles cholesterol biosynthetic complex that has been linked to lymphocyte development (Santori, et al. 2015)
ACACA	acetyl-CoA carboxylase α	-1.56	0.0000021	rate-limiting enzyme in long-chain fatty acid biosynthesis; inhibition of protein decreases Th17 cell formation and promotes anti-inflammatory Treg cell production (Berod, et al. 2014)
*DLG5**	discs, large homolog 5	1.63	0.0000443	role in signal transduction including receptor signaling complex scaffolds; SNP that reduces protein activity is a known risk factor for inflammatory bowel disease (Stoll, et al. 2004)

Table 4.7. Monocyte genes significantly up-regulated by exposure to HDE from APAP-treated human hepatocytes. Statistical significance was determined by linear contrast between APAP HDE and APAP mock control (FDR $p < 0.05$ and FC > |1.5|). Gene product functions were obtained from human UniProt annotations unless otherwise noted.

Gene Symbol	Gene Name	Gene FC	*p* -value	Relevant Gene Product Functions
C10orf2/PEO1	chromosome 10 open reading frame, coding for twinkle protein	1.81	0.0000198	helicase involved in mitochondrial organization and mtDNA replication, response to glucose stimulus, interacts with MCP-1
AGMAT	agmatinase	1.68	0.000181168	metal ion binding
CD1D	antigen-presenting glycoprotein CD1d	1.63	0.000164671	antigen presentation, innate immune response, differentially regulated in APAP healthy volunteer study (Fannin, et al)
BBS5	Bardet-Beidl syndrome 5	1.54	0.000255106	intracellular transport, carrier vesicle fusion to the plasma
SLC25A15	mitochondrial ornithine transporter 1	1.51	0.000181248	amino acid metabolism, urea cycle
CD38	cyclic ADP-ribose hydrolase 1	1.50	0.000450119	B cell receptor signaling, up-regulation of B cell proliferation, response to hypoxia and IL-1, down-regulates apoptosis
POLR3E	RNA polymerase III subunit RPC5	1.50	0.000564809	sensing intracellular pathogens, DNA sensor in innate immune response, induces NFκB

Table 4.8. Top 25 significantly down-regulated genes in monocytes exposed to APAP HDE. Gene product functions were obtained from human UniProt annotations or Ingenuity Knowledge Base unless otherwise noted.

Gene Symbol	Gene Name	FC	Relevant Gene Functions and Pathway Annotations
MVD	diphosphomevalonate decarboxylase	-4.64	isoprene biosynthesis
LIPG	endothelial lipase	-4.55	breakdown of triglycerides and HDL, heparin binding
HMGCS1	hydroxymethylglutaryl-CoA synthase	-4.12	lipid metabolism, cholesterol biosynthesis, drug binding, liver
TSC22D3	DSIP-immunoreactive peptide	-3.95	inhibits inflammatory effects of glucocorticoids and IL-10 in macrophages, supresses NFκB-mediated transcription, implicated in steatosis
LSS	lanosterol synthase	-3.64	steroid and cholesterol biosynthesis, protein aggregation
DHCR7	7-dehydroxycholesterol reductase	-3.64	steroid and cholesterol biosynthesis
INSIG1	insulin-induced gene 1	-3.48	down-regulation of cargo loading into COPII-coated vesicles, steroid biosynthesis, implicated in steatosis

Table 4.8. *continued*

Gene Symbol	Gene Name	FC	Relevant Gene Functions and Pathway Annotations
C6orf223	chromosome 6 open reading frame 223	-3.47	uncharacterized protein
BHLHE40	basic helix-loop-helix family member e40	-3.44	LXR/RXR co-repressor, implicated in steatosis, lymphocyte proliferation and activation
SCD	stearoyl-CoA desaturase	-3.26	phospholipid, cholesterol, and triglyceride biosynthesis, fatty acid oxidation, implicated in steatosis, down-regulated in non-responders in APAP healthy volunteer study (Fannin, et al. 2015)
LDLR	low-density lipoprotein receptor	-3.26	endocytosis (viral particles, LDL), lipid metabolism, clathrin and glycoprotein binding, implicated in hepatic fibrosis, steatosis, and cirrhosis; phagocyte and macrophage migration, leukocyte activation
CYTIP	cytohesin-interacting protein	-3.11	endosomal and cytoplasmic protein expressed in immune cells and regulating migration, extravasation, proliferation, adhesion (ICAM1), regulated by CD40L, IL-1β, TNF-α, etc.
ULBP2	retinoid acid early transcript 1H	-2.95	MHC class I molecule involved in cytokine and chemokine release for immune cell recruitment, leukocyte and lymphocyte activation

Table 4.8. *continued*

Gene Symbol	Gene Name	FC	Relevant Gene Functions and Pathway Annotations
RHOB	regualtor of G-protein signaling 2	-2.94	GPCR signaling, phospholipase activity, immune cell activation and migration (phagocytes, leukocytes, antigen-presenting cells)
SLC2A3	solute carrier family 2 facilitated glucose transporter member 3	-2.88	monosaccharide transmembrane transport, carbohydrate metabolism
LPIN1	phosphatidate phosphatase	-2.87	fatty acid metabolism, PPAR co-activator, insulin response, known SNP associated with NAFLD (Valenti, et al., 2012); lymphocyte proliferation
BTG2	B-cell translocation gene 2	-2.80	proliferation and differentiation, up-regulated in hepatocellular carcinoma and following partial hepatectomy (Zhang, et al. 2009)
SCML1	sex comb on midleg-like protein 1	-3.74	transcription factor activity

Table 4.8. *continued*

Gene Symbol	Gene Name	FC	Relevant Gene Functions and Pathway Annotations
MVK	mevalonate kinase	-3.61	cholesterol biosynthesis, down-regulation of inflammatory response, ATP binding
ALDOC	fructose-biphosphate aldolase C	-3.53	glycolysis, epithelial cell differentiation, fructose metabolism
SH2D3C	SH2 domain-containing 3C	-3.14	membrane modifications in cell migration, associated with leukocyte movement and lymphocyte proliferation, JNK signaling
TM7SF2	delta(14)-sterol reductase	-2.99	sterol and cholesterol biosynthesis, oxidoreductase activity
ACAT2	sterol O-acetyltransferase 2	-2.89	lipoprotein particle assembly, macrophage-derived foam cell differentiation, dietary cholesterol absorption
SULF2	extracellular sulfatase 2	-2.84	calcium binding, positive regulation of Wnt signaling and VEGF production, involved in hepatocyte proliferation and liver regeneration

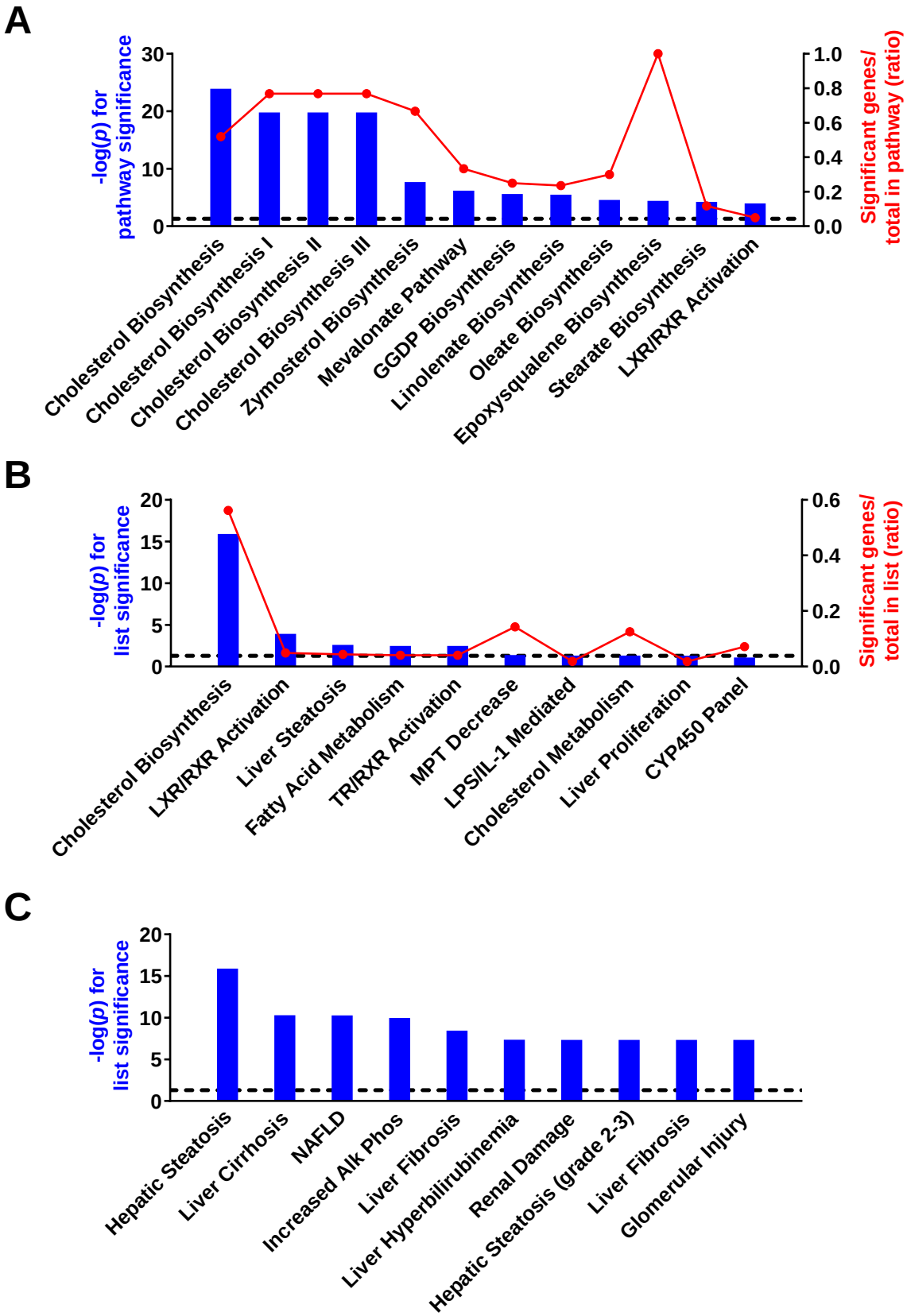
A
-log(p) for pathway significance
Significant genes/ total in pathway (ratio)
30
20
10
0
1.0
0.8
0.6
0.4
0.2
0.0
Cholesterol Biosynthesis
Cholesterol Biosynthesis I
Cholesterol Biosynthesis II
Cholesterol Biosynthesis III
Zymosterol Biosynthesis
Mevalonate Pathway
GGDP Biosynthesis
Linolenate Biosynthesis
Oleate Biosynthesis
Epoxysqualene Biosynthesis
Stearate Biosynthesis
LXR/RXR Activation
B
-log(p) for list significance
Significant genes/ total in list (ratio)
20
15
10
5
0
0.6
0.4
0.2
0.0
Cholesterol Biosynthesis
LXR/RXR Activation
Liver Steatosis
Fatty Acid Metabolism
TR/RXR Activation
MPT Decrease
LPS/IL-1 Mediated
Cholesterol Metabolism
Liver Proliferation
CYP450 Panel
C
-log(p) for list significance
20
15
10
5
0
Hepatic Steatosis
Liver Cirrhosis
NAFLD
Increased Alk Phos
Liver Fibrosis
Liver Hyperbilirubinemia
Renal Damage
Hepatic Steatosis (grade 2-3)
Liver Fibrosis
Glomerular Injury

Figure 4.21. Top pathways enriched among genes significantly associated with monocyte exposure to APAP HDE. Pathway enrichment was performed on the 126 significantly DE genes influenced by APAP HDE from primary human hepatocytes (n=5 donors). Canonical pathways (A), toxicity-related pathways (B), and pathologic associations (C) are represented (NAFLD: non-alcoholic fatty liver disease). The dashed line indicates a $-\log(p) > 1.3$ threshold for pathway significance.

Table 4.9. Differentially expressed genes and related immune pathways represented in monocytes exposed to APAP HDE . Pathways and significance were assigned by Ingenuity Knowledge Base.

Diseases or Functions Annotation	*p* -value	Differentially Expressed Genes in Significant Pathway
Antigen Presenting Cell Migration	9.88E-05	*CD38,IL10RA,LDLR,NDRG1,NPC1,PDPN,PTPN6,RHOB,S100A10,SREBF1, TRPM4*
B Lymphocyte Proliferation	4.01E-04	*ACLY,CD300A,CD38,CD72,FCGR2B,LPIN1,PTGER4,PTPN6,SH2D3C*
CD4+ T-lymphocyte Proliferation	5.40E-03	*BHLHE40,CYTIP,PPARD*
Cellular Infiltration by Macrophages	6.48E-03	*LDLR,NDRG1,NPC1,PTPN6,S100A10*
Cytotoxic and Helper T Cells	6.23E-03	*PTPN6*
Dendritic Cell Migration	4.69E-03	*CD38,IL10RA,PDPN,PTPN6,TRPM4*
Leukocyte Activation	1.43E-03	*BHLHE40,CD1D,CD300A,CD38,CD72,FCGR2B,LDLR,NDRG1,NPC1,PTGER4, PTPN6,RHOB,TRPM4,ULBP2*
Leukocyte Migration	1.21E-04	*CD1D,CD38,CYTIP,DPYSL2,FCGR2B,IL10RA,LDLR,NDRG1,NEDD9,NPC1, P2RX1,PDPN,PTPN6,RASGRP4,RHOB,S100A10,SH2D3C,SREBF1,TRPM4*
Lymphocyte Activation	3.20E-03	*BHLHE40,CD1D,CD38,CD72,FCGR2B,LDLR,PTGER4,PTPN6,RHOB,ULBP2*
Lymphocyte Proliferation	7.84E-06	*ACLY,BHLHE40,CD1D,CD300A,CD38,CD72,CYTIP,FCGR2B,JUND,LPIN1, NPC1,PPARD,PTGER4,PTPN6,RGS2,RRAS,SH2D3C,TSC22D3,ULBP2*
Lymphoid Tissue Morphology	3.89E-03	*ATP2B4,BHLHE40,BNIP3L,CD72,CYP51A1,FADS2,FCGR2B,FLVCR1, PDPN,PTPN6,TSC22D3*
Macrophage Cell Movement	4.64E-03	*LDLR,NDRG1,NPC1,PTPN6,RHOB,S100A10,SREBF1*
Movement of Phagocytes	2.10E-03	*CD38,IL10RA,LDLR,NDRG1,NPC1,PDPN,PTPN6,RASGRP4,RHOB,S100A10,SR EBF1,TRPM4*
Phagocyte Migration	5.11E-03	*CD38,IL10RA,LDLR,PDPN,PTPN6,RHOB,S100A10*
Quantity of Lymphatic System Cells	3.96E-03	*BHLHE40,BNIP3L,CD1D,CD38,CD72,CYTIP,FCGR2B,IL10RA,LDLR, NEDD9,NPC1,POLR3E,PTPN6,SH2D3C*
Quantity of Lymphocytes	5.04E-03	*BHLHE40,CD1D,CD38,CD72,CYTIP,FCGR2B,IL10RA,LDLR,NEDD9,NPC1, POLR3E,PTPN6,SH2D3C*
Quantity of Lymphoid Tissue	2.53E-03	*BHLHE40,BNIP3L,CD1D,CD72,FADS2,FCGR2B,NEDD9,POLR3E,SH2D3C*
Quantity of T Helper Lymphocytes	4.82E-03	*FCGR2B,IL10RA,LDLR,PTPN6*
Quantity of Th17 Cells	5.14E-03	*FCGR2B,IL10RA,LDLR*
Spleen Enlargement	4.98E-03	*BNIP3L,FADS2,FCGR2B,PTPN6*
T-lymphocyte Proliferation	3.11E-03	*BHLHE40,CD1D,CD38,CYTIP,FCGR2B,JUND,PPARD,PTGER4,PTPN6, RGS2,RRAS,TSC22D3*

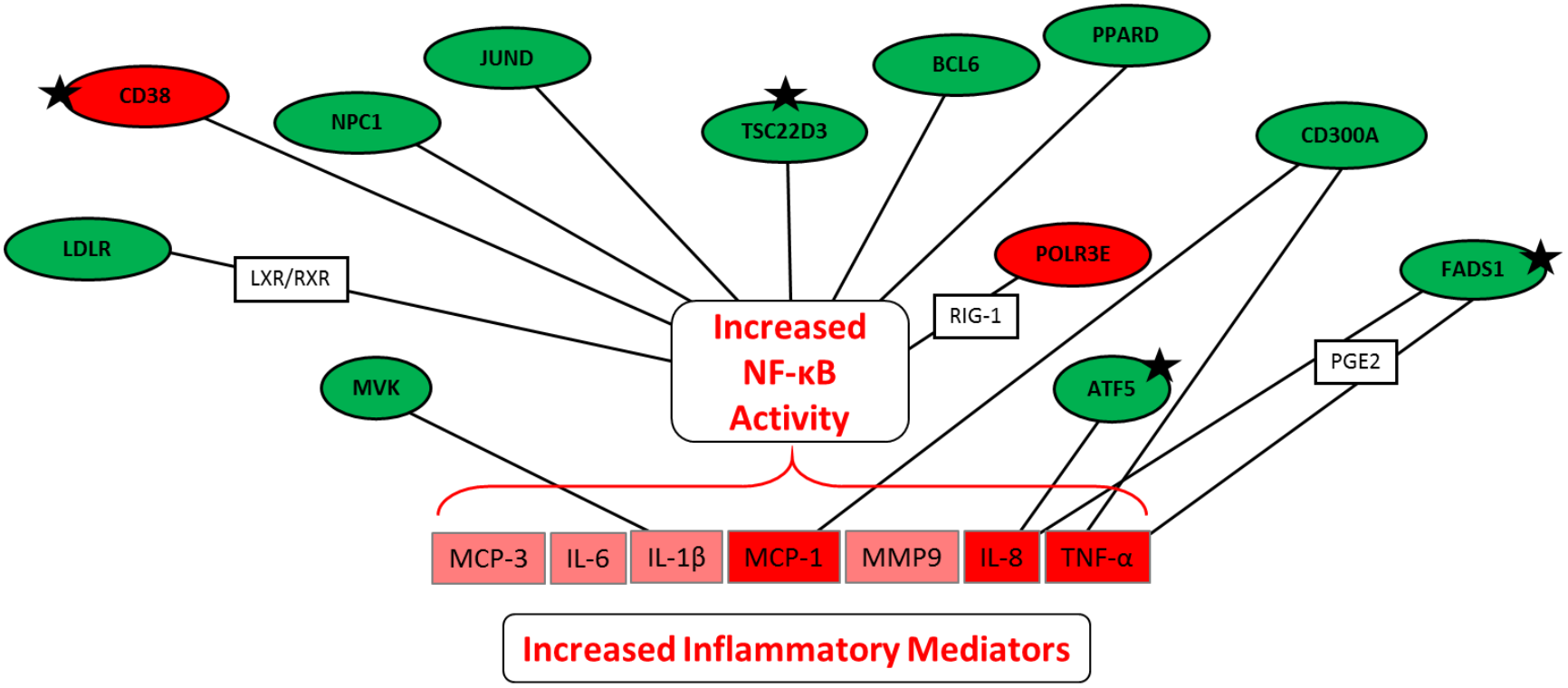

Figure 4.22. APAP HDE exposure causes gene expression changes in monocytes that may explain LPS response. Significant DE genes following APAP HDE exposure (red: up-regulated relative to mock; green: down-regulated relative to mock) that have been linked to increased pro-inflammatory response in databases and the literature. Associated inflammatory mediators expected to increase are indicated by red squares. Darker shading represents cytokines measured in this research. Stars indicate those genes whose activity has been directly associated with increased responsiveness to inflammatory activators such as LPS. *MVK*: (Cyster *et al.*, 2014); *ATF5*: (Chuang *et al.*, 2008); *TSC22D3*: (Koarai *et al.*, 2012); *FADS1*: (Fan *et al.*, 2012; Vij *et al.*, 2008); *POLR3E*: Uniprot, (Chiu *et al.*, 2009); *JUND*: (Rahmani *et al.*, 2001); *NPC1*: (Suzuki *et al.*, 2007); *LDLR*: IPA, (Calkin *et al.*, 2011); *CD300A*: (Nakahashi-Oda *et al.*, 2012); *PPARD*: (Adhikary *et al.*, 2015); *CD38*: (Manjarrez-Orduno *et al.*, 2007); *BCL6*: (Perez-Rosado *et al.*, 2008).

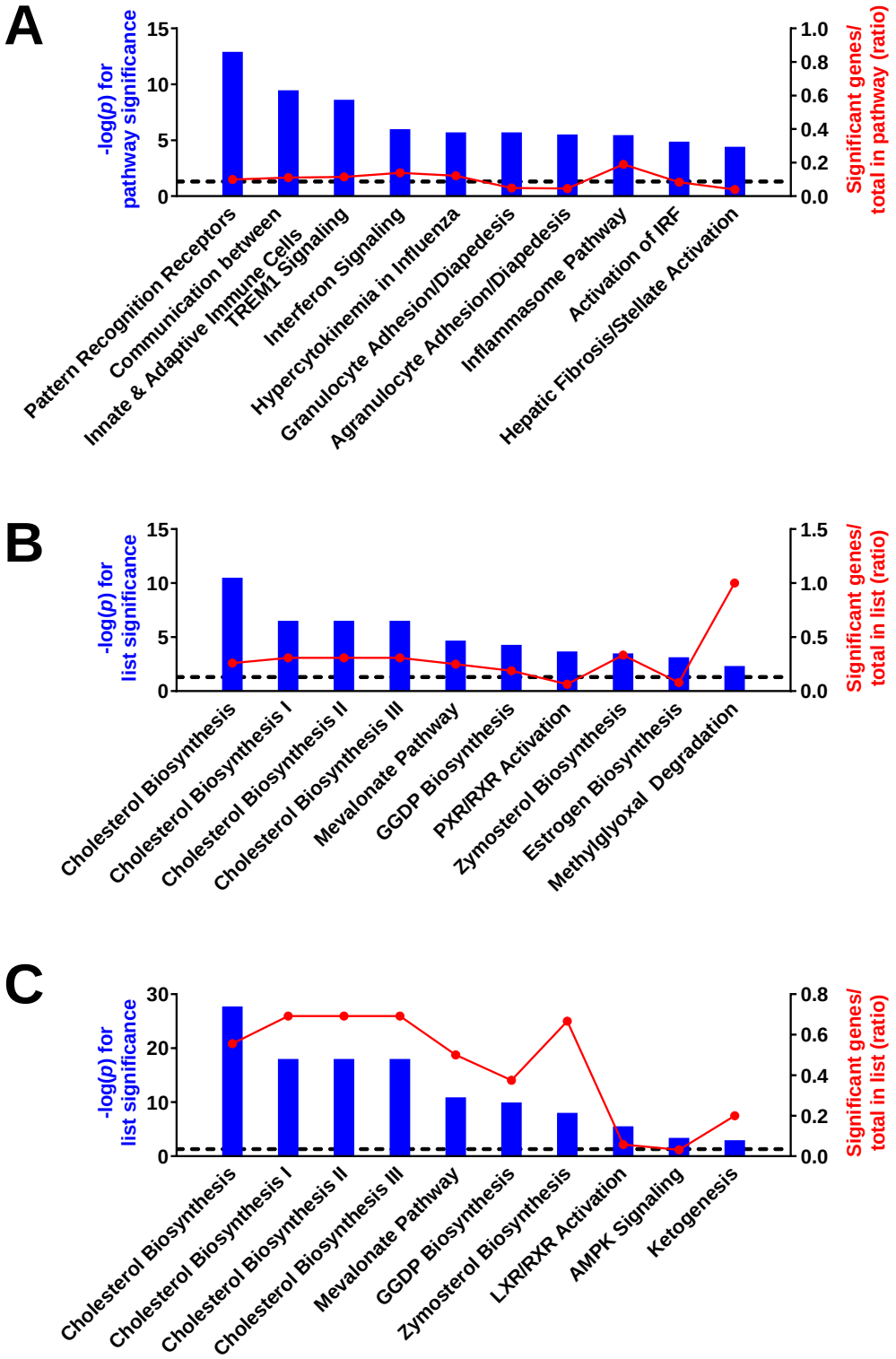
A
-log(p) for pathway significance
Significant genes/ total in pathway (ratio)
Pattern Recognition Receptors
Communication between Innate & Adaptive Immune Cells
TREM1 Signaling
Interferon Signaling
Hypercytokinemia in Influenza
Granulocyte Adhesion/Diapedesis
Agranulocyte Adhesion/Diapedesis
Inflammasome Pathway
Activation of IRF
Hepatic Fibrosis/Stellate Activation
B
-log(p) for list significance
Significant genes/ total in list (ratio)
Cholesterol Biosynthesis
Cholesterol Biosynthesis I
Cholesterol Biosynthesis II
Cholesterol Biosynthesis III
Mevalonate Pathway
GGDP Biosynthesis
PXR/RXR Activation
Zymosterol Biosynthesis
Estrogen Biosynthesis
Methylglyoxal Degradation
C
-log(p) for list significance
Significant genes/ total in list (ratio)
Cholesterol Biosynthesis
Cholesterol Biosynthesis I
Cholesterol Biosynthesis II
Cholesterol Biosynthesis III
Mevalonate Pathway
GGDP Biosynthesis
Zymosterol Biosynthesis
LXR/RXR Activation
AMPK Signaling
Ketogenesis

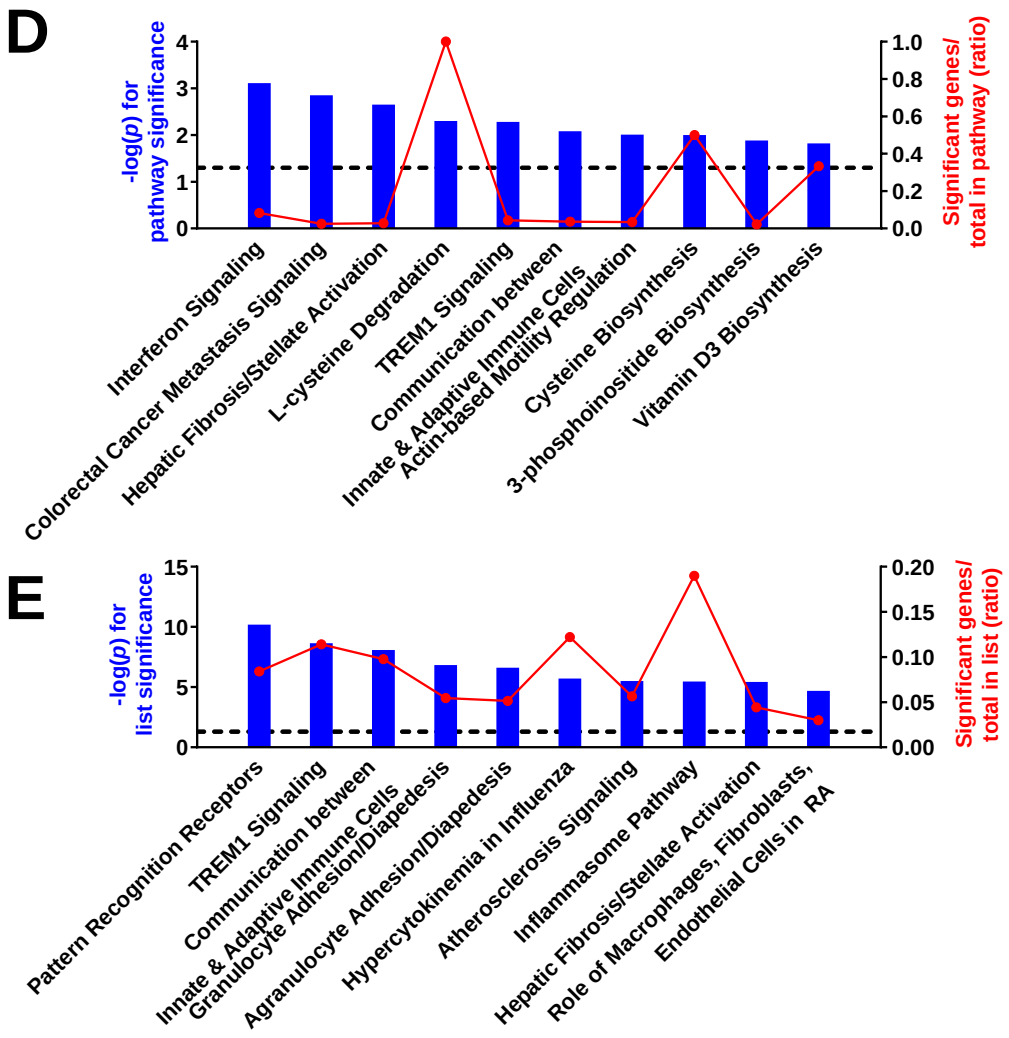

Figure 4.23. Top 10 pathways enriched among genes significantly associated with monocyte exposure to APAP HDE from individual donors. Pathway enrichment was performed on 100 of the genes most influenced by APAP HDE from each primary human hepatocyte donor. Pathways enriched as a result of APAP HDE exposure are presented in order of donor ID: Donor 1 (A), Donor 2 (B), Donor 3 (C), Donor 4 (D), Donor 5 (E). The dashed line indicates a –log(p) > 1.3 threshold for pathway significance. APAP HDE from donors 2 and 3 induced alterations in cholesterol-related pathways while HDE from donors 1, 4, and 5 modulated pathways related to immune responses.

Table 4.10. Common monocyte pathways associated with exposure to APAP HDE from individual donors. Pathways were assigned by Ingenuity Knowledge Base.

Shared Immune Pathways (Donors 1, 4, 5)
Acetate Conversion to Acetyl-CoA
Colorectal Cancer Metastasis Signaling
Communication between Innate and Adaptive Immune Cells
Hepatic Fibrosis / Hepatic Stellate Cell Activation
Interferon Signaling
Pathogenesis of Multiple Sclerosis
Role of Macrophages, Fibroblasts and Endothelial Cells in Rheumatoid Arthritis
Role of Pattern Recognition Receptors in Recognition of Bacteria and Viruses
TREM1 Signaling
Phagosome Formation

Shared Cholesterol Pathways (Donors 2, 3)
Acetate Conversion to Acetyl-CoA
Cholesterol Biosynthesis I
Cholesterol Biosynthesis II (via 24,25-dihydrolanosterol)
Cholesterol Biosynthesis III (via Desmosterol)
Estrogen Biosynthesis
FXR/RXR Activation
Ketogenesis
Lanosterol Biosynthesis
Mevalonate Pathway I
Oleate Biosynthesis II (Animals)
Sucrose Degradation V (Mammalian)
Superpathway of Cholesterol Biosynthesis
Superpathway of Geranylgeranyldiphosphate Biosynthesis I (via Mevalonate)
Triacylglycerol Degradation
Zymosterol Biosynthesis

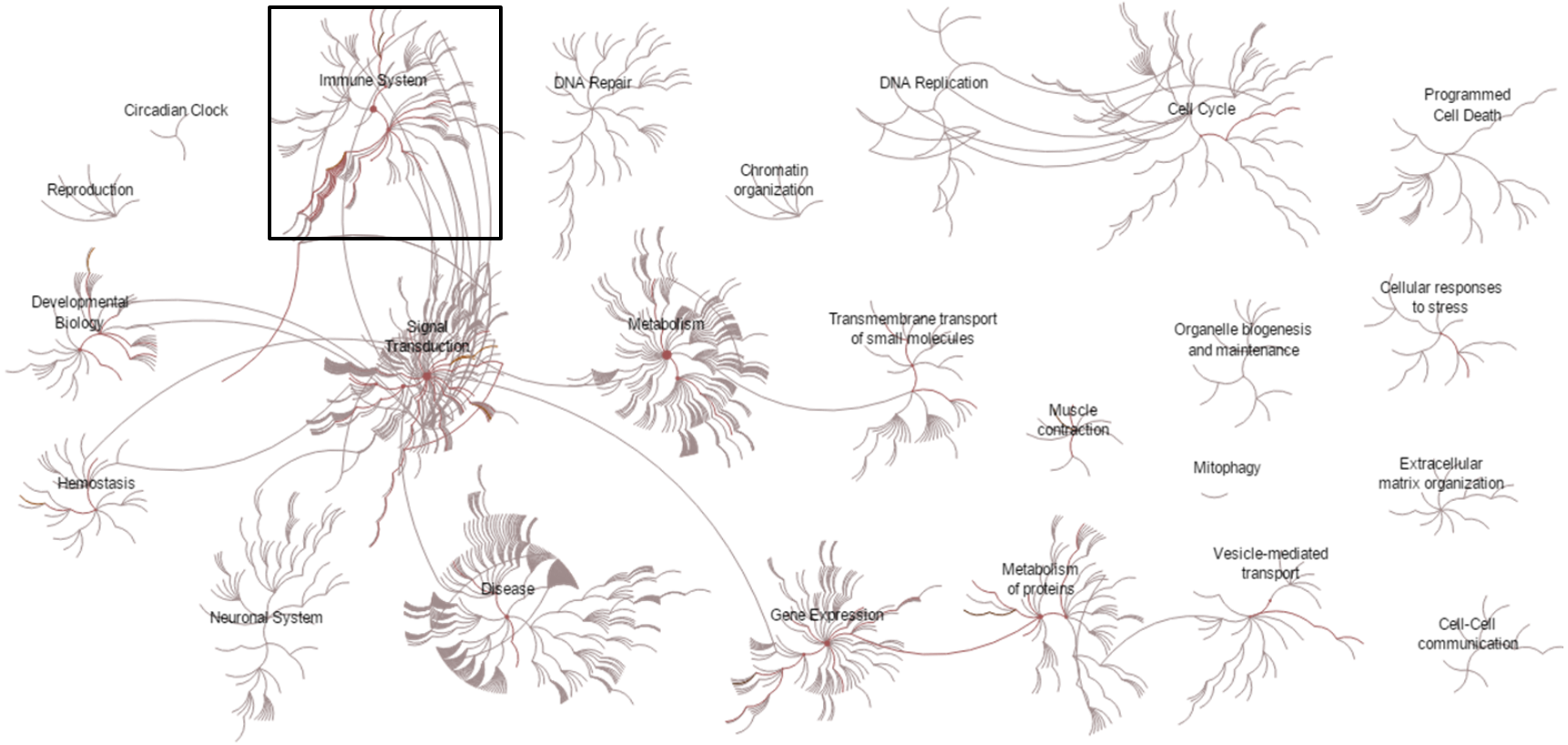

Figure 4.24a. Reactome analysis of common genes differentially regulated by APAP HDE from Donors 1, 4, and 5. Networks represent reactome data for 18 of 26 shared genes between donors in the immune subset. Red color saturation indicates greater enrichment of genes in a given network.

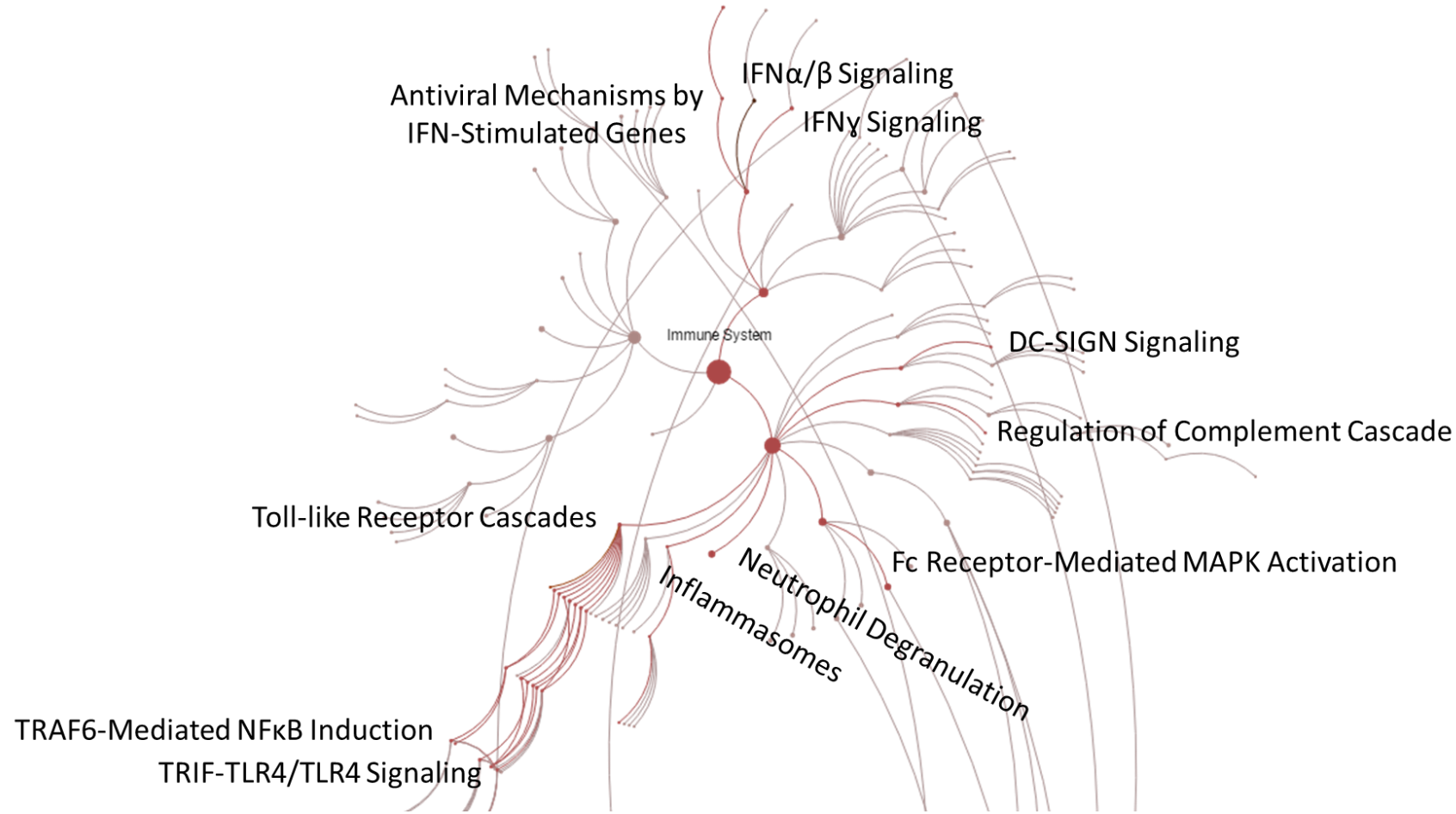

Figure 4.24b. Reactome analysis of common genes differentially regulated by APAP HDE from Donors 1, 4, and 5. Networks represent reactome data for 18 of 26 shared genes between donors in the immune subset. Red color saturation indicates greater enrichment of genes in a given network. Overrepresented pathways are labeled.

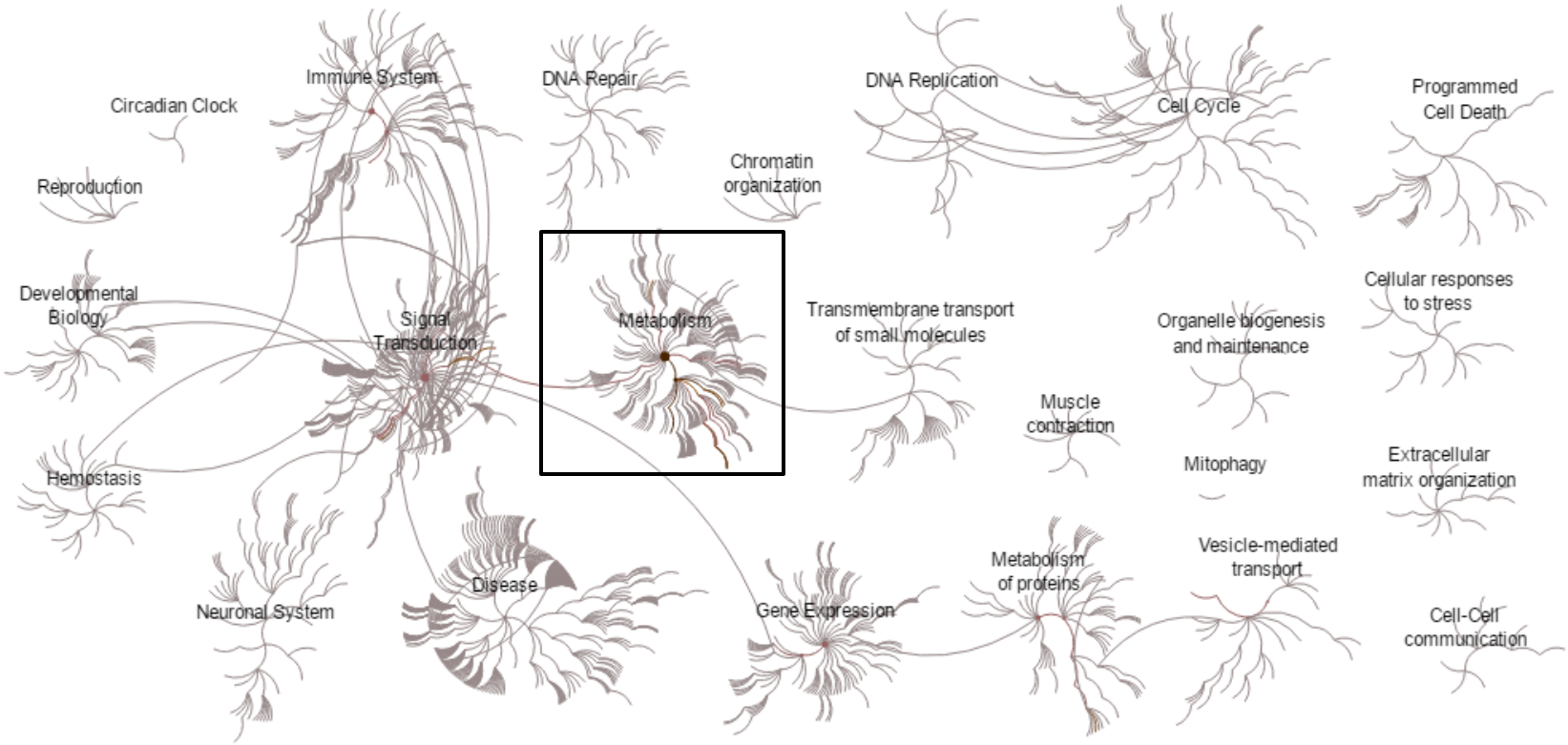

Figure 4.25a. Reactome analysis of common genes differentially regulated by APAP HDE from Donors 2 and 3. Networks represent reactome data for 13 of 15 shared genes between donors in the cholesterol subset. Red color saturation indicates greater enrichment of genes in a given network.

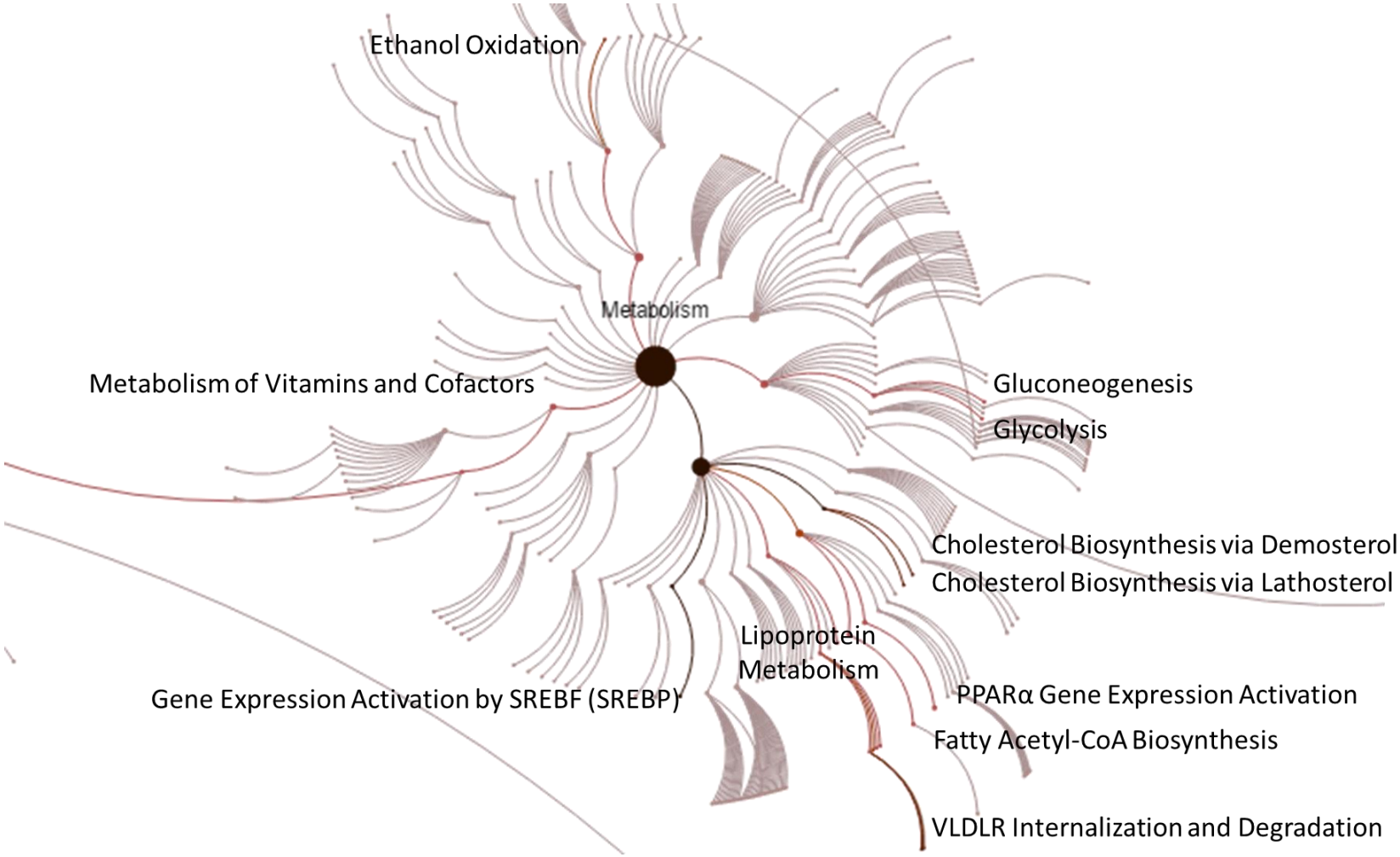

Figure 4.25b. Reactome analysis of common genes differentially regulated by APAP HDE from Donors 2 and 3. Networks represent reactome data for 13 of 15 shared genes between donors in the cholesterol subset. Red color saturation indicates greater enrichment of genes in a given network. Overrepresented pathways are labeled.

4.3.11 miRNA in HDE from drug-stressed hepatocytes are linked to gene expression effects in monocytes

Finally, we sought to integrate the content of HDE from APAP-treated human hepatocytes with the exosome-induced transcriptional changes we observed in monocytes. We have demonstrated previously that both albumin mRNA and miR-122 within primary human HDE are significantly altered by sub-toxic APAP exposure (Holman *et al.*, 2016), thus our interest was in the RNA content of HDE. While a number of studies have demonstrated the ability of EVs to transfer full-length mRNA that can be translated in recipient cells (Herrera *et al.*, 2010; Royo *et al.*, 2013), exosomal RNA translation has not yet been connected with functional changes in recipient cells. In addition, our RNA sequencing work and the research of others suggest that the majority of exosomal RNA is non-coding RNA (Huang *et al.*, 2013; Santangelo *et al.*, 2016). Exosomes are well known for carrying inherently regulatory RNAs like miRNA, and it has already been established that hepatocyte-like cells produce exosomes that can transfer functional miR-122 to monocytes (Momen-Heravi *et al.*, 2015a). Therefore, we integrated our novel data set of primary human HDE miRNA profiles with the observed gene expression effects in recipient monocytes to test the hypothesis that the immunomodulatory activity of HDE is mediated in part by the delivery of functional miRNAs to immune cells.

The 126 DE genes uniquely and significantly associated with APAP HDE across all donors were compared to miRNAs with the most marked fold changes in APAP HDE relative to control HDE in a 2-pronged approach. First, we worked backwards from DE genes in monocytes and predicted which miRNAs should be differentially enriched in APAP HDE to cause the significant decreases observed in monocyte gene expression.

Experimentally-validated human miRNA-target interactions (MTIs) were obtained from IPA or miRTarBase. The top 25 most significantly down-regulated monocyte genes were connected with differentially enriched miRNAs in APAP HDE (Table 4.11). 72% of the most down-regulated genes are known to be targeted by miRNAs whose levels increased in APAP HDE. In addition, a number of these miRNAs have been significantly elevated in *in vivo* rat and human studies of DILI caused by APAP overdose (Table 4.11). This concordance with previous APAP studies highlights the potential functional relevance of these miRNAs and the novelty of detecting increases in their abundance prior to overt hepatotoxicity.

Next, we used differentially enriched exosomal miRNAs across all donors to predict which genes and pathways could be targeted in THP-1 cells. Given that miRNAs typically have an inverse relationship with their target mRNA and that 94% of the genes significantly affected by APAP HDE were down-regulated, we predicted gene targets of the miRNAs with the greatest positive fold change. The top 50 most increased miRNA from APAP HDE and their fold changes were imported into IPA microRNA Target Filter. This software combined results from 3 different miRNA databases of experimentally observed MTIs to produce a list of known mRNA targets. Enrichment analysis was performed on the mRNA targets to produce pathways that could be reasonably anticipated to change if functional APAP HDE miRNA were transferred to monocytes (Figure 4.26). The most significant pathways predicted by APAP HDE miRNA content are almost identical to those actually affected in APAP HDE-treated monocytes (Figure 4.21). In addition, miRNAs differentially enriched in APAP HDE target all but one differentially expressed gene directly tied to increased pro-inflammatory response in Figure 4.22. These results suggest

that exosomal miRNA transfer may be one of the mechanisms used by drug-stressed hepatocytes to influence immune cell behavior.

In addition to evaluating the degree to which miRNA within APAP HDE corresponded with the observed pathway alterations from the global data set, we also examined these relationships on an individual donor basis (n=4 donors). The 50 most increased miRNA within APAP HDE relative to control HDE were determined for each donor. These miRNAs were analyzed with IPA microRNA Target Filter to identify validated relationships with target genes. Pathway enrichment was performed on predicted target genes for each donor and the results were compared to the pathway alterations observed in monocytes exposed to APAP HDE from that donor. Of the observed pathways associated with APAP HDE exposure, 30-73% were recapitulated in the target gene set predicted by donor-matched APAP HDE miRNA (Table 4.12). This degree of overlap provides additional evidence that exosomal miRNA may be mediating the gene expression changes observed in APAP HDE-treated monocytes. It is important to note that the concordance between predicted and observed pathways was generated using limited miRNA target information. Table 4.12 shows that of the 50 miRNAs used for target gene prediction, no more than 27 miRNAs from any donor had validated targeting information available. Therefore, the pathway overlap may have been considerably greater if additional MTI data were available.

Table 4.11. Enriched miRNAs in APAP HDE target a majority of the 25 most significantly down-regulated genes in monocytes exposed to APAP HDE. Annotation information was obtained from human UniProt, Ensembl, or Ingenuity Knowledge Base unless otherwise noted. MTI associations between miRNA and gene targets were obtained from Ingenuity Knowledge Base and bold miRNAs have also been elevated in at least 2 other rat and/or human APAP DILI models (Krauskopf *et al.*, 2015; Starkey Lewis *et al.*, 2011; Vliegenthart *et al.*, 2015; Ward *et al.*, 2014).

Gene Target	Gene Name	Top Up-regulated Exo miRNAs Targeting Down-regulated Gene	Gene FC	Relevant Gene Functions and Pathway Annotations
MVD	diphosphomevalonate decarboxylase	hsa-miR-26b-5p	-4.64	isoprene biosynthesis
LIPG	endothelial lipase	hsa-miR-342-3p	-4.55	breakdown of triglycerides and HDL, heparin binding
HMGCS1	hydroxymethylglutaryl-CoA synthase	hsa-miR-19b-3p **let-7b-5p**	-4.12	lipid metabolism, cholesterol biosynthesis, drug binding, liver development
TSC22D3	DSIP-immunoreactive peptide	hsa-miR-19b-3p	-3.95	inhibits inflammatory effects of glucocorticoids and IL-10 in macrophages, suppresses NFκB-mediated transcription, implicated in steatosis
LSS	lanosterol synthase	hsa miR-30a-5p **hsa-miR-125b-5p**	-3.64	steroid and cholesterol biosynthesis, protein aggregation
DHCR7	7-dehydroxycholesterol reductase	hsa-miR-34a-5p hsa-miR-451b	-3.64	steroid and cholesterol biosynthesis
INSIG1	insulin-induced gene 1	hsa-miR-29b-3p	-3.48	down-regulation of cargo loading into COPII-coated vesicles, steroid biosynthesis, implicated in steatosis

Table 4.11. *continued*

Gene Target	Gene Name	Top Up-regulated Exo miRNAs Targeting Down-regulated Gene	Gene FC	Relevant Gene Functions and Pathway Annotations
C6orf223	chromosome 6 open reading frame 223	**hsa-miR-192-3p**	-3.47	uncharacterized protein
BHLHE40	basic helix-loop-helix family member e40	hsa-miR-15a/b-5p, hsa-miR-16-5p, hsa-miR-195-5p	-3.44	LXR/RXR co-repressor, implicated in steatosis, lymphocyte proliferation and activation
SCD	stearoyl-CoA desaturase	**hsa-miR-125b-5p**, hsa-miR-30a-5p, **hsa-let-7b-5p**, hsa-miR-185-5p, hsa-miR-19/ba-3p, hsa-miR-142-5p ,hsa-miR-20a-5p, hsa-miR-17-5p, hsa-miR-106a/b-5p	-3.26	phospholipid, cholesterol, and triglyceride biosynthesis, fatty acid oxidation, implicated in steatosis, down-regulated in non-responders in APAP healthy volunteer study (Fannin, et a. 2015)
LDLR	low-density lipoprotein receptor	**hsa-let-7b-5p**, hsa-miR-106a/b-5p, hsa-miR-17-5p, hsa-miR-19a/b-3p, hsa-miR-20a-5p, hsa-miR-27a/b-3p, hsa-miR-30a-5p, hsa-miR-30C-5p, hsa-miR-30d-5p, hsa-miR-40e-5p	-3.26	endocytosis (virla particles, LDL), lipid metabolism, clathrin and glycoprotein binding, implicated in hepatic fibrosis, steatosis, and cirrhosis; phagocyte and macrophage migration, leukocyte activation
CYTIP	cytohesin-interacting protein	hsa-miR-26b-5p hsa-miR-146b-5p	-3.11	endosomal and cytoplasmic protein expressed in immune cells and regulating migration, extravasation, proliferation, adhesion (ICAM1), regulated by CD40L, IL-1β, TNF-α, etc.
ULBP2	retinoid acid early transcript 1H	hsa-miR-34a-5p hsa-miR-29b-3p	-2.95	MHC class I molecule involved in cytokine and chemokine release for immune cell recruitment, leukocyte and lymphocyte activation

Table 4.11. *continued*

Gene Target	Gene Name	Top Up-regulated Exo miRNAs Targeting Down-regulated Gene	Gene FC	Relevant Gene Functions and Pathway Annotations
RHOB	regualtor of G-protein signaling 2	**hsa-let-7f-5p**, hsa-miR-233-3p, **hsa-miR-let7b-5p**, **hsa-miR-let7c-5p**, **hsa-miR-21-5p**, hsa-miR-30a-5p, hsa-miR-19a/b-3p,	-2.94	GPCR signaling, phospholipase activity, immune cell activation and migration (phagocytes, leukocytes, antigen-presenting cells)
SLC2A3	solute carrier family 2 facilitated glucose transporter member 3	**hsa-miR-122-5p**, hsa-miR-195-5p, hsa-miR-34a-5p, **hsa-miR-148a-3p**, hsa-miR-106a-5p, hsa-miR-16-5p, hsa-miR-15a/b-5p	-2.88	monosaccharide transmembrane transport, carbohydrate metabolism
LPIN1	phosphatidate phosphatase	hsa-miR-17-5p hsa-miR-27a/b-5p	-2.87	fatty acid metabolism, PPAR co-activator, insulin response, known SNP associated with NAFLD (Valenti et al. 2012); lymphocyte proliferation
BTG2	B-cell translocation gene 2	**hsa-miR-21-5p**, hsa-miR-101-3p, hsa-miR-26b-5p, hsa-miR-16-5p, **hsa-let7b-5p**, hsa-miR-15a/b-5p, hsa-miR-195-5p, **hsa-miR-125b-5p**, hsa-miR-25-3p, hsa-miR-185-5p, hsa-miR-29b-3p, hsa-miR-20a-5p, hsa-miR-17-5p, hsa-miR-106a/b-5p, hsa-miR-27a/b-3p	-2.80	proliferation and differentiation, up-regulated in hepatocellular carcinoma and following partial hepatectomy (Zhang, et al. 2009)

Table 4.11. *continued*

Gene Target	Gene Name	Top Up-regulated Exo miRNAs Targeting Down-regulated Gene	Gene FC	Relevant Gene Functions and Pathway Annotations
SCML1	sex comb on midleg-like protein 1	N/A	-3.74	transcription factor activity
MVK	mevalonate kinase	N/A	-3.61	cholesterol biosynthesis, down-regulation of inflammatory response, ATP binding
ALDOC	fructose-biphosphate aldolase C	N/A	-3.53	glycolysis, epithelial cell differentiation, fructose metabolism
SH2D3C	SH2 domain-containing 3C	N/A	-3.14	membrane modifications in cell migration, associated with leukocyte movement and lymphocyte proliferation, JNK signaling
TM7SF2	delta(14)-sterol reductase	N/A	-2.99	sterol and cholesterol biosynthesis, oxidoreductase activity
ACAT2	sterol O-acetyltransferase 2	N/A	-2.89	lipoprotein particle assembly, macrophage-derived foam cell differentiation, dietary cholesterol absorption
SULF2	extracellular sulfatase 2	N/A	-2.84	calcium binding, positive regulation of Wnt signaling and VEGF production, involved in hepatocyte proliferation and liver regeneration

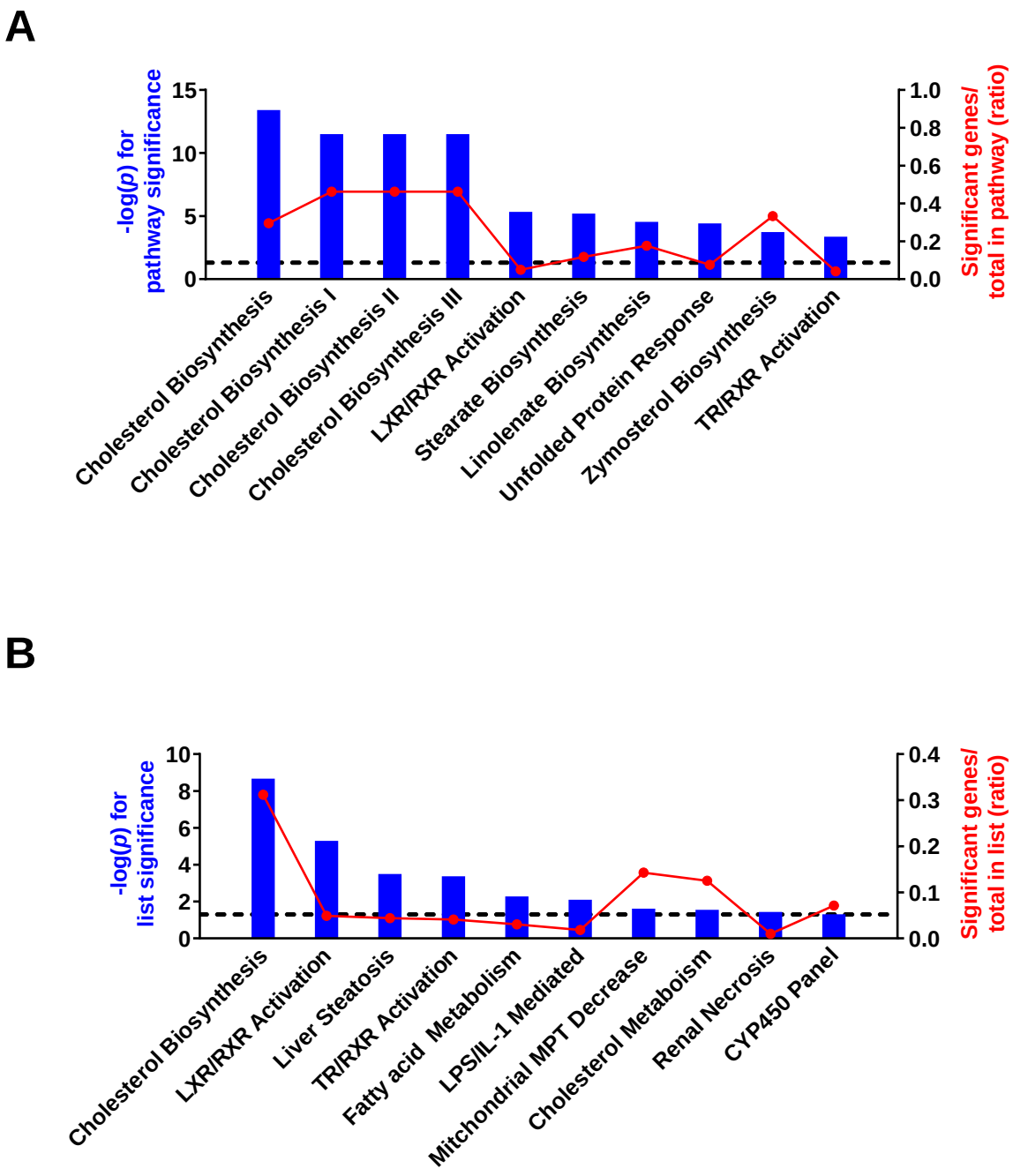

Figure 4.26. Monocyte pathway enrichment is predicted by mRNA targets of differentially enriched APAP HDE miRNA. Using experimentally validated targets of the top 50 miRNA with the highest FC in APAP HDE, monocyte gene targets were predicted. Pathway enrichment for top molecular functions (A) and toxicological mechanisms (B) was performed on the predicted target genes to confirm concordance with true DE pathways.

Table 4.12. Concordance of observed monocyte pathway enrichment with pathways predicted using target genes of miRNA enriched within individual donor APAP HDE . Observed pathways were generated from the 100 monocyte genes most impacted (down-regulated) by APAP HDE exposure. IPA microRNA Target Filter was used to identify validated gene targets of the 50 most increased miRNAs in APAP HDE relative to control HDE. Observed and predicted pathways were included in the analysis if the pathway significance score exceeded a $-\log(p) > 1.3$ threshold.

Donor ID	HDE miRNAs with validated targets	Pathways predicted by miRNA target genes	Pathways observed	Overlapping pathways	Observed pathways predicted by HDE miRNA
1	25	287	55	33	60%
2	27	29	27	18	67%
3	21	302	40	12	30%
4	19	234	70	51	73%

4.4 Discussion

The research presented here was performed to address knowledge gaps in the fields of HDE and DILI using primary human hepatocytes. Foremost, we sought to establish a role for HDE released by drug-stressed cells in mediating early, sub-toxic immune responses in DILI. In so doing, we profiled the mRNA and miRNA contents of HDE and linked the miRNA contents to the effects of HDE on immune cells, as we have already demonstrated sub-toxic APAP-induced alterations in mRNA and miRNA within HDE (Holman *et al.*, 2016).

To assess the immunomodulatory capacity of HDE, we exposed THP-1 human monocytes to HDE harvested from cultures of control- and APAP-treated primary human hepatocytes (n=5 donors). One set of THP-1 cells was stimulated with LPS to determine if HDE exposure affected prototypical immune responses such as cytokine (IL-8, TNF-α) and chemokine (MCP-1) secretion. HDE from control hepatocytes suppressed the secretion of IL-8 and TNF-α relative to LPS alone, suggesting an inherently anti-inflammatory influence. HDE from APAP-stressed hepatocytes reversed this trend and in some donors, increased cytokine levels beyond those of LPS alone. The IL-8 and TNF-α results indicate that the potential anti-inflammatory effects of HDE from healthy hepatocytes are lost upon drug-induced hepatocellular stress. Both control and APAP HDE stimulated MCP-1 release with and without LPS. Taken together, these data revealed two key findings regarding HDE activity: (1) HDE from healthy and drug-stressed hepatocytes appear to have direct immunomodulatory activity; and (2) the effects of APAP HDE on the release of inflammatory mediators indicates that they may sensitize monocytes to LPS stimulation.

To better define the effects of primary human HDE on immune cells, transcriptomic analysis was conducted on HDE-exposed THP-1 monocytes via microarrays. We present a novel method to account for the potential confounding effects of EQ precipitation reagent on gene expression analysis. Briefly, mock EQ controls were prepared from hepatocyte dosing solutions (medium control and 10 mM APAP) that were not incubated with hepatocytes. These solutions were concentrated and precipitated with EQ in the same fashion as the conditioned hepatocyte medium containing HDE. Application of these mock controls to monocytes alongside true HDE preparations enabled the isolation of gene expression effects due solely to HDE and not confounded by the potential influences of residual APAP or EQ. Differential gene expression (for global data set or individual donors) was determined by comparing the effects of HDE from control- and APAP-treated hepatocytes to monocytes treated with respective mock EQ controls. In general, exposure to HDE from control- or APAP-treated hepatocytes caused down-regulation of genes.

Inspection of genes with the greatest decreases induced by APAP HDE from individual donors revealed two distinct responses: APAP HDE from three donors (1, 4, 5) significantly affected genes in immune pathways while APAP HDE from two donors (2, 3) impacted genes associated with cholesterol metabolism pathways. These results provide the first evidence of immunologically relevant gene expression changes occurring as a result of exposure to HDE from drug-stressed cells. The present findings suggest that donor-specific hepatocellular responses to APAP—which were not apparent in cell viability and functionality data—are communicated to immune cells via HDE. This hypothesis is supported by the outcome of a healthy volunteer study that examined the peripheral blood transcriptome following therapeutic doses of APAP. Subjects were classified as responders

if they showed ALT elevations or non-responders if they did not. In responders, peripheral blood transcriptomic signatures indicated a loss of immune tolerance and increased inflammatory response (Fannin *et al.*, 2016). Conversely, non-responders had tolerogenic, anti-inflammatory transcriptomic signatures. The differential responses of monocytes to individual donor HDE observed here may represent the unique responses of hepatocytes to APAP.

When data from all hepatocyte donors were pooled, thirteen genes were significantly altered by control HDE versus mock EQ control treatments, suggesting that under these experimental conditions, HDE from healthy cells do not exert a strong effect on monocyte gene expression. However, 126 unique genes were differentially regulated by APAP HDE exposure in a statistically significant manner. Pathway analysis of these data revealed extensive enrichment for genes involved in cholesterol homeostasis and lipid metabolism processes. Most of the immune pathways affected by APAP HDE from donors 1, 4, and 5 were not among the pathways enriched in the global data set. There was, however, overlap of TREM1 signaling in both data sets. TREM1 is a glycoprotein surface receptor on monocytes and neutrophils whose activation mediates pro-inflammatory cytokine production and phagocytosis (Arts *et al.*, 2013). However, the current data do not indicate whether the TREM pathway would be activated or inactivated as a result of the observed gene expression changes.

There are a number of hypotheses that may explain why the majority of statistically significant transcriptomic alterations due to APAP HDE were related to cholesterol homeostasis, a process that is indirectly linked to immune response. The simplest interpretation of these data is that APAP HDE deliver excessive lipids and cholesterol to

monocytes, resulting in a compensatory down-regulation of cholesterol biosynthesis and lipid breakdown. The release of HDE carrying higher lipid loads following APAP exposure has been observed in rat models and may be adaptive for the hepatocyte (Royo *et al.*, 2016). Utilization of exosomes to maintain cholesterol homeostasis is a known adaptive mechanism (Strauss *et al.*, 2010) and is mechanistically plausible given that lysosomal accumulation of cholesterol is associated with increased susceptibility to APAP DILI (Baulies *et al.*, 2015). Thus, hepatocytes may be ridding themselves of excess cholesterol as a precautionary measure against APAP toxicity.

Exosomes are inherently enriched for cholesterol, sphingomyelin, ceramide, and phosphatidylserine externally but they can also carry bioactive lipids and lipid metabolizing enzymes as interior cargo (Kowal *et al.*, 2014; Royo *et al.*, 2016; Subra *et al.*, 2010). Exosomes are structurally distinct from the major source of cholesterol for extrahepatic cells, low-density lipoproteins (LDL), but they are now becoming recognized as highly effective vectors for lipid transport between cells (Berg *et al.*, 2002; Laulagnier *et al.*, 2004; Record *et al.*, 2014). The fact that control HDE also caused down-regulation of a handful of cholesterol-related genes but to a lesser extent supports the hypothesis that APAP HDE may be enriched in lipids and cholesterol relative to controls. In conjunction with our finding that monocytes do not differentially internalize control HDE and APAP HDE, these results suggest that the unique gene expression changes induced by APAP HDE are due to altered content rather than altered uptake.

The differential packaging of lipids into APAP HDE may very well mediate some of the biological effects of HDE. However, our data indicate that the differential gene expression in monocytes following APAP HDE exposure may be due to the transfer of

functional miRNA by APAP HDE. Exosomal miRNA profiling revealed that APAP HDE are enriched for miRNA that target many of the down-regulated genes in monocytes. Using experimentally validated miRNA-mRNA relationships, we predicted which monocyte genes would be targeted by the miRNA increased in APAP HDE across all donors. Pathway enrichment analysis was performed on the predicted gene list to compare the monocyte functions that would be affected if functional exosomal miRNA were delivered by APAP HDE. There was marked concordance between the most significantly affected predicted and observed pathways: 8 of 10 predicted canonical biological functions and 9 of 10 toxicity pathways were common to both data sets. Common pathways included cholesterol metabolism, LXR/RXR activation, mitochondrial membrane permeability decrease, and liver steatosis. There was also marked overlap between predicted and observed pathways on an individual donor basis. Despite having limited gene target information, exosomal miRNA predicted up to 73% of the pathways altered by a given donor in monocytes.

We propose that APAP HDE sensitized monocytes to LPS. In this work, two sets of monocytes were treated with HDE from APAP- or control-treated hepatocytes for 24 h. After 24 h, one set of monocytes was harvested for gene expression analysis and the other set was stimulated with LPS for cytokine analysis. Therefore, altered cytokine responses following LPS activation in HDE-treated monocytes reflect the influence of HDE on sensitivity to stimulus. Similar results have been obtained from application of T-cell derived exosomes to THP-1 monocytes. Exosome exposure resulted in cholesterol accumulation and enhanced TNF-α production (Zakharova *et al.*, 2006). In fact, many of the statistically significant genes affected by APAP HDE that are related to cholesterol homeostasis are also linked to LPS sensitization. For example, 25-hydroxycholesterol synergizes with a TLR3

agonist to enhance IL-8 secretion (Koarai *et al.*, 2012). One of the significantly down-regulated genes in our data set, *TSC22D3*, is responsible for this sensitization via negative regulation of NFκB activity (Koarai *et al.*, 2012). Through mechanisms that are not yet defined, 25-hydroxycholesterol also promotes secretion of IL-6 and macrophage colony stimulating factor (Cyster *et al.*, 2014). Another significantly decreased gene, *MVK*, has been associated with pro-inflammatory responses. In the genetic inflammatory disorder known as hyper IgD syndrome, low *MVK* expression is responsible for increases in the production of IL-1β (Cyster *et al.*, 2014). Usually considered a positive regulator, under certain conditions, down-regulation of *ATF5* may enhance the release of pro-inflammatory cytokine production following T cell activation (Chuang *et al.*, 2008). While 94% of the genes whose expression was significantly different in the APAP HDE group were decreased, some of the increased genes also have ties to immune response. For instance, *POLR3E* induces NFκB, which could lead to potentiation of an NFκB-mediated inflammatory response (Koarai *et al.*, 2012).

There is a well-recognized but poorly understood relationship between intracellular cholesterol levels and dysregulated immune response. Observations from cholesterol-loaded monocyte-derived macrophages demonstrate that these cells are sensitized to LPS and that myeloid cells from a high-fat environment are pre-disposed to adopt a pro-inflammatory phenotype, a phenomenon called myeloid skewing (Murphy *et al.*, 2014; Oiknine and Aviram, 1992). The mechanisms of this sensitization have not been fully defined, but at least three processes have been described in the literature. In the first process, cholesterol accumulation leads to formation of cholesterol crystals and excess LDL, which together can perform both of the priming steps required for inflammasome activation and pro-

inflammatory cytokine release (Tall and Yvan-Charvet, 2015). LPS sensitization may also occur as a result of failed compensatory mechanisms mediated by ABCG1 and ABCA1, which normally down-regulate toll-like receptor (TLR) signaling in response to cholesterol accumulation (Yvan-Charvet *et al.*, 2008; Zhu *et al.*, 2008). Without the proper function of these cholesterol-mediated feedback mechanisms, the TLR4 signaling pathway remains highly responsive to LPS stimulation. The facilitation of enhanced TLR and cytokine receptor-mediated signaling by increased density of lipid rafts is perhaps the most defined mechanism of cholesterol-mediated LPS sensitization. Cellular cholesterol and lipid levels are directly tied to membrane remodeling, which is a key aspect of immune signaling. For example, cholesterol accumulation increases the density of plasma membrane lipid rafts, which promote inflammatory receptor-mediated signaling, including that of TNFR, by serving as "platforms" for the assembly of signaling complexes (Fessler and Parks, 2011; Legler *et al.*, 2003). Cholesterol levels in the plasma membrane also mediate ligand-independent activation of receptors such as EGFR (Chen and Resh, 2002), and cholesterol flux influences the levels of LPS recognition proteins CD14 and TLR4 (Fessler and Parks, 2011). Lastly, low cholesterol levels cause displacement and shedding of TNFR1, TNFR2, and IL-6R in immune cells including THP-1 monocytes (Matthews *et al.*, 2003; Tellier *et al.*, 2008). It is hypothesized that cholesterol stabilizes these receptors, increasing the responsiveness of cholesterol-loaded immune cells to inflammatory stimuli.

It is difficult to conclude from these results whether the effects of APAP HDE on monocytes would exacerbate APAP injury, because cytokines play such varied roles in DILI depending upon the context of the injury. For instance, TNF-α is known to exacerbate the toxicity of certain I-DILI drugs including trovafloxacin (Maiuri *et al.*, 2015; Shaw *et al.*,

2010), but may also promote hepatocyte regeneration after APAP injury (Chiu *et al.*, 2003). Plasma levels of IL-8 and MCP-1 at presentation are correlated with the degree of injury in APAP overdose patients (James *et al.*, 2001; James *et al.*, 2005). In human APAP-induced liver injury, classical $CD14^{++}/CD16^{-}$ monocytes (the predominant circulating monocytes) are recruited to the liver in an MCP-1 dependent manner during the early phase of cell death, known as the "necroinflammatory" stage (Geissmann *et al.*, 2003; Shi and Pamer, 2011; Zigmond *et al.*, 2014). Once in the liver, these monocytes can differentiate into dendritic cells (DCs), macrophages, and possibly even hepatocyte stem-like cells (Shi and Pamer, 2011; Simon *et al.*, 2015). In fact, monocytes recruited to the liver by APAP toxicity have been shown to differentiate into macrophages that aid in the resolution phase of injury (Zigmond *et al.*, 2014). It is important to note that in the current research, 4 out of 5 human hepatocyte lots did not experience overt APAP cytotoxicity. Therefore, the observed alterations in monocyte cytokine response were produced by HDE released prior to fulminant necrosis. While the current research cannot determine the ultimate influence of HDE on the outcome of APAP DILI, the results presented here substantiate HDE as a mechanism of sub-toxic immune cell regulation by drug-stressed hepatocytes.

Although this work was not focused on the evaluation or HDE as biomarkers of DILI, the present RNA sequencing results suggest that global mRNA profiles in HDE may provide mechanistic information regarding cell stress. Despite the fact that exosomal mRNA represented approximately 2% of all mapped reads, control HDE data were substantiated by concordance with results from rat HDE transcriptomics (Royo *et al.*, 2013). In addition, mRNAs representing genes known to be up-regulated in hepatocytes during APAP DILI were enriched in APAP HDE relative to control HDE. These transcripts also showed

significant overlap with DE genes from APAP-treated primary human hepatocytes, and represented pathways that are mechanistically relevant in APAP DILI. Therefore, the mRNA content of HDE may provide information regarding gene expression at the hepatocyte level, which supports the hypothesis that HDE may serve as a "liquid biopsy" of hepatic gene expression changes in patients, potentially eliminating the need for invasive measures.

In summary, this research sought to verify the immunologic activity of HDE released by drug-stressed cells and evaluate HDE miRNA as potential mediators of said activity. HDE from APAP-treated hepatocytes induced different gene expression changes in monocytes depending upon the hepatocyte donor. One subset of donors (n=3) produced HDE in response to APAP exposure that regulated many immunologically relevant pathways. The second subset of donors (n=2) had the greatest impacts on cholesterol and lipid-related metabolic processes. When examined as a whole, the data revealed statistically significant alterations in cholesterol pathways as a result of monocyte exposure to APAP HDE. New evidence has identified differential lipid enrichment in HDE from APAP-treated cells, but the data presented here argue for a role of exosomal miRNA in the regulation of cholesterol pathways within monocytes. We associated these gene expression changes with miRNA delivered by APAP HDE, and determined that there was significant overlap between the observed DE pathways and those predicted by HDE miRNA targets. Control HDE appeared to induce compensatory and possibly even anti-inflammatory responses in monocytes. However, gene expression changes induced by APAP HDE indicate major effects on cholesterol accumulation and metabolism, processes that are linked to the LPS sensitization of immune cells that we observed. We conclude that exosomes from APAP-stressed primary human hepatocytes sensitize monocytes to LPS activation, a process

potentially mediated by exosomal miRNA regulation which may involve cholesterol homeostasis. This research presents the first evidence of direct immunomodulation by primary human HDE and alteration of this activity by drug-induced hepatocellular stress, thereby substantiating the role of HDE in early immune-mediated DILI events.

CHAPTER 5.

DISCUSSION

5.1 Summary and conclusions

The current research provided substantive evidence that hepatocyte-derived exosomes (HDE), a type of extracellular vesicle (EV), are directly involved in signaling to the immune system following drug-induced hepatocyte stress. EVs are membrane-bound particles that carry RNA, protein, and lipid cargo to recipient cells as a means of communication. It follows that EVs participate in myriad physiological processes including cell fate, regeneration, metastasis, and viral pathogenesis. Exosomes represent the smallest class of EV (<150 nm) and are widely recognized as effective mediators of immune function. Both innate and adaptive immune responses are key components of many intrinsic and idiosyncratic drug-induced liver injury (DILI) mechanisms. Thus HDE are of great interest in the field of DILI.

The field of HDE research is in its infancy, and the possibility that HDE form a link between hepatocytes and immune cells in the absence of overt hepatotoxicity had not been investigated prior to this research. Multiple studies have demonstrated that HDE are immunologically active in models of viral hepatitis, fatty liver disease, and alcohol-induced liver injury. Many of these experiments have utilized hepatocyte-like cell lines, which are characteristically dissimilar to primary hepatocytes. In this work, we sought to establish a

role for HDE in early, sub-toxic immune responses to drug-induced hepatocyte stress that could ultimately influence the outcome of DILI. With few methods or precedents in the literature, we intended to confirm the immunomodulatory capacity of HDE released by primary hepatocytes stressed with an intrinsic hepatotoxicant, acetaminophen (APAP). Although it was necessary to employ an intrinsic hepatotoxicant in this foundational work, it is fully anticipated that the findings presented here will be validated in models of idiosyncratic DILI (I-DILI) in the future.

This research addressed the global hypothesis that HDE from drug-stressed cells carry bioactive signals of hepatocellular stress to the immune system. We proposed that HDE could serve as functional regulators of early DILI events if the following conditions were met. First, given that HDE are constitutively released, their content or quantity should be significantly altered prior to overt drug-induced hepatotoxicity. Second, HDE content should be indicative of hepatocyte stress or of HDE function. Lastly, immune cells should respond to HDE, and this response should be distinct between HDE from control- and drug-treated hepatocytes. These conditions were investigated in three Specific Aims using APAP as a model DILI compound.

Chapter 2 of this work summarizes a year of extensive technique optimization and validation for the enrichment and analysis of primary rat and human HDE. There are no standardized methods for the study of exosomes and it is vital that techniques are developed and substantiated for each individual research question. In comparisons between ultracentrifugation (UC) and ExoQuick (EQ) polymer precipitation, EQ was selected as the ideal method for optimal HDE RNA and protein yields from rat plasma, rat hepatocyte cultures, and human hepatocyte cultures. The use of EQ allowed us to decrease the scale of

hepatocyte experiments by 10 to 20-fold relative to published methods. The absolute quantification of HDE mRNA was optimized by developing standard curves for quantitative real-time polymerase chain reaction (qRT-PCR) analysis of all rat and human targets. In addition, the use of exogenous mRNA was validated as a means of qRT-PCR data normalization in the absence of traditional housekeeping genes. Rarely in exosome literature are steps taken to generate absolute mRNA quantities and normalize qRT-PCR data. However, it is extremely important that these efforts be made because reliable housekeeping genes whose exosomal levels are unaffected by treatment have yet to be identified. The procedures developed in this research represent higher throughput and reliable methods for the analysis of HDE from primary rat and human hepatocytes.

In Chapter 3, the aforementioned techniques were employed to determine whether the content or quantity of HDE were altered prior to overt APAP hepatotoxicity. *In vivo*, rats were exposed to a single APAP dose (0, 500, or 1400 mg/kg) for a total of 0, 1, 2, 4, 8, 12, or 24 h (n=5-6/group). At these time points, samples were collected for plasma exosome precipitation, clinical chemistry, liver histopathology, and liver gene expression analysis. HDE were isolated from plasma and examined via qRT-PCR for the liver-specific RNAs albumin mRNA and miR-122. Currently available techniques cannot reliably separate exosomes released by a specific cell type from the heterogeneous mixture of exosomes in the circulation. Therefore, *in vivo* HDE studies rely upon liver-specific RNAs to verify the presence of HDE. For these studies, albumin mRNA and miR-122 were measured in exosomes as markers of HDE. As it can exist outside of exosomes, miR-122 was also measured in the protein-rich (non-exosomal) fraction of plasma. These data were compared to metrics of hepatic injury including liver histopathology scores and the plasma activity of

alanine aminotransferase (ALT), the gold-standard biomarker of hepatocellular necrosis *in vivo*. Histopathology and ALT results indicated that APAP DILI only developed in the high dose group after 24 h. Albumin mRNA in plasma HDE was significantly elevated in the high dose group at 12 h, prior to hepatocellular necrosis. HDE albumin was also significantly elevated in the low dose group at 24 h, in the absence of hepatocellular necrosis. These data supported the hypothesis that the RNA content of HDE was altered before development of DILI *in vivo*. Both the exosomal and protein-rich fractions of miR-122 were elevated prior to DILI, but these changes were not statistically significant. However, when exosomal miR-122 was plotted as a percentage of total circulating miR-122 (exosome + protein-rich), time-dependent decreases in the proportion of exosomal miR-122 relative to total were observed. These decreases were apparent as early as 2 h post-dose, and reached statistical significance at 12 h, before development of APAP DILI. These results confirmed that the majority of miR-122 released by hepatocytes as a function of APAP exposure is protein-rich, and also revealed that following exosomal miR-122 as a percent of total provided earlier indication of toxicity than measuring protein-rich miR-122 alone. Finally, the unique profiles of miR-122 and albumin mRNA within HDE support the assertion that RNAs are selectively and differentially packaged into HDE.

Corresponding *in vitro* studies were conducted using primary rat hepatocytes exposed to 0, 0.37, 1.1, 3.3, 10, or 30 mM APAP for 24 h. These experiments confirmed that *in vivo* HDE dynamics could be recapitulated *in vitro*. They were also used to evaluate the effect of drug stress on HDE quantity because, as mentioned previously, it is not yet possible to reliably separate HDE from other circulating exosome populations. Therefore, any investigation of changes in HDE quantity must be performed in an isolated monoculture

system. From these studies, we observed significant increases in HDE albumin mRNA beginning at 1.1 mM APAP, while cytotoxicity was not apparent until 30 mM APAP. Quantification of albumin mRNA in the hepatocytes themselves revealed that increases in exosomal albumin were not simply a passive reflection of increased transcription at the hepatocyte level. No statistically significant increases in HDE or protein-rich miR-122 were detected prior to overt hepatocellular injury. The unique increases in albumin mRNA that were not observed for miR-122 indicated a selective packaging of albumin mRNA into HDE following APAP exposure. Despite increases in albumin mRNA content, HDE number was not affected by any APAP concentration. Taken together, these results suggest that the significant alterations in HDE RNA observed *in vivo* and *in vitro* were caused by an increase in selective packaging of albumin mRNA as opposed to an increase in total HDE release.

The translational relevance of these findings was assessed using freshly isolated primary human hepatocytes (n=7). Cultures were exposed to 10 mM APAP for 24 h, after which samples were harvested for cytotoxicity, cellular and HDE RNA analysis, and HDE quantification. Across all donors, 10 mM APAP did not significantly increase LDH leakage, suggesting that 10 mM APAP was not overtly toxic. APAP-induced elevations in HDE albumin mRNA were observed but did not reach statistical significance. However, exosomal miR-122 showed statistically significant increases across all donors in response to APAP stress. In keeping with the rat hepatocyte results, HDE quantity was not affected by APAP exposure. These results confirmed that the RNA content, but not quantity, of HDE is altered by sub-toxic drug stress in rats, rat hepatocytes, and human hepatocytes. As these were the first studies to quantify mRNA in primary human HDE, baseline levels of additional liver-enriched mRNAs were measured across donors, and the influence of donor characteristics on

baseline HDE content were also examined. We observed a potential relationship between donor BMI and baseline quantities of albumin mRNA in HDE. These results may have implications for the role of HDE in fatty liver disease and related liver disorders.

In Chapter 4, we sought to comprehensively profile the mRNA and miRNA content of HDE from control- and APAP-treated primary human hepatocytes (n=5) (Aim 2). Next-generation sequencing techniques were employed to generate the first profiles of mRNA and miRNA in primary human HDE. Analysis revealed that mRNA and miRNA enrichment within HDE are influenced by sub-toxic APAP stress. RNA sequencing indicated that the most abundant transcripts in primary human HDE overlap with those identified as the most prevalent in primary rat HDE. Relative to control HDE, the mRNA enriched in APAP HDE represented pathways including oxidative phosphorylation and mitochondrial dysfunction, that are not only mechanistically relevant in APAP DILI but are also altered at the hepatocyte level. These results suggest that global alterations in HDE mRNA content may be indicative of hepatocellular gene expression, as we had originally hypothesized. Similarly, the miRNAs that were enriched in APAP HDE relative to control HDE have been associated with response to APAP in both rat and human *in vivo* studies.

HDE were then incubated with THP-1 human monocytes to address the hypothesis that HDE from drug-stressed hepatocytes are capable of immunomodulation in the absence of cell death (Aim 3). Gene expression profiling of monocytes revealed that exposure to control HDE and APAP HDE may alter cholesterol metabolism and lipid homeostasis pathways, with APAP HDE promoting the differential expression of 10 times more genes than control HDE. Depending on the hepatocyte donor, monocyte pathway enrichment indicated overrepresentation of immunologically relevant genes or those involved in

cholesterol metabolism. Analysis of the global data set revealed statistically significant effects on cholesterol homeostasis. In an effort to relate HDE content to this activity, miRNAs enriched in APAP HDE were used to predict the pathways anticipated to be differentially regulated in monocytes for individual donors as well as pooled data. Notably, the pathways known to be targeted by the miRNA in APAP HDE largely overlapped with the pathways actually affected in monocytes. These results strongly suggest that HDE regulation of monocyte gene expression may be caused by the horizontal transfer of functional miRNAs, a mechanism that has been substantiated for miR-122 delivery to monocytes via Huh7.5 HDE (Momen-Heravi *et al.*, 2015a).

We also provided evidence to suggest that the gene expression changes caused by APAP HDE may predispose monocytes to activation. Monocytes pre-treated with control or APAP HDE were stimulated with LPS to examine effects on cytokine response. Results demonstrated that control HDE caused a mild increase in MCP-1 secretion and generally decreased release of pro-inflammatory cytokines IL-8 and TNF-α. In contrast, APAP HDE promoted a pro-inflammatory phenotype with increases in all measured cytokines. We proposed that the gene expression changes induced by APAP HDE exposure promoted sensitization of monocytes to LPS stimulus, and provided evidence to support this claim. For the first time, this research demonstrates the immunomodulatory capacity of exosomes released by drug-stressed hepatocytes. The activity of HDE prior to overt cytotoxicity strongly suggests that through direct interactions with immune cells, HDE may be critical mediators of DILI outcomes.

5.2 Limitations

In the field of exosomes, there are several inherent limitations that must be considered, not the least of which is the inability to truly purify exosomes from other EVs. In any biofluid, exosomes are part of a heterogeneous mixture of other EVs, lipoproteins, protein aggregates, and protein-miRNA complexes. Current technologies for exosome isolation rely on separation by size, buoyant density, or specific protein markers. Many variations of size- and density-based methods exist, and none can truly isolate exosomes due to size and density overlap with non-exosomal particles. Selection for exosomes using immunoprecipitation via protein markers of the endolysosomal pathway such as CD9, CD63, CD81, or TSG101 is an attractive option. However, there is no single protein that has been unequivocally detected in all exosomes, therefore, immunoselection of this kind automatically creates a bias by ignoring exosome populations that are not positive for the marker of interest. It follows that the outcome of individual exosome investigations is highly dependent upon the enrichment method and functional endpoints. The current research employed a polymer precipitation reagent, which enriches for exosomes by size. Like all size-exclusion methods, this approach may co-precipitate miRNA-protein complexes and lipoproteins in exosome preparations. This limitation is particularly important when measuring miRNAs in the exosomal fraction, as we have done, because some of the miRNA signal may be due to extra-exosomal molecules. For this reason, we also measured exosomal mRNA such as albumin, which was not detected outside of exosomes and serves as a confirmatory marker. It is also important to note that standardized methods for exosome enrichment and analysis do not currently exist. It is for this reason that so much time and effort was invested in confirming that the approaches developed here were appropriate and

optimized for the research query. To ensure reproducibility, it is paramount to report all pertinent methods in exosome studies and work towards standardization in the field.

An area that will require significant optimization specifically for exosomes is the analysis of exosome content by RNA sequencing. RNA sequencing has become a popular approach for global profiling because it allows for more direct quantification of RNAs and can detect novel RNA species. Sample preparation is relatively simple, but there is a significant bottleneck in the data analysis stage that limits the feasibility for RNA sequencing for many purposes. In addition to the inherent complications of RNA sequencing, exosomes contain RNA profiles that are often distinct from those within their parent cell. RNA sequencing results have demonstrated that the majority of exosomal RNAs are miRNAs and other non-coding RNA species (Huang *et al.*, 2013; Nolte-'t Hoen *et al.*, 2012). This posed a challenge for the current research, which sought to identify coding mRNAs within HDE that could be reflective of hepatocyte gene expression. With such a low proportion of mappable reads, statistical comparisons between mRNAs in control HDE and APAP HDE could not be performed reliably. RNA sequencing is a strong analytical tool, but requires further optimization of specialized sample preparation and bioinformatics techniques before it can be readily applied to exosomes.

When conducting *in vitro* hepatotoxicity studies, it is important to recognize the limitations of each model system. In the present research, experiments were conducted on primary rat or human hepatocytes in monoculture on a collagen substratum, without the overlay applied in traditional sandwich culture. Sandwich culture of hepatocytes has remained the gold standard model for *in vitro* hepatotoxicity testing because the configuration supports metabolic function, canalicular development, and cell viability

(LeCluyse *et al.*, 1994; Swift *et al.*, 2010). However, evidence indicated that the sandwich culture overlay could impede exosome release and detection, and existing work using rat HDE did not utilize an overlay (Conde-Vancells *et al.*, 2008; Royo *et al.*, 2013). Since the current research was attempting to significantly scale down experiments relative to published methods, it was imperative to culture without an overlay to ensure maximal exosome collection. In the absence of an overlay, it is possible that the hepatocytes used in the present studies were experiencing stress at the time that they were exposed to APAP. Conversely, the cells were likely to have experienced more stress had they been cultured longer without an overlay.

While primary hepatocytes constitute an inherently more physiologically relevant system than hepatocyte-like cell lines, their biology is not ideally modeled in monocultures. In the liver, hepatocytes are surrounded by non-parenchymal cells that support and regulate their function, as well as their responses to toxicants, as our earlier work has shown (Rose *et al.*, 2016) (Appendix). The inability to separate HDE from other exosomes necessitated that hepatocytes be studied in monoculture to ensure that the exosomes being harvested and analyzed were hepatocyte-derived. Improvements on the methods available today would allow for the study of HDE in complex, multi-cellular models that more accurately recapitulate *in vivo* liver physiology.

5.3 Future directions

The current research presents the first evidence that immune cells are directly influenced by exosomes from primary human hepatocytes in response to sub-toxic drug treatment. These findings have exciting implications for the future study of DILI

mechanisms, as they implicate HDE as an early regulator of the immune system following drug-induced stress. A natural progression of this work would utilize the approaches described here to investigate the role of HDE in early responses to I-DILI drugs. I-DILI frequently involves the immune system, and HDE may be used to study the mechanisms of I-DILI or to identify and predict I-DILI in patients. The present work may also implicate HDE as mediators of inflammatory responses in other organs and underscores the importance of contextualizing the systemic effects of HDE release. For example, an as-yet undefined relationship exists between immune responses in the liver and the lung (Hilliard *et al.*, 2015). This axis, and others like it, may be mediated in part by the immunomodulatory functions of HDE.

Near-term future directions would be to further investigate the potentially bioactive exosome components identified here, namely miRNA. We reported increases in exosomal miRNAs that corresponded to regulation of targeted pathways in monocytes. Many of the potential miRNA regulators differentially enriched in APAP HDE have known associations with APAP DILI. To support the hypothesis that these miRNAs are responsible for the activity of APAP HDE on monocytes, molecular biology techniques should be employed to individually manipulate those miRNAs in monocytes and establish a causal relationship. First, the most abundant miRNAs in APAP HDE should be measured in monocytes by qRT-PCR before and after HDE exposure to confirm transfer. Ideally, miRNAs that are hepatocyte-specific and not expressed in monocytes, like miR-122, would be selected to strengthen the argument for exosomal transfer. Similar to the work of Momen-Heravi and colleagues, recipient monocytes should be treated with mimics and RNAi inhibitors of a given miRNA to examine the influence of that miRNA on the phenotype (Momen-Heravi *et*

al., 2015a). Recent evidence from primary rat HDE suggest that lipid profiles and metabolic enzymes within HDE are altered by APAP exposure (Royo *et al.*, 2016). These findings should be confirmed in primary human HDE, as exosomal lipid content may influence the activity of HDE and have implications for diseases involving lipid accumulation and inflammation, such as fatty liver disease.

While not the focus of the current work, HDE-mediated gene expression changes were also observed in SECs and macrophages. The activity of HDE demonstrated here warrants further investigation of these interactions, and provides justification for exposing primary monocytes and elutriated hepatic NPCs to HDE. The effects of HDE on primary NPCs would have implications for intrinsic and idiosyncratic DILI, especially for those drugs whose toxicity is known to involve NPCs (Rose *et al.*, 2016)(Appendix). In addition, application of HDE to non-immune NPCs such as SECs and stellate cells could reveal mechanisms by which HDE indirectly mediate immune responses. Lastly, to fully understand the complex dynamics between the cells of the liver, exosomes from NPCs should be applied to hepatocytes. Results from such experiments would be valuable in the field of DILI but also for understanding the mechanisms of exosome-mediated cell communication in liver disease as a whole.

APPENDIX.

CO-CULTURE OF HEPATOCYTES AND KUPFFER CELLS AS AN *IN VITRO* MODEL OF INFLAMMATION AND DRUG-INDUCED HEPATOTOXICITY[2]

Overview

Immune-mediated drug-induced hepatotoxicity is often unrecognized as a potential mode of action due to the lack of appropriate in vitro models. We have established an in vitro rat donor-matched hepatocyte and Kupffer cell co-culture (HKCC) model to study immune-related responses to drug exposure. Optimal cell culture conditions were identified for the maintenance of co-cultures based on cell longevity, monolayer integrity and cytokine response after LPS exposure. Hepatocyte mono-cultures and HKCCs were then used to test a subset of compounds associated with hepatotoxic effects with or without LPS. Cytokine levels and metabolic activity (Cyp3A) were measured after a 48 hr exposure to monitor endotoxin-induced changes in acute phase and functional endpoints. LPS-activated HKCCs, but not hepatocyte mono-cultures, treated with trovafloxacin (TVX) or acetaminophen (APAP), compounds associated with immune-mediated hepatotoxicity, showed LPS-dependent decreases in IL-6 production with concomitant increases in Cyp3A activity. Differential endotoxin- and model-dependent alterations were observed in cytokine profiles and Cyp3A activity levels that corresponded to specific compounds. These results indicate

[2] This chapter has been published as an original research article in the Journal of Pharmaceutical Sciences and is presented according to journal convention. The original citation is as follows: Rose K., Holman N., *et al*. 2016. Co-culture of hepatocytes and Kupffer cells as an *in vitro* model of inflammation and drug-induced hepatotoxicity, Journal of Pharmaceutical Sciences, 105:950-964; Epub 2015 Nov 17.

the utility of the HKCC model system to discern compound-specific effects that may lead to enhanced or mitigate hepatocellular injury due to innate or adaptive immune responses.

Introduction

Unexpected and unexplained hepatotoxicity continues to be one of the main adverse outcomes observed in humans during clinical trials and after-market withdrawals (Corsini *et al.*, 2012; Kaplowitz, 2005; Sunman *et al.*, 2004). Drug-induced hepatotoxic modes of action (MOA) are often complex, involving metabolic activation, multiple cell types and perturbation of biochemical pathways involving both hepatocytes and resident macrophages (i.e. Kupffer cells [KCs]) (DeLeve *et al.*, 1997; Evers *et al.*, 2013; Kmiec, 2001; Sunman *et al.*, 2004). Many complex, immune-mediated hepatocellular responses such as reactive metabolite formation, infectious disease, circulating cytokines, and gut-derived endotoxin inflammation require interactions between hepatocytes, endothelial cells and KCs (DeLeve *et al.*, 1997; Evers *et al.*, 2013; Liu and Kaplowitz, 2006; Sunman *et al.*, 2004).

KCs constitute the largest resident macrophage population in the body, and are crucial for the regulation of immune-mediated hepatotoxicity and liver injury (Dixon *et al.*, 2013). In their primary scavenger role, KCs endocytose foreign particles and bacterial endotoxins, which causes their activation and production of a number of cell signaling and stress pathway modulators, such as reactive oxygen species and cytokines, including TNF-α and IL-1 (Kolios *et al.*, 2006). Cell damage and soluble stress signals during drug-induced hepatocellular injury cause a similar KC activation, which modulates hepatocyte and non-parenchymal cell death by apoptosis (Dixon *et al.*, 2013; Kolios *et al.*, 2006; Roberts *et al.*, 2007). In addition, cytokines and chemokines secreted by KCs during injury modulate the metabolic activity of hepatocytes and induce the expression of acute phase proteins, such as

C-reactive protein and *NOS2*, while causing the suppression of genes involved in the metabolism and clearance of xenobiotics, including cytochrome P-450 enzymes, uridine 5'-diphospho(UDP)-glucuronosyl transferase systems and uptake and efflux transporters (Higuchi *et al.*, 2007; Hoebe *et al.*, 2001; Morgan, 2009; Sunman *et al.*, 2004; Wu *et al.*, 2006).

KCs constitute the largest resident macrophage population in the body, and are crucial for the regulation of immune-mediated hepatotoxicity and liver injury (Dixon *et al.*, 2013). In their primary scavenger role, KCs endocytose foreign particles and bacterial endotoxins, which causes their activation and production of a number of cell signaling and stress pathway modulators, such as reactive oxygen species and cytokines, including TNF-α and IL-1 (Kolios *et al.*, 2006). Cell damage and soluble stress signals during drug-induced hepatocellular injury cause a similar KC activation, which modulates hepatocyte and non-parenchymal cell death by apoptosis (Dixon *et al.*, 2013; Kolios *et al.*, 2006; Roberts *et al.*, 2007). In addition, cytokines and chemokines secreted by KCs during injury modulate the metabolic activity of hepatocytes and induce the expression of acute phase proteins, such as C-reactive protein and *NOS2*, while causing the suppression of genes involved in the metabolism and clearance of xenobiotics, including cytochrome P-450 enzymes, uridine 5'-diphospho(UDP)-glucuronosyl transferase systems and uptake and efflux transporters (Higuchi *et al.*, 2007; Hoebe *et al.*, 2001; Morgan, 2009; Sunman *et al.*, 2004; Wu *et al.*, 2006).

These complex and dynamic cellular interactions are not adequately captured in traditional hepatocyte mono-cultures. As such, indirect hepatocellular toxicity caused by immune cell activation and hepatic inflammation is often overlooked as a potential mode of

action (Evers *et al.*, 2013). Development of an optimized co-culture system that incorporates KCs will be imperative to study these events. In addition, there is a growing body of evidence for the role of genetic variability and adaptive immune responses within the human population that accounts for some idiosyncratic drug-induced liver injury and its severity in some patients (Corsini *et al.*, 2012). This also becomes even more important when using inbred strains of rodents or animal models with rare or unique genetic backgrounds (Harrill *et al.*, 2009a).

Clearly, to better assess the potential of compounds to cause immune-mediated hepatotoxicity, more reliable and predictive culture models that incorporate donor-matched cell types are needed. Previously, we developed a rodent-based co-culture model using a commercial source of cryopreserved KCs and observed enhanced drug-induced hepatotoxicity under glucocorticoid-free medium conditions (Bonzo *et al.*, 2015). In the current study, we present a more metabolically competent *in vitro* rat hepatic co-culture system that incorporates donor-matched primary hepatocytes and KCs (HKCC) to assess immune-mediated hepatotoxicity over an extended culture period. The effects of different medium formulations and glucocorticoid levels were investigated to define suitable experimental conditions prior to compound testing (Waxman *et al.*, 1990). Validation studies were conducted under predefined culture conditions using a set of hepatotoxic compounds, including trovafloxacin (TVX), an antibiotic associated with immune-related hepatotoxicity, and acetaminophen (APAP), an analgesic and antipyretic agent associated with reactive metabolite formation and oxidative stress. As part of these studies, we determined the concentration-dependent responses of a set of test compounds on functional endpoints (Cyp3A activity) and cytokine profiles (IL-6, TNF-α) in the presence and absence

of lipopolysaccharide (LPS). Our results indicate that this enhanced co-culture model system provides a more stable and physiologically relevant platform by which to investigate drug-induced, immune-mediated reactions that can lead to acute hepatotoxic effects.

Materials and methods

Reagents

Trovafloxacin, levofloxacin, allyl alcohol and acetaminophen were purchased from Sigma-Aldrich (St. Louis, MO). Triclosan (Irgacare MP) was obtained from Ciba-Geigy AG (Basel, Switzerland). Propiconazole and Acetochlor were purchased from Chem Service (West Chester, PA). All other compounds were purchased from Sigma-Aldrich and were of the highest grade available. Compound stocks were prepared in dimethyl sulfoxide (DMSO, Sigma-Aldrich) so that the final concentration did not exceed 0.1%. Lipopolysaccharide (LPS) from E. coli strain 0127:B8 (Sigma-Aldrich, Cat # L4516) was dissolved in sterile phosphate buffered saline (PBS).

Isolation of Primary Hepatocytes and KCs

Donor-matched hepatocytes and Kupffer cells (KCs) were co-isolated from individual adult (200-300g) male Sprague-Dawley rats (Charles River Laboratories) using differential, density gradient and counter-flow elutriation centrifugation methods (LeCluyse *et al.*, 1996; Valatas *et al.*, 2003). Briefly, *in situ* perfusions were performed following a modified two-step digestion method using a collagenase/protease enzyme blend according to the manufacturer's recommendations (Vitacyte, Indianapolis, IN). After digestion, the liver tissue was dissected, placed in a sterile 150-mm petri dish containing HBSS supplemented with 1% BSA, 15 mM HEPES and 1 g/L glucose (Thermo-Fisher/Life Technologies, Grand

Island, NY), and transferred to a sterile biosafety cabinet. After removing the outer membrane (Glisson's capsule) with sterile forceps, the digested liver tissue was gently shaken to remove the parenchymal cells from the vascular tree without direct mechanical manipulation. The crude cell slurry was poured through a mesh filter (105-µm) into 50 mL tubes and centrifuged at 70 g for 3 min, which enriched for the mature hepatocytes in the pellet and NPCs in the supernatant. Supernatants were collected for KC isolation and the hepatocyte pellets were further subjected to Percoll density gradient centrifugation (GE Healthcare, Marlborough, MA) which yielded >99% pure population of hepatocytes (LeCluyse *et al.*, 1996). Final hepatocyte yields and viabilities were determined using a Vision CBA Image Cytometry System (Nexcelom Bioscience, Lawrence, MA), and seeded as described below.

For the isolation of KCs, the liver remnant with residual parenchymal and non-parenchymal cells (NPCs) was placed in a 250-mL specimen cup containing 100 mL of supplemented HBSS with 1% BSA and 100□g/mL DNase and further dissociated by gentle stirring for 5 min. Afterwards, the cell slurry was filtered through a 297-micron mesh and centrifuged, along with the supernatants from the initial hepatocyte low-speed spin, at 500 *g* for 6 min at 4ºC (DeLeve *et al.*, 2006). Crude NPC pellets were resuspended in supplemented HBSS, filtered using a 70-micron snap-cap filter, and loaded into a sterile 10-mL syringe. KCs were then further separated from other NPCs by a combination of Optiprep (Sigma-Aldrich) density gradient and counterflow elutriation centrifugation using an Avanti J-26XP centrifuge (Beckman-Coulter, Brea, CA) and a JE-5.0 rotor equipped with a 5-mL standard chamber following a modified version of the methods described by Valatas et al (Valatas *et al.*, 2003). Adjustments were made to the elutriation protocol as necessary until

KC purity was determined to be greater than 90% based on flow cytometry results (see *Flow Cytometry*).

Plating of Primary Cell Co-cultures

Hepatocyte-Kupffer cell co-cultures (HKCC) were plated at a 2:1 ratio onto 48-well Type I collagen-coated plates. The ratio of KC and hepatocytes was initially optimized as part of the development of the co-culture system with the goal to achieve maximum cytokine production in the presence of LPS (Bonzo *et al.*, 2015). Whereas normal KC:hepatocyte ratios are on average closer to 1:4 across the liver acinar structure, the 1:2 ratio that was utilized for the co-culture model does represent a near physiological condition when considering their enrichment in the periportal region under inflammatory conditions *in vivo* (Adams *et al.*, 2010).

For initial studies exploring effects of dexamethasone, co-cultures were plated in Advanced DMEM supplemented with penicillin-streptomycin, GlutaMax and 10% fetal bovine serum (Life Technologies, Grand Island, NY). For later studies investigating effects of hydrocortisone and screening compounds, co-cultures were plated in DMEM-HG supplemented with MEM Non-Essential Amino Acids, penicillin-streptomycin, 10% fetal bovine serum (Life Technologies) and insulin (10 mg/mL; Sigma-Aldrich). Hepatocytes were plated at 375,000/well and allowed to attach for ~ 1 h at 37°C/5% CO_2 with manual gentle shaking every fifteen minutes. After hepatocyte attachment, medium with unattached cells was removed and donor-matched KCs in supplemented plating medium were added at 187,500/well. KCs were allowed to attach for approximately 1 hr in the incubator with gentle shaking every 15 min and transferred into maintenance medium prior to use.

Flow Cytometry

Cell sample preparation and flow cytometry measurements were performed using a modification of methods described previously (Hanna *et al.*, 2011). Small aliquots of NPC fractions were collected from the final cell pellets after elutriation and density gradient separation as described above. Cells were then washed with PBS containing 2.5mM EDTA and pelleted by centrifugation at 300 *g* for 5 minutes. Cells were then resuspended at $1x10^6$ per 100µl staining buffer (BD Biosciences, San Jose, CA) containing 2.5mM EDTA. To measure viability, cells were stained with a fixable LIVE/DEAD stain (ThermoFisher, Waltham, MA) according to the manufacturer's recommendations. Cells were then blocked with Fc□ receptor (BD Biosciences) for 15 min and stained with AlexaFluor 488-conjugated CD163 (AbD Serotec, Raleigh, NC) for 30 min at 4ºC. For intracellular staining of CD68, cells were fixed and permeabilized using BD IntraSure Kit (BD Biosciences). AlexaFluor 647-conjugated CD68 antibody (AbD Serotec) was added in 100µl of staining buffer and incubated for 30 min at 4ºC.

Flow cytometry and cell fluorescence measurements were performed using a BD Cantos II flow cytometer (BD Biosciences) and analyzed with FlowJo software (Tree Star, version 10.0.6). Samples were analyzed using 100,000 events based on NPC population. Parameters for FSC/SSC were set to include all cell types potentially present in liver cell isolation and elutriation fractions (i.e., endothelial cells, stellate cells, KCs, and hepatocytes). Populations were first interpreted using relative cell size and complexity in FSC/SSC, viability, and the presence or absence of cellular markers. Calculations for the percentage of each cell type were based on live cell populations as determined by viability analysis. KCs

were identified as CD68+, with CD163 determining maturation. Mature KCs were defined as CD68+/CD163+. Liver sinusoidal endothelial cells were identified by exclusion.

Immunocytochemistry

To visually confirm KC enrichment in elutriated fractions and KC localization within HKCCs, KC mono-cultures and HKCCs were stained with antibodies against CD68 and CD163. Cultures were activated with LPS (1 μg/mL) for 48 hr after 24 hr acclimation. Cells were fixed and permeabilized with ice-cold methanol. Cultures were washed 2x with DPBS and blocked using BSA Stain Buffer (BD Pharminogen) containing diluted Hoechst 33342 nuclear dye (ThermoFisher). Individual wells were probed for CD68 or CD163 using mouse anti-rat primary antibodies (AbD Serotec) incubated for 6 hr at 4°C. Cultures were washed and incubated with a goat anti-mouse AlexaFluor 488 secondary antibody (ThermoFisher) for 1 hr at room temperature. After washing, cells were visualized with the EVOS FL Cell Imaging System (ThermoFisher,).

Comparison of Maintenance Media

To extend HKCC longevity, four different maintenance medium formulations were evaluated: Advanced DMEM (A-DMEM) (Life Technologies), Modified Chee's Medium (MCM) (Life Technologies), Williams' E Medium (WEM) (Life Technologies), or Hepatocyte Maintenance Media (HMM) (Lonza, Walkersville, MD). HKCCs were plated as previously described above, and transitioned to one of four maintenance media formulations supplemented with ITS+ and penicillin-streptomycin (ThermoFisher) 30 min after KC attachment. After a 24 hr acclimation period, cultures were exposed to LPS (1 μg/mL) for 48 hr. Cell viability after 48 hr LPS exposure was assessed by measuring cellular ATP levels as described below.

Glucocorticoid Effects on LPS-mediated Responses

To identify a plating and treatment regimen that would provide HKCCs with sufficient glucocorticoids to sustain hepatocytes over a 3-4 day culture period with minimal suppression of LPS-induced cytokine production, pre-treatment of hepatocytes and/or KCs with normal and reduced levels of dexamethasone (Dex) and hydrocortisone (HC) were evaluated. Pretreatment with Dex was initially evaluated by exposing both hepatocytes and KCs during the respective attachment stages to supplemented Advanced DMEM containing 1 µM Dex. After attachment, the cells were washed, medium replaced with Dex-free MCM, and HKCCs were treated with LPS (1 µg/mL) for a 48 hr period followed by assessment of cytokine production levels and morphological integrity. Additional experiments in which only the hepatocyte fraction was initially plated in Advanced DMEM containing Dex (20 nM) were conducted. Prior to adding KCs in Dex-free medium, hepatocyte monolayers were washed with Dex-free medium. HKCCs were then treated with LPS in Dex-free MCM as described in the previous section followed by evaluation of cytokine production levels and morphological integrity.

To ensure appropriate KC-mediated events were recapitulated in HKCCs exposed to HC, effects of TVX and LVX, a toxic and non-toxic fluoroquinolone antibiotic, respectively, on cytokine release and HKCC viability were determined. Hepatocytes were allowed to attach (approximately 1 hr) in plating medium containing 1µM HC before addition of KC. HKCC were maintained in MCM as described above, and co-exposed to TVX or LVX (0-200 µM) in the presence of absence of LPS on culture day 1 for 48 hr.

In a separate set of experiments, the concentration- and time-dependent effects of hydrocortisone (HC) on LPS-mediated cytokine production in HKCCs were examined by exposing hepatocytes and KCs to plating medium containing 1 or 10 µM HC for a 2 hr or 24 hr

duration, prior to changing cells into Dex-free maintenance medium (MCM). HKCCs were then treated with LPS (1 µg/mL) and samples were collected for determination of cytokine production, Cyp3A activity, and gene expression as described below.

Measurement of Cytokine Production

Cytokine levels were measured as described previously (Bonzo *et al.*, 2015). Briefly, cell culture supernatant samples were collected at indicated time points after treatment with compounds in the presence or absence of 1 µg/mL LPS and stored at -80°C until analysis. Individual cytokine levels were measured using rat IL-6 and TNF-α ELISA kits according to the manufacturer's recommendations (Life Technologies/ThermoFisher) and quantified using a SpectroMax M5 plate reader and utilizing SoftMax Pro software (Molecular Devices, Sunnyvale, CA). Additional multiplex measurements were performed on select medium samples using the Cytokine Rat 10-Plex Panel (ThermoFisher) for the Luminex® platform. Data were collected and analyzed using the Bio-Plex System (Bio-Rad, Hercules, CA).

Measurement of Cytochrome P450 3A (Cyp3A) Activity

Cyp3A metabolic activity was measured in intact cultures as described previously (Bonzo *et al.*, 2015). Briefly, HKCCs were cultured and treated with compounds in the presence or absence of LPS for 48 hours as indicated above. Cytochrome P450 3A (Cyp3A) activity was measured directly in wells using the P450-Glo™ CYP3A4 Assay with Luciferin-IPA (Cat # V9001, Promega, Madison, WI) according to the manufacturer's instructions for cultured cells, and utilizing a Luciferin standard curve (Beetle Luciferin, Cat # E1601, Promega). Plates were analyzed using a SpectroMax M5 plate reader and utilizing SoftMax Pro software. Values are reported as units of Luciferin (nM).

Gene Expression Profiling

At the end of the 48 hr treatment period, RNA was extracted from HKCCs using the RNeasy Miniprep Kit (Qiagen, Valencia, CA) according to the manufacturer's protocol. RNA samples were reverse transcribed with the High Capacity RNA-to-cDNA Kit following the manufacturer's instructions (Applied Biosystems/Life Technologies, Grand Island, NY). Quantitative PCR reactions (technical duplicates) were performed with 10 ng of cDNA per well using TaqMan® Universal PCR Master Mix (Applied Biosystems) and manufacturer recommended "best coverage" TaqMan® Gene Expression Assays for *Crp, Nos2, Tat,* and *Alb* (Applied Biosystems). Reactions were carried out using an ABI 7900HT Fast Real-Time PCR System with sample analysis performed using Sequence Detection Systems software (version 2.4; Life Technologies). Relative quantities (RQ) were calculated for each gene of interest by normalizing to *Hprt1* and are presented as a percent of the respective HC vehicle control group for each set of treatments.

ATP Content

For measurement of ATP levels as a representation of overall cell viability, the CellTiter-Glo® Luminescent Cell Viability Assay was performed on cell cultures maintained with different medium conditions according to manufacturer's instructions and utilizing an ATP standard curve (Promega). Plates were analyzed using a SpectroMax M5 plate reader and utilizing SoftMax Pro software. Values are reported as µM ATP.

Screening with Test Compounds

After a 24 hr post-plating acclimation period in MCM with 1 µM HC, HKCC or corresponding mono-cultures of hepatocytes were treated with several compounds associated with liver injury over a range of concentrations in the presence or absence of LPS (1 µg/mL) for

an additional 48 hr. Effects on cytokine production (IL-6, TNF-α and Cyp3A activity were determined as described in previous sections. Compounds tested were TVX, APAP, triclosan (TCS), acetochlor, propiconazole, and allyl alcohol.

Data Analysis

Each treatment condition was performed in a minimum of two replicate culture wells. The average or mean ± SD was calculated from the data for each treatment group unless otherwise specified. Statistical tests and significance levels utilized are described in individual figure legends where applicable.

Results

Establishment of HKCC Model with Donor-matched Hepatocytes and KCs

The main goal of this project was to extend and expand upon our previous efforts to develop a robust co-culture model of primary rat hepatocytes and liver-derived macrophages (KCs) that would ultimately lead to a corresponding human cell-based system for drug and chemical screening purposes (Bonzo *et al.*, 2015). In this work, we developed novel methods to produce donor-matched primary hepatocyte and KC fractions from the same liver tissue that, under optimized culture conditions, allow an extended compound exposure period compared to our previous culture system (DeLeve *et al.*, 2006; LeCluyse *et al.*, 1996; Valatas *et al.*, 2003). The inherent sequence of events during the isolation process allowed for the rapid preparation of hepatocyte fractions first, which were pre-plated at the appropriate density and allowed to attach while the NPC fractions were processed using modified density gradient and elutriation centrifugation methods.

Confirmation of the identity and purity of the KC fractions was performed using a combination of flow cytometry and immuno-fluorescence microscopy. The isolated cells were stained for CD68 and CD163, which indicate monocyte lineage and mature macrophage phenotype, respectively, and purity was assessed using flow cytometry (Fig. 1). Flow analysis confirmed the enrichment of KCs (>90%) with very small amounts of contaminating cell types (Fig. 1D). The ratio of KCs and hepatocytes was previously optimized as part of the development of a rodent-based co-culture system with the goal to achieve maximum cytokine production after treatment with LPS (Bonzo *et al.*, 2015). Phase-contrast and fluorescent images of HKCCs illustrated the localization of KCs relative to hepatocytes in these co-cultures (Supplementary Fig.1) (Bonzo *et al.*, 2015). KCs were well-distributed around and amongst the hepatocyte chords that formed as a result of the seeding conditions described in the Materials and Methods section. LPS treatment did not appear to have an impact on the localization or distribution of the KCs among the hepatocytes (Supplementary Fig. 1B,D).

Effect of Medium Formulation on HKCC Integrity and Viability

As part of our model development strategy, we further explored the effects of four commercially available cell maintenance media (Advanced DMEM [A-DMEM], Modified Chee's Medium [MCM], Williams' E Medium [WEM], or Williams' E-based Hepatocyte Maintenance Media [HMM]) on HKCC viability and morphological integrity over a 72 hr period in the presence and absence of LPS. In keeping with previous study conditions, no glucocorticoids were utilized during these media comparison experiments (Bonzo *et al.*, 2015). The results showed that MCM maintained the greatest overall ATP levels in HKCCs on culture day 3, representing contributions from both hepatocytes and KCs, followed by A-

DMEM, regardless of LPS stimulation (Fig. 2A,B). Corresponding photomicrographs depicting the unstimulated HKCCs at 72 hours confirmed that the overall health and integrity of the co-cultures was best supported using MCM (Supplementary Fig. 2). As a result of these experiments, all subsequent experiments were performed using glucocorticoid-free MCM as the basal maintenance medium formulation.

Effects of Glucocorticoids on LPS-induced Responses

In order to develop a more physiologically relevant medium formulation that included glucocorticoids to support native hepatocyte metabolic function, the impact of Dex or HC exposure on cell morphology and LPS-induced inflammatory cytokine responses in HKCCs was explored. Initial experiments were performed using Dex because of its prevalent use and acceptance as a potent synthetic glucocorticoid for hepatocyte cell culture experimentation in the pharmaceutical and chemical industries. The impact of Dex on HKCC monolayer integrity and cytokine response was investigated after brief exposure (2 hr) to medium containing 1 µM Dex during the post-isolation hepatocyte and KC attachment phase. As has previously been shown, the presence of 1 µM Dex enhanced the overall appearance of the monolayers and the cuboidal architecture of the hepatocytes (data not shown) (LeCluyse *et al.*, 1999; LeCluyse *et al.*, 1996). However, the LPS-induced production of TNF-α was reduced by ~80% from no LPS levels and IL-6 was completely eradicated in Dex-treated HKCCs (Fig. 3A, C).

We further explored the tenacity of the Dex-mediated effects on LPS-induced cytokine response by exposing only the hepatocytes during the attachment step to an even smaller amount of Dex (20 nM). Upon hepatocyte attachment, the Dex-containing medium was removed and cultures were washed with fresh Dex-free medium prior to addition of KCs

to the hepatocyte monolayers. Photomicrographs of HKCCs with and without 20 nM Dex in the plating medium during hepatocyte and KC attachment showed minor effects on cell morphology after day 1 (Supplementary Fig. 3A,C). However, there were marked differences in the overall monolayer integrity and cuboidal structure of the hepatocytes by day 3 in the absence of Dex (Supplementary Fig. 3B). LPS-induced TNF-α levels were reduced ~33% of those without Dex while IL-6 production was reduced ~70% (Fig. 3B,D). The results from an expanded list of cytokines as represented in Table 1 confirmed that the major pro-inflammatory cytokines, e.g. IL-6, IL-1α, IL-12, GM-CSF, and IFN-γ, were drastically reduced, whereas the anti-inflammatory cytokines, e.g. IL-10 and IL-4, were minimally affected. The combined results from these experiments indicated that Dex would not be a suitable glucocorticoid supplement for subsequent use in experiments to investigate compound-induced effects on adaptive immune responses, even if only employed at low levels during the cell attachment stage.

Hydrocortisone as a Substitute Glucocorticoid in HKCCs for Immune-based Toxicity Testing

Given the tenacity of Dex pretreatment on cytokine response to LPS exposure in HKCCs, we explored whether brief exposure to low concentrations of hydrocortisone (HC), a glucocorticoid with lower *in vitro* stability and potency, would serve as a suitable substitute. For these experiments, hepatocytes and KCs were seeded in attachment medium containing 1 μM HC, which was subsequently replaced with HC-free maintenance medium. Cultures were then treated with trovafloxacin (TVX) over a range of concentrations (0-200 μM) known to cause differential effects on cytokine profiles and cytotoxicity in the presence of LPS after a 48 hr exposure period (Shaw *et al.*, 2007; Waring *et al.*, 2006). As a negative control, the experiments were run in parallel using HKCCs treated with the non-toxic analog

levofloxacin (LVX) with or without LPS. As anticipated, the results showed statistically significant increases in both TNF-α and IL-6 production levels in LPS-activated HKCCs compared to those that were not (Fig. 4A,B). TVX caused decreased ATP levels with LPS co-treatment (Fig. 4C), while no significant decreases in ATP levels were observed in LVX-treated HKCCs under any condition (Fig. 4D). TVX produced concentration-dependent increases in TNF-α production (Fig. 4A) and corresponding decreases in IL-6 production (Fig. 4B) at 22 μM prior to overt toxicity at the highest concentration tested (200 μM). TVX and LPS co-exposure significantly impacted both TNF-α and IL-6 production (interaction term $p<0.0001$). LPS and LVX co-exposure caused significant increases in TNF-α that were independent of LVX concentration (Fig. 4A). In contrast, LPS and LVX interact (interaction term $p<0.05$) to increase IL-6 at 66 μM with respect to LVX vehicle control. These data recapitulate previous data collected from rat co-culture systems without HC (Bonzo *et al.*, 2015).

As a result of these initial outcomes, we further expanded on these findings by exploring the effects of low levels of HC on Cyp3A metabolic activity and cytokine levels in LPS-activated HKCCs. Inflammatory cytokines, such as IL-6, are known to reduce the drug metabolizing capacity of the liver in both animal models and isolated primary hepatocytes (Abdel-Razzak *et al.*, 1993; Ashino *et al.*, 2004; Poüs *et al.*, 1990). Therefore, cells were exposed to either 1 or 10 μM HC during attachment (~2 hr) or continuously for the first 24 hr in culture, followed by treatment for an additional 48 hr with LPS and TVX (50 μM), which causes well-defined alterations in IL-6 and Cyp3A activity levels without overt hepatocellular injury in the previous experiments. Under all HC treatment conditions tested, the expected suppression of Cyp3A activity was observed in the absence of TVX as a result

of the corresponding increases in IL-6 and TNF-α production in LPS-activated HKCCs (Fig. 5). Moreover, the corresponding reversal of this suppressive effect was observed in activated co-cultures treated with 50 μM TVX regardless of the HC concentration or exposure period. These outcomes were further confirmed by the concomitant LPS-induced changes in the pro-inflammatory cytokine profiles of IL-6 and TNF-α in the presence and absence of TVX (Fig. 5BC,E,F).

The corresponding morphological effects of short-term (2 hr) versus long-term (24 hr) exposure to HC prior to LPS stimulation were also examined on HKCCs using phase-contrast microscopy. The results indicated that treatment with 1 or 10 μM HC sustained or improved the over morphological integrity and longevity of the cultures compared to those maintained in HC-free medium over the course of the study period (Supplementary Fig. 4).

HC Effects on LPS- and TVX-induced Gene Expression in HKCCs

To further elucidate the impact of brief versus prolonged exposure of HKCCs to 1 or 10 μM HC on liver-specific gene expression, we investigated the changes in the mRNA levels of two glucocorticoid receptor-dependent genes (*Alb, Tat*) and two oxidative-stress and acute phase-response (OSAR) genes (*Crp, Nos2*). The results, represented as a percentage of respective HC-free controls, indicate that brief exposure to 1 μM HC did not cause significant changes in the expression levels of the four genes under any treatment condition (Fig. 6A-D). However, 24 hr exposure to 1 μM HC caused a decrease in the acute-phase response gene *Crp* in the absence of LPS, whereas it caused an overall decrease in the expression of *Nos2* under all treatment conditions (Fig 6A,B). Addition of LPS reversed *Crp* suppression brought about by 24 hr of 1 μM HC exposure. HKCCs exhibited a global increase for all four genes when exposed to 10 μM HC at plating, regardless of LPS or TVX

treatments (Fig. 6E-H). As seen with 24hr 1 µM HC, LPS-induced *Crp* expression increased with 24hr of 10 µM HC (Fig. 6E). Another similarity to 24 hr of 1 µM HC results is the overall decrease in expression of *Nos2* under all treatment conditions when combined with 24 hr of 10 µM HC (Fig. 6F). While no differences in *Tat* expression were observed between the different 10 µM HC exposure times tested, a trend in the up-regulation of *Alb* was observed in HKCCs exposed to 10 µM HC for 24 hr (Fig. 6G, H).

Immune-mediated Toxicity Testing Using the Modified HKCC System

Overall, the combined results from the previous experiments demonstrated that HKCCs exposed to HC in the first 24 hr of culture exhibited better viability, morphology and hepatic gene expression profiles while successfully recapitulating the *in vitro* changes in metabolic function, cytokine profiles and hepatotoxic effects known to occur under glucocorticoid-free conditions (Bonzo *et al.*, 2015). As a result of these findings, MCM medium supplemented with 1 µM HC for a 24 hr period prior to treatment with LPS was selected as our system of choice for screening additional compounds for immune-mediated changes in cytokine profiles and hepatocellular functions. For these experiments, a subset of compounds with known associations with liver injury and inflammation was selected from a list of hepatotoxic compounds published previously (Rodrigues *et al.*, 2013). After a 24 hr post-plating acclimation period, mono-cultures of hepatocytes and matching HKCCs were treated with compounds over a range of concentrations in the presence or absence of LPS to assess effects on cytokine production and metabolic (Cyp3A) activity. These experiments were designed to show the impact of KC activation in the presence of LPS on the concentration-dependent effects of 6 hepatotoxic compounds (Fig. 8). Matching mono-cultures of hepatocytes alone (Fig. 7) were treated in an identical fashion to discriminate

between intrinsic compound-dependent hepatocellular injury in the absence of a KC-mediated inflammatory response.

The results are represented in Figures 7 (mono-cultures) and 8 (co-cultures) as a percent change in each endpoint at each concentration compared to the initial vehicle control value from the corresponding groups treated with or without LPS. Corresponding actual values for each endpoint in mono-cultures and co-cultures treated with each compound are included as supplementary tables (Suppl. Tables 1 and 2). In mono-cultures of hepatocytes, TVX caused a 2-fold increase in Cyp3A activity at the highest concentration tested but no net change in cytokine production regardless of LPS treatment (Fig. 7A,B). This same overall pattern was observed in HKCCs in the absence of LPS (Fig. 8A). However, in the presence of LPS (i.e. KC activation), TVX caused a concentration-dependent decrease in IL-6 levels that was concomitant with a pronounced ~ 5-fold increase in Cyp3A activity and enhanced hepatotoxicity (at the highest concentration) compared to the other treatment groups (Fig. 8B). Little or no concentration-dependent effects were observed on TNF-α levels. Upon closer inspection of the absolute values of the endpoint data for the HKCCs with and without LPS, it was apparent that the activation of KCs in the vehicle control HKCCs treated with LPS caused a 50% reduction of Cyp3A activity concomitant with a marked increase in both IL-6 and TNF-α levels (Suppl.Table 2A). The data also showed that the TVX-mediated increase in the Cyp3A activity correlated with a concentration-dependent decrease in IL-6 production without effect on the corresponding production of TNF-α.

APAP also caused a concentration-dependent increase (~3-fold) in Cyp3A activity in mono-cultures of hepatocytes relative to the vehicle controls without a major change in the corresponding cytokine levels regardless of LPS treatment (Fig. 7C,D). This pattern of

effects also occurred on Cyp3A and cytokine profiles in APAP-treated HKCCs in the absence of LPS (Fig. 8C). In APAP-treated HKCCs in the presence of LPS, there was a concomitant concentration-dependent reduction in IL-6 levels and >5-fold change in Cyp3A activity at the highest concentration without a corresponding effect on TNF-α levels (Fig. 8D). The shift in Cyp3A activity was again associated with the reversal of IL6-mediated suppression of Cyp3A similar to what was observed with TVX (Suppl Table 2A).

TCS caused no significant changes in Cyp3A activity or cytokine levels in mono-cultures of hepatocytes regardless of LPS treatment prior to observing overt toxicity, which occurred at the highest concentration tested (100 µM) (Fig. 7E,F). In HKCCs treated with LPS, TCS also did not cause a significant change in Cyp3A activity or cytokine levels at subtoxic concentrations. A slight reduction in IL-6 levels was observed in the presence of LPS, but it was less pronounced compared to TVX and did not result in reversing the IL-6 suppression of Cyp3A activity levels (Suppl. Table 2A). Acetochlor also did not cause marked changes in Cyp3A activity or cytokine levels in mono-cultures of hepatocytes relative to vehicle controls prior to overt toxicity, which also occurred at the highest concentration tested (100 µM) (Fig. 7G,H). In HKCCs, acetochlor caused a slight increase in TNF-α which resulted in a slight decrease in Cyp3A activity, but no net effect on IL-6 levels until the highest concentration (Fig. 8G). By contrast, it caused a reduction in IL-6 levels in HKCCS treated with LPS, without concomitant effects on TNF-α or Cyp3A (Fig. 8H), which was not observed in corresponding mono-cultures of hepatocytes (Suppl. Tables 1,2). Notably, the overt cytotoxicity observed in acetochlor-treated mono-cultures at the highest concentration was attenuated in HKCCs (data not shown).

Propiconazole treatment of mono-cultures caused a large ~10-fold increase in Cyp3A activity at the lowest concentration tested; followed by a complete inhibition of Cyp3A activity at the higher concentrations (Fig. 7I,J). By contrast, it had minimal effects on cytokine levels that were related to the LPS treatment (Suppl. Table 1A). Propiconazole-treated HKCCs in the absence of LPS exhibited a reduced 4-fold increase in Cyp3A activity at the lowest concentration followed by complete inhibition of metabolic activity at the higher concentrations (Fig. 8I; Suppl. Table 2A). However, the induction of Cyp3A activity at the lower concentration was nearly completely attenuated in LPS-activated HKCCs (Fig. 8J). Little or no effects were observed on the cytokine levels in HKCCs regardless of the LPS treatment with the exception of LPS-treated co-cultures at the highest propiconazole concentration tested, where reduced IL-6, but not TNF-α, and enhanced cytotoxicity were observed (Suppl. Table 2A).

Allyl alcohol (AA) caused little or no changes IL-6 or TNF-α levels in mono-cultures of hepatocytes in the absence of LPS (Fig. 7K). However, there was a slight concentration-dependent increase in IL-6 in LPS-treated mono-cultures (Fig. 7L). Regardless of the LPS treatment, a marked reduction in Cyp3A activity was observed in mono-cultures at concentrations ≥100 µM, which coincided with the onset of overt cytotoxicity (Fig. 7K,L; Suppl. Table 1B). Treatment of HKCCs with AA caused more pronounced changes in cytokine levels in the presence of LPS at concentrations ≥100 µM (Fig. 8K,L). Notably, there were more-pronounced concentration-dependent decreases in Cyp3A activity at the lower concentrations of AA in HKCCs compared to mono-cultures, but less-pronounced decreases in Cyp3A activity at higher AA concentrations (Fig. 8K,L). Upon closer

inspection of the separate endpoint values, AA caused a concentration-dependent decrease in Cyp3A activity that was independent of LPS treatment (Suppl. Table 2B).

Discussion

Drug- and chemical-induced hepatotoxicity continues to be a major concern for during development and compound prioritization in the pharmaceutical and agrochemical industries, despite the scientific advancements in our understanding of the clearance, disposition and exposure for most compounds. Many hepatotoxic responses are caused or exacerbated by an immune system component, which cannot be mimicked in simple mono-cultures of hepatocytes (Evers *et al.*, 2013; Kaplowitz, 2005). More advanced, multicellular models incorporating both primary adult hepatocytes and resident immune cells, i.e. KCs, recapitulate the interaction between parenchymal and immune cells under controlled conditions (LeCluyse *et al.*, 2012). LPS- and treatment-mediated KC activation also has been shown to contribute to a number of adverse effects produced by hepatotoxic compounds (Jaeschke, 2007; Jaeschke *et al.*, 2002; LeCluyse *et al.*, 2012). Hypotheses for the key molecular events and cellular pathways that may be involved in the mechanisms of action and progression of the hepatotoxic effects *in vivo* have been elegantly described and illustrated previously (Roberts *et al.*, 2007; Shaw *et al.*, 2010). Accordingly, the direct as well as indirect effects of compounds on important cell-cell interactions, shifts in cytokine levels and changes in metabolic clearance can only be examined more systematically *in vitro* using more sophisticated co-culture systems that incorporate the key cell types that possess biochemical pathways.

In a previous study, we described an *in vitro* co-culture model using rat primary hepatocytes and cryopreserved KCs (Bonzo *et al.*, 2015). We established conditions that

facilitated short-term culture of both cell types while maintaining responsiveness to LPS activation and TVX-dependent hepatocellular injury. TVX is one of the most highly studied and best described examples of immune-mediated enhanced hepatoxicity (Beggs *et al.*, 2014; Shaw *et al.*, 2009). Previous work has shown that TNF-α is a key mediator of TVX effects on caspase-dependent hepatocellular injury by direct effects on resident macrophages (e.g. KCs) and increasing its biosynthesis and slowing its elimination (Poulsen *et al.*, 2014; Shaw *et al.*, 2010). LVX, a structural analog of TVX, does not exhibit the direct effects on KCs nor the corresponding hepatotoxic properties *in vivo* or *in vitro*.

In our previous work, we employed KCs from a commercial source (Life Technologies/ThermoFisher) and avoided the use of glucocorticoids due to their known anti-inflammatory effects. As an extension of our previous work, our goal was to establish methods of isolating donor-matched hepatocytes and KCs from the same tissue specimen in order to establish a model for studying the role of innate and adaptive immunity in idiosyncratic drug-induced liver injury (IDILI). The ability to isolate and culture donor-matched cell types also would allow studies to be performed using the matched cell types from knock-out animals and specific strains from murine genetic diversity panels (Harrill *et al.*, 2009a; Harrill *et al.*, 2009b). Moreover, we are exploring the genetic variability that accounts for the idiosyncratic drug-induced liver injury and its severity in some patient populations (Corsini *et al.*, 2012). In order to conduct these studies it is important to eliminate any artifactual immune response that could be due to HLA/MHC differences or mismatches across donors. This becomes even more important when using inbred strains of rodents or precious human tissue samples from patients that have very rare or unique genetic backgrounds. In addition to having donor-matched liver cells, we also intended to identify a

more suitable medium formulation incorporating low levels of glucocorticoids, if possible, in order to prolong the useful life-span of HKCCs and to better understand drug-induced hepatotoxic events under more physiologic conditions.

In order to isolate liver cells from the same tissue, we combined methods from the literature that had been originally designed to isolate individual cell types and modified them until we were able to obtain suitable quantities of hepatocytes and KCs with acceptable purity and viability (DeLeve *et al.*, 2006; LeCluyse *et al.*, 1996; Valatas *et al.*, 2003). As demonstrated in Figure 1, we were able to obtain relatively pure populations of KCs that exhibited >90% enrichment of macrophage-specific markers, CD68 and CD163. Further examination by phase-contrast and immuno-fluorescence microscopy confirmed the presence of KCs that stained positive for these same markers. We also established a protocol for plating the hepatocytes and KCs sequentially, which followed the natural progression of the isolation stages, such that the hepatocytes were isolated first and allowed to attach for 45-60 min while the KCs were purified from the NPC-enriched supernatant fractions. Freshly-isolated KCs were then added to the attached hepatocyte monolayer, after which they became integrated in between individual hepatocytes, as illustrated in Figure 2.

Following the establishment of our isolation protocols, we explored different formulations of culture media that had been employed for the maintenance of primary hepatocytes (LeCluyse *et al.*, 1999; LeCluyse *et al.*, 1996). The results from the medium experiments indicated that modified Chee's medium (MCM) provided greater support for optimal co-culture morphology and viability over a 72 hr culture period, which was deemed suitable for investigating compound effects on immune-related responses and hepatocellular injury. Notably, MCM had been identified previously as a 'preferred' medium for

maintaining primary hepatocyte function and viability over longer culture periods, but this is the first report to show evidence of its beneficial effects on maintenance of HKCC monolayer integrity and functionality (LeCluyse *et al.*, 1999; Waxman *et al.*, 1990).

We then attempted to identify suitable conditions under which we could incorporate glucocorticoids to sustain hepatocyte gene expression and metabolic capacity, while retaining the HKCC cytokine response to LPS (LeCluyse *et al.*, 2012; Waxman *et al.*, 1990). Our initial experiments confirmed that the use of potent and stable glucocorticoids, such as Dex, completely abolish the activation of KC by LPS in both KC mono-cultures and co-cultures even after limited exposure during the initial attachment phase. However, subsequent results suggest that HKCCs, exposed to low levels of HC (1□M) for up to 24 hr after plating, could still respond normally to LPS treatment, recapitulating key events such as TNF-□ and IL-6 cytokine production and concentration-dependent TVX toxicity. Importantly, cytokine production directly resulted in the down-regulation of CYP activity, which was reversed by TVX treatment, a benchmark result from a prototype compound that is known to elicit adverse effects *in vitro* and *in vivo,* especially under inflammatory conditions (Bonzo *et al.*, 2015; Morgan, 2009; Roberts *et al.*, 2007; Shaw *et al.*, 2007). Moreover, gene expression levels of liver-specific and OSAR genes were maintained at higher levels in HKCCs with HC pretreatment compared to those without it.

After establishing the culture conditions for maintaining cell longevity and improved hepatocyte functionality while retaining LPS responsiveness, a subset of known hepatotoxicants was tested using the modified HKCC model system (Borlak *et al.*, 2013; Rodrigues *et al.*, 2013). The compounds were tested over a 48 hr exposure period at several concentrations that were relevant to their exposure *in vivo* or that had been shown to cause

hepatocellular injury *in vitro*. We then examined their immune-mediated (LPS-induced) and direct effects (without LPS) on the production of key cytokines, namely TNF-α and IL-6, as well as metabolic capacity as represented by Cyp3A activity. Cytotoxicity was monitored either visually by phase-contrast microscopy and/or biochemically by measuring changes in intracellular ATP levels.

Firstly, the data confirmed the fidelity of the modified HKCC model to recapitulate the key events exhibited by the benchmark compound TVX, including the concentration-dependent alteration in IL-6/TNF-α ratios and corresponding shift in Cyp3A suppression that has been described previously (Bonzo *et al.*, 2015). HKCCs treated with APAP also exhibited a similar trend in LPS-mediated effects on cytokine profiles and CYP activity. In addition, APAP caused a greater cellular ATP decrease in LPS-treated HKCCs relative to co-cultures not exposed to LPS, which was similar to what was observed with TVX (data not shown). Notably, APAP is another compound known to be associated with immune-mediated enhanced hepatotoxic events leading to severe liver injury and liver failure in some individuals (Borlak *et al.*, 2013). Although it is well established in the literature that APAP is metabolically activated to a reactive metabolite (NAPQI), which depletes GSH as a key initiating event leading to oxidative stress and hepatocellular injury, our results provide confirmation that there may be secondary pathways involved in its hepatotoxic mechanism, such as changes in cytokine profiles and metabolic capacity, that may be responsible for enhancement of toxicity in LPS-activated HKCCs, outside the classical APAP-induced cytotoxic effects from NAPQI formation. Notably, the 'idiosyncratic' nature of the severity of APAP toxicity in some patients has been linked to the patient's adaptive immune

responses, suggesting that it too may fall into a category of a 'TVX-like' mechanism (Borlak *et al.*, 2013; Harrill *et al.*, 2009b).

Other hepatotoxic compounds that were tested using the enhanced HKCC system exhibited unique trends in their effects on either cytokine profiles and/or CYP activity that seemed to lead to exacerbated or attenuated cytotoxicity. For the most part, the compound-induced effects observed in the HKCC model system are likely to be a reflection of their mode of action on KC activation and/or hepatocellular functions. For example, it's been shown that TCS causes LPS-independent perturbations in thyroxine disposition (Paul *et al.*, 2012). Chloroacetanilide pesticides, such as acetochlor and alachlor, exhibit metabolism-dependent hepatoxicity (Kale *et al.*, 2008; Rodrigues *et al.*, 2013). Many antifungals, such as propiconazole, are known to be potent inhibitors and inducers of liver cytochrome P450 enzymes and nongenotoxic tumor promoters, events which are exacerbated by inflammatory responses (Wolf *et al.*, 2006). Allyl alcohol has been shown to exhibit selective hepatocellular damage around the periportal region that was shown to be related to localized gradients in oxygen and inflammatory responses (Przybocki *et al.*, 1992).

Taken together these results suggest that the HKCC model could provide additional information and insights into the true potential of compounds in development to cause hepatocellular injury and toxicity. We propose that the HKCC model system could potentially be utilized to stratify toxic compounds into sub-categories of immune-mediated hepatotoxic responses as observed in this study, for example: 1) compounds that caused KC-mediated decreases in IL-6 levels with concomitant in metabolic activity leading to enhanced cytotoxicity, e.g. TVX, APAP; 2) compounds that caused hepatocellular effects and cytotoxicity that were independent of inflammatory mediators, e.g. TCS; 3) compounds

exhibiting KC-mediated attenuation of hepatocellular effects and cytotoxicity, e.g. acetochlor; allyl alcohol; and 4) compounds that cause marked changes in metabolic capacity (i.e. induction, inhibition of Cyp3A), with enhanced KC-mediated cytotoxicity in the absence of distinct cytokine effects, e.g. propiconazole. Moreover, our findings underscore the need for more biologically relevant, multicellular culture models to study these complex biological and toxicological events. Further research is warranted in order to explore the mechanisms of the LPS-enhanced and KC-mediated secondary and adaptive events leading to enhanced or diminished hepatocellular injury.

Conclusion

We have demonstrated the utility of an optimized donor-matched HKCC model for exploring possible mechanisms of immune-mediated drug responses. Our HKCC system responds to prototype effector molecules of inflammation and toxicity and corresponds closely with results observed previously *in vitro* and *in vivo* for prototype hepatotoxic compounds. Application of this model system to screening a limited set of compounds associated with liver injury indicated that APAP displayed enhanced immune-mediated effects similar to that of TVX, a known IDILI compound. Other compounds had unique direct or indirect effects on cytokine levels and metabolic capacity that appeared to reflect known *in vitro* and *in vivo* effects or modes of action (Borlak *et al.*, 2013; Liu *et al.*, 2015; Rodrigues *et al.*, 2013; Rotroff *et al.*, 2010). Overall, these findings support the use of HKCCs, with proper medium formulation, as a valuable *in vitro* tool to evaluate and stratify compounds with hepatotoxic liability that would otherwise be overlooked using hepatocytes

alone. Moreover, this novel approach can be extended to development of a human-based co-culture model to explore population diversity in innate immunity and its role in IDILI.

Abbreviations

hepatocyte and Kupffer cell co-culture, HKCC; Kupffer cell, KC; oxidative-stress and acute phase-response, OSAR; lipopolysaccharide, LPS; cytochrome P450 3A, Cyp3A; trovafloxacin, TVX; triclosan, TCS; acetaminophen, APAP; non-parenchymal cells, NPCs; Hank's Balanced Salt Solution, HBSS; bovine serum albumin, BSA; Dulbecco's modified Eagle's medium-high glucose, DMEM-HG; ethylenediaminetetraacetic acid, EDTA; Dulbecco's phosphate-buffered saline, DPBS; Advanced DMEM, A-DMEM; Modified Chee's Medium, MCM; Williams' E Medium, WEM; Hepatocyte Maintenance Medium, HMM; hydrocortisone, HC; dexamethasone, Dex; interleukin-6, IL-6; tumor necrosis factor alpha, TNF-α

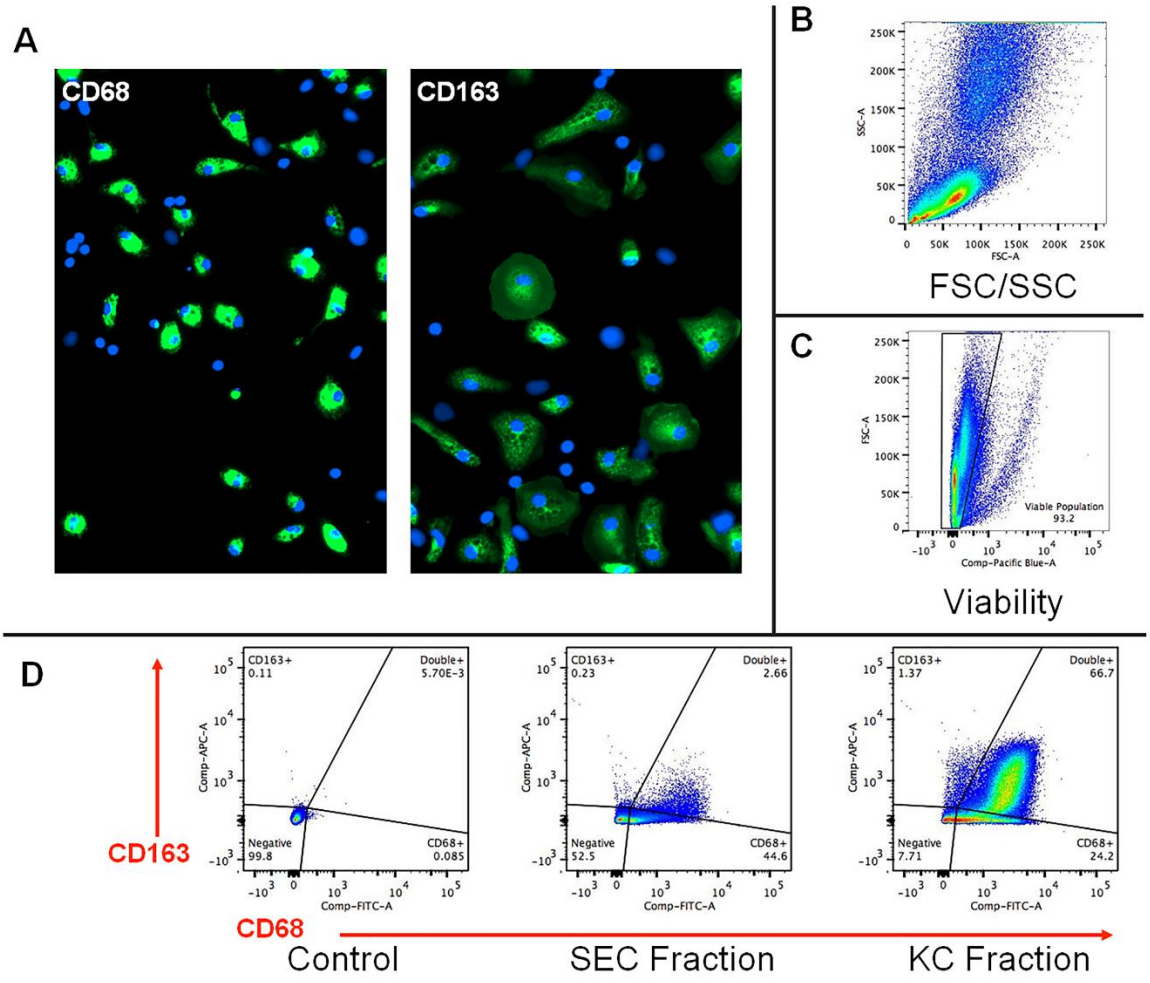

Figure 1. Flow cytometric analysis of freshly isolated rat NPC- and KC-containing fractions. A, Representative fluorescent images of cells analyzed by flow cytometry and counter-stained with antibodies against CD68 and CD163 for visual verification of cells with macrophage lineage (i.e. KCs). Original magnification, 100x. B, FSC/SSC plot representing entire population present after elutriating liver cells for KC. Counts were recorded for 100,000 events within the population of interest. All cells are shown in FSC/SSC to ensure maximum collection of KC during elutriation. C, Cell viability is represented by dye exclusion. Only viable cell populations were utilized for subsequent cell marker analysis. D, Flow analysis of cell fractions using CD68 and CD163 as markers of cell lineage and relative fraction purity with corresponding gating strategy. Representative plots for unstained control sample, SEC fraction, and KC fraction are shown. Quadrants display cells that are both CD68- and CD163-, single CD68+, single CD163+, and double CD68+/CD163+. Data are representative of three separate elutriations.

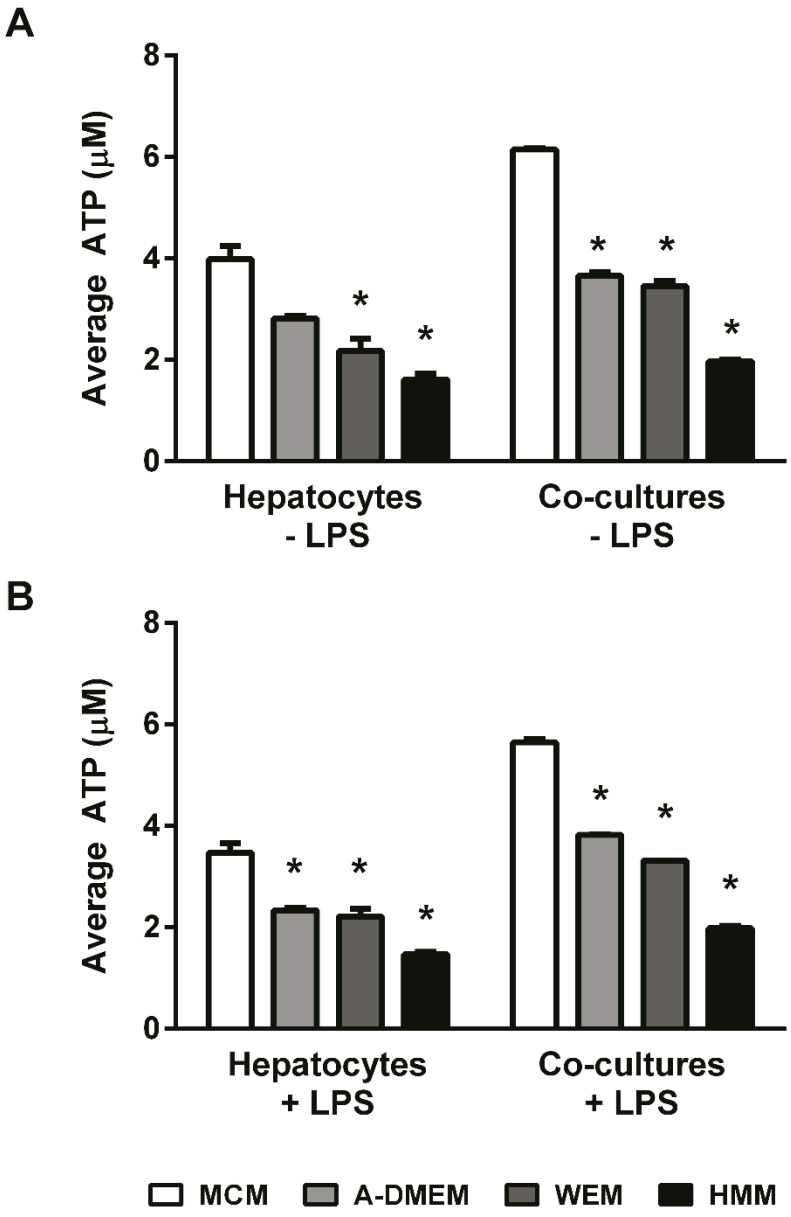

Figure 2. Effect of maintenance medium formulation on intracellular ATP levels in HKCCs. Hepatocyte mono-cultures and HKCC were cultured for 48 hr with or without LPS in four different types of maintenance media. A, cell viability across medium formulations without LPS stimulation. B, cell viability across medium formulations with LPS stimulation. An (*) denotes a significant difference between ATP values for a given medium and those for MCM, after a Bonferroni post-test (p<0.001).

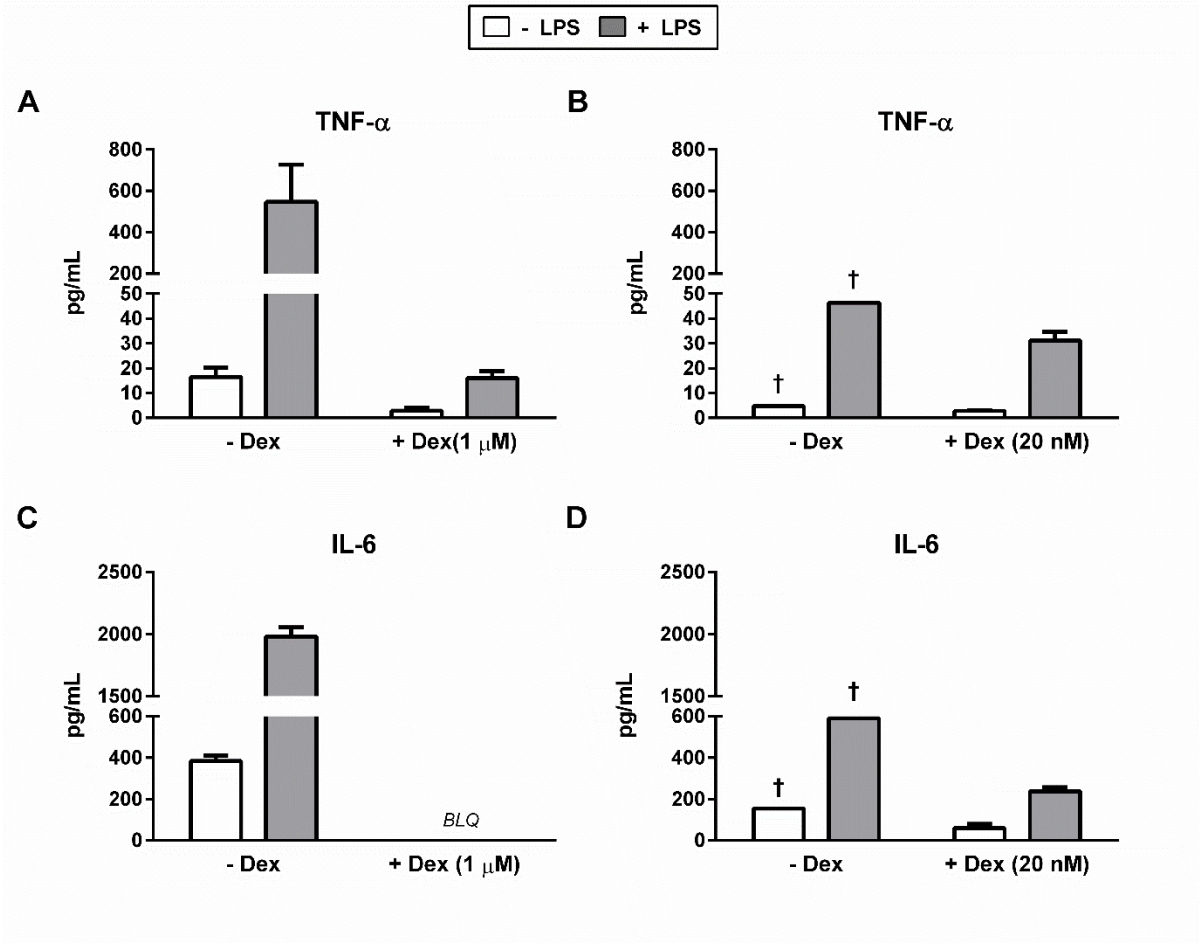

Figure 3. Effects of Dex supplementation in hepatocyte and KC plating medium on HKCC cytokine release. TNF-α and IL-6 release from HKCCs in which Heps and KCs were plated in media containing Dex (A,C, 1 μM; B, D, 20 nM) (†, values from biological singlet wells). Significance of Dex treatment on cytokine release in LPS stimulated HKCC was determined by two-tailed Student's t-test (****, $p<0.0001$); (***, $p<0.001$); (**, $p<0.01$); (BLQ, below limit of quantification).

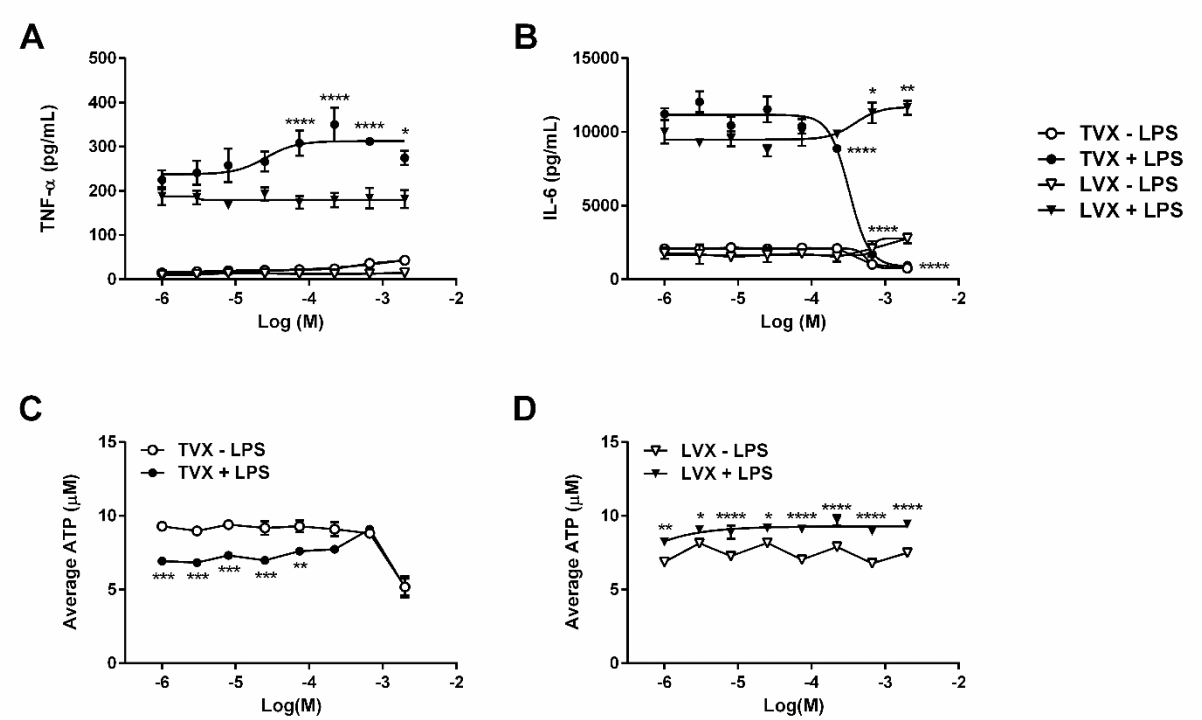

Figure 4. Validation of immune-mediated biology in HKCC with prototypical positive and negative control compounds. HKCCs were exposed to a concentration range (0-200 μm) of TVX or LVX in the presence and absence of LPS. Levels of TNF-α (A) and IL-6 (B) in collected medium samples were assayed by ELISA after 48 hr of compound exposure. Combined effects of LPS and compound were analyzed for each cytokine by two-way ANOVA with Dunnett's post-test and compared to compound vehicle control (*: $p<0.05$);(**: $p<0.01$); (***; $p<0.001$); (****: $p<0.0001$). Matching data for levels of ATP in HKCC after treatment with TVX (C) or with LVX (D) in the presence or absence of LPS found that relative to no LPS control, LPS significantly increases ATP levels for LVX and significantly decreases ATP for low TVX concentrations. ATP statistics were done by 2-way ANOVA with Bonferroni's post-test to compare no LPS to LPS (*: $p<0.05$); (**: $p<0.01$) ;(***, $p<0.001$); (****: $p<0.0001$).

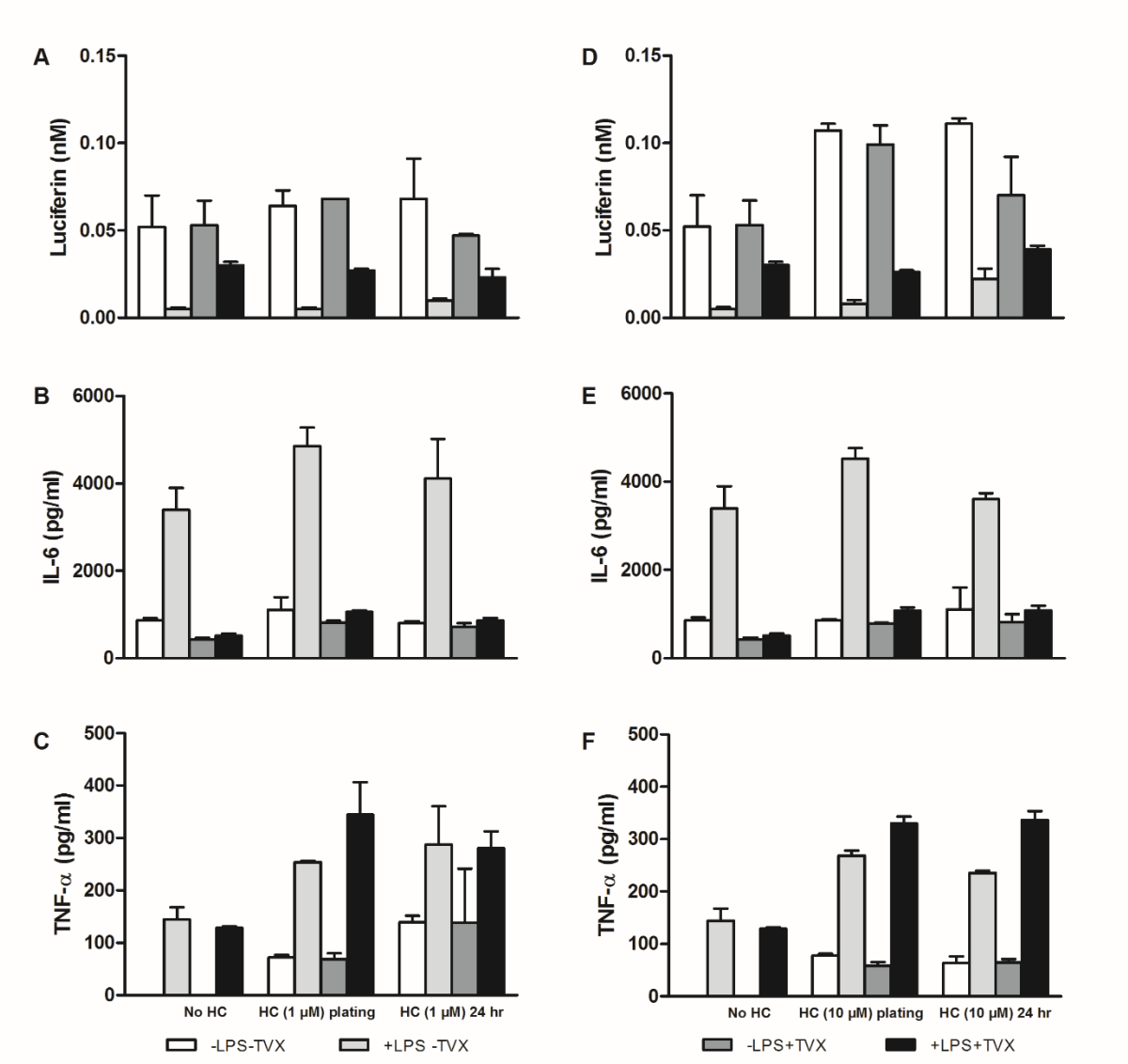

Figure 5. Effects of 1 μM and 10 μM HC on Cyp3A activity and IL-6/TNF-α levels in HKCCs. HKCCs were exposed to 1 or 10 μM HC briefly (~2 hr) at plating or for 24 hr, and then were treated with 1 μg/mL LPS, 50 μM TVX and/or respective controls for 48 hr. Cyp3A activity was assessed (A, 1 μM HC; D, 10 μM HC) and media was collected and frozen for IL-6 (B, 1 μM HC; E, 10 μM HC) and TNF-α (C, 1 μM HC; F, 10 μM HC) analyses as described in Materials and Methods.

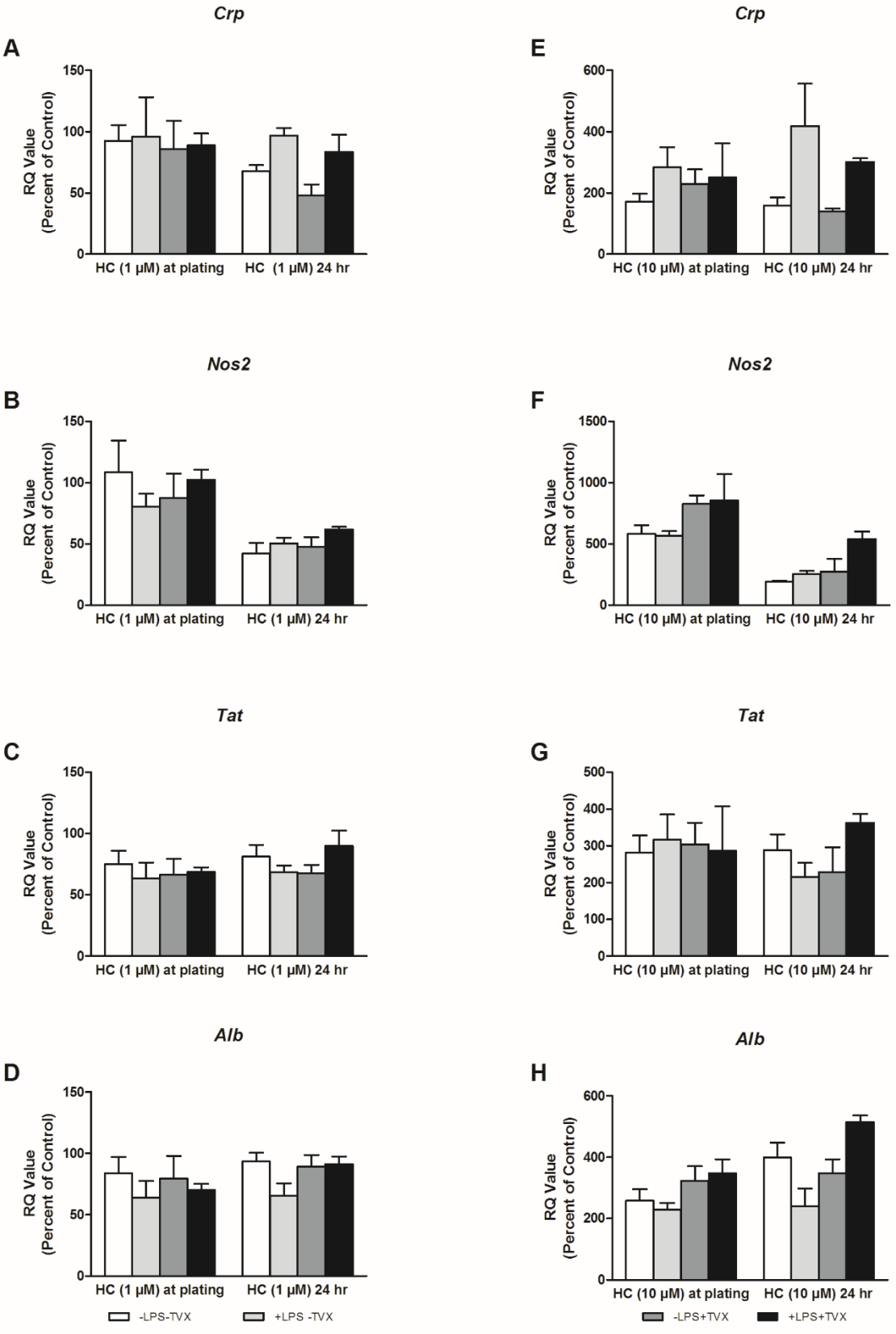
A
Crp
RQ Value
(Percent of Control)
150
100
50
0
HC (1 µM) at plating
HC (1 µM) 24 hr
B
Nos2
RQ Value
(Percent of Control)
150
100
50
0
HC (1 µM) at plating
HC (1 µM) 24 hr
C
Tat
RQ Value
(Percent of Control)
150
100
50
0
HC (1 µM) at plating
HC (1 µM) 24 hr
D
Alb
RQ Value
(Percent of Control)
150
100
50
0
HC (1 µM) at plating
HC (1 µM) 24 hr
-LPS-TVX
+LPS -TVX
E
Crp
RQ Value
(Percent of Control)
600
400
200
0
HC (10 µM) at plating
HC (10 µM) 24 hr
F
Nos2
RQ Value
(Percent of Control)
1500
1000
500
0
HC (10 µM) at plating
HC (10 µM) 24 hr
G
Tat
RQ Value
(Percent of Control)
500
400
300
200
100
0
HC (10 µM) at plating
HC (10 µM) 24 hr
H
Alb
RQ Value
(Percent of Control)
600
400
200
0
HC (10 µM) at plating
HC (10 µM) 24 hr
-LPS+TVX
+LPS+TVX

Figure 6. Gene expression in HKCC after exposure to 1 or 10 µM HC. HKCC were exposed to 1 or 10 µM HC briefly (~2 hr) at plating or for 24 hr, and then were treated with 1 µg/mL LPS and 50 µM TVX and/or respective controls for 48 hr. Panels A-D represent levels of gene expression after 1 µM HC exposure, E-H after 10 µM HC exposure. *Crp* expression is shown in panels A and E, *Nos2* in B and F, *Tat* in C and G, and *Alb* in D and H.

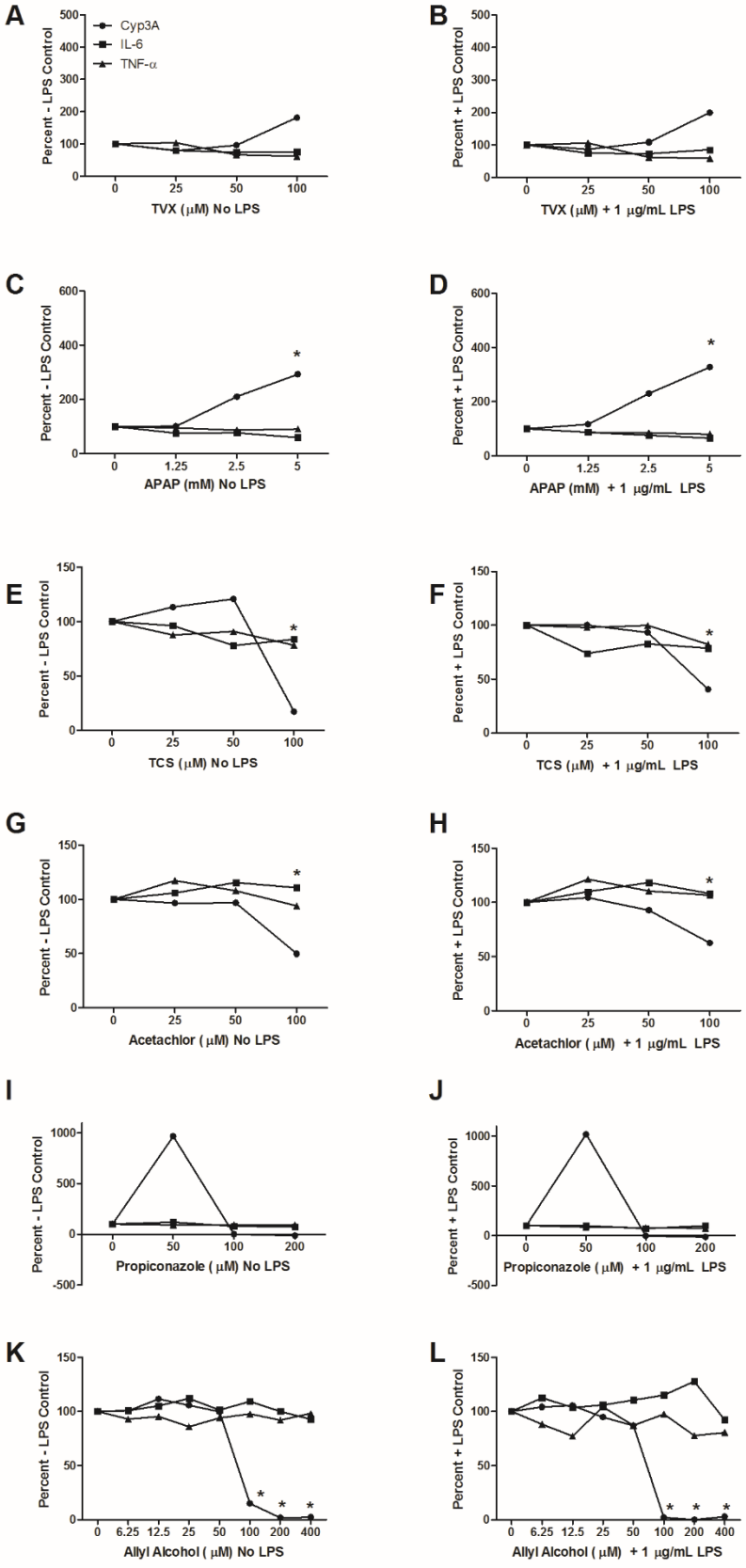
A
Cyp3A
IL-6
TNF-α
Percent - LPS Control
TVX (μM) No LPS
B
Percent + LPS Control
TVX (μM) + 1 μg/mL LPS
C
Percent - LPS Control
APAP (mM) No LPS
D
Percent + LPS Control
APAP (mM) + 1 μg/mL LPS
E
Percent - LPS Control
TCS (μM) No LPS
F
Percent + LPS Control
TCS (μM) + 1 μg/mL LPS
G
Percent - LPS Control
Acetachlor (μM) No LPS
H
Percent + LPS Control
Acetachlor (μM) + 1 μg/mL LPS
I
Percent - LPS Control
Propiconazole (μM) No LPS
J
Percent + LPS Control
Propiconazole (μM) + 1 μg/mL LPS
K
Percent - LPS Control
Allyl Alcohol (μM) No LPS
L
Percent + LPS Control
Allyl Alcohol (μM) + 1 μg/mL LPS

Figure 7. Effects of known hepatotoxic compounds on Cyp3A activity and IL-6/TNF-α levels in mono-cultures of hepatocytes with or without LPS. Data expressed as % +/- LPS controls. 24 hr post-plating, hepatocytes were treated with varying doses of TVX (A,B), APAP (C,D), TCS (E,F), acetochlor (G,H), propiconazole (I,J), or allyl alcohol (K,L) with or without 1 μg/mL LPS for 48 hr. Cyp3A activity was assessed and media was collected and frozen for IL-6 and TNF-α analyses as described in Materials and Methods. Data are representative of a single experiment and expressed as a percentage of the respective LPS-free or LPS-containing vehicle controls as shown on y-axis. * = toxicity evident in in photomicrographs or ATP studies for this compound (data not shown).

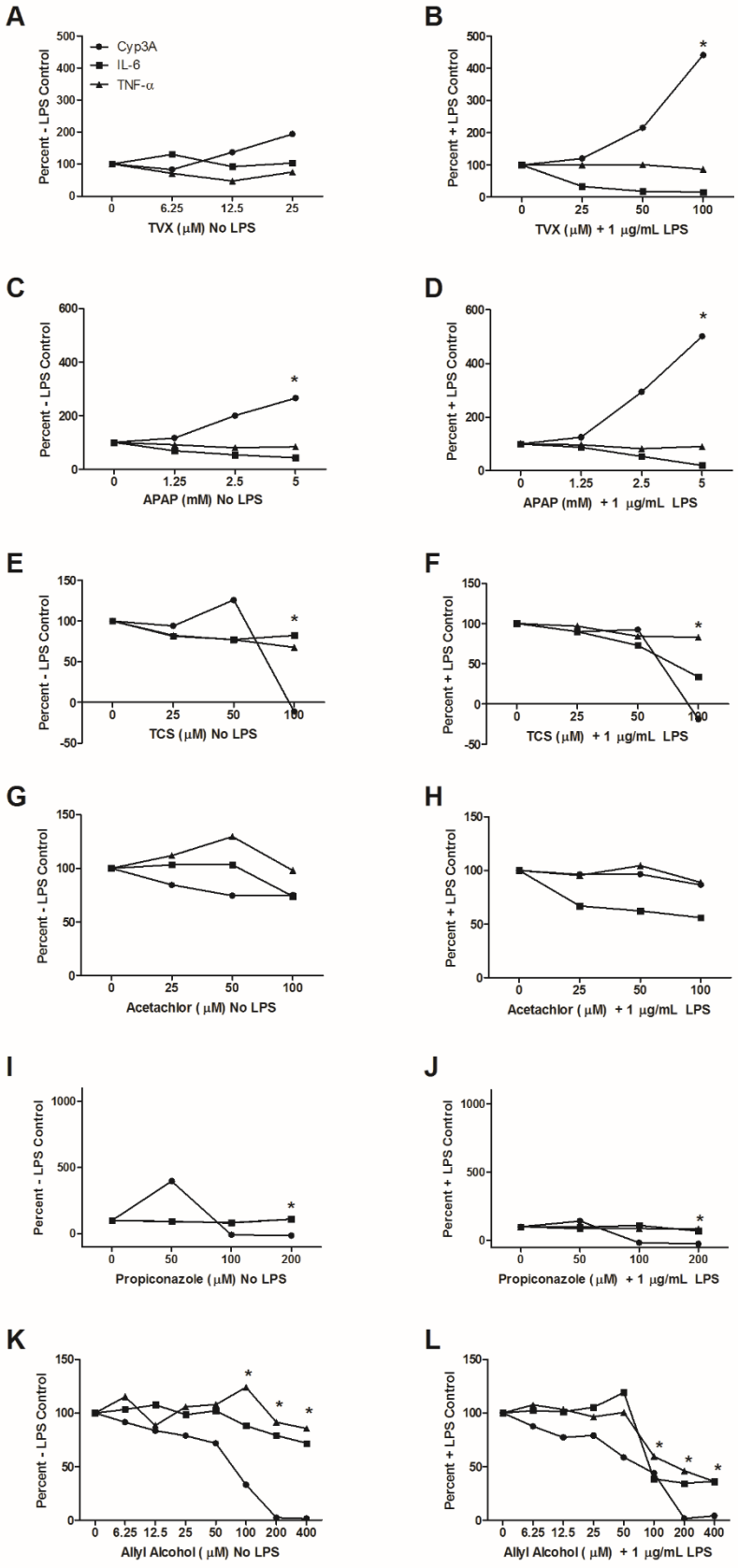
A
Cyp3A
IL-6
TNF-α
Percent - LPS Control
TVX (μM) No LPS
B
Percent + LPS Control
TVX (μM) + 1 μg/mL LPS
C
Percent - LPS Control
APAP (mM) No LPS
D
Percent + LPS Control
APAP (mM) + 1 μg/mL LPS
E
Percent - LPS Control
TCS (μM) No LPS
F
Percent + LPS Control
TCS (μM) + 1 μg/mL LPS
G
Percent - LPS Control
Acetachlor (μM) No LPS
H
Percent + LPS Control
Acetachlor (μM) + 1 μg/mL LPS
I
Percent - LPS Control
Propiconazole (μM) No LPS
J
Percent + LPS Control
Propiconazole (μM) + 1 μg/mL LPS
K
Percent - LPS Control
Allyl Alcohol (μM) No LPS
L
Percent + LPS Control
Allyl Alcohol (μM) + 1 μg/mL LPS

Figure 8. Effects of known hepatotoxic compounds on Cyp3A activity and IL-6/TNF-α levels in HKCCs with or without LPS. Data expressed as % of +/- LPS controls. HKCC were treated with varying doses of TVX (A,B), APAP (C,D), TCS (E,F), acetochlor (G,H), propiconazole (I,J), or allyl alcohol (K,L) with or without 1 μg/mL LPS for 48 hr. Cyp3A activity was assessed and media was collected and frozen for IL-6 and TNF-α analyses as described in Materials and Methods. Data are representative of a single experiment and expressed as a percentage of the respective LPS-free or LPS-containing vehicle controls as shown on y-axis. * = toxicity evident in in photomicrographs or ATP studies for this compound (data not shown).

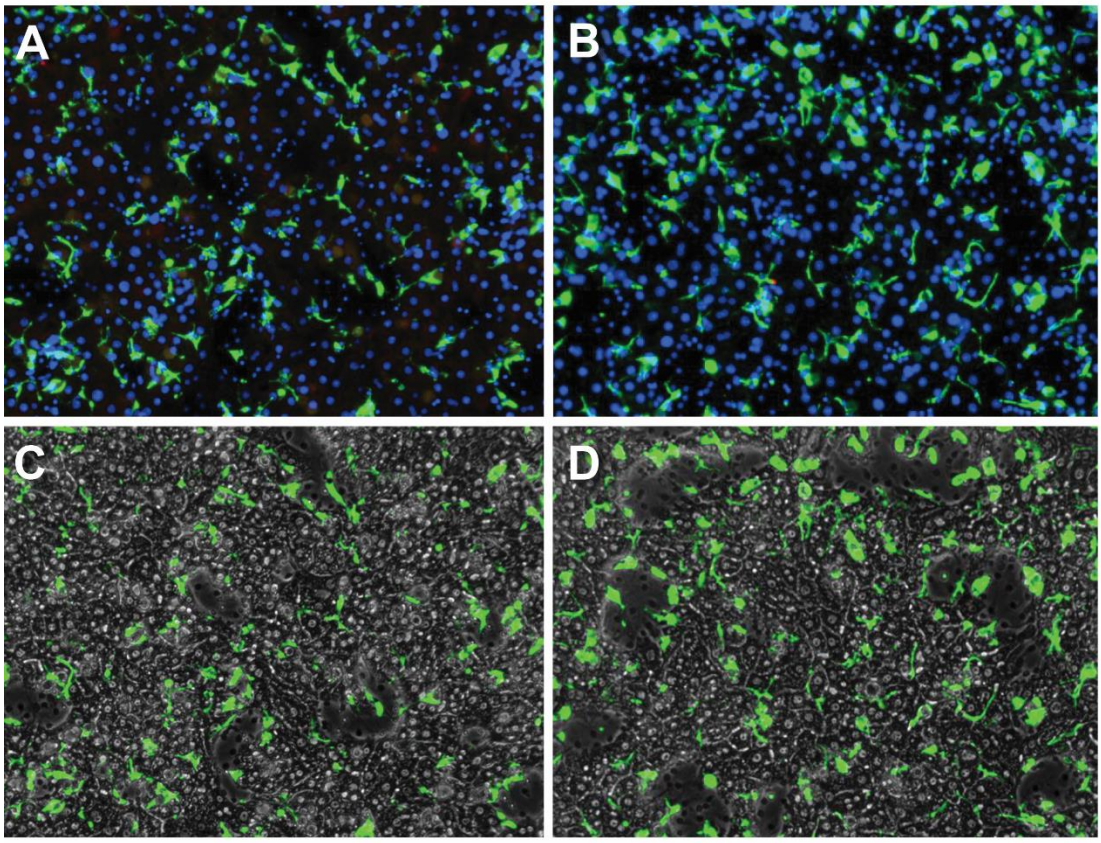

Supplementary Figure 1. Immunofluorescent imaging of HKCCs. Representative HKCCs (1:2 KC to hepatocyte) on day 3 of culture in the absence (A,C) and presence (B,D) of LPS stimulation for 48 hr. A, No LPS control: CD68 positive KC (green) and nuclei (blue). B, LPS-treated: CD68 positive KC (green) and nuclei (blue); C, No LPS: Overlay of phase contrast and GFP channel; D, LPS-treated: Overlay of phase contrast and GFP channel, demonstrating LPS-induced KC localization to hepatocyte junctions.

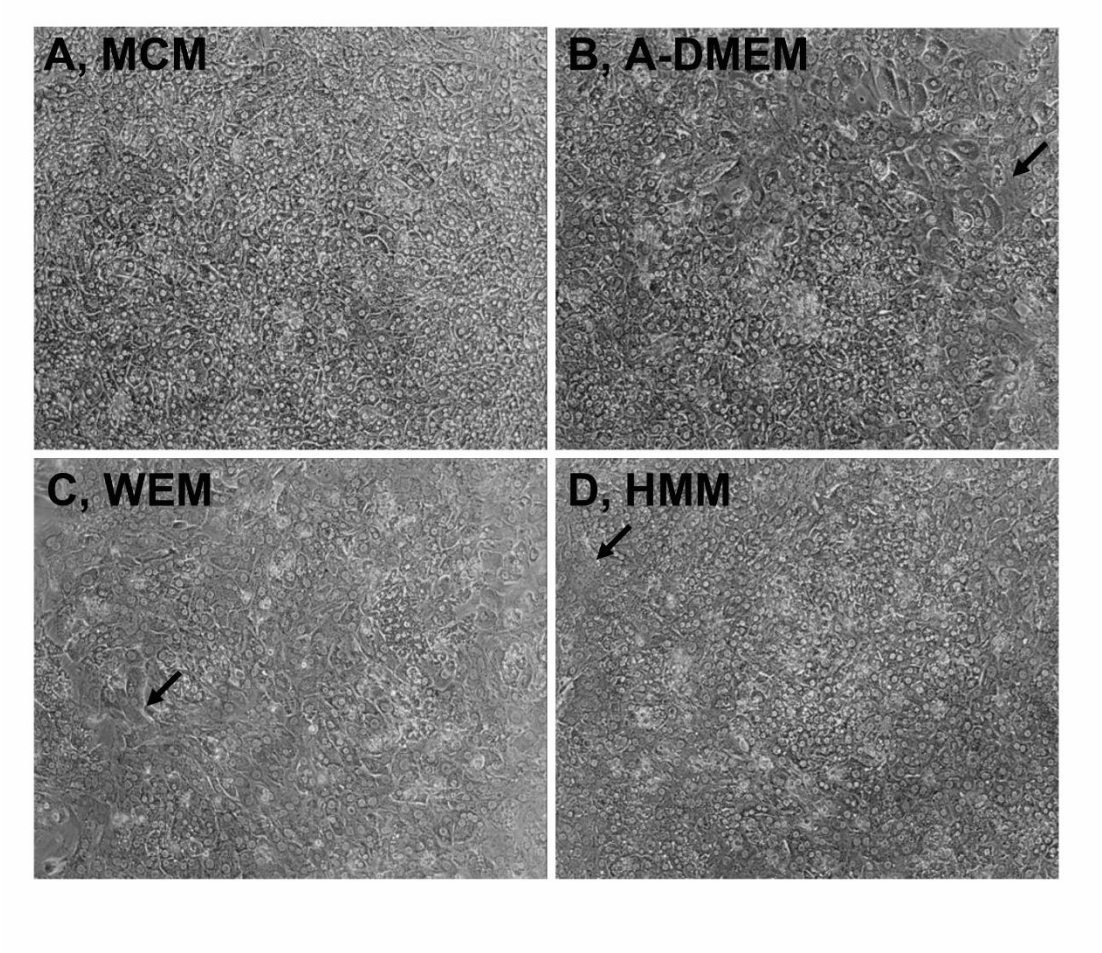

Supplementary Figure 2. Effect of maintenance medium formulation on hepatocyte morphology in HKCCs. Hepatocyte mono-cultures and HKCC were cultured for 48 hr without LPS in four different types of maintenance media. Photo-micrographs depict the corresponding non-stimulated HKCCs on culture day 3 in various medium formulations: A, MCM; B, A-DMEM; C, WEM; D, HMM (original magnification, 100x). Arrows indicate areas of cell morphology distortion and lack of proper attachment.

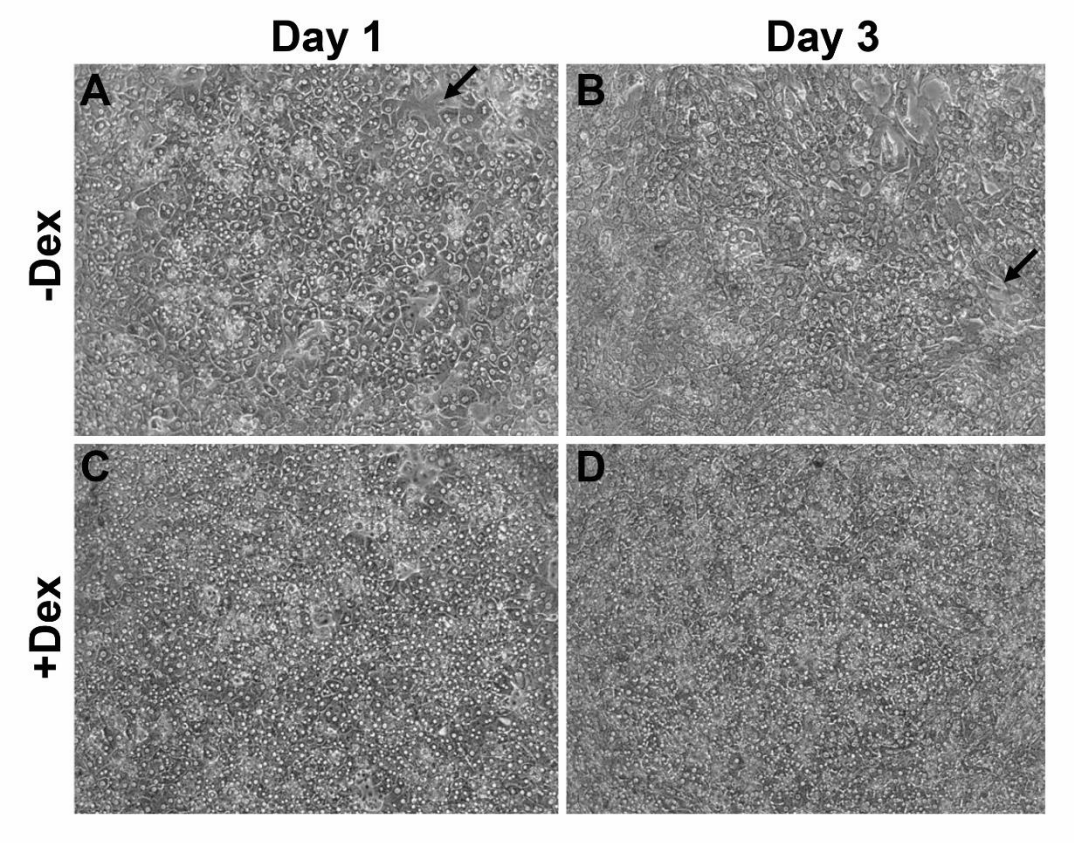

Supplementary Figure 3. Effects of Dex supplementation in hepatocyte and KC plating medium on HKCC morphology. Photo-micrographs (A-D) depict the long-term effects of Dex (20 nM) in hepatocyte plating medium only (original magnification, 100x). Arrows indicate areas of cell distortion and lack of proper attachment.

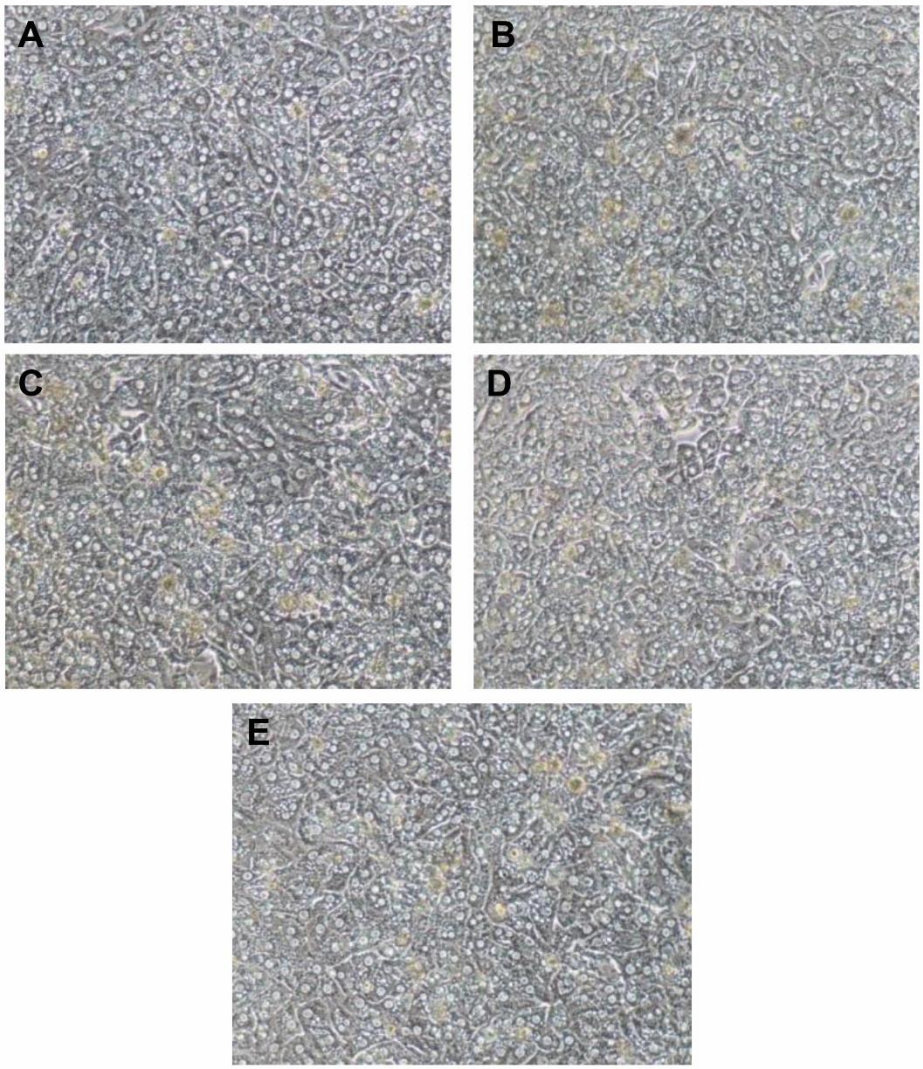

Supplementary Figure 4. Effects of HC supplementation on HKCC morphology. Co-cultures were plated in 1 µM HC for ~ 2 hr (A) or 24 hr (B), or in 10 µM HC for ~2 hr (C) or 24 hr (D), or no HC (E). HCCCs shown were not treated with LPS or other compounds. Cultures are shown 48 hr after initiation of treatment, and therefore are 72 hr post-plating. Original magnification, 200x.

Table 1. Effects of dexamethasone (20 nM) in hepatocyte plating medium on subsequent HKCC cytokine release.

No LPS Activation		Analyte	LPS Activation	
- Dex	***+ Dex***	**(pg/mL)**	***- Dex***	***+ Dex***
16.6 ± 6.5	3.0 ± 2.0[a]	TNF-α	547.65 ± 311.3	16.0 ± 5.2
384.25 ± 47.6	ND	IL-6	1981.1 ± 130.9	ND
5.7 ± 0.9[a]	6.6 ± 1.4[a]	GM-CSF	115.9 ± 12.1	ND
1.0 ± 3.8[a]	ND	INF-γ	12.2 ± 34.4	ND
ND	ND	IL-1α	148.78 ± 38.0	ND
20.3 ± 1.4[a]	6.4 ± 3.1[a]	IL-1β	135.1 ± 26.1	7.0 ± 0.7[a]
93.2 ± 2.1	41.6 ± 0.9[a]	IL-2	381.5 ± 11.6	48.4 ± 1.4[a]
0.4 ± 1.3[a]	0.4 ± 0.5[a]	IL-4	0.4 ± 0.9[a]	0.4 ± 0.6[a]
55.2 ± 1.3[a]	65.6 ± 2.7[a]	IL-10	162.83 ± 5.1	117.3 ± 2.1
23.3 ± 1.1[a]	22.0 ± 0.8[a]	IL-12	203.1 ± 8.9	6.0 ± 0.5[a]

Supplementary Table 1. Use of hepatocyte monocultures for screening effects of compounds on Cyp3A activity and IL-6/TNF-α levels, data expressed as units of luciferin (nM), IL-6 or TNF- α (both pg/ml). 24 hr post-plating, hepatocytes were treated with varying doses of 1A, TVX, APAP, TCS , Acetachlor, propiconazole, or 1B, allyl alcohol with or without 1 μg/mL LPS for 48 hr. Cyp3A activity was assessed and media was collected and frozen for IL-6 and TNF-α analysis as described in Materials and Methods.

Supplementary Table 1A.

Trovafloxacin				Acetaminophen				Triclosan				Acetochlor				Propiconazole			
Conc (μM)	LPS	CYP3A (Luciferin, nM)		Conc (mM)	LPS	CYP3A (Luciferin, nM)		Conc (μM)	LPS	CYP3A (Luciferin, nM)		Conc (μM)	LPS	CYP3A (Luciferin, nM)		Conc (μM)	LPS	CYP3A (Luciferin, nM)	
		Mean	SD			Mean	SD			Mean	SD			Mean	SD			Mean	SD
0	-	10.25	0.55	0	-	7.57	0.22	0	-	10.25	0.55	0	-	10.40	1.50	0	-	9.66	3.27
0	+	8.39	0.60	0	+	6.96	0.36	0	+	11.08	1.74	0	+	9.76	2.30	0	+	8.60	1.57
25	-	8.08	1.94	1.25	-	7.67	1.13	25	-	11.61	2.44	25	-	10.05	4.12	50	-	93.52	13.51
25	+	7.24	1.08	1.25	+	8.10	0.77	25	+	11.10	3.94	25	+	10.19	2.66	50	+	87.58	4.57
50	-	9.84	1.89	2.5	-	15.90	4.45	50	-	12.38	1.69	50	-	10.07	2.25	100	-	0.03	0.15
50	+	9.10	1.80	2.5	+	16.03	1.56	50	+	10.35	1.76	50	+	9.06	2.71	100	+	-0.14	0.00
100	-	18.65	1.42	5	-	22.18	3.13	100	-	1.77	2.03	100	-	5.18	2.30	200	-	-1.22	0.07
100	+	16.76	2.42	5	+	22.81	0.27	100	+	4.46	0.15	100	+	6.12	3.24	200	+	-1.20	0.10
Conc (μM)	LPS	IL-6 pg/ml		Conc (mM)	LPS	IL-6 pg/ml		Conc (μM)	LPS	IL-6 pg/ml		Conc (μM)	LPS	IL-6 pg/ml		Conc (μM)	LPS	IL-6 pg/ml	
		Mean	SD			Mean	SD			Mean	SD			Mean	SD			Mean	SD
0	-	573.74	11.07	0	-	923.15	61.98	0	-	770.23	46.19	0	-	595.06	35.16	0	-	854.32	51.31
0	+	632.56	89.50	0	+	782.30	64.30	0	+	866.33	89.18	0	+	557.70	36.12	0	+	942.50	5.74
25	-	457.40	132.64	1.25	-	695.20	19.35	25	-	741.52	62.75	25	-	631.27	17.90	50	-	1030.47	64.89
25	+	475.28	0.53	1.25	+	681.61	3.03	25	+	639.09	14.74	25	+	613.19	82.94	50	+	919.79	283.78
50	-	424.30	20.28	2.5	-	707.78	139.26	50	-	599.63	24.22	50	-	687.42	103.88	100	-	689.93	94.80
50	+	462.24	12.35	2.5	+	588.44	47.94	50	+	716.74	71.92	50	+	659.84	39.08	100	+	689.43	158.08
100	-	436.33	36.77	5	-	548.44	61.08	100	-	643.64	53.82	100	-	659.09	15.92	200	-	647.93	0.13
100	+	540.42	98.22	5	+	508.57	46.28	100	+	681.71	55.54	100	+	604.34	84.14	200	+	920.07	120.74
Conc (μM)	LPS	TNF-α pg/ml		Conc (mM)	LPS	TNF-α pg/ml		Conc (μM)	LPS	TNF-α pg/ml		Conc (μM)	LPS	TNF-α pg/ml		Conc (μM)	LPS	TNF-α pg/ml	
		Mean	SD			Mean	SD			Mean	SD			Mean	SD			Mean	SD
0	-	27.54	3.19	0	-	48.87	0.13	0	-	48.90	2.76	0	-	62.22	1.96	0	-	72.78	7.67
0	+	28.77	1.17	0	+	55.59	4.72	0	+	50.17	2.27	0	+	69.87	6.25	0	+	77.62	1.40
25	-	28.56	2.10	1.25	-	46.42	4.34	25	-	42.84	2.84	25	-	73.06	17.65	50	-	67.49	3.54
25	+	30.55	4.55	1.25	+	48.62	2.79	25	+	49.16	1.03	25	+	84.87	20.45	50	+	66.11	1.12
50	-	18.28	3.98	2.5	-	42.57	7.08	50	-	44.37	3.91	50	-	67.24	8.93	100	-	67.12	2.66
50	+	17.79	3.21	2.5	+	47.27	5.68	50	+	50.09	8.51	50	+	77.22	4.45	100	+	63.05	4.92
100	-	17.06	11.11	5	-	44.30	0.00	100	-	38.31	8.09	100	-	58.56	5.96	200	-	67.93	3.10
100	+	16.91	4.68	5	+	44.50	2.08	100	+	41.27	5.70	100	+	74.51	14.59	200	+	57.77	3.50

Supplementary Table 1B.

Allyl Alcohol							
		CYP3A (Luciferin, nM)		IL-6 pg/ml		TNF-α pg/ml	
Conc	LPS	Mean	SD	Mean	SD	Mean	SD
0	-	10.72	0.69	489.22	28.17	71.73	10.31
0	+	9.50	1.50	521.23	21.94	75.80	1.50
6.25	-	10.76	0.83	492.94	27.05	66.61	10.54
6.25	+	9.88	1.23	586.44	18.09	66.83	4.81
12.5	-	11.96	1.05	513.80	72.95	68.25	6.64
12.5	+	10.02	0.73	540.52	5.80	58.50	1.74
25	-	11.33	0.94	548.32	7.10	61.65	0.25
25	+	9.01	0.00	551.86	35.50	78.98	16.09
50	-	10.69	1.50	495.40	92.43	67.47	2.07
50	+	8.26	0.64	575.69	44.40	67.47	2.07
100	-	1.61	1.64	534.00	82.61	70.04	3.40
100	+	0.19	0.00	599.53	57.16	73.87	2.23
200	-	0.19	0.00	489.52	40.42	65.92	19.19
200	+	0.00	0.00	665.25	152.67	58.96	12.59
400	-	0.23	0.27	453.39	97.05	70.46	10.27
400	+	0.26	0.04	480.43	7.08	60.94	11.72

Supplementary Table 2. Use of HKCC for screening effects of compounds on Cyp3A activity and IL-6/TNF-α levels, data expressed as units of luciferin (nM), IL-6 or TNF- α (both pg/ml). 24 hr post-plating, HKCC were treated with varying doses of 2A, TVX, APAP, TCS , Acetachlor , propiconazole, or 2B, allyl alcohol with or without 1 μg/mL LPS for 48 hr. Cyp3A activity was assessed and media was collected and frozen for IL-6 and TNF-α analysis as described in Materials and Methods.

Supplementary Table 2A.

Trovafloxacin				Acetaminophen				Triclosan				Acetochlor				Propiconazole			
Conc (μM)	LPS	CYP3A (Luciferin, nM)		Conc (mM)	LPS	CYP3A (Luciferin, nM)		Conc (μM)	LPS	CYP3A (Luciferin, nM)		Conc (μM)	LPS	CYP3A (Luciferin, nM)		Conc (μM)	LPS	CYP3A (Luciferin, nM)	
		Mean	SD			Mean	SD			Mean	SD			Mean	SD			Mean	SD
0	-	8.32	0.50	0	-	5.75	0.00	0	-	8.32	0.50	0	-	8.94	0.90	0	-	8.26	0.12
0	+	4.19	0.17	0	+	3.04	0.58	0	+	3.91	0.53	0	+	4.85	0.87	0	+	4.87	0.36
25	-	6.91	1.29	1.25	-	6.76	0.94	25	-	7.84	0.15	25	-	7.56	0.44	50	-	32.83	9.27
25	+	5.04	0.26	1.25	+	3.79	0.72	25	+	3.52	0.31	25	+	4.66	0.27	50	+	6.94	2.90
50	-	11.43	1.56	2.5	-	11.51	1.13	50	-	10.46	0.24	50	-	6.67	0.63	100	-	-0.74	0.17
50	+	9.01	2.30	2.5	+	8.93	0.84	50	+	3.62	0.07	50	+	4.68	1.06	100	+	-0.79	0.10
100	-	16.14	0.55	5	-	15.30	3.99	100	-	-0.93	0.24	100	-	6.70	0.39	200	-	-1.20	0.00
100	+	18.50	3.79	5	+	15.24	4.91	100	+	-0.72	0.05	100	+	4.20	0.34	200	+	-1.17	0.10
Conc (μM)	LPS	IL-6 pg/ml		Conc (mM)	LPS	IL-6 pg/ml		Conc (μM)	LPS	IL-6 pg/ml		Conc (μM)	LPS	IL-6 pg/ml		Conc (μM)	LPS	IL-6 pg/ml	
		Mean	SD			Mean	SD			Mean	SD			Mean	SD			Mean	SD
0	-	830.70	46.47	0	-	1,235.13	178.20	0	-	1,259.48	93.66	0	-	954.53	37.95	0	-	1,109.18	214.22
0	+	5,458.89	826.96	0	+	5,254.73	1,517.98	0	+	6,239.17	180.70	0	+	5,804.68	1,772.41	0	+	5,284.44	78.09
25	-	1,085.76	107.67	1.25	-	852.79	30.09	25	-	1,026.48	126.64	25	-	985.65	31.76	50	-	1,029.44	127.36
25	+	1,821.30	160.57	1.25	+	4,613.34	760.71	25	+	5,622.33	225.15	25	+	3,876.60	1,138.50	50	+	5,171.19	325.95
50	-	766.66	15.04	2.5	-	666.07	29.21	50	-	975.82	135.13	50	-	984.68	109.64	100	-	942.05	32.04
50	+	991.32	0.67	2.5	+	2,793.74	666.08	50	+	4,544.56	129.95	50	+	3,618.00	512.20	100	+	5,798.60	1,006.62
100	-	861.48	99.77	5	-	536.22	50.42	100	-	1,036.57	90.66	100	-	707.40	33.71	200	-	1,222.24	61.81
100	+	868.44	0.80	5	+	1,045.73	37.35	100	+	2,119.92	761.07	100	+	3,257.77	229.83	200	+	3,649.02	474.19
Conc (μM)	LPS	TNF-α pg/ml		Conc (mM)	LPS	TNF-α pg/ml		Conc (μM)	LPS	TNF-α pg/ml		Conc (μM)	LPS	TNF-α pg/ml		Conc (μM)	LPS	TNF-α pg/ml	
		Mean	SD			Mean	SD			Mean	SD			Mean	SD			Mean	SD
0	-	42.32	18.42	0	-	58.35	5.24	0	-	56.01	6.29	0	-	73.07	13.08	0	-	63.85	6.18
0	+	72.59	4.07	0	+	120.10	6.70	0	+	106.97	0.27	0	+	129.23	16.58	0	+	118.40	7.51
25	-	30.01	2.49	1.25	-	53.29	3.38	25	-	46.12	1.36	25	-	81.67	1.16	50	-	59.52	8.56
25	+	72.54	0.12	1.25	+	116.31	6.11	25	+	103.59	5.53	25	+	123.38	22.29	50	+	102.79	10.65
50	-	19.89	2.84	2.5	-	47.26	5.14	50	-	43.11	2.19	50	-	94.69	4.81	100	-	51.72	2.10
50	+	73.37	4.52	2.5	+	99.51	4.69	50	+	90.11	1.66	50	+	134.92	1.89	100	+	102.42	11.77
100	-	31.80	0.45	5	-	49.12	3.13	100	-	37.86	9.81	100	-	71.60	9.17	200	-	69.77	5.99
100	+	63.05	12.67	5	+	108.43	1.27	100	+	88.95	2.86	100	+	114.82	5.67	200	+	100.17	4.63

Supplementary Table 1B.

Allyl Alcohol							
		CYP3A (Luciferin, nM)		IL-6 pg/ml		TNF-α pg/ml	
Conc	LPS	Mean	SD	Mean	SD	Mean	SD
0	-	7.66	0.44	632.41	21.63	67.48	0.21
0	+	4.21	0.83	1645.39	500.35	145.77	3.46
6.25	-	7.01	0.91	653.20	4.90	77.70	24.91
6.25	+	3.68	0.05	1682.78	221.82	156.58	7.61
12.5	-	6.39	1.12	680.58	110.09	59.70	0.80
12.5	+	3.25	1.01	1663.95	383.13	150.40	23.43
25	-	6.04	0.31	623.34	83.60	71.35	0.92
25	+	3.32	0.56	1730.74	264.13	140.37	12.46
50	-	5.49	0.42	645.36	52.95	72.80	1.21
50	+	2.47	0.32	1959.00	216.86	146.42	4.08
100	-	2.54	0.00	557.21	60.85	83.61	14.29
100	+	1.85	2.02	635.66	125.48	86.77	28.82
200	-	0.19	0.00	500.11	9.07	61.62	3.73
200	+	0.08	0.06	566.31	95.58	67.39	5.64
400	-	0.14	0.03	453.80	13.04	57.61	5.67
400	+	0.17	0.07	596.27	74.90	52.32	2.91

REFERENCES

Abdel-Razzak, Z., Loyer, P., Fautrel, A., Gautier, J. C., Corcos, L., Turlin, B., Beaune, P., and Guillouzo, A. (1993). Cytokines down-regulate expression of major cytochrome P-450 enzymes in adult human hepatocytes in primary culture. *Molecular pharmacology* **44**(4), 707-715.

Adams, D. H., Ju, C., Ramaiah, S. K., Uetrecht, J., and Jaeschke, H. (2010). Mechanisms of immune-mediated liver injury. *Toxicological sciences : an official journal of the Society of Toxicology* **115**(2), 307-21.

Adhikary, T., Wortmann, A., Schumann, T., Finkernagel, F., Lieber, S., Roth, K., Toth, P. M., Diederich, W. E., Nist, A., Stiewe, T., *et al.* (2015). The transcriptional PPARbeta/delta network in human macrophages defines a unique agonist-induced activation state. *Nucleic acids research* **43**(10), 5033-51.

Admyre, C., Johansson, S. M., Qazi, K. R., Filen, J. J., Lahesmaa, R., Norman, M., Neve, E. P., Scheynius, A., and Gabrielsson, S. (2007). Exosomes with immune modulatory features are present in human breast milk. *Journal of immunology* **179**(3), 1969-78.

Al-Nedawi, K., Meehan, B., Micallef, J., Lhotak, V., May, L., Guha, A., and Rak, J. (2008). Intercellular transfer of the oncogenic receptor EGFRvIII by microvesicles derived from tumour cells. *Nature cell biology* **10**(5), 619-24.

Aliotta, J. M., Sanchez-Guijo, F. M., Dooner, G. J., Johnson, K. W., Dooner, M. S., Greer, K. A., Greer, D., Pimentel, J., Kolankiewicz, L. M., Puente, N., *et al.* (2007). Alteration of marrow cell gene expression, protein production, and engraftment into lung by lung-derived microvesicles: a novel mechanism for phenotype modulation. *Stem cells* **25**(9), 2245-56.

Alvarez, M. L., Khosroheidari, M., Kanchi Ravi, R., and DiStefano, J. K. (2012). Comparison of protein, microRNA, and mRNA yields using different methods of urinary exosome isolation for the discovery of kidney disease biomarkers. *Kidney international* **82**(9), 1024-32.

Andaloussi, S. E. L., Mager, I., Breakefield, X. O., and Wood, M. J. (2013). Extracellular vesicles: biology and emerging therapeutic opportunities. *Nature reviews. Drug discovery* **12**(5), 347-57.

Anders, S., and Huber, W. (2010). Differential expression analysis for sequence count data. *Genome biology* **11**(10), R106.

Andrade, R. J., Lucena, M. I., Fernandez, M. C., Pelaez, G., Pachkoria, K., Garcia-Ruiz, E., Garcia-Munoz, B., Gonzalez-Grande, R., Pizarro, A., Duran, J. A., *et al.* (2005). Drug-induced liver injury: an analysis of 461 incidences submitted to the Spanish registry over a 10-year period. *Gastroenterology* **129**(2), 512-21.

Andre, F., Schartz, N. E., Movassagh, M., Flament, C., Pautier, P., Morice, P., Pomel, C., Lhomme, C., Escudier, B., Le Chevalier, T., *et al.* (2002). Malignant effusions and immunogenic tumour-derived exosomes. *Lancet* **360**(9329), 295-305.

Antoine, D. J., Dear, J. W., Starkey Lewis, P., Platt, V., Coyle, J., Masson, M., Thanacoody, R. H., Gray, A. J., Webb, D. J., Moggs, J. G., *et al.* (2013). Mechanistic biomarkers provide early and sensitive detection of acetaminophen-induced acute liver injury at first presentation to hospital. *Hepatology (Baltimore, Md.)* **58**(2), 777-787.

Antoine, D. J., Harrill, A. H., Watkins, P. B., and Park, B. K. (2014). Safety biomarkers for drug-induced liver injury – current status and future perspectives. *Toxicol. Res.* **3**(2), 75-85.

Antoniades, C. G., Quaglia, A., Taams, L. S., Mitry, R. R., Hussain, M., Abeles, R., Possamai, L. A., Bruce, M., McPhail, M., Starling, C., *et al.* (2012). Source and characterization of hepatic macrophages in acetaminophen-induced acute liver failure in humans. *Hepatology* **56**(2), 735-46.

Applied Biosystems (2010). Factors Influencing Multiplex Real-Time PCR.

Arroyo, J. D., Chevillet, J. R., Kroh, E. M., Ruf, I. K., Pritchard, C. C., Gibson, D. F., Mitchell, P. S., Bennett, C. F., Pogosova-Agadjanyan, E. L., Stirewalt, D. L., *et al.* (2011). Argonaute2 complexes carry a population of circulating microRNAs independent of vesicles in human plasma. *Proceedings of the National Academy of Sciences of the United States of America* **108**(12), 5003-8.

Arts, R. J., Joosten, L. A., van der Meer, J. W., and Netea, M. G. (2013). TREM-1: intracellular signaling pathways and interaction with pattern recognition receptors. *Journal of leukocyte biology* **93**(2), 209-15.

Aryani, A., and Denecke, B. (2016). Exosomes as a Nanodelivery System: a Key to the Future of Neuromedicine? *Molecular neurobiology* **53**(2), 818-34.

Asea, A., Jean-Pierre, C., Kaur, P., Rao, P., Linhares, I. M., Skupski, D., and Witkin, S. S. (2008). Heat shock protein-containing exosomes in mid-trimester amniotic fluids. *Journal of reproductive immunology* **79**(1), 12-7.

Ashino, T., Oguro, T., Shioda, S., Horai, R., Asano, M., Sekikawa, K., Iwakura, Y., Numazawa, S., and Yoshida, T. (2004). Involvement of interleukin-6 and tumor necrosis factor α in CYP3A11 and 2C29 down-regulation by Bacillus Calmette-Guérin and lipopolysaccharide in mouse liver. *Drug Metabolism and Disposition* **32**(7), 707-714.

Bala, S., Csak, T., Momen-Heravi, F., Lippai, D., Kodys, K., Catalano, D., Satishchandran, A., Ambros, V., and Szabo, G. (2015). Biodistribution and function of extracellular miRNA-155 in mice. *Scientific reports* **5**, 10721.

Bala, S., Petrasek, J., Mundkur, S., Catalano, D., Levin, I., Ward, J., Alao, H., Kodys, K., and Szabo, G. (2012). Circulating microRNAs in exosomes indicate hepatocyte injury and inflammation in alcoholic, drug-induced, and inflammatory liver diseases. *Hepatology* **56**(5), 1946-57.

Bandiera, S., Pfeffer, S., Baumert, T. F., and Zeisel, M. B. (2015). miR-122--a key factor and therapeutic target in liver disease. *Journal of hepatology* **62**(2), 448-57.

Bass, N. M., and Ockner, R. K. (1996). *Drug-Induced Liver Disease*. 3 ed. W.B. Saunders Company.

Baulies, A., Ribas, V., Nunez, S., Torres, S., Alarcon-Vila, C., Martinez, L., Suda, J., Ybanez, M. D., Kaplowitz, N., Garcia-Ruiz, C., *et al.* (2015). Lysosomal Cholesterol Accumulation Sensitizes To Acetaminophen Hepatotoxicity by Impairing Mitophagy. *Scientific reports* **5**, 18017.

Beggs, K. M., Fullerton, A. M., Miyakawa, K., Ganey, P. E., and Roth, R. A. (2014). Molecular mechanisms of hepatocellular apoptosis induced by trovafloxacin-tumor necrosis factor-alpha interaction. *Toxicological sciences : an official journal of the Society of Toxicology* **137**(1), 91-101.

Beninson, L. A., and Fleshner, M. (2014). Exosomes: an emerging factor in stress-induced immunomodulation. *Seminars in immunology* **26**(5), 394-401.

Berg, J. M., Tymozcko, J. L., and Stryer, L. (2002). *Biochemistry*. 5 ed. WH Freeman, New York.

Bernal, W., Auzinger, G., Dhawan, A., and Wendon, J. (2010). Acute liver failure. *Lancet* **376**(9736), 190-201.

Bessems, J. G., and Vermeulen, N. P. E. (2001). Paracetamol (acetaminophen)-induced toxicity: molecular and biochemical mechanisms, analogues and protective approaches. *Critical Reviews in Toxicology* **31**(1), 55-138.

Beutler, E., Gelbart, T., and Kuhl, W. (1990). Interference of heparin with the polymerase chain reaction. *BioTechniques* **9**(2), 166.

Bigagli, E., Luceri, C., Guasti, D., and Cinci, L. (2016). Exosomes secreted from human colon cancer cells influence the adhesion of neighboring metastatic cells: Role of microRNA-210. *Cancer biology & therapy* doi: 10.1080/15384047.2016.1219815, 1-8.

Bobrie, A., Colombo, M., Raposo, G., and Thery, C. (2011). Exosome secretion: molecular mechanisms and roles in immune responses. *Traffic* **12**(12), 1659-68.

Bonzo, J. A., Rose, K. A., Freeman, K., Deibert, E., Amaral, K. B., Ferguson, S. S., Andersen, M. E., Witek, R. P., and LeCluyse, E. L. (2015). Differential effects of trovafloxacin on TNF-alpha and IL-6 profiles in a rat hepatocyte-Kupffer cell co-culture system. *Appl In Vitro Toxicol* **1**(1), 45-54.

Borlak, J., Chatterji, B., Londhe, K. B., and Watkins, P. B. (2013). Serum acute phase reactants hallmark healthy individuals at risk for acetaminophen-induced liver injury. *Genome Med* **5**(9), 86.

Bossink, A. W., Paemen, L., Jansen, P. M., Hack, C. E., Thijs, L. G., and Van Damme, J. (1995). Plasma levels of the chemokines monocyte chemotactic proteins-1 and -2 are elevated in human sepsis. *Blood* **86**(10), 3841-7.

Bretz, N. P., Ridinger, J., Rupp, A. K., Rimbach, K., Keller, S., Rupp, C., Marme, F., Umansky, L., Umansky, V., Eigenbrod, T., *et al.* (2013). Body fluid exosomes promote secretion of inflammatory cytokines in monocytic cells via Toll-like receptor signaling. *The Journal of biological chemistry* **288**(51), 36691-702.

Brodsky, S. V., Facciuto, M. E., Heydt, D., Chen, J., Islam, H. K., Kajstura, M., Ramaswamy, G., and Aguero-Rosenfield, M. (2008). Dynamics of Circulating Microparticles in Liver Transplant Patients. *J. Gastrointestin. Liver Dis.* **17**(3), 261-268.

Brown, A. P., Morrissey, R. L., Tolhurst, T. A., Crowell, J. A., and Levine, B. S. (2000). Oral toxicity of 1,2-dithiole-3-thione, a potential cancer chemopreventive agent, in the rat. *International Journal of Toxicology* **19**(6), 375-381.

Bukong, T. N., Momen-Heravi, F., Kodys, K., Bala, S., and Szabo, G. (2014). Exosomes from hepatitis C infected patients transmit HCV infection and contain replication competent viral RNA in complex with Ago2-miR122-HSP90. *PLoS pathogens* **10**(10), e1004424.

Caby, M. P., Lankar, D., Vincendeau-Scherrer, C., Raposo, G., and Bonnerot, C. (2005). Exosomal-like vesicles are present in human blood plasma. *International immunology* **17**(7), 879-87.

Calkin, A. C., Goult, B. T., Zhang, L., Fairall, L., Hong, C., Schwabe, J. W., and Tontonoz, P. (2011). FERM-dependent E3 ligase recognition is a conserved mechanism for targeted degradation of lipoprotein receptors. *Proceedings of the National Academy of Sciences of the United States of America* **108**(50), 20107-12.

Cattaneo, M., Lecchi, A., Zighetti, M. L., and Lussana, F. (2007). Platelet aggregation studies: autologous platelet-poor plasma inhibits platelet aggregation when added to platelet-rich plasma to normalize platelet count. *Haematologica* **92**(5), 694-697.

Chargaff, E., and West, R. (1946). The biological significance of the thromboplastic protein of blood. *The Journal of biological chemistry* **166**(1), 189-97.

Chen, X., and Resh, M. D. (2002). Cholesterol depletion from the plasma membrane triggers ligand-independent activation of the epidermal growth factor receptor. *The Journal of biological chemistry* **277**(51), 49631-7.

Chensue, S. W., Warmington, K. S., Ruth, J. H., Sanghi, P. S., Lincoln, P., and Kunkel, S. L. (1996). Role of monocyte chemoattractant protein-1 (MCP-1) in Th1 (mycobacterial) and Th2 (schistosomal) antigen-induced granuloma formation: relationship to local inflammation, Th cell expression, and IL-12 production. *Journal of immunology* **157**(10), 4602-8.

Chiba, M., Kimura, M., and Asari, S. (2012). Exosomes secreted from human colorectal cancer cell lines contain mRNAs, microRNAs and natural antisense RNAs, that can transfer into the human hepatoma HepG2 and lung cancer A549 cell lines. *Oncology reports* **28**(5), 1551-8.

Chiu, H., Gardner, C. R., Dambach, D. M., Durham, S. K., Brittingham, J. A., Laskin, J. D., and Laskin, D. L. (2003). Role of tumor necrosis factor receptor 1 (p55) in hepatocyte proliferation during acetaminophen-induced toxicity in mice. *Toxicology and applied pharmacology* **193**(2), 218-27.

Chiu, Y. H., Macmillan, J. B., and Chen, Z. J. (2009). RNA polymerase III detects cytosolic DNA and induces type I interferons through the RIG-I pathway. *Cell* **138**(3), 576-91.

CHPA (2014). Awareness of acetaminophen safe use increasing (press release). In (doi. Consumer Healthcare Products Association.

Chuang, H. C., Wang, J. M., Hsieh, W. C., Chang, Y., and Su, I. J. (2008). Up-regulation of activating transcription factor-5 suppresses SAP expression to activate T cells in hemophagocytic syndrome associated with Epstein-Barr virus infection and immune disorders. *The American journal of pathology* **173**(5), 1397-405.

Conde-Vancells, J., Rodriguez-Suarez, E., Embade, N., Gil, D., Matthiesen, R., Valle, M., Elortza, F., Lu, S. C., Mato, J. M., and Falcon-Perez, J. M. (2008). Characterization and comprehensive proteome profiling of exosomes secreted by hepatocytes. *Journal of proteome research* **7**(12), 5157-66.

Corsini, A., Ganey, P., Ju, C., Kaplowitz, N., Pessayre, D., Roth, R., Watkins, P. B., Albassam, M., Liu, B., Stancic, S., *et al.* (2012). Current challenges and controversies in drug-induced liver injury. *Drug Saf* **35**(12), 1099-117.

Cvjetkovic, A., Lotvall, J., and Lasser, C. (2014). The influence of rotor type and centrifugation time on the yield and purity of extracellular vesicles. *Journal of extracellular vesicles* **3**.

Cyster, J. G., Dang, E. V., Reboldi, A., and Yi, T. (2014). 25-Hydroxycholesterols in innate and adaptive immunity. *Nature reviews. Immunology* **14**(11), 731-43.

Davidson, D. G., and Eastham, W. N. (1966). Acute liver necrosis following overdose of paracetamol. *British medical journal* **2**(5512), 497-9.

de Jong, O. G., Verhaar, M. C., Chen, Y., Vader, P., Gremmels, H., Posthuma, G., Schiffelers, R. M., Gucek, M., and van Balkom, B. W. (2012). Cellular stress conditions are reflected in the protein and RNA content of endothelial cell-derived exosomes. *Journal of extracellular vesicles* **1**.

De Maio, A. (2011). Extracellular heat shock proteins, cellular export vesicles, and the Stress Observation System: a form of communication during injury, infection, and cell damage. *Cell stress & chaperones* **16**(3), 235-49.

Dear, J. W., and Antoine, D. J. (2014). Stratification of paracetamol overdose patients using new toxicity biomarkers: current candidates and future challenges. *Expert review of clinical pharmacology* **7**(2), 181-9.

DeLeve, L. D., Wang, X., Kaplowitz, N., Shulman, H. M., Bart, J. A., and van der Hoek, A. (1997). Sinusoidal endothelial cells as a target for acetaminophen toxicity. Direct action versus requirement for hepatocyte activation in different mouse strains. *Biochem Pharmacol* **53**(9), 1339-45.

DeLeve, L. D., Wang, X., McCuskey, M. K., and McCuskey, R. S. (2006). Rat liver endothelial cells isolated by anti-CD31 immunomagnetic separation lack fenestrae and sieve plates. *Am J Physiol Gastrointest Liver Physiol* **291**(6), G1187-9.

Dixon, L. J., Barnes, M., Tang, H., Pritchard, M. T., and Nagy, L. E. (2013). Kupffer cells in the liver. *Comprehensive Physiology* **3**(2), 785-97.

Dokland, T. (2006). Electron microscopy of biological samples. In *Techniques in Microscopy for Biomedical Applications* (T. Dokland, Hutmacher, D.W., Ng, M.L., Schantz, J.T. , Eds.) doi. World Scientific Press, Singapore.

Dreux, M., Garaigorta, U., Boyd, B., Decembre, E., Chung, J., Whitten-Bauer, C., Wieland, S., and Chisari, F. V. (2012). Short-range exosomal transfer of viral RNA from infected cells to plasmacytoid dendritic cells triggers innate immunity. *Cell host & microbe* **12**(4), 558-70.

Eldh, M., Ekstrom, K., Valadi, H., Sjostrand, M., Olsson, B., Jernas, M., and Lotvall, J. (2010). Exosomes communicate protective messages during oxidative stres; possible role of exosomal shuttle RNA. *PloS one* **5**(12), e15353.

Eldh, M., Lotvall, J., Malmhall, C., and Ekstrom, K. (2012). Importance of RNA isolation methods for analysis of exosomal RNA: evaluation of different methods. *Molecular immunology* **50**(4), 278-86.

Evers, R., Dallas, S., Dickmann, L. J., Fahmi, O. A., Kenny, J. R., Kraynov, E., Nguyen, T., Patel, A. H., Slatter, J. G., and Zhang, L. (2013). Critical review of preclinical approaches to investigate cytochrome p450-mediated therapeutic protein drug-drug

interactions and recommendations for best practices: a white paper. *Drug metabolism and disposition: the biological fate of chemicals* **41**(9), 1598-609.

Fan, Y. Y., Monk, J. M., Hou, T. Y., Callway, E., Vincent, L., Weeks, B., Yang, P., and Chapkin, R. S. (2012). Characterization of an arachidonic acid-deficient (Fads1 knockout) mouse model. *J Lipid Res* **53**(7), 1287-95.

Fannin, R. D., Gerrish, K., Sieber, S. O., Bushel, P. R., Watkins, P. B., and Paules, R. S. (2015). Blood transcript immune signatures distinguish a subset of people with elevated serum ALT from others given acetaminophen. *Clinical pharmacology and therapeutics* doi: 10.1002/cpt.328.

Fannin, R. D., Gerrish, K., Sieber, S. O., Bushel, P. R., Watkins, P. B., and Paules, R. S. (2016). Blood transcript immune signatures distinguish a subset of people with elevated serum ALT from others given acetaminophen. *Clinical pharmacology and therapeutics* **99**(4), 432-41.

Faure, J., Lachenal, G., Court, M., Hirrlinger, J., Chatellard-Causse, C., Blot, B., Grange, J., Schoehn, G., Goldberg, Y., Boyer, V., *et al.* (2006). Exosomes are released by cultured cortical neurones. *Molecular and cellular neurosciences* **31**(4), 642-8.

FDA (2016). *Acetaminophen Information*2016.

FDA CDER, C. (2009). Guidance for Industry, Drug-Induced Liver Injury: Premarketing Clinical Evaluation. In (F. a. D. A. U.S. Department of Health and Human Services, Ed.) Eds.) doi. FDA Maryland.

Ferreira, D. W., Goedken, M. J., Rommelaere, S., Chasson, L., Galland, F., Naquet, P., and Manautou, J. E. (2016). Enhanced hepatotoxicity by acetaminophen in Vanin-1 knockout mice is associated with deficient proliferative and immune responses. *Biochimica et biophysica acta* **1862**, 662-669.

Fessler, M. B., and Parks, J. S. (2011). Intracellular lipid flux and membrane microdomains as organizing principles in inflammatory cell signaling. *Journal of immunology* **187**(4), 1529-35.

Fonsato, V., Collino, F., Herrera, M. B., Cavallari, C., Deregibus, M. C., Cisterna, B., Bruno, S., Romagnoli, R., Salizzoni, M., Tetta, C., *et al.* (2012). Human liver stem cell-derived microvesicles inhibit hepatoma growth in SCID mice by delivering antitumor microRNAs. *Stem cells* **30**(9), 1985-98.

Fontana, R. J. (2014). Pathogenesis of idiosyncratic drug-induced liver injury and clinical perspectives. *Gastroenterology* **146**(4), 914-28.

Gamazon, E. R., Innocenti, F., Wei, R., Wang, L., Zhang, M., Mirkov, S., Ramirez, J., Huang, R. S., Cox, N. J., Ratain, M. J., *et al.* (2013). A genome-wide integrative study of microRNAs in human liver. *BMC genomics* **14**(395).

Gatti, S., Bruno, S., Deregibus, M. C., Sordi, A., Cantaluppi, V., Tetta, C., and Camussi, G. (2011). Microvesicles derived from human adult mesenchymal stem cells protect against ischaemia-reperfusion-induced acute and chronic kidney injury. *Nephrology, dialysis, transplantation : official publication of the European Dialysis and Transplant Association - European Renal Association* **26**(5), 1474-83.

Geissmann, F., Jung, S., and Littman, D. R. (2003). Blood monocytes consist of two principal subsets with distinct migratory properties. *Immunity* **19**(1), 71-82.

Giugliano, S., Kriss, M., Golden-Mason, L., Dobrinskikh, E., Stone, A. E., Soto-Gutierrez, A., Mitchell, A., Khetani, S. R., Yamane, D., Stoddard, M., *et al.* (2015). Hepatitis C virus infection induces autocrine interferon signaling by human liver endothelial cells and release of exosomes, which inhibits viral replication. *Gastroenterology* **148**(2), 392-402 e13.

Gyorgy, B., Szabo, T. G., Pasztoi, M., Pal, Z., Misjak, P., Aradi, B., Laszlo, V., Pallinger, E., Pap, E., Kittel, A., *et al.* (2011). Membrane vesicles, current state-of-the-art: emerging role of extracellular vesicles. *Cellular and molecular life sciences : CMLS* **68**(16), 2667-88.

Han, D., Hanawa, N., Saberi, B., and Kaplowitz, N. (2006). Mechanisms of liver injury. III. Role of glutathione redox status in liver injury. *Am J Physiol Gastrointest Liver Physiol* **291**(1), G1-7.

Hanawa, N., Shinohara, M., Saberi, B., Gaarde, W. A., Han, D., and Kaplowitz, N. (2008). Role of JNK translocation to mitochondria leading to inhibition of mitochondria bioenergetics in acetaminophen-induced liver injury. *The Journal of biological chemistry* **283**(20), 13565-77.

Hanna, R. N., Carlin, L. M., Hubbeling, H. G., Nackiewicz, D., Green, A. M., Punt, J. A., Geissmann, F., and Hedrick, C. C. (2011). The transcription factor NR4A1 (Nur77) controls bone marrow differentiation and the survival of Ly6C- monocytes. *Nature immunology* **12**(8), 778-85.

Harrill, A. H., Ross, P. K., Gatti, D. M., Threadgill, D. W., and Rusyn, I. (2009a). Population-based discovery of toxicogenomics biomarkers for hepatotoxicity using a laboratory strain diversity panel. *Toxicological sciences : an official journal of the Society of Toxicology* **110**(1), 235-43.

Harrill, A. H., Watkins, P. B., Su, S., Ross, P. K., Harbourt, D. E., Stylianou, I. M., Boorman, G. A., Russo, M. W., Sackler, R. S., Harris, S. C., *et al.* (2009b). Mouse population-guided resequencing reveals that variants in CD44 contribute to acetaminophen-induced liver injury in humans. *Genome research* **19**(9), 1507-15.

Harris, D. A., Patel, S. H., Gucek, M., Hendrix, A., Westbroek, W., and Taraska, J. W. (2015). Exosomes released from breast cancer carcinomas stimulate cell movement. *PloS one* **10**(3), e0117495.

Harwood, N. M., Golden-Mason, L., Cheng, L., Rosen, H. R., and Mengshol, J. A. (2016). HCV-infected cells and differentiation increase monocyte immunoregulatory galectin-9 production. *Journal of leukocyte biology* **99**(3), 495-503.

Hegyi, G., Kardos, J., Kovacs, M., Malnasi-Csizmadia, A., Nyitray, L., Pal, G., Radnai, L., Remenyi, A., and Venekei, I. (2013). Introduction to Practical Biochemistry. In (doi. Eotvos Lorand University, Hungary.

Henegariu, O., Heerema, N. A., Dlouhy, S. R., Vance, G. H., and Vogt, P. H. (1997). Multiplex PCR: Critical Parameters and Step-by-Step Protocol. *BioTechniques* **23**(3), 504-511.

Herrera, M. B., Fonsato, V., Gatti, S., Deregibus, M. C., Sordi, A., Cantarella, D., Calogero, R., Bussolati, B., Tetta, C., and Camussi, G. (2010). Human liver stem cell-derived microvesicles accelerate hepatic regeneration in hepatectomized rats. *Journal of cellular and molecular medicine* **14**(6B), 1605-18.

Higuchi, S., Wu, R., Zhou, M., Ravikumar, T. S., and Wang, P. (2007). Downregulation of hepatic cytochrome P-450 isoforms and PPAR-gamma: their role in hepatic injury and proinflammatory responses in a double-hit model of hemorrhage and sepsis. *The Journal of surgical research* **137**(1), 46-52.

Hill, A. F., Pegtel, D. M., Lambertz, U., Leonardi, T., O'Driscoll, L., Pluchino, S., Ter-Ovanesyan, D., and Nolte-'t Hoen, E. N. (2013). ISEV position paper: extracellular vesicle RNA analysis and bioinformatics. *Journal of extracellular vesicles* **2**.

Hilliard, K. L., Allen, E., Traber, K. E., Yamamoto, K., Stauffer, N. M., Wasserman, G. A., Jones, M. R., Mizgerd, J. P., and Quinton, L. J. (2015). The Lung-Liver Axis: A Requirement for Maximal Innate Immunity and Hepatoprotection during Pneumonia. *American journal of respiratory cell and molecular biology* **53**(3), 378-90.

Hinson, J. A., Roberts, D. W., and James, L. P. (2010). Mechanisms of acetaminophen-induced liver necrosis. *Handbook of experimental pharmacology* doi: 10.1007/978-3-642-00663-0_12(196), 369-405.

Hirsova, P., and Gores, G. J. (2015). Death Receptor-Mediated Cell Death and Proinflammatory Signaling in Nonalcoholic Steatohepatitis. *Cellular and molecular gastroenterology and hepatology* **1**(1), 17-27.

Hirsova, P., Ibrahim, S. H., Krishnan, A., Verma, V. K., Bronk, S. F., Werneburg, N. W., Charlton, M. R., Shah, V. H., Malhi, H., and Gores, G. J. (2016). Lipid-induced Signaling Causes Release of Inflammatory Extracellular Vesicles from Hepatocytes. *Gastroenterology* **150**(4), 956-967.

Hisada, Y., Alexander, W., Kasthuri, R., Voorhees, P., Mobarrez, F., Taylor, A., McNamara, C., Wallen, H., Witkowski, M., Key, N. S., *et al.* (2016). Measurement of microparticle tissue factor activity in clinical samples: A summary of two tissue factor-dependent FXa generation assays. *Thrombosis research* **139**, 90-7.

Hodgman, M. J., and Garrard, A. R. (2012). A review of acetaminophen poisoning. *Critical care clinics* **28**(4), 499-516.

Hoebe, K. H., Witkamp, R. F., Fink-Gremmels, J., Van Miert, A. S., and Monshouwer, M. (2001). Direct cell-to-cell contact between Kupffer cells and hepatocytes augments endotoxin-induced hepatic injury. *Am J Physiol Gastrointest Liver Physiol* **280**(4), G720-8.

Holman, N. S., Mosedale, M., Wolf, K. K., LeCluyse, E. L., and Watkins, P. B. (2016). Subtoxic Alterations in Hepatocyte-Derived Exosomes: An Early Step in Drug-Induced Liver Injury? *Toxicological sciences : an official journal of the Society of Toxicology* **151**(2), 365-75.

Holt, M. P., Cheng, L., and Ju, C. (2008). Identification and characterization of infiltrating macrophages in acetaminophen-induced liver injury. *Journal of leukocyte biology* **84**(6), 1410-21.

Hornby, R. J., Starkey Lewis, P., Dear, J., Goldring, C., and Park, B. K. (2014). MicroRNAs as potential circulating biomarkers of drug-induced liver injury: key current and future issues for translation to humans. *Expert review of clinical pharmacology* **7**(3), 349-62.

Hou, Y., Zhang, H., Miranda, L., and Lin, S. (2010). Serious overestimation in quantitative PCR by circular (supercoiled) plasmid standard: microalgal pcna as the model gene. *PloS one* **5**(3), e9545.

Huang, X., Yuan, T., Tschannen, M., Sun, Z., Jacob, H., Du, M., Liang, M., Dittmar, R. L., Liu, Y., Liang, M., *et al.* (2013). Characterization of human plasma-derived exosomal RNAs by deep sequencing. *BMC genomics* **14**(319).

Huebener, P., Pradere, J. P., Hernandez, C., Gwak, G. Y., Caviglia, J. M., Mu, X., Loike, J. D., Jenkins, R. E., Antoine, D. J., and Schwabe, R. F. (2015). The HMGB1/RAGE axis triggers neutrophil-mediated injury amplification following necrosis. *The Journal of clinical investigation* **125**(2), 539-50.

Hunt, C. M. (2010). Mitochondrial and immunoallergic injury increase risk of positive drug rechallenge after drug-induced liver injury: a systematic review. *Hepatology* **52**(6), 2216-22.

Hussaini, S. H., and Farrington, E. A. (2014). Idiosyncratic drug-induced liver injury: an update on the 2007 overview. *Expert opinion on drug safety* **13**(1), 67-81.

Izquierdo-Useros, N., Naranjo-Gomez, M., Archer, J., Hatch, S. C., Erkizia, I., Blanco, J., Borras, F. E., Puertas, M. C., Connor, J. H., Fernandez-Figueras, M. T., *et al.* (2009). Capture and transfer of HIV-1 particles by mature dendritic cells converges with the exosome-dissemination pathway. *Blood* **113**(12), 2732-41.

Jaeschke, H. (2007). Kupffer cells In *Textbook of Hepatology: From Basic Science to Clinical Practice* (J. Rodes, J. Benhamou, A. Blei, J. Reichen, and M. Rizzetto, Eds.) doi: 3 ed., pp. 36-42

Wiley-Blackwell Publishing Malden.

Jaeschke, H. (2008). Toxic Responses of the Liver. In *Casarett and Doull's Toxicology: The Basic Science of Poisons* (C. D. Klaassen, Eds.) doi: 7 ed. McGraw Hill.

Jaeschke, H., Gores, G. J., Cederbaum, A. I., Hinson, J. A., Pessayre, D., and Lemasters, J. J. (2002). Mechanisms of hepatotoxicity. *Toxicological sciences : an official journal of the Society of Toxicology* **65**(2), 166-76.

Jaeschke, H., Williams, C. D., Ramachandran, A., and Bajt, M. L. (2012). Acetaminophen hepatotoxicity and repair: the role of sterile inflammation and innate immunity. *Liver international : official journal of the International Association for the Study of the Liver* **32**(1), 8-20.

Jaeschke, H., Xie, Y., and McGill, M. R. (2014). Acetaminophen-induced Liver Injury: from Animal Models to Humans. *Journal of clinical and translational hepatology* **2**(3), 153-61.

James, L. P., Farrar, H. C., Darville, T. L., Sullivan, J. E., Givens, T. G., Kearns, G. L., Wasserman, G. S., Simpson, P. M., Hinson, J. A., Pediatric Pharmacology Research Unit Network, N. I. o. C. H., *et al.* (2001). Elevation of serum interleukin 8 levels in acetaminophen overdose in children and adolescents. *Clinical pharmacology and therapeutics* **70**(3), 280-6.

James, L. P., Mayeux, P. R., and Hinson, J. A. (2003). Acetaminophen-induced hepatotoxicity. *Drug metabolism and disposition: the biological fate of chemicals* **31**(12), 1499-506.

James, L. P., Simpson, P. M., Farrar, H. C., Kearns, G. L., Wasserman, G. S., Blumer, J. L., Reed, M. D., Sullivan, J. E., and Hinson, J. A. (2005). Cytokines and toxicity in acetaminophen overdose. *Journal of clinical pharmacology* **45**(10), 1165-71.

Jiang, J., Briede, J. J., Jennen, D. G., Van Summeren, A., Saritas-Brauers, K., Schaart, G., Kleinjans, J. C., and de Kok, T. M. (2015). Increased mitochondrial ROS formation by acetaminophen in human hepatic cells is associated with gene expression changes suggesting disruption of the mitochondrial electron transport chain. *Toxicology letters* **234**(2), 139-50.

Johnson, M. L., Navanukraw, C., Grazul-Bilska, A. T., Reynolds, L. P., and Redmer, D. A. (2003). Heparinase treatment of RNA before quantitative real-time RT-PCR. *BioTechniques* **35**(6), 1140-2, 1144.

Johnston, S., Gallaher, Z., and Czaja, K. (2012). Exogenous reference gene normalization for real-time reverse transcription-polymerase chain reaction analysis under dynamic endogenous transcription. *Neural Regeneration Research* **7**(14), 1064-1072.

Jollow, D. J., Mitchell, J. R., Potter, W. Z., Davis, D. C., Gillette, J. R., and Brodie, B. B. (1973). Acetaminophen-induced hepatic necrosis. II. Role of covalent binding in vivo. *The Journal of pharmacology and experimental therapeutics* **187**(1), 195-202.

Jollow, D. J., Thorgeirsson, S. S., Potter, W. Z., Hashimoto, M., and Mitchell, J. R. (1974). Acetaminophen-induced hepatic necrosis. VI. Metabolic disposition of toxic and nontoxic doses of acetaminophen. *Pharmacology* **12**(4-5), 251-71.

Ju, C., and Reilly, T. (2012). Role of immune reactions in drug-induced liver injury (DILI). *Drug metabolism reviews* **44**(1), 107-15.

Ju, C., Reilly, T. P., Bourdi, M., Radonovich, M. F., Brady, J. N., George, J. W., and Pohl, L. R. (2002). Protective role of Kupffer cells in acetaminophen-induced hepatic injury in mice. *Chem Res Toxicol* **15**, 1504-1513.

Kakazu, E., Mauer, A. S., Yin, M., and Malhi, H. (2015). Hepatocytes release ceramide-enriched pro-inflammatory extracellular vesicles in an IRE1alpha-dependent manner. *Journal of Lipid Research* **57**(2), 233-245.

Kale, V. M., Miranda, S. R., Wilbanks, M. S., and Meyer, S. A. (2008). Comparative cytotoxicity of alachlor, acetochlor, and metolachlor herbicides in isolated rat and cryopreserved human hepatocytes. *Journal of biochemical and molecular toxicology* **22**(1), 41-50.

Kaplowitz, N. (2005). Idiosyncratic drug hepatotoxicity. *Nature reviews. Drug discovery* **4**(6), 489-99.

Kaufman, D. W., Kelly, J. P., Rohay, J. M., Malone, M. K., Weinstein, R. B., and Shiffman, S. (2012). Prevalence and correlates of exceeding the labeled maximum dose of acetaminophen among adults in a U.S.-based internet survey. *Pharmacoepidemiology and drug safety* **21**(12), 1280-8.

Kaur, S., Singh, S. P., Elkahloun, A. G., Wu, W., Abu-Asab, M. S., and Roberts, D. D. (2014). CD47-dependent immunomodulatory and angiogenic activities of extracellular vesicles produced by T cells. *Matrix biology : journal of the International Society for Matrix Biology* **37**, 49-59.

Kesimer, M., Scull, M., Brighton, B., DeMaria, G., Burns, K., O'Neal, W., Pickles, R. J., and Sheehan, J. K. (2009). Characterization of exosome-like vesicles released from human tracheobronchial ciliated epithelium: a possible role in innate defense. *FASEB*

journal : official publication of the Federation of American Societies for Experimental Biology **23**(6), 1858-68.

Kia, R., Kelly, L., Sison-Young, R. L., Zhang, F., Pridgeon, C. S., Heslop, J. A., Metcalfe, P., Kitteringham, N. R., Baxter, M., Harrison, S., *et al.* (2015). MicroRNA-122: a novel hepatocyte-enriched in vitro marker of drug-induced cellular toxicity. *Toxicological sciences : an official journal of the Society of Toxicology* **144**(1), 173-85.

Kim, D. J., Linnstaedt, S., Palma, J., Park, J. C., Ntrivalas, E., Kwak-Kim, J. Y., Gilman-Sachs, A., Beaman, K., Hastings, M. L., Martin, J. N., *et al.* (2012). Plasma components affect accuracy of circulating cancer-related microRNA quantitation. *The Journal of molecular diagnostics : JMD* **14**(1), 71-80.

Kim, S. Y., Lee, J. G., Cho, W. S., Cho, K. H., Sakong, J., Kim, J. R., Chin, B. R., and Baek, S. H. (2010). Role of NADPH oxidase-2 in lipopolysaccharide-induced matrix metalloproteinase expression and cell migration. *Immunology and cell biology* **88**(2), 197-204.

Kmiec, Z. (2001). Cooperation of liver cells in health and disease. *Adv Anat Embryol Cell Biol* **161**, III-XIII, 1-151.

Koarai, A., Yanagisawa, S., Sugiura, H., Ichikawa, T., Kikuchi, T., Furukawa, K., Akamatsu, K., Hirano, T., Nakanishi, M., Matsunaga, K., *et al.* (2012). 25-hydroxycholesterol enhances cytokine release and toll-like receptor 3 response in airway epithelial cells. *Respiratory Research* **13**(63).

Koeck, E. S., Iordanskaia, T., Sevilla, S., Ferrante, S. C., Hubal, M. J., Freishtat, R. J., and Nadler, E. P. (2014). Adipocyte exosomes induce transforming growth factor beta pathway dysregulation in hepatocytes: a novel paradigm for obesity-related liver disease. *The Journal of surgical research* **192**(2), 268-75.

Kolios, G., Valatas, V., and Kouroumalis, E. (2006). Role of Kupffer cells in the pathogenesis of liver disease. *World journal of gastroenterology* **12**(46), 7413-20.

Kowal, J., Tkach, M., and Thery, C. (2014). Biogenesis and secretion of exosomes. *Current opinion in cell biology* **29**, 116-25.

Krauskopf, J., Caiment, F., Claessen, S. M., Johnson, K. J., Warner, R. L., Schomaker, S. J., Burt, D. A., Aubrecht, J., and Kleinjans, J. C. (2015). Application of high-throughput sequencing to circulating microRNAs reveals novel biomarkers for drug-induced

liver injury. *Toxicological sciences : an official journal of the Society of Toxicology* **143**(2), 268-76.

Kwak, M. K., Itoh, K., Yamamoto, M., and Kensler, T. W. (2002). Enhanced Expression of the Transcription Factor Nrf2 by Cancer Chemopreventive Agents: Role of Antioxidant Response Element-Like Sequences in the nrf2 Promoter. *Molecular and Cellular Biology* **22**(9), 2883-2892.

Laine, J. E., Auriola, S., Pasanen, M., and Juvonen, R. O. (2009). Acetaminophen bioactivation by human cytochrome P450 enzymes and animal microsomes. *Xenobiotica; the fate of foreign compounds in biological systems* **39**(1), 11-21.

Larson, A. M., Polson, J., Fontana, R. J., Davern, T. J., Lalani, E., Hynan, L. S., Reisch, J. S., Schiodt, F. V., Ostapowicz, G., Shakil, A. O., *et al.* (2005). Acetaminophen-induced acute liver failure: results of a United States multicenter, prospective study. *Hepatology* **42**(6), 1364-72.

Laulagnier, K., Motta, C., Hamdi, S., Roy, S., Fauvelle, F., Pageaux, J. F., Kobayashi, T., Salles, J. P., Perret, B., Bonnerot, C., *et al.* (2004). Mast cell- and dendritic cell-derived exosomes display a specific lipid composition and an unusual membrane organization. *The Biochemical journal* **380**(Pt 1), 161-71.

LeCluyse, E., Bullock, P., Madan, A., Carroll, K., and Parkinson, A. (1999). Influence of extracellular matrix overlay and medium formulation on the induction of cytochrome P-450 2B enzymes in primary cultures of rat hepatocytes. *Drug metabolism and disposition: the biological fate of chemicals* **27**(8), 909-15.

LeCluyse, E. L., Audus, K. L., and Hochman, J. H. (1994). Formation of extensive canalicular networks by rat hepatocytes cultured in collagen-sandwich configuration. *The American journal of physiology* **266**(6 Pt 1), C1764-74.

LeCluyse, E. L., Bullock, P. L., Parkinson, A., and Hochman, J. H. (1996). Cultured rat hepatocytes. *Pharm Biotechnol* **8**, 121-59.

LeCluyse, E. L., Witek, R. P., Andersen, M. E., and Powers, M. J. (2012). Organotypic liver culture models: meeting current challenges in toxicity testing. *Crit Rev Toxicol* **42**(6), 501-48.

Legler, D. F., Micheau, O., Doucey, M. A., Tschopp, J., and Bron, C. (2003). Recruitment of TNF receptor 1 to lipid rafts is essential for TNFalpha-mediated NF-kappaB activation. *Immunity* **18**(5), 655-64.

Li, J., Liu, K., Liu, Y., Xu, Y., Zhang, F., Yang, H., Liu, J., Pan, T., Chen, J., Wu, M., *et al.* (2013). Exosomes mediate the cell-to-cell transmission of IFN-alpha-induced antiviral activity. *Nature immunology* **14**(8), 793-803.

Lin, C., Chen, Y., and Pan, T. (2011). Quantification bias caused by plasmid DNA conformation in quantitative real-time PCR assay. *PloS one* **6**(12), e29101.

Liu, J., Mansouri, K., Judson, R. S., Martin, M. T., Hong, H., Chen, M., Xu, X., Thomas, R. S., and Shah, I. (2015). Predicting hepatotoxicity using ToxCast in vitro bioactivity and chemical structure. *Chem Res Toxicol* **28**(4), 738-51.

Liu, S., Stolz, D. B., Sappington, P. L., Macias, C. A., Killeen, M. E., Tenhunen, J. J., Delude, R. L., and Fink, M. P. (2006). HMGB1 is secreted by immunostimulated enterocytes and contributes to ctyomix-induced hyperpermeability of Caco-2 monolayers. *Am J Physiol Cell Physiol* **290**, C990-C992.

Liu, Z. X., and Kaplowitz, N. (2006). Role of innate immunity in acetaminophen-induced hepatotoxicity. *Expert Opin Drug Metab Toxicol* **2**(4), 493-503.

Love, M. I., Huber, W., and Anders, S. (2014). Moderated estimation of fold change and dispersion for RNA-seq data with DESeq2. *Genome biology* **15**(12), 550.

Maiuri, A. R., Breier, A. B., Gora, L. F., Parkins, R. V., Ganey, P. E., and Roth, R. A. (2015). Cytotoxic Synergy Between Cytokines and NSAIDs Associated With Idiosyncratic Hepatotoxicity Is Driven by Mitogen-Activated Protein Kinases. *Toxicological sciences : an official journal of the Society of Toxicology* **146**(2), 265-80.

Manjarrez-Orduno, N., Moreno-Garcia, M. E., Fink, K., and Santos-Argumedo, L. (2007). CD38 cross-linking enhances TLR-induced B cell proliferation but decreases IgM plasma cell differentiation. *European journal of immunology* **37**(2), 358-67.

Masyuk, A. I., Huang, B. Q., Ward, C. J., Gradilone, S. A., Banales, J. M., Masyuk, T. V., Radtke, B. R., Splinter, P. L., and Larusso, N. F. (2010). Biliary exosomes influence cholangiocyte regulatory mechanisms and proliferation through interaction with primary cilia. *Am J Physiol Gastrointest Liver Physiol* **299**, G990-G999.

Matsumura, T., Takesue, M., Westerman, K. A., Okitsu, T., Sakaguchi, M., Fukazawa, T., Totsugawa, T., Noguchi, H., Yamamoto, S., Stolz, D. B., *et al.* (2004). Establishment of an immortalized human-liver endothelial cell line with SV40T and hTERT. *Transplantation* **77**(9), 1357-1365.

Matthews, V., Schuster, B., Schutze, S., Bussmeyer, I., Ludwig, A., Hundhausen, C., Sadowski, T., Saftig, P., Hartmann, D., Kallen, K. J., *et al.* (2003). Cellular cholesterol depletion triggers shedding of the human interleukin-6 receptor by ADAM10 and ADAM17 (TACE). *The Journal of biological chemistry* **278**(40), 38829-39.

Mazaleuskaya, L. L., Sangkuhl, K., Thorn, C. F., FitzGerald, G. A., Altman, R. B., and Klein, T. E. (2015). PharmGKB summary: pathways of acetaminophen metabolism at the therapeutic versus toxic doses. *Pharmacogenetics and genomics* **25**(8), 416-26.

McGill, M. R., Williams, C. D., Xie, Y., Ramachandran, A., and Jaeschke, H. (2012). Acetaminophen-induced liver injury in rats and mice: comparison of protein adducts, mitochondrial dysfunction, and oxidative stress in the mechanism of toxicity. *Toxicology and applied pharmacology* **264**(3), 387-94.

McKelvey, K. J., Powell, K. L., Ashton, A. W., Morris, J. M., and McCracken, S. A. (2015). Exosomes: Mechanisms of Uptake. *Journal of Circulating Biomarkers* doi: 10.5772/61186, 1.

Miyamoto, M., Yanai, M., Ookubo, S., Awasaki, N., Takami, K., and Imai, R. (2008). Detection of cell-free, liver-specific mRNAs in peripheral blood from rats with hepatotoxicity: a potential toxicological biomarker for safety evaluation. *Toxicological sciences : an official journal of the Society of Toxicology* **106**(2), 538-45.

Momen-Heravi, F., Bala, S., Kodys, K., and Szabo, G. (2015a). Exosomes derived from alcohol-treated hepatocytes horizontally transfer liver specific miRNA-122 and sensitize monocytes to LPS. *Scientific reports* **5**, 9991.

Momen-Heravi, F., Saha, B., Kodys, K., Catalano, D., Satishchandran, A., and Szabo, G. (2015b). Increased number of circulating exosomes and their microRNA cargos are potential novel biomarkers in alcoholic hepatitis. *Journal of translational medicine* **13**, 261.

Morgan, E. T. (2009). Impact of infectious and inflammatory disease on cytochrome P450-mediated drug metabolism and pharmacokinetics. *Clinical pharmacology and therapeutics* **85**(4), 434-8.

Mossanen, J. C., Krenkel, O., Ergen, C., Govaere, O., Liepelt, A., Puengel, T., Heymann, F., Kalthoff, S., Lefebvre, E., Eulberg, D., *et al.* (2016). Chemokine (C-C motif) receptor 2-positive monocytes aggravate the early phase of acetaminophen-induced acute liver injury. *Hepatology* doi: 10.1002/hep.28682.

Mulcahy, L. A., Pink, R. C., and Carter, D. R. (2014). Routes and mechanisms of extracellular vesicle uptake. *Journal of extracellular vesicles* **3**.

Muller, L., Hong, C. S., Stolz, D. B., Watkins, S. C., and Whiteside, T. L. (2014). Isolation of biologically-active exosomes from human plasma. *Journal of immunological methods* **411**, 55-65.

Murphy, A. J., Dragoljevic, D., and Tall, A. R. (2014). Cholesterol efflux pathways regulate myelopoiesis: a potential link to altered macrophage function in atherosclerosis. *Frontiers in immunology* **5**, 490.

Nakahashi-Oda, C., Tahara-Hanaoka, S., Shoji, M., Okoshi, Y., Nakano-Yokomizo, T., Ohkohchi, N., Yasui, T., Kikutani, H., Honda, S., Shibuya, K., *et al.* (2012). Apoptotic cells suppress mast cell inflammatory responses via the CD300a immunoreceptor. *The Journal of experimental medicine* **209**(8), 1493-503.

New England Biolabs *Guidelines for PCR Optimization with Taq DNA Polymerase*. Accessed 6/9/2015 doi.

Nolte-'t Hoen, E. N., Buermans, H. P., Waasdorp, M., Stoorvogel, W., Wauben, M. H., and t Hoen, P. A. (2012). Deep sequencing of RNA from immune cell-derived vesicles uncovers the selective incorporation of small non-coding RNA biotypes with potential regulatory functions. *Nucleic acids research* **40**(18), 9272-85.

Ogawa, Y., Miura, Y., Harazono, A., Kanai-Azuma, M., Akimoto, Y., Kawakami, H., Yamaguchi, T., Toda, T., Endo, T., Tsubuki, M., *et al.* (2011). Proteomic analysis of two types of exosomes in human whole saliva. *Biological & pharmaceutical bulletin* **34**(1), 13-23.

Oiknine, J., and Aviram, M. (1992). Increased susceptibility to activation and increased uptake of low density lipoprotein by cholesterol-loaded macrophages. *Arteriosclerosis and Thrombosis* **12**(6), 745-753.

Okubo, S., Miyamoto, M., Takami, K., Kanki, M., Ono, A., Nakatsu, N., Yamada, H., Ohno, Y., and Urushidani, T. (2013). Identification of novel liver-specific mRNAs in plasma for biomarkers of drug-induced liver injury and quantitative evaluation in rats treated with various hepatotoxic compounds. *Toxicological sciences : an official journal of the Society of Toxicology* **132**(1), 21-31.

Ostapowicz, G., Fontana, R. J., Schiodt, F. V., Larson, A., Davern, T. J., Han, S. H., McCashland, T. M., Shakil, A. O., Hay, J. E., Hynan, L., *et al.* (2002). Results of a prospective study of acute liver failure at 17 tertiary care centers in the United States. *Ann Intern Med* **137**(12), 947-54.

Park, E. K., Jung, H. S., Yang, H. I., Yoo, M. C., and Kim, K. S. (2007). Optimized THP-1 differentiation is required for the detection of responses to weak stimuli. *Inflammation Research* **56**, 45-50.

Paul, K. B., Hedge, J. M., Bansal, R., Zoeller, R. T., Peter, R., DeVito, M. J., and Crofton, K. M. (2012). Developmental triclosan exposure decreases maternal, fetal, and early neonatal thyroxine: a dynamic and kinetic evaluation of a putative mode-of-action. *Toxicology* **300**(1-2), 31-45.

Perez-Rosado, A., Artiga, M., Vargiu, P., Sanchez-Aguilera, A., Alvarez-Barrientos, A., and Piris, M. (2008). BCL6 represses NFkappaB activity in diffuse large B-cell lymphomas. *The Journal of pathology* **214**(4), 498-507.

Pisitkun, T., Shen, R. F., and Knepper, M. A. (2004). Identification and proteomic profiling of exosomes in human urine. *Proceedings of the National Academy of Sciences of the United States of America* **101**(36), 13368-73.

Poulsen, K. L., Albee, R. P., Ganey, P. E., and Roth, R. A. (2014). Trovafloxacin Potentiation of Lipopolysaccharide-Induced Tumor Necrosis Factor Release from RAW 264.7 Cells Requires Extracellular Signal-Regulated Kinase and c-Jun N-Terminal Kinase. *The Journal of pharmacology and experimental therapeutics* **349**(2), 185-91.

Poüs, C., Giroud, J. P., Damais, C., Raichvarg, D., and Chauvelot-Moachon, L. (1990). Effect of recombinant human interleukin-1 beta and tumor necrosis factor alpha on

liver cytochrome P-450 and serum alpha-1-acid glycoprotein concentrations in the rat. *Drug Metabolism and Disposition* **18**(4), 467-470.

Premier Biosoft *PCR Primer Design Guidelines*. Accessed 6/9/2015 doi.

Prescott, L. F. (1981). Treatment of severe acetaminophen poisoning with intravenous acetylcysteine. *Archives of internal medicine* **141**(3 Spec No), 386-9.

Przybocki, J. M., Reuhl, K. R., Thurman, R. G., and Kauffman, F. C. (1992). Involvement of nonparenchymal cells in oxygen-dependent hepatic injury by allyl alcohol. *Toxicology and applied pharmacology* **115**(1), 57-63.

Rahmani, M., Peron, P., Weitzman, J., Bakiri, L., Lardeux, B., and Bernuau, D. (2001). Functional cooperation between JunD and NF-kappaB in rat hepatocytes. *Oncogene* **20**(37), 5132-42.

Raposo, G., Nijman, H. W., Stoorvogel, W., Liejendekker, R., Harding, C. V., Melief, C. J., and Geuze, H. J. (1996). B lymphocytes secrete antigen-presenting vesicles. *The Journal of experimental medicine* **183**(3), 1161-72.

Raposo, G., and Stoorvogel, W. (2013). Extracellular vesicles: exosomes, microvesicles, and friends. *The Journal of cell biology* **200**(4), 373-83.

Ratajczak, J., Miekus, K., Kucia, M., Zhang, J., Reca, R., Dvorak, P., and Ratajczak, M. Z. (2006). Embryonic stem cell-derived microvesicles reprogram hematopoietic progenitors: evidence for horizontal transfer of mRNA and protein delivery. *Leukemia* **20**(5), 847-56.

Record, M., Carayon, K., Poirot, M., and Silvente-Poirot, S. (2014). Exosomes as new vesicular lipid transporters involved in cell-cell communication and various pathophysiologies. *Biochimica et biophysica acta* **1841**(1), 108-20.

Revilla-Fernandez, S., Wallner, B., Truschner, K., Benczak, A., Brem, G., Schmoll, F., Mueller, M., and Steinborn, R. (2005). The use of endogenous and exogenous reference RNAs for qualitative and quantitative detection of PRRSV in porcine semen. *Journal of virological methods* **126**(1-2), 21-30.

Robbins, P. D., and Morelli, A. E. (2014). Regulation of immune responses by extracellular vesicles. *Nature reviews. Immunology* **14**(3), 195-208.

Roberts, R. A., Ganey, P. E., Ju, C., Kamendulis, L. M., Rusyn, I., and Klaunig, J. E. (2007). Role of the Kupffer cell in mediating hepatic toxicity and carcinogenesis. *Toxicological sciences : an official journal of the Society of Toxicology* **96**(1), 2-15.

Rodrigues, R. M., Bouhifd, M., Bories, G., Sacco, M. G., Gribaldo, L., Fabbri, M., Coecke, S., and Whelan, M. P. (2013). Assessment of an automated in vitro basal cytotoxicity test system based on metabolically-competent cells. *Toxicology in vitro : an international journal published in association with BIBRA* **27**(2), 760-7.

Rose, K. A., Holman, N. S., Green, A. M., Andersen, M. E., and LeCluyse, E. L. (2016). Co-culture of Hepatocytes and Kupffer Cells as an In Vitro Model of Inflammation and Drug-Induced Hepatotoxicity. *Journal of pharmaceutical sciences* **105**(2), 950-64.

Rotroff, D. M., Beam, A. L., Dix, D. J., Farmer, A., Freeman, K. M., Houck, K. A., Judson, R. S., LeCluyse, E. L., Martin, M. T., Reif, D. M., *et al.* (2010). Xenobiotic-metabolizing enzyme and transporter gene expression in primary cultures of human hepatocytes modulated by ToxCast chemicals. *J Toxicol Environ Health B Crit Rev* **13**(2-4), 329-46.

Royo, F., and Falcon-Perez, J. M. (2012). Liver extracellular vesicles in health and disease. *Journal of extracellular vesicles* **1**.

Royo, F., Palomo, L., Mleczko, J., Gonzalez, E., Alonso, C., Martinez, I., Perez-Cormenzana, M., Castro, A., and Falcon-Perez, J. M. (2016). Metabolically active extracellular vesicles released from hepatocytes under drug-induced liver-damaging conditions modify serum metabolome and might affect different pathophysiological processes. *European journal of pharmaceutical sciences : official journal of the European Federation for Pharmaceutical Sciences* doi: 10.1016/j.ejps.2016.10.020.

Royo, F., Schlangen, K., Palomo, L., Gonzalez, E., Conde-Vancells, J., Berisa, A., Aransay, A. M., and Falcon-Perez, J. M. (2013). Transcriptome of extracellular vesicles released by hepatocytes. *PloS one* **8**(7), e68693.

Russmann, S., Kullak-Ublick, G. A., and Grattagliano, I. (2009). Current concepts of mechanisms in drug-induced hepatotoxicity. *Current Medicinal Chemistry* **16**, 4041-3053.

Santangelo, L., Giurato, G., Cicchini, C., Montaldo, C., Mancone, C., Tarallo, R., Battistelli, C., Alonzi, T., Weisz, A., and Tripodi, M. (2016). The RNA-Binding Protein SYNCRIP Is a Component of the Hepatocyte Exosomal Machinery Controlling MicroRNA Sorting. *Cell reports* **17**(3), 799-808.

Schildberger, A., Rossmanith, E., Eichhorn, T., Strassl, K., and Weber, V. (2013). Monocytes, peripheral blood mononuclear cells, and THP-1 cells exhibit different cytokine expression patterns following stimulation with lipopolysaccharide. *Mediators of inflammation* **2013**, 697972.

Serper, M., Wolf, M., Parikh, N. A., Tillman, H., Lee, W. M., and Ganger, D. R. (2016). Risk factors, clinical presentation, and outcomes in overdose with acetaminophen alone or with combination products. *J Clin Gastroenterol* **50**(1), 85-91.

Shaw, P. J., Ganey, P. E., and Roth, R. A. (2009). Tumor necrosis factor alpha is a proximal mediator of synergistic hepatotoxicity from trovafloxacin/lipopolysaccharide coexposure. *The Journal of pharmacology and experimental therapeutics* **328**(1), 62-8.

Shaw, P. J., Ganey, P. E., and Roth, R. A. (2010). Idiosyncratic drug-induced liver injury and the role of inflammatory stress with an emphasis on an animal model of trovafloxacin hepatotoxicity. *Toxicological sciences : an official journal of the Society of Toxicology* **118**(1), 7-18.

Shaw, P. J., Hopfensperger, M. J., Ganey, P. E., and Roth, R. A. (2007). Lipopolysaccharide and Trovafloxacin Coexposure in Mice Causes Idiosyncrasy-Like Liver Injury Dependent on Tumor Necrosis Factor-Alpha. *Toxicological Sciences* **100**(1), 259-266.

Shi, C., and Pamer, E. G. (2011). Monocyte recruitment during infection and inflammation. *Nature reviews. Immunology* **11**(11), 762-74.

Siekevitz, P. (1972). Biological membranes: the dynamics of their organization. *Annual review of physiology* **34**, 117-40.

Simon, L., Lopez, M., Uribe-Cruz, C., Vergara, D. F., Silla, L., and Matte, U. (2015). Injured hepatocyte-released microvesicles induce bone marrow-derived mononuclear cells differentiation. *Differentiation; research in biological diversity* doi: 10.1016/j.diff.2015.09.001.

Skazik-Voogt, C., Kuhler, K., Ott, H., Czaja, K., Zwadlo-Klarwasser, G., Merk, H. F., Amann, P. M., and Baron, J. M. (2016). Myeloid human cell lines lack functional regulation of aryl hydrocarbon receptor-dependent phase I genes. *Altex* **33**(1), 37-46.

Smith, R. D., Brown, B., Ikonomi, P., and Schechter, A. N. (2003). Exogenous reference RNA for normalization of real-time quantitative PCR. *BioTechniques* **34**(1), 88-91.

Starckx, S., Batheja, A., Verheyen, G. R., Jonghe, S. D., Steemans, K., Dijck, B. V., Singer, M., Bogdan, N., Snoeys, J., Vinken, P., *et al.* (2013). Evaluation of miR-122 and other biomarkers in distinct acute liver injury in rats. *Toxicologic pathology* **41**(5), 795-804.

Starkey Lewis, P. J., Dear, J., Platt, V., Simpson, K. J., Craig, D. G., Antoine, D. J., French, N. S., Dhaun, N., Webb, D. J., Costello, E. M., *et al.* (2011). Circulating microRNAs as potential markers of human drug-induced liver injury. *Hepatology* **54**(5), 1767-76.

Strauss, K., Goebel, C., Runz, H., Mobius, W., Weiss, S., Feussner, I., Simons, M., and Schneider, A. (2010). Exosome secretion ameliorates lysosomal storage of cholesterol in Niemann-Pick type C disease. *The Journal of biological chemistry* **285**(34), 26279-88.

Subra, C., Grand, D., Laulagnier, K., Stella, A., Lambeau, G., Paillasse, M., De Medina, P., Monsarrat, B., Perret, B., Silvente-Poirot, S., *et al.* (2010). Exosomes account for vesicle-mediated transcellular transport of activatable phospholipases and prostaglandins. *J Lipid Res* **51**(8), 2105-20.

Sunman, J. A., Hawke, R. L., LeCluyse, E. L., and Kashuba, A. D. (2004). Kupffer cell-mediated IL-2 suppression of CYP3A activity in human hepatocytes. *Drug metabolism and disposition: the biological fate of chemicals* **32**(3), 359-63.

Suzuki, M., Sugimoto, Y., Ohsaki, Y., Ueno, M., Kato, S., Kitamura, Y., Hosokawa, H., Davies, J. P., Ioannou, Y. A., Vanier, M. T., *et al.* (2007). Endosomal accumulation of Toll-like receptor 4 causes constitutive secretion of cytokines and activation of signal transducers and activators of transcription in Niemann-Pick disease type C (NPC) fibroblasts: a potential basis for glial cell activation in the NPC brain. *The Journal of neuroscience : the official journal of the Society for Neuroscience* **27**(8), 1879-91.

Swift, B., Pfeifer, N. D., and Brouwer, K. L. (2010). Sandwich-cultured hepatocytes: an in vitro model to evaluate hepatobiliary transporter-based drug interactions and hepatotoxicity. *Drug metabolism reviews* **42**(3), 446-71.

System Biosciences (2013). ExoQuick Exosome Precipitation Solution User Manual. In (Vol. ver 8-2013-02-22. System Biosciences.

Tahaoglu, K., Atac, G., Sevim, T., Tarun, T., Yazicioglu, O., Horzum, G., Gemci, I., Ongel, A., Kapakli, N., and Aksoy, E. (2001). The management of anti-tuberculosis drug-induced hepatotoxicity. *The international journal of tuberculosis and lung disease : the official journal of the International Union against Tuberculosis and Lung Disease* **5**(1), 65-9.

Tall, A. R., and Yvan-Charvet, L. (2015). Cholesterol, inflammation and innate immunity. *Nature reviews. Immunology* **15**(2), 104-16.

Taylor, D. D., Gercel-Taylor, C., Lyons, K. S., Stanson, J., and Whiteside, T. L. (2003). T-cell apoptosis and suppression of T-cell receptor/CD3-zeta by Fas ligand-containing membrane vesicles shed from ovarian tumors. *Clinical cancer research : an official journal of the American Association for Cancer Research* **9**(14), 5113-9.

Taylor, D. D., and Shah, S. (2015). Methods of isolating extracellular vesicles impact down-stream analyses of their cargoes. *Methods* **87**, 3-10.

Taylor, D. D., Zacharias, W., and Gercel-Taylor, C. (2011). Exosome isolation for proteomic analyses and RNA profiling. *Methods in molecular biology* **728**, 235-46.

Tellier, E., Canault, M., Poggi, M., Bonardo, B., Nicolay, A., Alessi, M. C., Nalbone, G., and Peiretti, F. (2008). HDLs activate ADAM17-dependent shedding. *Journal of cellular physiology* **214**(3), 687-93.

Torregrosa Paredes, P., Esser, J., Admyre, C., Nord, M., Rahman, Q. K., Lukic, A., Radmark, O., Gronneberg, R., Grunewald, J., Eklund, A., *et al.* (2012). Bronchoalveolar lavage fluid exosomes contribute to cytokine and leukotriene production in allergic asthma. *Allergy* **67**(7), 911-9.

Tujios, S., and Fontana, R. J. (2011). Mechanisms of drug-induced liver injury: from bedside to bench. *Nature reviews. Gastroenterology & hepatology* **8**(4), 202-11.

Turchinovich, A., Samatov, T. R., Tonevitsky, A. G., and Burwinkel, B. (2013). Circulating miRNAs: cell-cell communication function? *Frontiers in genetics* **4**, 119.

Turchinovich, A., Weiz, L., Langheinz, A., and Burwinkel, B. (2011). Characterization of extracellular circulating microRNA. *Nucleic acids research* **39**(16), 7223-33.

Uetrecht, J. (2008). Idiosyncratic Drug Reactions: Past, Present, and Future. *Chem. Res. Toxicol.* **21**, 84-92.

Uetrecht, J., and Naisbitt, D. J. (2013). Idiosyncratic adverse drug reactions: current concepts. *Pharmacological reviews* **65**(2), 779-808.

Ulrich, R. G. (2007). Idiosyncratic toxicity: a convergence of risk factors. *Annual review of medicine* **58**, 17-34.

Urban, T. J., Daly, A. K., and Aithal, G. P. (2014). Genetic basis of drug-induced liver injury: present and future. *Seminars in liver disease* **34**(2), 123-33.

Valadi, H., Ekstrom, K., Bossios, A., Sjostrand, M., Lee, J. J., and Lotvall, J. O. (2007). Exosome-mediated transfer of mRNAs and microRNAs is a novel mechanism of genetic exchange between cells. *Nature cell biology* **9**(6), 654-9.

Valatas, V., Xidakis, C., Roumpaki, H., Kolios, G., and Kouroumalis, E. A. (2003). Isolation of rat Kupffer cells: a combined methodology for highly purified primary cultures. *Cell Biol Int* **27**(1), 67-73.

Van Deun, J., Mestdagh, P., Sormunen, R., Cocquyt, V., Vermaelen, K., Vandesompele, J., Bracke, M., De Wever, O., and Hendrix, A. (2014). The impact of disparate isolation methods for extracellular vesicles on downstream RNA profiling. *Journal of extracellular vesicles* **3**.

Vella, L. J., Sharples, R. A., Lawson, V. A., Masters, C. L., Cappai, R., and Hill, A. F. (2007). Packaging of prions into exosomes is associated with a novel pathway of PrP processing. *The Journal of pathology* **211**(5), 582-90.

Verma, V. K., Li, H., Wang, R., Hirsova, P., Mushref, M., Liu, Y., Cao, S., Contreras, P. C., Malhi, H., Kamath, P. S., *et al.* (2016). Alcohol stimulates macrophage activation through caspase-dependent hepatocyte derived release of CD40L containing extracellular vesicles. *Journal of hepatology* **64**(3), 651-60.

Vickers, K. C., Palmisano, B. T., Shoucri, B. M., Shamburek, R. D., and Remaley, A. T. (2011). MicroRNAs are transported in plasma and delivered to recipient cells by high-density lipoproteins. *Nature cell biology* **13**(4), 423-33.

Vij, N., Amoako, M. O., Mazur, S., and Zeitlin, P. L. (2008). CHOP transcription factor mediates IL-8 signaling in cystic fibrosis bronchial epithelial cells. *American journal of respiratory cell and molecular biology* **38**(2), 176-84.

Villarroya-Beltri, C., Baixauli, F., Gutierrez-Vazquez, C., Sanchez-Madrid, F., and Mittelbrunn, M. (2014). Sorting it out: regulation of exosome loading. *Seminars in cancer biology* **28**, 3-13.

Vliegenthart, A. D., Shaffer, J. M., Clarke, J. I., Peeters, L. E., Caporali, A., Bateman, D. N., Wood, D. M., Dargan, P. I., Craig, D. G., Moore, J. K., *et al.* (2015). Comprehensive microRNA profiling in acetaminophen toxicity identifies novel circulating biomarkers for human liver and kidney injury. *Scientific reports* **5**, 15501.

Vojtech, L., Woo, S., Hughes, S., Levy, C., Ballweber, L., Sauteraud, R. P., Strobl, J., Westerberg, K., Gottardo, R., Tewari, M., *et al.* (2014). Exosomes in human semen carry a distinctive repertoire of small non-coding RNAs with potential regulatory functions. *Nucleic acids research* **42**(11), 7290-304.

Wahlgren, J., Karlson Tde, L., Glader, P., Telemo, E., and Valadi, H. (2012). Activated human T cells secrete exosomes that participate in IL-2 mediated immune response signaling. *PloS one* **7**(11), e49723.

Walgren, J. L., Mitchell, M. D., and Thompson, D. C. (2005). Role of metabolism in drug-induced idiosyncratic hepatotoxicity. *Critical Reviews in Toxicology* **34**(4), 325-361.

Wang, K., Zhang, S., Marzolf, B., Troisch, P., Brightman, A., Hu, Z., Hood, L. E., and Galas, D. J. (2009). Circulating microRNAs, potential biomarkers for drug-induced liver injury. *Proceedings of the National Academy of Sciences of the United States of America* **106**(11), 4402-7.

Ward, J., Kanchagar, C., Veksler-Lublinsky, I., Lee, R. C., McGill, M. R., Jaeschke, H., Curry, S. C., and Ambros, V. R. (2014). Circulating microRNA profiles in human patients with acetaminophen hepatotoxicity or ischemic hepatitis. *Proceedings of the National Academy of Sciences of the United States of America* **111**(33), 12169-74.

Waring, J. F., Liguori, M. J., Luyendyk, J. P., Maddox, J. F., Ganey, P. E., Stachlewitz, R. F., North, C., Blomme, E. A. G., and Roth, R. A. (2006). Microarray Analysis of Lipopolysaccharide Potentiation of Trovafloxacin-Induced Liver Injury in Rats Suggests a Role for Proinflammatory Chemokines and Neutrophils. *Journal of Pharmacology and Experimental Therapeutics* **316**(3), 1080-1087.

Waxman, D. J., Morrissey, J. J., Naik, S., and Jauregui, H. O. (1990). Phenobarbital induction of cytochromes P-450. High-level long-term responsiveness of primary rat hepatocyte cultures to drug induction, and glucocorticoid dependence of the phenobarbital response. *The Biochemical journal* **271**(1), 113-9.

Welch, J. D., Williams, L. A., DiSalvo, M., Brandt, A. T., Marayati, R., Sims, C. E., Allbritton, N. L., Prins, J. F., Yeh, J. J., and Jones, C. D. (2016). Selective single cell isolation for genomics using microraft arrays. *Nucleic acids research* **44**(17), 8292-301.

Wetmore, B. A., Brees, D. J., Singh, R., Watkins, P. B., Andersen, M. E., Loy, J., and Thomas, R. S. (2010). Quantitative analyses and transcriptomic profiling of circulating messenger RNAs as biomarkers of rat liver injury. *Hepatology* **51**(6), 2127-2139.

Widmann, J. J., and Fahimi, H. D. (1975). Proliferation of mononuclear phagocytes (Kupffer cells) and endothelial cells in regenerating rat liver. A light and electron microscopic cytochemical study. *The American journal of pathology* **80**(3), 349-66.

Wilke, R. A., Lin, D. W., Roden, D. M., Watkins, P. B., Flockhart, D., Zineh, I., Giacomini, K. M., and Krauss, R. M. (2007). Identifying genetic risk factors for serious adverse drug reactions: current progress and challenges. *Nature reviews. Drug discovery* **6**(11), 904-16.

Williams, C. D., Bajt, M. L., Sharpe, M. R., McGill, M. R., Farhood, A., and Jaeschke, H. (2014). Neutrophil activation during acetaminophen hepatotoxicity and repair in mice and humans. *Toxicology and applied pharmacology* **275**(2), 122-33.

Witek, R. P., Yang, L., Liu, R., Jung, Y., Omenetti, A., Syn, W. K., Choi, S. S., Cheong, Y., Fearing, C. M., Agboola, K. M., *et al.* (2009). Liver cell-derived microparticles activate hedgehog signaling and alter gene expression in hepatic endothelial cells. *Gastroenterology* **136**(1), 320-330 e2.

Witwer, K. W., Buzas, E. I., Bemis, L. T., Bora, A., Lasser, C., Lotvall, J., Nolte-'t Hoen, E. N., Piper, M. G., Sivaraman, S., Skog, J., *et al.* (2013). Standardization of sample collection, isolation and analysis methods in extracellular vesicle research. *Journal of extracellular vesicles* **2**.

Wojdyla, K., Wrzesinski, K., Williamson, J., Fey, S. J., and Rogowska-Wrzesinska, A. (2016). Acetaminophen-induced S-nitrosylation and S-sulfenylation signalling in 3D cultured hepatocarcinoma cell spheroids. *Toxicology Research* **5**(3), 905-920.

Wolf, D. C., Allen, J. W., George, M. H., Hester, S. D., Sun, G., Moore, T., Thai, S. F., Delker, D., Winkfield, E., Leavitt, S., *et al.* (2006). Toxicity profiles in rats treated with tumorigenic and nontumorigenic triazole conazole fungicides: Propiconazole, triadimefon, and myclobutanil. *Toxicologic pathology* **34**(7), 895-902.

Wolf, P. (1967). The nature and significance of platelet products in human plasma. *British journal of haematology* **13**(3), 269-88.

Wu, R., Cui, X., Dong, W., Zhou, M., Simms, H. H., and Wang, P. (2006). Suppression of hepatocyte CYP1A2 expression by Kupffer cells via AhR pathway: the central role of proinflammatory cytokines. *International journal of molecular medicine* **18**(2), 339-46.

Yang, X., Weng, Z., Mendrick, D. L., and Shi, Q. (2014). Circulating extracellular vesicles as a potential source of new biomarkers of drug-induced liver injury. *Toxicology letters* **225**(3), 401-6.

Yang, Y., Han, Q., Hou, Z., Zhang, C., Tian, Z., and Zhang, J. (2016). Exosomes mediate hepatitis B virus (HBV) transmission and NK-cell dysfunction. *Cellular & molecular immunology* doi: 10.1038/cmi.2016.24.

Yu, Y., Ping, J., Chen, H., Jiao, L., Zheng, S., Han, Z. G., Hao, P., and Huang, J. (2010). A comparative analysis of liver transcriptome suggests divergent liver function among human, mouse and rat. *Genomics* **96**(5), 281-9.

Yuana, Y., Bertina, R. M., and Osanto, S. (2011). Pre-analytical and analytical issues in the analysis of blood microparticles. *Thrombosis and haemostasis* **105**(3), 396-408.

Yuana, Y., Levels, J., Grootemaat, A., Sturk, A., and Nieuwland, R. (2014). Co-isolation of extracellular vesicles and high-density lipoproteins using density gradient ultracentrifugation. *Journal of extracellular vesicles* **3**.

Yvan-Charvet, L., Welch, C., Pagler, T. A., Ranalletta, M., Lamkanfi, M., Han, S., Ishibashi, M., Li, R., Wang, N., and Tall, A. R. (2008). Increased inflammatory gene expression in ABC transporter-deficient macrophages: free cholesterol accumulation, increased signaling via toll-like receptors, and neutrophil infiltration of atherosclerotic lesions. *Circulation* **118**(18), 1837-47.

Zakharova, L., Svetlova, M., and Fomina, A. F. (2006). T cell exosomes induced cholesterol accumulation in human monocytes via phosphatidylserine receptor. *Journal of cellular physiology* **212**, 174-181.

Zhang, X., Zhang, Z., Dai, F., Shi, B., Chen, L., Zhang, X., Zang, G., Zhang, J., Chen, X., Qian, F., *et al.* (2014). Comparison of circulating, hepatocyte-specific messenger RNA and microRNA as biomarkers of chronic hepatitis B and C. *PloS one* **9**(3), e92112.

Zhu, X., Lee, J. Y., Timmins, J. M., Brown, J. M., Boudyguina, E., Mulya, A., Gebre, A. K., Willingham, M. C., Hiltbold, E. M., Mishra, N., *et al.* (2008). Increased cellular free cholesterol in macrophage-specific Abca1 knock-out mice enhances pro-inflammatory response of macrophages. *The Journal of biological chemistry* **283**(34), 22930-41.

Zigmond, E., Samia-Grinberg, S., Pasmanik-Chor, M., Brazowski, E., Shibolet, O., Halpern, Z., and Varol, C. (2014). Infiltrating monocyte-derived macrophages and resident kupffer cells display different ontogeny and functions in acute liver injury. *Journal of immunology* **193**(1), 344-53.

Zisman, D. A., Kunkel, S. L., Strieter, R. M., Tsai, W. C., Bucknell, K., Wilkowski, J., and Standiford, T. J. (1997). MCP-1 protects mice in lethal endotoxemia. *The Journal of clinical investigation* **99**(12), 2832-6.